

## DISSERTATION

# New Aspects of the Quantum Geometric Phase

ausgeführt zum Zwecke der Erlangung des akademischen Grades eines  
Doktors der technischen Wissenschaften unter der Leitung von

o. Univ. Prof. Dipl. Ing. Dr. Helmut Rauch  
E 141 - Atominstitut der Österreichischen Universitäten

eingereicht an der Technischen Universität Wien  
Fakultät für Technische Physik

von

Dipl. Ing. Stefan Filipp  
Matrikelnummer 9725660  
Herzgasse 14/5, 1100 Wien, Austria  
[sfilipp@ati.ac.at](mailto:sfilipp@ati.ac.at)

Wien, am 5. September 2006



## **Abstract**

The quantum geometric phase is a fascinating demonstration how geometry affects standard quantum mechanics already on the level of Hilbert space structure. A prominent classical analogue is Foucault's pendulum proving besides the rotation of the earth also that it is not flat. After twenty-four hours the plane of oscillation does not return to its initial direction, a typical geometric effect of the curvature of Earth. In quantum mechanics a similar effect causes a phase difference between initial and final state of a system depending only on the evolution path traced out by the state vector in its state space. If it is not flat, as for instance a sphere for the neutron spin state, a geometric phase factor shows up. This thesis deals with the geometric phase in several ways. First, based on the geometric phase for mixed states, I will present two definitions of off-diagonal geometric phases for mixed states, which provide topological information about state space also if the usual mixed state geometric phase is undefined. The second part contains the description of a neutron interferometry experiment, where a geometric phase arising from the path degree of freedom in an interferometer is demonstrated. A double-loop perfect-crystal neutron interferometer is used in order to measure the phase induced in one loop relative to a reference beam. For particular absorption and phase shifter parameters this relative phase is purely geometric. Finally, according to several theoretical investigations the geometric phase seems to be a good candidate to achieve quantum gates with high reliability. In the third part, a possible experimental test of this feature using ultra-cold neutrons subjected to fluctuating magnetic fields is discussed. Numerical studies provide insight in the feasibility of such an experiment and demonstrate the prospective difficulties.



## **Kurzfassung**

Die geometrische Phase zeigt, wie schon die Vorhersagen der Standard-Quantenmechanik von der Geometrie des zugrundeliegenden Hilbertraumes beeinflusst werden. Ein anschauliches und bekanntes Beispiel aus der klassischen Physik ist das Foucaultsche Pendel. Dieses diente in der Mitte des 19. Jahrhunderts als Beweis der Rotation der Erde, und nebenher noch als Demonstration ihrer Kugelgestalt. Die Schwingungsebene rotiert aus der Sicht des fix auf der Erde stehenden Beobachters, kehrt aber im Allgemeinen nicht nach 24 Stunden zu seiner Ausgangslage zurück. Dieser Effekt beruht auf der Krümmung der Erdoberfläche. In der Quantenmechanik tritt ein analoger Effekt auf: Es kommt zu einer zusätzlichen Phasendifferenz zwischen dem Anfangs- und Endzustand eines quantenmechanischen Systems, wenn der Zustandsraum eine Krümmung aufweist. Weiters hängt diese Phase - im Gegensatz zur dynamischen Phase - nur vom Pfad ab und nicht von der benötigten Zeit oder der Energie des Zustandes. Ein typisches Beispiel ist der Spin-Zustand eines Neutrons, dessen Zustandsraum als Kugeloberfläche dargestellt werden kann, und eine Manipulation des Spins führt daher zu einer geometrischen Phase. Die vorliegende Dissertation behandelt einige Aspekte dieser geometrischen Phase. Zum einen werden sogenannte nicht-diagonale geometrische Phasen für gemischte Zustände definiert, welche Information über die Topologie des Zustandsraumes bietet, falls die gewöhnliche geometrische Phase nicht wohldefiniert ist. Im zweiten Teil taucht die geometrische Phase im Kontext der Neutroneninterferometrie auf. Ein Interferometer mit zwei Kreisen wird verwendet, um die in einem Kreis generierte Phase relative zu einem Referenzstrahl zu messen. Der Zustand in diesem Kreis kann durch geeignete Wahl eines Absorbers und eines Phasenschiebers so verändert werden, dass schlussendlich nur eine geometrische Phase gemessen wird. Diese folgt wiederum aus der Geometrie des sphärischen Zustandsraumes. Schließlich wird die Frage des Einflusses von äußeren Störungen auf die geometrische Phase aufgegriffen. Einige theoretische Überlegungen kommen zum Schluß, dass diese gut geeignet sei um quantenmechanische Schaltungen zu realisieren. Dieses Verhalten könnte mit ultrakalten Neutronen getestet werden. Numerische Simulationen in Hinblick auf ein zukünftiges Experiment werden präsentiert.



# Acknowledgements

Without the support, the contributions and the help of several other people the completion, not even the beginning of this thesis would have been possible. It was a pleasure for me to work with many talented and friendly colleagues guiding me towards new insights and expanding my horizons. I want to thank my supervisor and mentor Helmut Rauch for his thought-provoking impulses and helpful discussions - not only on topics connected to this thesis. Pointing out an abundance of interesting physical questions was as important for the physical understanding as his consent and allowance that enabled scientific exchange, acquirement of new knowledge and formation of ideas on various workshops, conferences and schools. In equal measure, I want to say thanks to Yuji Hasegawa who contributed significantly to the accomplishment of this thesis. His competence in doing experiments was indispensable for this work, his advice and his ideas were of great help all along my studies.

What would a working day be without interesting and enlightening discussions - about physics or more mundane issues, without regular coffee breaks, without interaction and cooperation, without exchange of knowledge and experience and without lunch at the notorious restaurant “Knusperhäuschen”. For all these things I acknowledge the tireless commitment of my colleagues and friends at the Atominstitut, especially of Jürgen Klepp, Hartmut Lemmel, Stephan Sponar, Matthias Baron, Matthias Lettner and Martin Trinker. I also want to say thanks to all those I met during my stay at the Institut Laue Langevin in Grenoble. I owe Hans Börner as the head of the Nuclear and Particle Physics Group a debt of gratitude for the hospitality I found there. It was a pleasure for me to meet many sociable and avid people, most notably Christian Plonka, Rudi Loidl, Torsten Soldner, Monica Jimenez-Ruiz, Jochen Krempel, Tinka Spehr, Karin Schmalzl and Peter Geltenbort, and all the others who made my stay at the ILL an unforgettable experience. I want to thank Erik Sjöqvist from Uppsala University for many discussions and suggestions concerning geometric phases. It was him who introduced me into the fascinating physics of the geometric phase and whose thoughts and ideas have been very important for the progress of this work. Furthermore, I thank Karl Svozil from the Technical University Vienna as my former supervisor for the close collaboration on Bell-type inequalities in continuation of my diploma thesis. I also want to acknowledge many fruitful discussions and meetings with Reinhold Bertlmann, Katharina Durstberger and Beatrix Hiesmayr from the University of Vienna. In the course of my PhD-studies it turned out that more than pencil, paper and a computer is needed and, therefore, I want to thank Peter Pataki and Erich Tischler for their support and patience when it came to the realisation of various utensils needed for experiments.

Beyond the immediate involvement on the progress of my thesis of those mentioned above I wish to express my sincere thanks to my parents who really formed the basis of all this work. Without their encouraging support, without their engagement from the very beginning of my career and without the untroubled family background it would be impossible for me to accomplish this work.

Above all, I am indebted to my beloved girlfriend Claudia Führer, my support in almost all aspects of everyday life. It is due to her that I could maintain balance in life and it was her who had to bear the immediate consequences of time-consuming major and minor difficulties turning up every now and then. Her endurance and her understanding were key ingredients of this dissertation.

This work has been supported by the Austrian Science Foundation (FWF) within the Spezialforschungsbereich (SFB) “Control and Measurement of Coherent Quantum Systems”.

# Contents

<b>Acknowledgements</b>	<b>vii</b>
<b>Preface</b>	<b>xiii</b>
<b>1 Geometric Phase - Introduction</b>	<b>1</b>
1.1 Mathematical analogue . . . . .	1
1.2 Berry's phase and generalisations . . . . .	2
1.2.1 Derivation of Berry's phase . . . . .	3
1.2.2 Non-adiabatic evolution . . . . .	9
1.2.3 Non-cyclic and non-adiabatic evolution . . . . .	11
1.2.4 Kinematic Approach . . . . .	17
1.3 Experiments on the geometric phases . . . . .	23
1.4 Facts to remember . . . . .	24
<b>2 Geometric Phase For Mixed States</b>	<b>27</b>
2.1 Mixed states . . . . .	27
2.2 Geometric Phase for Mixed States . . . . .	32
2.3 Interferometric mixed state geometric phase . . . . .	33
2.3.1 Parallel transport . . . . .	35
2.3.2 Gauge invariance . . . . .	36
2.3.3 Degenerate density matrices . . . . .	37
2.3.4 Non-unitary evolution . . . . .	38
2.4 Uhlmann Holonomies . . . . .	38
2.4.1 Construction of amplitudes . . . . .	39
2.4.2 Parallelity of states . . . . .	40
2.4.3 Parallel transport . . . . .	42
2.4.4 Hamiltonian motion . . . . .	44
<b>3 Off-diagonal Geometric Phases</b>	<b>49</b>
3.1 Pure state off-diagonal geometric phase . . . . .	49
3.2 Off-diagonal Geometric Phase for Mixed States - Interferometric approach .	52
3.2.1 Orthogonality . . . . .	52
3.2.2 Consistency and normalisation . . . . .	57

3.2.3	Off-diagonal mixed state geometric phase . . . . .	58
3.2.4	Computation of off-diagonal mixed state phases . . . . .	59
3.2.5	Projection phase . . . . .	61
3.2.6	Explicit calculations for a simple path . . . . .	62
3.2.7	Kinematic approach to off-diagonal geometric phases . . . . .	67
3.2.8	Experimental verification . . . . .	68
3.3	Off-diagonal holonomies following Uhlmann's definition . . . . .	72
3.3.1	Nodal points of Uhlmann holonomies . . . . .	72
3.3.2	Definition of off-diagonal quantum holonomies . . . . .	72
3.3.3	Comparison with the interferometric off-diagonal geometric phase . . . . .	75
3.3.4	Examples . . . . .	75
3.3.5	Spin Flip Operation on a Mixture of Bell States . . . . .	77
3.4	Conclusions . . . . .	79
<b>4</b>	<b>Spatial Geometric Phase</b>	<b>81</b>
4.1	Neutron Interferometry . . . . .	82
4.1.1	Phase Shifter . . . . .	86
4.1.2	Induced phase shift . . . . .	89
4.1.3	Absorber . . . . .	90
4.2	Description of the setup . . . . .	91
4.3	Dynamical contribution . . . . .	94
4.4	Paths on Bloch-sphere - A geometrical interpretation . . . . .	95
4.4.1	Calculation of the surface integrals . . . . .	96
4.5	Measurement procedure . . . . .	99
4.6	Experimental results . . . . .	99
4.6.1	Thickness ratio $d_1/d_2 \approx 1/8$ . . . . .	100
4.6.2	Thickness ratio $d_1/d_2 \approx 1/4$ . . . . .	106
4.6.3	Thickness ratio $d_1/d_2 \approx 1/2$ . . . . .	107
4.6.4	Thickness ratio $d_1/d_2 = 1$ . . . . .	109
4.6.5	Cyclic geometric phase . . . . .	110
4.7	Wagh's critical comments . . . . .	111
4.8	Systematic deviations due to partial overlap . . . . .	112
4.8.1	Coherence properties . . . . .	112
4.8.2	Correlation Function approach . . . . .	114
4.8.3	Coherence volume in a neutron interferometer . . . . .	115
4.8.4	Three Beam superposition . . . . .	116
4.9	Dephasing effects . . . . .	119
4.10	Conclusions . . . . .	122
<b>5</b>	<b>Geometric phase and adiabatic fluctuations</b>	<b>123</b>
5.1	Spin-1/2 in a fluctuating magnetic field . . . . .	125
5.1.1	Theoretical considerations . . . . .	126

5.1.2	Region of applicability of the first-order approximation . . . . .	130
5.1.3	Dynamical Contribution . . . . .	131
5.1.4	Explanation in terms of domains of integration . . . . .	133
5.2	Removing the dynamical phase . . . . .	134
5.3	Spin Echo . . . . .	135
5.4	Possible Experimental setups . . . . .	138
5.4.1	Interferometric setup . . . . .	138
5.4.2	Polarimetric setup . . . . .	139
5.4.3	Ultra cold neutrons . . . . .	142
5.5	Spin gymnastics . . . . .	144
5.5.1	Time Sequence . . . . .	150
5.6	Numerical Simulations . . . . .	150
5.6.1	Evolution algorithm for the spin state . . . . .	152
5.6.2	Noise model . . . . .	153
5.6.3	Numerical results for different parameter settings . . . . .	157
5.6.4	More spin flips . . . . .	164
5.7	Conclusions . . . . .	165
<b>6</b>	<b>Conclusions and Outlook</b>	<b>167</b>
<b>A</b>	<b>About Noise</b>	<b>171</b>
A.1	Definition of a stochastic process . . . . .	171
A.2	Langevin equation . . . . .	175
A.3	Ornstein-Uhlenbeck process . . . . .	176
A.4	Integral of an O.U. process . . . . .	177
A.5	Generation of an O. U.-process by its spectral representation . . . . .	178
A.6	Example: Current noise in an electric circuits . . . . .	179
<b>B</b>	<b>Calculation of a geodesic on a sphere</b>	<b>181</b>
<b>C</b>	<b>Adiabatic Theorem</b>	<b>184</b>
<b>D</b>	<b>Details of UCN measurement</b>	<b>186</b>
D.1	Description of the components . . . . .	187
D.1.1	Neutron guides . . . . .	187
D.1.2	Shutter . . . . .	188
D.1.3	Switch . . . . .	188
D.1.4	Polarisation foil . . . . .	188
D.1.5	Storage volume . . . . .	189
D.1.6	Helmholtz coils . . . . .	189
D.1.7	Mu-metal shielding chamber . . . . .	194
D.1.8	Detector . . . . .	194
D.1.9	Control units . . . . .	195

D.2	Unavoidable influences . . . . .	195
D.2.1	Inhomogeneities of the magnetic field of the coils . . . . .	195
D.2.2	Fluctuating stray magnetic fields . . . . .	198
D.2.3	Vessel too small . . . . .	199
D.2.4	Insufficient rise & fall time of the electrical components . . . . .	199
D.2.5	Inductance of Helmholtz coil could spoil high frequency noise . . . . .	199
D.3	How to measure? . . . . .	200
<b>E</b>	<b>Notation</b>	<b>202</b>
	<b>Curriculum Vitae</b>	<b>217</b>

# Preface

Foucault's pendulum experiment is an important and remarkable demonstration that the Earth is rotating beneath our feet from the mid-nineteenth century (and also a intriguing book by Umberto Eco [Eco88]). Moreover, not only the rotation, but also that fact the Earth is a sphere and not a disc is established. Placing the pendulum on a flat rotating earth instead, one would expect that it lasts 24 hours that the plane of oscillation returns to its original position. However, this is not the case, depending on the circle of latitude the pendulum lags behind the rotation and after twenty-four hours there will be an angle difference, a *holonomy*, with respect to its original oscillation plane accounting for the curved geometry of the earth. The underlying geometry of an experiment has an influence on the measured results. The possible oscillation states of the pendulum have to reflect the curvature, an evolution from one state to another gives rise to an observable holonomy. Moreover, the angle difference is the same irrespective of how fast the rotation is - a pendulum placed on Neptune exhibits the same angle difference although one Neptune day is only about 16 hours.

What is the connection to the geometric phase and in the following to neutron interferometry? Well, what can be learnt from the pendulum is that the subjacent state space must not be neglected. The same is valid in quantum mechanics, where the states of a quantum system are "living" in a complex vector space, the *Hilbert space*, and it is the phase of a state that mirrors the geometry of the system's Hilbert space. Probably the most famous effect based on the topology of the state space is the Aharonov-Bohm effect [AB59], where the transport of a charged particle around, but not through, a magnetic field region affects the phase of the state, although there is no interaction. Earlier, Pancharatnam [Pan56] investigated the phase change of light when changing its polarisation by use of filters. The phase change is based on the spherical shape of the polarisation state space. The catalyst for a vast number of investigations in the geometry of state space was finally a seminal paper by Berry [Ber84] in 1984 demonstrating that the adiabatic and cyclic transport of a quantum mechanical system involves a phase contribution to the final state that is neither dependent on the evolution time from the initial to the final state nor on the energies involved. A simple example is the spin of a neutron subjected to a magnetic field which slowly changes its direction. The spin follows the motion of the field. If the initial spin is parallel to the magnetic field and the evolution is cyclic the final state has picked up a phase factor. The accumulated phase along the path of the state can be separated into one term which depends on the energy-splitting associated with the magnitude of the magnetic field, the dynamical phase, and a second term that depends on the geometry of the Hilbert space representing the spin degree of freedom.

Fortunately, in this simple case the state space is equivalent to a sphere and analogous to Foucault's pendulum the geometric phase difference is due to the curvature of the sphere and proportional to the area enclosed by the path of the spin state.

In Chapter 1 the notion of Berry's phase factor along with some extensions to more general evolutions will be discussed. For example, the restriction to adiabatic motion has been released soon after [AA87], followed by the extension to non-cyclic paths [SB88]. That the notion of the geometric phase is not connected to any dynamics at all becomes explicit in a kinematic theory [MS93] relating the geometric phase to geodesic lines connecting quantum states.

In view of realistic models of Nature an entirely pure state description of quantum systems seems inappropriate. Quantum systems interacting with the environment tend to dissipate energy, exchange phase information and are found finally in mixed states. Therefore, a definition of a general geometric phase for mixed state and non-unitary evolutions is expedient. In Chapter 2 the notion of mixed states is introduced and two possible ways towards a geometric phase associated to the paths of mixed state are presented - first, an operationally intuitive definition via interference of states [SPE<sup>+</sup>00] and secondly, a mathematically appealing approach by representing mixed states as pure state vectors in a larger Hilbert space [Uhl86].

The question arises whether the geometric phase can be measured for all possible paths. Do particular evolutions exist where nothing can be said about the subjacent geometry? For pure states such a situation is encountered if initial and final state are orthogonal [MP00] and one has to resort to the off-diagonal geometric phase. This concept is generalised to mixed states for the interferometric definition of the mixed state geometric phase [FS03b, FS03a, SF03] as well as for purification alternative [FS05] in Chapter 3.

The canonical example of a geometric phase is definitely the spin-1/2 particle like a neutron in a magnetic field. In Chapter 4, it is shown that not only the neutrons' spin can be used to play with geometric phases, but also the two possible ways through an interferometer give rise to a non-trivial spatial state space of the neutron and, consequently, to a geometric phase connected to the spatial degree of freedom. An experiment on a cyclic evolution [HZR96] provided first evidence of the spatial geometric phase. For the recent experiment [FHLR05b, FHLR05a] the theory has been refined to fully explain non-cyclic paths in order to refute the criticism on the previous [Wag99]. The paths on the Bloch sphere, the belonging state space, have been devised in order to obtain analytic results purely from geometric considerations. These are compared with the measured data and are found to be fully coherent, so that one can disprove any critical voices with a clear conscience.

Finally, the attention is turned back again to the geometric phase in connection with open quantum systems in Chapter 5. It is widely believed that the power of the geometric phase lies in its robustness with respect to environmental influences and a multitude of studies support or refute such claims. However, to the best of my knowledge no experiments on this issue have been performed yet. I will focus particularly on the effects of perturbations in the magnetic field driving adiabatically the spin of a neutron. The perturbations induce a

statistical spread of the geometric phase, the boundary of the surface area enclosed by the perturbed path looks frayed. Most interestingly, for long evolution times the uncertainty in the geometric phase tends to zero. Besides numerical studies in order to estimate a set of feasible parameters for a subsequent experimental realisation, details of a possible measurement scheme involving ultra-cold neutrons are presented. Such neutrons are slow enough to trap them in an appropriate storage vessel and when applying magnetic fields their spin polarisation can be manipulated.

As for the notation a list of symbols used for parameters and variables can be found in the Appendix E.



# Chapter 1

## Geometric Phase - Introduction

In this section an overview on the *geometric phase* business in general is given. First, we consider a mathematical analogue from spherical geometry to catch a glimpse on the importance of a curved state space, then we move on to Berry's seminal paper [Ber84] about a *quantum phase* "accompanying adiabatic changes" of a system. This is - as it turned out later - only a special case of more general concepts. Simon [Sim83] immediately realised the link between Berry's phase factor and geometry in terms of fibre bundle (gauge) theory, viz. that Berry's phase is a holonomy invariant associated with a particular connection in a line bundle over the parameter space. Wilczek and Zee considered non-abelian holonomy invariants for Hamiltonians with degenerate eigenvalue spectrum, still for cyclic adiabatic processes. Aharonov and Anandan [AA87] relaxed the condition of adiabaticity and Samuel and Bhandari [SB88] formulated the geometric phase for even more general non-cyclic evolutions bringing in Pancharatnam's ideas from the 1950's [Pan56]. Without resorting to any particular dynamics of the system Mukunda and Simon [MS93] formulated the geometric phase in a quantum kinematic picture. To give a conceptual overview a sketch of some of these papers is presented in the following and at the end some experiments on the geometric phase are mentioned.

### 1.1 Mathematical analogue

Let us first consider an example of elementary geometry analogous to the *geometric phase* to clarify what we are talking about. Take a sphere and mount a vector onto some point on the sphere pointing in an arbitrary direction and transport this vector along a geodesic line to the equator, then along the equator and back on a geodesic to the original point (see Figure 1.1). During this transport the vector has to stay tangential to the (curved) surface all the time, it must not change its magnitude and the angle between the vector and the (geodesic) path must not change, so that there is no rotation about the instantaneous normal to the surface. This transport is called a *parallel transport*. After completing the closed path (i. e. the loop) we notice that the vector has changed its direction compared to the initial one by an angle  $\varphi$  although we thoroughly paid attention to keep it parallel. Thus, we obtained a so called

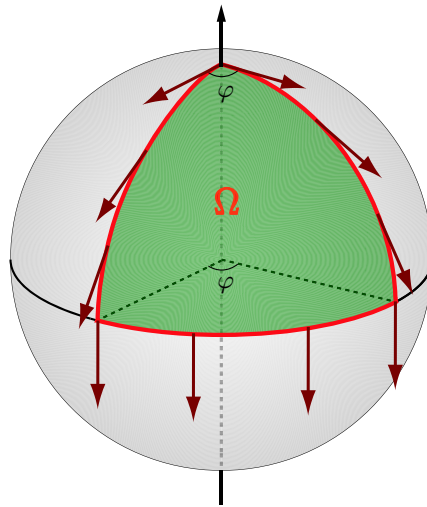


Figure 1.1: Parallel transport of a vector on a sphere

*holonomy* distinguishing the vector before and after the transport only due to the curvature of the sphere. This angle  $\varphi$  equals the solid angle  $\Omega$  enclosed by the loop,  $\Omega = 2\pi \frac{\varphi}{2\pi} = \varphi$ , where  $2\pi$  is the solid angle of a half-sphere and by multiplication with  $\frac{\varphi}{2\pi}$  we get the portion surrounded by the loop.

This concept can be generalised to any surface using a proper definition of the parallel transport. By dealing with such a surface (mostly referred to as a *manifold* to ensure that it is smooth and one can define differentiable coordinate patches [Ber96, CBDMDB77]) with intrinsic curvature we get a holonomy after a transport of a vector around a loop. If the surface is flat the vector points in the same direction after a closed path.

Another illustrative example is a path on a cone. A cone can be formed by taking a piece of paper shaped like a sector of a circle and joining the paper at its edges. During this process the paper is neither stretched nor compressed and, consequently, the cone has no intrinsic curvature except at its vertex (which can be smoothed out so that the curvature is finite everywhere). Therefore, a vector transported along a path not enclosing the vertex acquires no holonomy, there is no difference to a parallel transport on a flat surface. But a vector  $\vec{V}$  parallel-transported around a closed curve to  $\vec{V}'$  enclosing the vertex undergoes a rotation (Figure 1.2). This is in fact the geometry responsible for the *Aharonov-Bohm* effect, “the curvature at the vertex can be regarded as analogous to the magnetic field within the cylinder in the Aharonov-Bohm experiment [AB59], while the zero intrinsic curvature everywhere else corresponds to the vanishing of the magnetic field outside the cylinder.” [Ana92]

## 1.2 Berry’s phase and generalisations

In 1984 Berry published a paper entitled “*Quantal phase factors accompanying adiabatic changes*” [Ber84] describing the geometric phase factor acquired by (slowly) transporting a

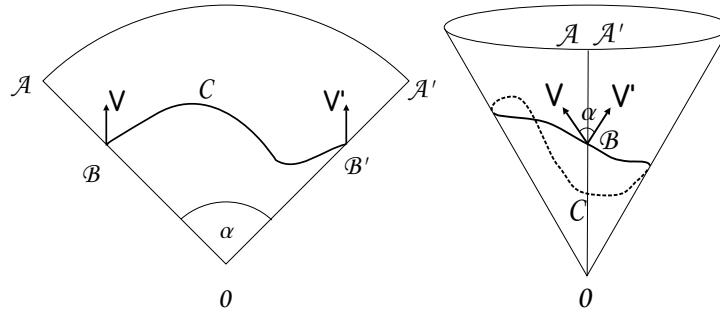


Figure 1.2: Parallel transport on a cone

quantum system governed by the Hamiltonian  $H(\vec{R})$  round a circuit by varying its parameters  $\vec{R}$ . This phase is non-integrable, because it depends directly on the path connecting the endpoints of the evolution.

### 1.2.1 Derivation of Berry's phase

The parameters  $\vec{R}$  of the Hamiltonian  $H(\vec{R})$  should change slowly in time so that the adiabatic theorem holds [Mes62]. Then the system will remain in an eigenstate of  $H(\vec{R}(t))$  at any time  $t$ , if the system is initially in an eigenstate of  $H$ . If the evolution is cyclic ( $\vec{R}(0) = \vec{R}(T)$ ) the Hamiltonian takes on its original form at the final time  $T$  and the system returns to its initial state. The state has been transported around a loop  $C : t \in [0, T] \mapsto |\psi(t)\rangle$  in parameter space with  $|\psi(t)\rangle$  denoting the instantaneous state of the system, which is equivalent to the eigenstate  $|n(\vec{R}(t))\rangle$  of the instantaneous Hamiltonian (Figure 1.3) defined by  $H(\vec{R}(t))|n(\vec{R}(t))\rangle = E_n(t)|n(\vec{R}(t))\rangle$ .  $E_n(t)$  denotes the energy of the  $n$ -th eigenstate.

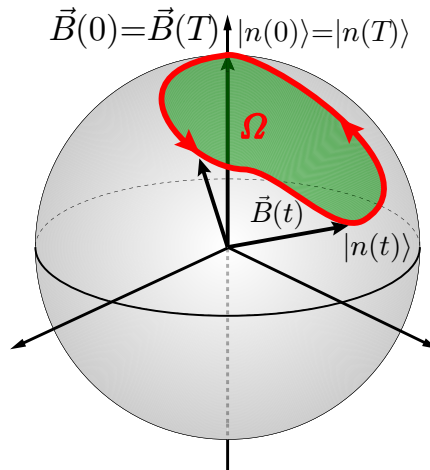


Figure 1.3: The curve  $C$  traced out on the sphere ( $S^2$ ) encloses the solid angle  $\Omega$  which is proportional to the geometric phase. The parameter space  $S^2$  of the magnetic field coincides with the state space of a spin-1/2 particle, if the magnitude of the magnetic field is kept fixed.

In detail, the evolution of the system's state vector  $|\psi(t)\rangle$  is given by the Schrödinger

equation

$$H(\vec{R}(t))|\psi(t)\rangle = i\hbar \frac{d}{dt}|\psi(t)\rangle. \quad (1.2.1)$$

Let the initial state  $|\psi(0)\rangle = |n(\vec{R}(0))\rangle$  be an eigenstate of  $H(\vec{R})$  at time  $t = 0$ . Assuming adiabatic evolution the solution of this equation at time  $t$  reads

$$|\psi(t)\rangle = e^{i\Phi(t)}|n(\vec{R}(t))\rangle, \quad (1.2.2)$$

To determine  $\Phi(t)$  we insert (1.2.2) into equation (1.2.1), obtaining

$$-i\hbar \left( i\dot{\Phi}(t)e^{i\Phi(t)}|n(\vec{R}(t))\rangle + e^{i\Phi(t)}|\dot{n}(\vec{R}(t))\rangle \right) = e^{i\Phi(t)}E_n(\vec{R}(t))|n(\vec{R}(t))\rangle, \quad (1.2.3)$$

where a dot denotes the time derivative. Multiplying  $\langle n(\vec{R}(t))|e^{-i\Phi(t)}$  from the left yields

$$\begin{aligned} -\hbar\dot{\Phi}(t) + i\hbar\langle n(\vec{R}(t))|\dot{n}(\vec{R}(t))\rangle &= E_n(\vec{R}(t)) \\ \Rightarrow \dot{\Phi}(t) &= -\frac{1}{\hbar}E_n(\vec{R}(t)) + i\langle n(\vec{R}(t))|\dot{n}(\vec{R}(t))\rangle. \end{aligned} \quad (1.2.4)$$

This equation has to be integrated from  $t = 0$  to the final time  $t = T$  (setting  $\Phi(0) = 0$ ),

$$\Phi(T) = -\frac{1}{\hbar} \int_0^T E_n(\vec{R}(t))dt + i \int_0^T \langle n(\vec{R}(t))|\frac{d}{dt}|n(\vec{R}(t))\rangle dt.$$

We see that the last term does not depend explicitly on the time parameter and the chain rule can be applied,

$$\langle n(\vec{R}(t))|\frac{d}{dt}|n(\vec{R}(t))\rangle = \frac{d\vec{R}(t)}{dt} \cdot \langle n(\vec{R})|\vec{\nabla}_{\vec{R}}|n(\vec{R})\rangle,$$

to find

$$\Phi(T) = -\frac{1}{\hbar} \int_0^T E_n(\vec{R}(t))dt + i \oint_{\mathcal{C}} d\vec{R} \cdot \langle n(\vec{R})|\vec{\nabla}_{\vec{R}}|n(\vec{R})\rangle \quad (1.2.5)$$

for a closed path  $\mathcal{C}$  in the parameter space with the choice  $|n(\vec{R}(T))\rangle = |n(\vec{R}(0))\rangle$ . The first term corresponds to the usual expression of the phase accumulated by a system in a state with energy  $E(t)$  for a time  $T$ , the *dynamical phase*

$$\phi_d \equiv -\frac{1}{\hbar} \int_0^T E_n(\vec{R}(t))dt. \quad (1.2.6)$$

The *geometric phase* is defined by the additional second term

$$\phi_g(\mathcal{C}) \equiv i \oint_{\mathcal{C}} d\vec{R} \cdot \langle n(\vec{R})|\vec{\nabla}_{\vec{R}}|n(\vec{R})\rangle, \quad (1.2.7)$$

an integral in parameter space independent of the rate at which the loop  $\mathcal{C}$  is traversed and independent of the energy. That  $\phi_g$  is reparametrisation invariant (independent of the rate of

traversal) can be seen by substituting  $t \mapsto \tau(t)$  and  $dt \mapsto \frac{d\tau}{dt}d\tau$ ,

$$\begin{aligned}\phi_g &= i \int_{t_1}^{t_2} \langle n(\vec{R}(t)) | \frac{d}{dt} | n(\vec{R}(t)) \rangle dt = i \int_{\tau(t_1)}^{\tau(t_2)} \langle n(\vec{R}(\tau)) | \frac{d\tau}{dt} \frac{d}{d\tau} | n(\vec{R}(\tau)) \rangle \frac{dt}{d\tau} d\tau \\ &= i \int_{\tau(t_1)}^{\tau(t_2)} \langle n(\vec{R}(\tau)) | \frac{d}{d\tau} | n(\vec{R}(\tau)) \rangle d\tau = \phi_g\end{aligned}\quad (1.2.8)$$

for equal initial and final time  $\tau(t_1) = t_1$  and  $\tau(t_2) = t_2$ .

Normalisation guarantees that  $\phi_g(\mathcal{C})$  is purely imaginary: From  $\langle n(s) | n(s) \rangle = 1$  (while simplifying the notation by skipping the  $\vec{R}$  dependence of  $|n\rangle$ ) it follows that  $\frac{d}{ds} (\langle n(s) | n(s) \rangle) = 0$  and consequently

$$\langle \dot{n}(s) | n(s) \rangle = -\langle n(s) | \dot{n}(s) \rangle = -(\langle \dot{n}(s) | n(s) \rangle)^*.$$

Hence,

$$\text{Re} \langle n(s) | \dot{n}(s) \rangle = 0 \quad (1.2.9)$$

and  $\phi_g = i \oint_{\mathcal{C}} \langle n(s) | \dot{n}(s) \rangle$  is purely imaginary.

It is also gauge invariant, i. e. by choosing a different phase of the eigenvectors  $|n(t)\rangle$   $\phi_g$  does not change. If this would be the case, this quantity would not be physical since the choice of the phase of the eigenvectors is arbitrary for each instant of time. To proof this proposition we have a look at the geometric phase after the gauge transformation  $|n(t)\rangle \mapsto |n'(t)\rangle = e^{i\alpha(t)} |n(t)\rangle$ :

$$\begin{aligned}\phi'_g &= i \int dt \langle n'(t) | \dot{n}'(t) \rangle = i \int dt \langle n(t) | e^{-i\alpha(t)} \frac{d}{dt} (e^{i\alpha(t)} |n(t)\rangle) \\ &= i \int dt (\langle n(t) | \dot{n}(t) \rangle + i\dot{\alpha}(t)) = \phi_g - \int_0^T \dot{\alpha}(t) dt.\end{aligned}\quad (1.2.10)$$

When choosing single valued eigenvalue bases the initial and final eigenstates can differ only by a phase of integer multiples of  $2\pi$ ,  $|n'(0)\rangle = e^{in2\pi} |n'(T)\rangle$  (and same for the unprimed eigenstates  $|n(t)\rangle$ ). Therefore,  $\alpha(T) - \alpha(0) = \int_0^T \dot{\alpha}(t) dt = 2n\pi$  and  $\phi'_g = \phi_g$  modulo  $2\pi$ .

**Transformation to a surface integral** For simpler evaluation of  $\phi_g$  the circuit integral can be transformed into a surface integral over the surface in parameter space whose boundary is  $\mathcal{C}$ . This can easily be done in a 3-dimensional parameter space using *Stokes' theorem*, for higher dimensions the theory of differential forms [Nak03] has to be applied by transforming (1.2.7) into the integral of a 2-form over the surface  $\mathcal{F}$  bounded by  $\mathcal{C}$  ( $\mathcal{C} = \partial\mathcal{F}$ ). In three dimensions we get by using vector calculus and decomposing  $|\vec{\nabla}n\rangle$  into the basis states  $|m\rangle$

$$\begin{aligned}\phi_g(\mathcal{C}) &= i \int_{\mathcal{F}} d\vec{S} \cdot \vec{\nabla} \times \langle n | \vec{\nabla} n \rangle = i \int_{\mathcal{F}} d\vec{S} \cdot \langle \vec{\nabla} n | \times | \vec{\nabla} n \rangle \\ &= i \int_{\mathcal{F}} d\vec{S} \cdot \sum_{m \neq n} \langle \vec{\nabla} n | m \rangle \times \langle m | \vec{\nabla} n \rangle,\end{aligned}\quad (1.2.11)$$

whereas  $d\vec{S}$  denotes the area element in parameter space and the restriction  $n \neq m$  in the sum is justified, because  $\langle n|\vec{\nabla}n\rangle$  is purely imaginary. Therefore the product  $\langle \vec{\nabla}n|n\rangle \times \langle n|\vec{\nabla}n\rangle$  is purely real and must therefore vanish since it would contribute to a real part in the geometric phase which we have already excluded above. To calculate the other elements in the sum we use

$$\begin{aligned}\vec{\nabla}(H|n\rangle) &= (\vec{\nabla}H)|n\rangle + H|\vec{\nabla}n\rangle = (\vec{\nabla}E_n)|n\rangle + E_n|\vec{\nabla}n\rangle \\ \langle m|\vec{\nabla}H|n\rangle &= E_n\langle m|\vec{\nabla}n\rangle - \langle m|H|\vec{\nabla}n\rangle = (E_n - E_m)\langle m|\vec{\nabla}n\rangle\end{aligned}$$

which finally yields

$$\langle m|\vec{\nabla}n\rangle = \langle m|\vec{\nabla}H|n\rangle / (E_n - E_m). \quad (1.2.12)$$

Thus, we have calculated *Berry's phase*  $\phi_g$  as

$$\phi_g = - \int_{\mathcal{F}} d\vec{S} \cdot \vec{V}_n(\vec{R}), \quad (1.2.13)$$

with

$$\vec{V}_n(\vec{R}) = \text{Im} \sum_{m \neq n} \frac{\langle n(\vec{R})|\vec{\nabla}H(\vec{R})|m(\vec{R})\rangle \times \langle m(\vec{R})|\vec{\nabla}H(\vec{R})|n(\vec{R})\rangle}{(E_m(\vec{R}) - E_n(\vec{R}))^2}. \quad (1.2.14)$$

### Example - Neutron in a magnetic field

To illustrate this idea, we consider a neutron with spin angular momentum  $S = \frac{\hbar}{2}$  in a magnetic field  $\vec{B}$  with magnitude  $B \equiv |\vec{B}|$ . A spin-1/2 state is commonly represented by a complex vector in a two dimensional Hilbert space. The basis states are commonly denoted by either  $\{|\uparrow\rangle, |\downarrow\rangle\}$ ,  $\{|z+\rangle, |z-\rangle\}$  or  $\{|0\rangle, |1\rangle\}$  as eigenvectors of the Pauli matrix  $\sigma_z$  to the eigenvalues  $+1$  and  $-1$ . In the following either one of these notations will be used alternatively. The Pauli spin matrices  $\{\sigma_x, \sigma_y, \sigma_z\}$  along with the identity constitute a complete set of generators of the unitary group  $U(2)$ , i. e. each unitary operator acting on the spin states can be decomposed in terms of these basis operators. They satisfy the identities

$$\sigma_i \sigma_j = \delta_{ij} + i\epsilon_{ijk} \sigma_k \quad (1.2.15)$$

$$\sigma_i \sigma_j + \sigma_j \sigma_i = 2\delta_{ij} \quad (1.2.16)$$

and have the matrix representation

$$\sigma_x = \begin{pmatrix} 0 & 1 \\ 1 & 0 \end{pmatrix}, \quad \sigma_y = \begin{pmatrix} 0 & i \\ i & 0 \end{pmatrix}, \quad \text{and } \sigma_z = \begin{pmatrix} 1 & 0 \\ 0 & -1 \end{pmatrix}. \quad (1.2.17)$$

An arbitrary spin state can be parametrised in terms of the polar and azimuthal angle  $\theta$  and  $\phi$ , respectively,

$$|\psi\rangle = \cos \frac{\theta}{2} |\uparrow\rangle + \sin \frac{\theta}{2} |\downarrow\rangle = \begin{pmatrix} \cos \frac{\theta}{2} \\ e^{i\phi} \sin \frac{\theta}{2} \end{pmatrix}, \quad (1.2.18)$$

which is already normalised. This parametrisation suggests the visualisation of a spin state on a 2-sphere known as *Bloch sphere* or *Poincaré sphere*<sup>1</sup> (Figure 1.4).

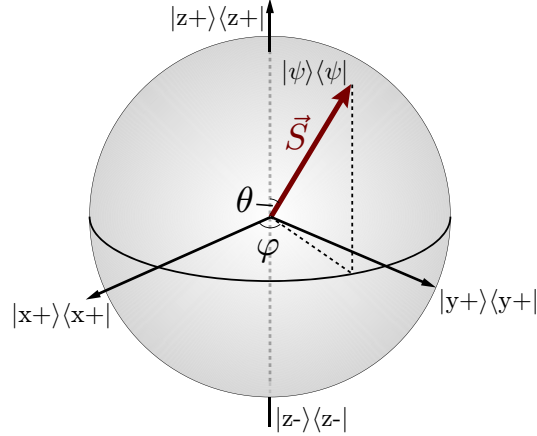


Figure 1.4: Bloch-sphere representation of a spin-1/2 state  $|\psi\rangle = \cos\theta/2|z+\rangle + e^{i\phi}\sin\theta/2|z-\rangle$  by the polar angle  $\theta$  and the azimuthal angle  $\phi$ .

The polarisation vector  $\vec{S}$  can be obtained by calculating the expectation values of the Pauli matrices

$$\vec{S} = \begin{pmatrix} \text{Tr}[\sigma_x|\psi\rangle\langle\psi|] \\ \text{Tr}[\sigma_y|\psi\rangle\langle\psi|] \\ \text{Tr}[\sigma_z|\psi\rangle\langle\psi|] \end{pmatrix} = \begin{pmatrix} \sin\theta\cos\phi \\ \sin\theta\sin\phi \\ \cos\theta \end{pmatrix} \quad (1.2.19)$$

The Hamiltonian of the magnetic field is given by

$$H_{mag}(t) = -\vec{\mu}_n \cdot \vec{B}(t), \quad (1.2.20)$$

where  $\vec{\mu}_n = \mu_n\vec{\sigma}$  denotes the magnetic moment of the neutron  $\mu_n = -9.66 \times 10^{-27} J/T$ .

In the simplest case,  $H_{mag}$  is static and for further convenience let the direction of the magnetic field determine the quantisation axis,

$$H_{mag} = -\mu_n B \sigma_z. \quad (1.2.21)$$

A neutron initially in the eigenstate  $|\psi(0)\rangle = |z+\rangle$  evolves according to the Schrödinger equation and we find the state at a later time

$$|\psi(t)\rangle = e^{-i\frac{Ht}{\hbar}} |\psi(0)\rangle. \quad (1.2.22)$$

---

<sup>1</sup>‘Poincaré sphere’ is usually used for the representation of light polarisation, but since the representation is same for both these expressions can be used alternatively.

Utilising the Euler identity  $e^{iA} = \cos A + i \sin A$  for the exponential we get

$$e^{-i\frac{Ht}{\hbar}} = e^{i\frac{\mu_n B_z \sigma_z}{\hbar} t} = \cos\left(\frac{\omega_L t}{2} \sigma_z\right) + i \sin\left(\frac{\omega_L t}{2} \sigma_z\right), \quad (1.2.23)$$

where we have defined the *Larmor frequency*

$$\omega_L \equiv \frac{2\mu_n B}{\hbar} \quad (1.2.24)$$

The property  $\sigma_z^2 = \mathbb{1}$  makes life particularly simple since the series expansion of the cosine contains only even powers of the  $\sigma_z$  and the sinus only odd powers, so that we end up with

$$e^{-i\frac{Ht}{\hbar}} = \cos\left(\frac{\omega_L t}{2}\right) + i\sigma_z \sin\left(\frac{\omega_L t}{2}\right) = \begin{pmatrix} e^{i\frac{\omega_L t}{2}} & 0 \\ 0 & e^{-i\frac{\omega_L t}{2}} \end{pmatrix}. \quad (1.2.25)$$

and the final state

$$|\psi(T)\rangle = e^{i\frac{\omega_L T}{2}} |z+\rangle. \quad (1.2.26)$$

The phase factor  $e^{i\frac{\omega_L t}{2}}$  is just the dynamical phase proportional to the Zeeman energy splitting  $\Delta E = \hbar\omega_L$  and the time  $t$ . Since the Hamiltonian did not vary in time there is no geometric phase ( $d/dt|n(t)\rangle = 0$ ).

In contrast, for a slow change of the Hamilton operator (adiabatic evolution) the neutron spin direction will be pinned to the direction of the magnetic field  $\vec{B}(t)$  at any time and will acquire in addition a geometric (Berry) phase  $\phi_g$  independent of the Larmor frequency  $\omega_L$  and time. Let us parametrise the direction of the field by the spherical coordinates  $\theta$  and  $\phi$ ,

$$\vec{B}(t) = B\vec{n}(t), \quad \vec{n}(t) = \begin{pmatrix} \cos\phi(t) \sin\theta(t) \\ \sin\phi(t) \sin\theta(t) \\ \cos\theta(t) \end{pmatrix}.$$

The eigenvectors to the Hamiltonian  $H = -\mu_n B \vec{n}(t) \cdot \vec{\sigma}$  are given by

$$|\psi_{\uparrow}(\theta, \phi)\rangle = \begin{pmatrix} \cos\frac{\theta(t)}{2} \\ e^{i\phi(t)} \sin\frac{\theta(t)}{2} \end{pmatrix} \quad \text{and} \quad |\psi_{\downarrow}(\theta, \phi)\rangle = \begin{pmatrix} \sin\frac{\theta(t)}{2} \\ -e^{i\phi} \cos\frac{\theta(t)}{2} \end{pmatrix}. \quad (1.2.27)$$

To find for instance the geometric phase  $\phi_g^{\uparrow}$  associated to the spin-up state we have to calculate the terms in Eq. (1.2.7),

$$\begin{aligned} \langle \psi_{\uparrow} | \frac{\partial}{\partial \theta} | \psi_{\uparrow} \rangle &= 0, \\ \langle \psi_{\uparrow} | \frac{\partial}{\partial \phi} | \psi_{\uparrow} \rangle &= \frac{i}{2} (1 - \cos\theta(t)). \end{aligned}$$

For the sake of simplicity we choose constant  $\theta$ , i. e. an evolution along a circle of latitude

and obtain Berry's phase by integrating

$$\phi_g^\uparrow = i \int_0^{2\pi} \frac{i}{2} (1 - \cos \theta(t)) d\phi = -\pi(1 - \cos \theta).$$

We notice that  $\phi_g$  is proportional to the solid angle  $\Omega$  enclosed by the path,  $\phi_g^\uparrow = -\Omega/2$ . For example, if  $\theta = \pi/2$ , a walk along the equatorial line,  $\phi_g^\uparrow = -\pi$  and the encompassed solid angle as seen from the degeneracy point  $\vec{B} = 0$  is half of the sphere  $\Omega = 2\pi$ . Such a rotation of  $\vec{B}$  produces a sign change ( $\phi_g = \pi$ ) of the fermionic wave function, which is equivalent to the sign change of spinors undergoing a  $SU(2)$  rotation.

The crucial point is that the magnetic field has a singularity at  $B = 0$  which is encircled by the path of the state. This gives rise to a non-trivial topology of the parameter space and enables the appearance of a geometric phase.

### 1.2.2 Non-adiabatic evolution

Aharonov and Anandan [AA87] generalised the Berry's phase by considering not only adiabatic but any cyclic evolution of a quantum system. Starting from the Schrödinger equation

$$H(t)|\psi(t)\rangle = i\hbar \frac{d}{dt} |\psi(t)\rangle \quad (1.2.28)$$

the normalised initial state  $|\psi(0)\rangle \in \mathcal{N}_0$  evolves to the final state  $|\psi(T)\rangle \in \mathcal{N}_0$  such that

$$|\psi(T)\rangle = e^{i\Phi} |\psi(0)\rangle, \quad \Phi \text{ real.} \quad (1.2.29)$$

$\mathcal{N}_0$  stands for the set of normalised non-zero states in  $\mathcal{H}$ ,  $\mathcal{N}_0 = \{|\psi\rangle \in \mathcal{H} \mid \langle\psi|\psi\rangle = 1\}$ . The point is that the system does in this general setting not stay in an eigenstate of the Hamiltonian and the geometric phase cannot be associated to the parameter space of the Hamilton operator's parameters. The focus is shifted towards state space that does not coincide anymore with parameter space as in the adiabatic case.

In order to obtain a notion of the geometric phase the *ray space* or *projective Hilbert space* has to be introduced. It is a general property of quantum mechanical states that these are only defined modulo a  $U(1)$  phase factor without physical relevance. All states that differ merely by a phase factor give rise to the same physics. One might argue then that the discussion about the geometric phase is immaterial from this point of view, but a relative phase difference between two states in superposition,  $|\Psi\rangle = |\psi\rangle + e^{i\Phi} |\psi'\rangle$  gives a different state. It is only a global phase which can be neglected, i. e.  $|\Psi\rangle$  and in  $e^{i\beta} |\Psi\rangle$  are equivalent. The projective Hilbert space comprises all states in  $\mathcal{N}_0$  where the states differing only by a phase factor are identified. This is denoted by  $\mathcal{P} = \mathcal{N}_0 / \sim$ , where  $\sim$  is an equivalence relation. The projection map

$$\pi : \mathcal{N}_0 \rightarrow \mathcal{P} \quad (1.2.30)$$

maps all vectors in  $\mathcal{N}_0$  to the projective Hilbert space  $\mathcal{P}$ . An equivalence class of states in

ray space is denoted by

$$P_\psi \equiv |\psi\rangle\langle\psi|, \quad (1.2.31)$$

which is equally well a projection operator to the equivalence class represented by  $|\psi\rangle$ . A path  $\mathcal{C}$  traced out by  $|\psi(t)\rangle$  satisfying (1.2.29) is therefore projected to a closed curve  $\tilde{\mathcal{C}}$  in  $\mathcal{P}$ , as  $|\psi(0)\rangle$  and  $|\psi(T)\rangle$  represent the same point in  $\mathcal{P}$ ,  $P_\psi(T) = e^{i\Phi}|\psi(0)\rangle\langle\psi(0)|e^{-i\Phi} = |\psi(0)\rangle\langle\psi(0)| = P_\psi(0)$ . For a geometrical interpretation see Figure (1.5).

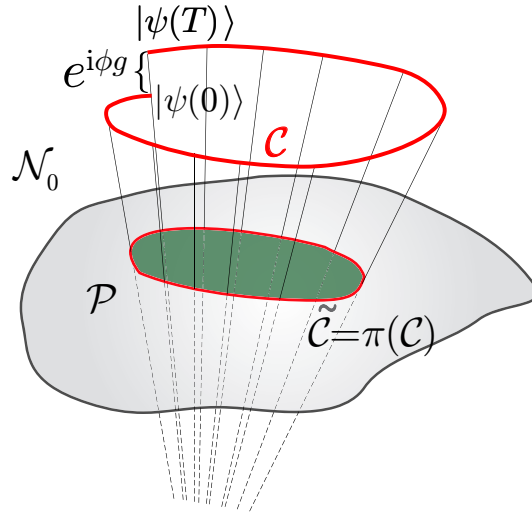


Figure 1.5: Projective Hilbert space (ray space) of  $\mathcal{N}_0$ . The rays denote states differing only by a U(1) phase factor.

We now have the freedom to add additional phases at any point along the curve without changing the curve in projective Hilbert space. If we define a state  $|\phi(t)\rangle \in \mathcal{N}_0$  such that

$$|\phi(t)\rangle = e^{-if(t)}|\psi(t)\rangle \quad \text{and} \quad f(T) - f(0) = \Phi, \quad (1.2.32)$$

it follows from equation (1.2.29) that  $|\phi(T)\rangle = |\phi(0)\rangle$  and from (1.2.28) that

$$\frac{df}{dt} = -\frac{1}{\hbar}\langle\psi(t)|H|\psi(t)\rangle + i\langle\phi(t)|\frac{d}{dt}|\phi(t)\rangle. \quad (1.2.33)$$

Having Figure (1.5) in mind, we can look at the curve traced out by  $|\phi(t)\rangle$  as another Hilbert space representative of the curve  $\tilde{\mathcal{C}} \in \mathcal{P}$ , thus the “shadows” of the curves traced out by  $|\psi(t)\rangle$  and  $|\phi(t)\rangle$  are the same. Indeed, we have the choice among many different curves in  $\mathcal{N}_0$  projecting to the same curve  $\tilde{\mathcal{C}} \in \mathcal{P}$  under the map defined in (1.2.30). The special choice (1.2.32) for  $f(t)$  has the advantage that the final phase difference  $\Phi$  is split into a dynamical and a geometrical part. Integration of Eq. (1.2.33) in the interval  $t \in [0, T]$  results in

$$f(T) - f(0) = -\frac{1}{\hbar} \int_0^T \langle\psi(t)|H|\psi(t)\rangle dt + i \int_0^T \langle\phi(t)|\frac{d}{dt}|\phi(t)\rangle dt = \Phi, \quad (1.2.34)$$

where the dynamical part is given by the first term  $-\frac{1}{\hbar} \int_0^T dt \langle\psi(t)|H|\psi(t)\rangle$  and the geometric

phase  $\phi_g$  stems from the second term in (1.2.34) and can be defined as

$$\phi_g \equiv \Phi + \frac{1}{\hbar} \int_0^T \langle \psi(t) | H | \psi(t) \rangle dt = i \int_0^T \langle \phi(t) | \frac{d}{dt} | \phi(t) \rangle dt. \quad (1.2.35)$$

As there are many curves  $\mathcal{C}_j$  in  $\mathcal{H}$  projecting to the same  $\tilde{\mathcal{C}} \in \mathcal{P}$  that are generated by different Hamiltonians  $H_j$  and because we can find the same  $|\phi(t)\rangle$  for each  $H_j$  by an appropriate choice of  $f(t)$ , the phase factor  $e^{i\phi_g}$  is independent of  $H$  for a given closed curve  $\tilde{\mathcal{C}} \in \mathcal{P}$ .  $\phi_g$  is furthermore independent of the choice of the parameter  $t$  (reparametrisation invariance) and is uniquely defined up to  $2\pi n$ ,  $n$  integer. In fact, consider two curves  $\mathcal{C}', \mathcal{C}'' \in \mathcal{N}_0$  with the same image  $\tilde{\mathcal{C}} \in \mathcal{P}$  traced out by the corresponding state vectors  $|\psi'(t)\rangle, |\psi''(t)\rangle \in \mathcal{N}_0$  related via  $|\psi''(t)\rangle = e^{-i\alpha(t)} |\psi'(t)\rangle$  with  $\alpha(T) - \alpha(0) = 2\pi n$ . They share the same geometric phase factor  $e^{i\phi_g}$  due to

$$\begin{aligned} \phi_g &= i \int_0^T \langle \psi''(t) | \frac{d}{dt} | \psi''(t) \rangle dt = i \int_0^T \left( -i\dot{\alpha}(t) + \langle \psi'(t) | \frac{d}{dt} | \psi'(t) \rangle \right) dt \\ &= 2\pi n + i \int_0^T \langle \psi'(t) | \frac{d}{dt} | \psi'(t) \rangle dt. \end{aligned} \quad (1.2.36)$$

Hence all curves in  $\mathcal{N}_0$  that project to the same (closed) curve in  $\mathcal{P}$  have the same geometric phase modulo  $2\pi$ . Consequently,  $\phi_g$  is only dependent upon the geometry of the curve  $\tilde{\mathcal{C}} \in \mathcal{P}$ . The geometric phase is a property of ray space only.

### 1.2.3 Non-cyclic and non-adiabatic evolution

Until now, the curves in the projective Hilbert space  $\mathcal{P}$  have still to be closed in order find a well-defined relative phase between initial and final state,  $\Phi \equiv \arg \langle \psi(T) | \psi(0) \rangle$ . For the further generalisation to open curves in  $\mathcal{P}$  it is necessary to find a way to compare the phases between two non-equivalent states, states that do not live on the same ray when referring to Figure 1.5. Samuel and Bhandari [SB88] based their investigations on the work of Pancharatnam [Pan56, Sjö02] on the interference of polarised light and generalised *Berry's phase* to a non-cyclic and even non-unitary evolution of a quantum system.

#### Pancharatnam's phase difference

Take two (normalised) state vectors  $|A\rangle$  and  $|B\rangle$  (either polarisation states of light as considered by Pancharatnam or state vectors representing a quantum system) and let them interfere. Then it is quite natural to ask about their relative phase. If

$$|A\rangle = e^{i\Phi} |B\rangle, \quad (1.2.37)$$

thus if  $|A\rangle$  and  $|B\rangle$  describe the same quantum/polarisation state, this phase is obviously  $\Phi$ .

But what to do if  $|A\rangle \neq e^{i\Phi} |B\rangle$ ? In this case we can nevertheless set up an interferometry

experiment [WRFI98] to measure the intensity of the interference between  $|A\rangle$  and  $|B\rangle$

$$I = |e^{i\chi}|A\rangle + |B\rangle|^2 = 2 + 2|\langle A|B\rangle| \cos(\chi - \arg\langle A|B\rangle), \quad (1.2.38)$$

where a  $U(1)$  phase shift is imposed on  $|A\rangle$ . If  $|A\rangle$  is orthogonal to  $|B\rangle$  ( $|A\rangle \perp |B\rangle$  if  $|\langle A|B\rangle| = 0$ ) we do not get any information about the phase  $\arg\langle A|B\rangle$ , but if they are not orthogonal we can measure the intensity and regard the two state vectors as “*in-phase*” when the intensity is at maximum. The Pancharatnam relative phase  $\Phi$  is defined as  $\Phi \equiv \arg\langle A|B\rangle$  and it is well-defined (for nonorthogonal states) even if (1.2.37) is not satisfied. Two states are called in-phase if  $\langle A|B\rangle$  is real and positive which is known as *Pancharatnam's connection*.

It is remarkable that  $\Phi$  is non-transitive: if  $|A\rangle$  is in phase with  $|B\rangle$ , and  $|B\rangle$  is in phase with a third state  $|C\rangle$ , then  $|C\rangle$  need not to be in phase with  $|A\rangle$ , but to  $|A'\rangle = e^{i\Phi}|A\rangle$ :

$$|A\rangle \triangleleft |B\rangle \triangleleft |C\rangle \triangleleft |A'\rangle \not\triangleleft |A\rangle, \quad (1.2.39)$$

where  $\triangleleft$  denotes the “in-phase” relation.

The phase  $\Phi$  depends again on the subjacent geometry of state space. Pancharatnam deduced this result already in 1956 [Pan56] by considering the relative phase of two “in phase” polarisation states  $|A\rangle$  and  $|C\rangle$  of light both being projected onto a third state  $|B\rangle$ . Their relative phase becomes then

$$\arg[\langle A|B\rangle\langle B|B\rangle\langle B|C\rangle] = \arg[\langle A|B\rangle\langle B|C\rangle\langle C|A\rangle] \equiv \Delta(A, B, C), \quad (1.2.40)$$

where  $\arg\langle A|C\rangle = 0$  has been used.  $\Delta(A, B, C)$  is independent of the choice of Hilbert space representatives (invariant under transformations like  $|A\rangle \rightarrow e^{i\alpha}|A\rangle$ ) and is therefore a property of the projective Hilbert space. For 2-level systems (spin-1/2 particles)  $|A\rangle$ ,  $|B\rangle$ , and  $|C\rangle$  can be visualised as points on the Bloch sphere. Calculating  $\Delta(A, B, C)$  results then in

$$\Delta(A, B, C) = -\Delta(A, C, B) = -\frac{1}{2}\Omega_{ABC}, \quad (1.2.41)$$

with  $\Omega_{ABC}$  as the solid angle enclosed by the spherical triangle  $ABC$  (Figure 1.6).  $\Delta(A, B, C)$  is intimately related to the geometric phase since it reflects also the properties of the state space without paying attention to any particular dynamics. These considerations are also subject of the kinematic definition of the geometric phase by Mukunda and Simon [MS93], where the quantity  $\Delta(A, B, C)$  appears as a *Bargmann invariant* [Bar64].

**Parallel-transport law** In Section 1.2.2 we have encountered special paths in Hilbert space for which the dynamical phase vanishes and the remaining phase difference is purely geometric. The condition was that the integral  $\int_0^T \langle \psi(t)|H|\psi(t)\rangle$  vanishes which leads naturally to the *parallel transport* condition, viz. that the integrand  $\langle \psi(t)|H|\psi(t)\rangle$  has to vanish

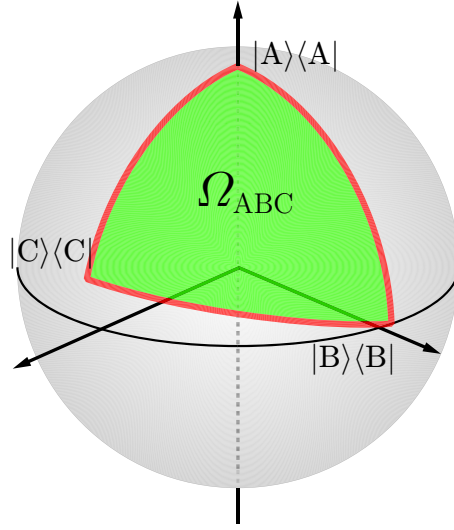


Figure 1.6: Spherical triangle on the Bloch sphere. If two states that are *in phase* are projected to a third one their phase difference depends on the enclosed solid angle  $\Omega_{ABC}$ .

for all  $t$ . From the Schrödinger equation we obtain

$$\langle \psi(t) | \frac{d}{dt} | \psi(t) \rangle = 0, \quad (1.2.42)$$

which denotes the in-phase relation between two adjacent states.

The other way round one can explicitly construct a state vector with zero dynamical phase corresponding to choosing a curve  $\mathcal{C}$  in Hilbert space for which the dynamical phase vanishes, a so called *horizontal lift* (or *parallel lift*) of the curve  $\tilde{\mathcal{C}} \in \mathcal{P}$ . Such a state is  $|\varphi(t)\rangle \in \mathcal{N}_0$  associated to the original state vector  $|\psi(t)\rangle \in \mathcal{N}_0$  by

$$|\varphi(t)\rangle = \exp\left[\frac{i}{\hbar} \int_0^t h(t') dt'\right] |\psi(t)\rangle, \quad (1.2.43)$$

where

$$h(t) = \text{Re} \langle \psi(t) | H(t) | \psi(t) \rangle \langle \psi(t) | \psi(t) \rangle^{-1}. \quad (1.2.44)$$

With this specific choice of  $h(t)$ , the dynamical phase factor is removed from  $|\psi(t)\rangle$  and only a geometric phase can be left.

From the evolution of  $|\varphi(t)\rangle$  we get back the parallel transport condition: The time evolution of  $|\psi(t)\rangle$  is given by the Schrödinger equation (1.2.28) and replacing  $|\psi\rangle$  with  $|\varphi\rangle$  we find the time evolution for  $|\varphi(t)\rangle$ ,

$$i\hbar \frac{d}{dt} |\varphi(t)\rangle = [H(t) - h(t)] |\varphi(t)\rangle. \quad (1.2.45)$$

Multiplying with  $\langle \varphi(t) |$  from the left and using the definition of  $h(t)$  (Eq. 1.2.44) we obtain

$$\begin{aligned} i\hbar \langle \varphi(t) | \frac{d}{dt} | \varphi(t) \rangle &= \langle \varphi(t) | H(t) | \varphi(t) \rangle - \langle \varphi(t) | h(t) | \varphi(t) \rangle \\ &= \langle \psi(t) | H(t) | \psi(t) \rangle - \text{Re} \langle \psi(t) | H(t) | \psi(t) \rangle \\ &= \text{Im} \langle \psi(t) | H(t) | \psi(t) \rangle. \end{aligned} \quad (1.2.46)$$

The *parallel-transport condition* is therefore given by

$$\text{Im} \langle \varphi(t) | \frac{d}{dt} | \varphi(t) \rangle = 0, \quad (1.2.47)$$

which is also valid for non-Hermitian  $H$ . For Hermitian  $H$  (unitary evolutions) we obtain the more familiar expression

$$\langle \varphi(t) | \frac{d}{dt} | \varphi(t) \rangle = 0, \quad (1.2.48)$$

which follows from the fact that  $\langle \varphi(t) | \frac{d}{dt} | \varphi(t) \rangle$  is already purely imaginary due to normalisation.

**Alternative approach to the parallel transport law** The parallel transport condition (1.2.48) can be more intuitively derived in the following way: Consider a curve  $\tilde{\mathcal{C}}$  in the projective Hilbert space  $\mathcal{P}$  (see Section 1.2.2) parametrised by  $s$ ,

$$\tilde{\mathcal{C}} : s \in [s_1, s_2] \mapsto |\varphi(s)\rangle \langle \varphi(s)|, \quad (1.2.49)$$

of a state  $|\varphi(s)\rangle$  on the associated ray in  $\mathcal{N}_0$ .  $|\varphi(s)\rangle$  varies smoothly above the curve  $\tilde{\mathcal{C}}$  and is therefore a Hilbert space representative of  $\tilde{\mathcal{C}}$ . Natural conditions for a parallel transport are now that the length of  $|\varphi\rangle$  is preserved, i. e.  $\langle \varphi(s) | \varphi(s) \rangle = \text{const.}$ , and furthermore that  $|\varphi(s)\rangle$  and an infinitesimally displaced  $|\varphi(s+ds)\rangle$  have the same phase, i. e.  $\langle \varphi(s) | \varphi(s+ds) \rangle$  is real and positive - see Figure (1.7). From a series expanding of  $\langle \varphi(s) | \varphi(s+ds) \rangle$  we find

$$\langle \varphi(s) | \varphi(s+ds) \rangle = \langle \varphi(s) | \varphi(s) \rangle + \langle \varphi(s) | \frac{d}{ds} | \varphi(s) \rangle ds + \mathcal{O}(ds^2), \quad (1.2.50)$$

which is real in first order of  $ds$  if

$$\text{Im} \langle \varphi(s) | \frac{d}{ds} | \varphi(s) \rangle = 0. \quad (1.2.51)$$

Evidently this is equivalent to the Pancharatnam connection for infinitesimally close states.

**Cyclic evolution** Now we can derive the cyclic geometric phase within this formalism. As pointed out above any open curve in Hilbert space traced out by  $|\varphi(s)\rangle$ ,  $s \in [s_1, s_2]$  can be projected to  $\mathcal{P}$  and if  $|\varphi(s_2)\rangle = e^{i\alpha} |\varphi(s_1)\rangle$ ,  $\alpha \in \mathbb{R}$  the curve in  $\mathcal{P}$  is closed (see Figure 1.5). For the curve in  $\mathcal{N}_0$  we can write the tangent vector as  $|u(s)\rangle = \frac{d}{ds} |\varphi(s)\rangle$  and define a quantity

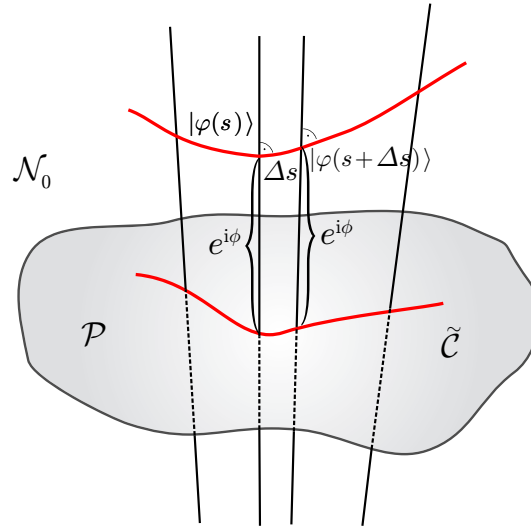


Figure 1.7: Parallel transport law: Two infinitesimally close states are called parallel if they are in-phase, i. e. if  $\arg\langle\phi(s)|\phi(s+\Delta s)\rangle = 0$ .

$A_s$  by

$$A_s = \text{Im}\langle\varphi(s)|u(s)\rangle. \quad (1.2.52)$$

Going back one step and look at the path traced out by the original state  $|\psi(s)\rangle$  we notice that if  $|\psi(s)\rangle$  is a cyclic solution of the Schrödinger equation, the projection of this curve to  $\mathcal{P}$  is closed. But we are not interested in the dynamical part of the phase factor acquired during the evolution, thus we have to ask for the curve  $c : s \mapsto |\varphi(s)\rangle$  defined by equation (1.2.45) which is a horizontal lift of the curve traced out by  $|\psi(s)\rangle$ .  $c$  is determined by the parallel-transport condition (1.2.51), which implies that  $A_s = 0$  (from (1.2.52)) along the curve. Note that in the language of fibre bundles  $A_s$  is interpreted as a connection one-form which defines horizontal lift [Ber96]. Consider now the integral

$$\phi_g = \oint A_s ds \quad (1.2.53)$$

along the curve  $c$  in  $\mathcal{N}_0$  closed by the vertical curve joining  $|\varphi(s_2)\rangle$  and  $|\varphi(s_1)\rangle$ .  $A_s$  vanishes along the curve  $|\varphi(s)\rangle$ , consequently only this vertical line contributes to this loop integral and  $\phi_g$  is therefore given by the phase difference  $\arg\langle\varphi(s_1)|\varphi(s_2)\rangle$ .

Due to the gauge invariance of the integral (1.2.53) this can be regarded as an integral in projective Hilbert space  $\mathcal{P}$ . We can use *Stokes' theorem* and express (1.2.53) as a surface integral in  $\mathcal{P}$ ,

$$\phi_g = \int_S dA_s, \quad (1.2.54)$$

where  $S$  is the surface in  $\mathcal{P}$  bounded by the closed curve  $\mathcal{C}(s)$  and  $dA_s$  is a two-form ( $dA_s$  denotes the exterior derivative of  $A_s$ , which is equivalent to the curl of  $A_s$  in 3 dimensions).

**Non-cyclic evolution** Until now the above was only a new formalism yielding an already known result. Therefore, let us consider now a non-cyclic (but still unitary) evolution of the quantum system. The state vector may not return to the initial ray, thus the curve  $\tilde{C}$  in  $\mathcal{P}$  is not necessarily closed and we need a method to compare the phase at two different rays. Pancharatnam's connection discussed earlier is the appropriate tool for this!

The most important fact derived by Samuel and Bhandari [SB88] is that one can express the *Pancharatnam phase difference*  $\beta = \arg\langle\varphi_1|\varphi_2\rangle$  ( $|\varphi_1\rangle, |\varphi_2\rangle \in \mathcal{N}_0, |\varphi_1\rangle \not\propto |\varphi_2\rangle$ ) as a line integral of  $A_s$  along a geodesic. In fact, they proved that, by choosing a geodesic curve  $\mathcal{G}$  with respect to the Fubini-Study metric connecting  $|\varphi_1\rangle$  and  $|\varphi_2\rangle$ , the phase difference is given by

$$\beta = \arg\langle\varphi_1|\varphi_2\rangle = \int_{\mathcal{G}} A_s ds. \quad (1.2.55)$$

The phase  $\phi_g$  of a state vector  $|\varphi(s)\rangle$  achieved by evolving from  $s = 0$  to  $s = T$  can consequently be expressed as

$$\phi_g = \oint_{\mathcal{G}+c} A_s ds = \int_c A_s ds + \int_{\mathcal{G}} A_s ds = \int_{\mathcal{G}} A_s ds, \quad (1.2.56)$$

where  $c$  denotes the horizontal curve. Integration along  $\mathcal{G}$  yields the Pancharatnam phase difference, the integral along  $c$  vanishes due to the parallel transport and we end up with the same expression as in the cyclic case (1.2.53).  $\phi_g = \oint A_s ds$  can again be expressed as the surface integral (1.2.54) over a 2-form in the projective Hilbert space (Figure 1.8) where the geodesic connection from the initial to the final point closes the boundary of the surface.

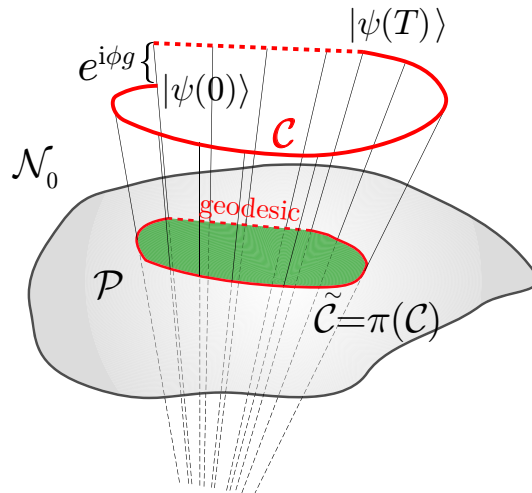


Figure 1.8: Geodesic closure to obtain loop in  $\mathcal{P}$ . For a non-cyclic path the curve  $\tilde{C}$  is closed by a geodesic.

### 1.2.4 Kinematic Approach

A theory of the geometric phase based entirely on kinematic ideas has been presented by Mukunda and Simon [MS93]. In their approach the geometric phase is decoupled from any (Hamiltonian) dynamics of the quantum system, but it is treated as a property of curves connecting state vectors. As before, the state vectors  $|\psi\rangle$  are elements of the set  $\mathcal{N}_0$  of normalised vectors which is a subset of the set of nonzero vectors  $\mathcal{N}$  of the Hilbert space  $\mathcal{H}$ , i. e.  $\mathcal{N}_0 \subset \mathcal{N} \subset \mathcal{H}$ .

In searching for interesting invariants under the U(1) gauge transformation

$$|\psi\rangle \mapsto |\psi'\rangle = e^{i\alpha}|\psi\rangle \in \mathcal{N}_0,$$

one immediately recognises the importance of the modulus of the inner product of two vectors,

$$|\langle\psi'_1|\psi'_2\rangle| = |\langle\psi_1|\psi_2\rangle| = U(1) \times U(1)\text{-invariant} \quad (1.2.57)$$

with independent transformations

$$|\psi'_1\rangle = e^{i\alpha_1}|\psi_1\rangle, \quad |\psi'_2\rangle = e^{i\alpha_2}|\psi_2\rangle.$$

Extending this scheme to even more vectors, naturally *Bargmann-invariants* [Bar64] of the form

$$\langle\psi_1|\psi_2\rangle\langle\psi_2|\psi_3\rangle\cdots\langle\psi_n|\psi_1\rangle = \underbrace{U(1) \times U(1) \cdots U(1)}_{n\text{-times}} \quad (1.2.58)$$

come into play. The modulus of the inner product (1.2.57) is a simple case of this kind of invariants:

$$\text{tprob}(\psi_1, \psi_2) \equiv |\langle\psi_1|\psi_2\rangle|^2 = \langle\psi_1|\psi_2\rangle\langle\psi_2|\psi_1\rangle$$

denotes the *transition probability* between two states  $|\psi_1\rangle$  and  $|\psi_2\rangle$ . In the following we will first consider a smooth curve and find its geometric invariant (geometric phase) and then derive the same quantity in terms of Bargmann invariants by dividing the curve into small segments.

**Invariant of a smooth curve** A smooth curve  $\mathcal{C}_0 \subset \mathcal{N}_0$  is given by the map

$$\mathcal{C}_0 : s \in [s_1, s_2] \mapsto |\psi(s)\rangle \in \mathcal{N}_0, \quad s_1, s_2 \in \mathbb{R}. \quad (1.2.59)$$

From the constant norm of the states  $|\psi(s)\rangle$  along the curve  $\mathcal{C}_0$  we can deduce that the quantity  $\langle\psi(s)|\dot{\psi}(s)\rangle$  is purely imaginary (c. f. Eq. 1.2.9), where the dot stands for the derivative  $d/ds$ . Moreover  $\langle\psi(s)|\dot{\psi}(s)\rangle$  is evidently invariant under a *global* gauge transformation

$$|\psi(s)\rangle \mapsto |\tilde{\psi}\rangle(s) = e^{i\alpha}|\psi(s)\rangle, \quad \alpha \in \mathbb{R}. \quad (1.2.60)$$

Under the *local* gauge transformation

$$\mathcal{C}_0 \mapsto \mathcal{C}'_0 : |\psi(s)\rangle \mapsto |\tilde{\psi}\rangle(s) = e^{ia(s)}|\psi(s)\rangle, \quad (1.2.61)$$

determined by the smooth real function  $a(s)$ , it transforms like

$$\langle\psi(s)|\frac{d}{ds}|\psi(s)\rangle \mapsto \langle\psi'(s)|\frac{d}{ds}|\psi'(s)\rangle = \langle\psi(s)|\dot{\psi}(s)\rangle + \dot{a}(s). \quad (1.2.62)$$

For the definition of a geometric phase we have to find a functional of the curve  $\mathcal{C}_0$  that is invariant under the local gauge transformation (1.2.61), i. e. which is the same for different  $\mathcal{C}_0$  and  $\mathcal{C}'_0$ . This local gauge transformation corresponds to the choice of a different Hamiltonian projecting to the same curve in  $\mathcal{P}$ .

Such a functional is given by

$$\phi_g[\mathcal{C}_0] \equiv \arg\langle\psi(s_1)|\psi(s_2)\rangle - \text{Im} \int_{s_1}^{s_2} ds \langle\psi(s)|\dot{\psi}(s)\rangle. \quad (1.2.63)$$

Replacing  $|\psi(s)\rangle$  by  $|\psi'(s)\rangle$  yields the same expression which can be verified easily by inserting Eq. (1.2.62) into Eq. (1.2.63). Consequently,  $\phi_g = \phi'_g$  and therefore gauge invariant.

It is also reparametrisation invariant by the same argument as in Eq. (1.2.8) since  $|\psi(s_1)\rangle = |\psi'(s'_1)\rangle$  and  $|\psi(s_2)\rangle = |\psi'(s'_2)\rangle$ .

The U(1) gauge invariance means that the quantity  $\phi_g$  is independent of the particular phase factors at each point  $s$  and consequently it is a property of ray space  $\mathcal{P}$ . As already discussed previously (Figure 1.8) the gauge transformation can be used to project the curve  $\mathcal{C}_0$  onto the curve  $\tilde{\mathcal{C}}_0$  in  $\mathcal{P}$ . The functional  $\phi_g[\tilde{\mathcal{C}}_0]$  defines the geometric phase associated with the smooth curve  $\tilde{\mathcal{C}}_0$ . The argument  $\tilde{\mathcal{C}}_0$  stresses that the geometric phase is a property of the projective Hilbert space. If, instead of  $\mathcal{C}_0$ ,  $\tilde{\mathcal{C}}_0$  is initially given one may choose any lift  $\mathcal{C}_0$  which projects to  $\tilde{\mathcal{C}}_0$  ( $\pi(\mathcal{C}_0) = \tilde{\mathcal{C}}_0$ ) and calculate  $\phi_g$  for the most convenient one.

Note, that  $\phi_g[\tilde{\mathcal{C}}]$  is undefined for orthogonal initial and final states  $|\psi(s_1)\rangle$  and  $|\psi(s_2)\rangle$ , since the transition probability  $\text{tprob}(\psi(s_1), \psi(s_2)) = |\langle\psi_1|\psi_2\rangle|^2$  vanishes and therefore the argument  $\arg\langle\psi(s_1)|\psi(s_2)\rangle$  is undefined.

Naturally, the two terms on the right hand side of Eq. (1.2.63) can be interpreted as the total phase

$$\Phi[\mathcal{C}_0] = \arg\langle\psi(s_1)|\psi(s_2)\rangle \quad (1.2.64)$$

and the dynamical phase

$$\phi_d[\mathcal{C}_0] \equiv \text{Im} \int_{s_1}^{s_2} ds \langle\psi(s)|\dot{\psi}(s)\rangle. \quad (1.2.65)$$

These phases depend on the curve  $\mathcal{C}_0$  in Hilbert space, it is only their difference  $\phi_g$  that depends only on the curve  $\tilde{\mathcal{C}}_0$  in ray space.

There are several possibilities to choose a lift to make one or the other term vanish. On the one hand side a curve  $\mathcal{C}_0$  can be found such that the total phase  $\Phi$  vanishes,  $|\psi(s_1)\rangle$  and  $|\psi(s_2)\rangle$  are then said to be “*in-phase*” and  $\phi_g = -\phi_d$ . On the other hand the dynamical phase

## 1. GEOMETRIC PHASE - INTRODUCTION

can be made to vanish by the requirement that the dynamical phase  $\phi_d$  vanishes along the curve, in other words, to choose a so called *horizontal lift* which fulfils the parallel transport condition,

$$\mathcal{C} \text{ horizontal} \leftrightarrow \text{Im}\langle\psi(s)|\dot{\psi}(s)\rangle = 0 \leftrightarrow \langle\dot{\psi}(s)|\psi(s)\rangle = 0 \rightarrow \phi_d = 0. \quad (1.2.66)$$

**Bargmann invariants** It is not difficult to derive the geometric phase functional (1.2.63) in terms of Bargmann invariants as introduced in Eq. (1.2.58). For this purpose the arbitrary path  $\mathcal{C}_0 : s \in [s_1, s_2] \mapsto |\psi(s)\rangle$  is divided into  $N$  pieces such that in the limit  $N \rightarrow \infty$  the original path is recovered. Instead of a continuous paths we get a ordered set of states  $\mathcal{C}_0 = \{|\psi_1\rangle, |\psi_2\rangle, \dots, |\psi_N\rangle\} \in \mathcal{N}_0$ , where  $|\psi_1\rangle = |\psi(s_1)\rangle$  and  $|\psi_N\rangle = |\psi(s_2)\rangle$ . To make all dynamical phase contributions vanish the parallel transport condition (1.2.48) has to hold for each pair of adjacent states. The discrete version of this condition is to link adjacent states by a *horizontal geodesic* that is defined as the horizontal lift  $g$  of a geodesic  $\tilde{\mathcal{G}}$  in ray space [MS93] (Figure 1.9). In other words, we have to re-gauge each  $|\psi_i\rangle \mapsto |\psi'_i\rangle = e^{i\alpha_i} |\psi_i\rangle$  such

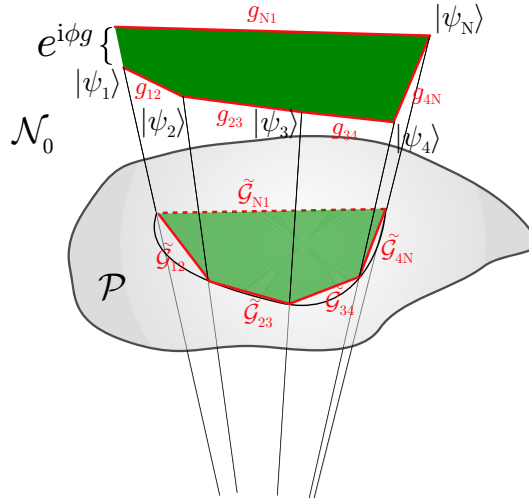


Figure 1.9: Discrete path where adjacent states  $|\psi_r\rangle$  and  $|\psi_{r+1}\rangle$  are connected by geodesics  $g_{r,r+1}$ .

that all states in the re-gauged set  $\mathcal{C}'_0 = \{|\psi'_1\rangle, |\psi'_2\rangle, \dots, |\psi'_N\rangle\}$  are linked by a horizontal geodesic. The geometric phase of a curve is given by the difference of the total phase and the dynamical phase,

$$\phi_g[\tilde{\mathcal{C}}_0] = \Phi[\mathcal{C}_0] - \phi_d[\mathcal{C}_0] = \arg\langle\psi_1|\psi_N\rangle - \sum_{r=1}^{N-1} \phi_d[g_{r,r+1}]$$

using Eq. (1.2.63). Using (1.2.63) once more for the sum on the right hand side we find

$$\sum_{r=1}^{N-1} \phi_d[g_{r,r+1}] = \sum_{r=1}^{N-1} \left\{ \Phi[g_{r,r+1}] - \phi_g[\tilde{\mathcal{G}}_{r,r+1}] \right\} = \sum_{r=1}^{N-1} \arg\langle\psi_r|\psi_{r+1}\rangle,$$

where the last equality follows from the fact that the geometric phase vanishes along a geodesic  $\mathcal{G}$ ,  $\phi_g[\mathcal{G}] = 0$ . Altogether the geometric phase reads

$$\phi_g[\tilde{\mathcal{C}}_0] = \arg\langle\psi_1|\psi_N\rangle - \sum_{r=1}^{N-1} \arg\langle\psi_r|\psi_{r+1}\rangle = -\arg\langle\psi_1|\psi_2\rangle\langle\psi_2|\psi_3\rangle\cdots\langle\psi_{N-1}|\psi_N\rangle\langle\psi_N|\psi_1\rangle, \quad (1.2.67)$$

the argument of a Bargmann invariant associated with the discrete path  $\mathcal{C}_0$ . For the special construction where we have chosen  $|\psi_r\rangle$  and  $|\psi_{r+1}\rangle$  to be “in-phase” ( $\arg\langle\psi_r|\psi_{r+1}\rangle = 0$ ) by choosing a horizontal geodesic

$$\phi_g = -\arg\langle\psi_N|\psi_1\rangle$$

. In general, the dynamical phase along a lifted geodesic in  $\mathcal{N}_0$  does not vanish, it is the horizontal property that disposes of the dynamical contributions.

**Limit of infinitesimally close states** In the limit  $N \rightarrow \infty$  the form (1.2.63) is recovered.  $\phi_g[\tilde{\mathcal{C}}_0]$  is given by

$$\begin{aligned} \phi_g[\tilde{\mathcal{C}}_0] &= \lim_{N \rightarrow \infty} \{-\arg\langle\psi_1|\psi_2\rangle\langle\psi_2|\psi_3\rangle\cdots\langle\psi_{N-1}|\psi_N\rangle\langle\psi_N|\psi_1\rangle\} \\ &= \arg\langle\psi(s_1)|\psi(s_2)\rangle - \lim_{N \rightarrow \infty} \arg \prod_{r=1}^N \langle\psi(\sigma_r)|\psi(\sigma_{r+1})\rangle \end{aligned}$$

where we have the following subdivision of the curve  $\tilde{\mathcal{C}}_0$  in mind:

$$\begin{array}{ccccccc} & 1 & \Delta s & 2 & \Delta s & 3 & & & & r & r+1 & & & & N-1 & N \\ & | & & | & & | & \cdots & & & | & & | & \cdots & & | & & | \\ s_1 = \sigma_1 & & \sigma_2 & & \sigma_3 & & & & & \sigma_r & & \sigma_{r+1} & & & \sigma_{N-1} & & \sigma_N = s_2 \end{array}$$

Expanding  $|\psi(\sigma_{r+1})\rangle = |\psi(\sigma_r + \Delta s)\rangle$  yields

$$\begin{aligned} \phi_g[\tilde{\mathcal{C}}_0] &\approx \arg\langle\psi(s_1)|\psi(s_2)\rangle - \lim_{N \rightarrow \infty} \arg \prod_{r=1}^N \langle\psi(\sigma_r)|\psi(\sigma_r) + \Delta s \dot{\psi}(\sigma_r)\rangle, \\ &= \arg\langle\psi(s_1)|\psi(s_2)\rangle - \lim_{N \rightarrow \infty} \arg \prod_{r=1}^N (1 + \Delta s \langle\psi(\sigma_r)|\dot{\psi}(\sigma_r)\rangle) \\ &\approx \arg\langle\psi(s_1)|\psi(s_2)\rangle - \lim_{N \rightarrow \infty} \arg \exp\left(\sum_{r=1}^N \Delta s \langle\psi(\sigma_r)|\dot{\psi}(\sigma_r)\rangle\right). \end{aligned}$$

Finally, the sum can be converted into an integral in the limit  $N \rightarrow \infty$  and we obtain

$$\phi_g[\tilde{\mathcal{C}}_0] = \arg\langle\psi(s_1)|\psi(s_2)\rangle - \arg \exp\left(\int_{s_1}^{s_2} ds \langle\psi(\sigma_r)|\dot{\psi}(\sigma_r)\rangle\right). \quad (1.2.68)$$

In summary, the kinematic approach derives the geometric phase for any set of states whether they belong to a continuous path or not. The latter describes for instance measurement

processes, whereas the former is connected to systems obeying Schrödinger equation dynamics.

### Non-unitary evolution

The kinematic approach is easily extensible to non-unitary evolutions by admitting also non-normalised state vectors  $|\psi\rangle \in \mathcal{N} \not\subseteq \mathcal{N}_0$ . Consider the smooth curve

$$\mathcal{C} : s \mapsto \psi(s) \in \mathcal{N}, s \in [s_1, s_2] \subset \mathbb{R}. \quad (1.2.69)$$

In the unitary case we have due to the conservation of the norm that  $\langle \psi(s) | \dot{\psi}(s) \rangle$  is purely imaginary, whereas in the non-unitary case this quantity can be real as well. As usual we will consider a projection  $\tilde{\mathcal{C}}_0$  of the curve  $\mathcal{C}$  onto ray space  $\mathcal{P} = \mathcal{N}_0/U(1)$ , but now the curve  $\tilde{\mathcal{C}}$  need not comprise only normalised states.

The use of the ray space suggests the use of unnormalised pure state density operators  $\rho(s) = |\psi(s)\rangle\langle\psi(s)|$  so that the curve  $\tilde{\mathcal{C}}$  is determined by

$$\tilde{\mathcal{C}} : s \mapsto \rho(s), s \in [s_1, s_2] \subset \mathbb{R}. \quad (1.2.70)$$

The (pure state) density operator has to fulfil the following conditions:

$$\rho(s)^\dagger = \rho(s) \text{ (hermitian)} \quad (1.2.71)$$

$$\rho(s) \geq 0 \text{ (positive)} \quad (1.2.72)$$

$$\rho(s)^2 = \rho(s) \text{Tr} \rho(s) \text{ (modified projection operator condition)}. \quad (1.2.73)$$

The last condition follows from  $\rho^2 = |\psi\rangle\langle\psi|\psi\rangle\langle\psi| = |\psi\rangle\langle\psi| \text{Tr}(|\psi\rangle\langle\psi|) = \rho \text{Tr} \rho$ .

In the case of constant norm the definition of the geometric phase relies on the search for a quantity invariant under local  $U(1)$  transformations, i. e. for transformations of the curve  $\mathcal{C}_0 \mapsto \tilde{\mathcal{C}}_0 : |\tilde{\psi}_0(s)\rangle = e^{i\alpha(s)}|\psi_0(s)\rangle$ , where  $|\psi_0\rangle \in \mathcal{N}_0$  and  $\alpha(s) \in \mathbb{R}$ . Only the phase of the state is modified. Such a quantity is then a property only of the path itself in ray space. Here in contrast the relevant transformation is given by

$$\mathcal{C} \mapsto \tilde{\mathcal{C}} : |\tilde{\psi}(s)\rangle = a(s)|\psi(s)\rangle \quad (1.2.74)$$

with a complex-valued function  $a(s) \in \mathbb{C}$ .

According to [MS93] the natural generalisation to the former definition (1.2.63) is given by the complex quantity

$$\mathcal{X} \equiv \frac{\langle \psi(s_1) | \psi(s_2) \rangle}{\langle \psi(s_2) | \psi(s_2) \rangle} \exp \left( - \int_{s_1}^{s_2} ds \frac{\langle \psi(s) | \dot{\psi}(s) \rangle}{\langle \psi(s) | \psi(s) \rangle} \right). \quad (1.2.75)$$

$\mathcal{X}$  transforms under the scale transformation in Eq. (1.2.74) as

$$\begin{aligned}
 \tilde{\mathcal{X}} &= \frac{\langle \tilde{\psi}(s_1) | \tilde{\psi}(s_2) \rangle}{\langle \tilde{\psi}(s_2) | \tilde{\psi}(s_2) \rangle} \exp \left( - \int_{s_1}^{s_2} ds \frac{\langle \tilde{\psi}(s) | \dot{\tilde{\psi}}(s) \rangle}{\langle \tilde{\psi}(s) | \tilde{\psi}(s) \rangle} \right) \\
 &= \frac{a^*(s_1) a(s_2) \langle \psi(s_1) | \psi(s_2) \rangle}{a^*(s_2) a(s_2) \langle \psi(s_2) | \psi(s_2) \rangle} \exp \left( - \int_{s_1}^{s_2} ds \frac{\langle \psi(s) | \dot{\psi}(s) \rangle}{\langle \psi(s) | \psi(s) \rangle} \right) \exp \left( - \int_{s_1}^{s_2} ds \frac{a^*(s) \dot{a}(s)}{a^*(s) a(s)} \right) \\
 &= \frac{a^*(s_1) a(s_2) \langle \psi(s_1) | \psi(s_2) \rangle}{a^*(s_2) a(s_2) \langle \psi(s_2) | \psi(s_2) \rangle} \exp \left( - \int_{s_1}^{s_2} ds \frac{\langle \psi(s) | \dot{\psi}(s) \rangle}{\langle \psi(s) | \psi(s) \rangle} \right) \exp \left( - \int_{a(s_1)}^{a(s_2)} \frac{da(s)}{a(s)} \right) \\
 &= \frac{a^*(s_1) a(s_2) \langle \psi(s_1) | \psi(s_2) \rangle}{a^*(s_2) a(s_2) \langle \psi(s_2) | \psi(s_2) \rangle} \exp \left( - \int_{s_1}^{s_2} ds \frac{\langle \psi(s) | \dot{\psi}(s) \rangle}{\langle \psi(s) | \psi(s) \rangle} \right) \exp(-\ln a(s_2) + \ln a(s_1)) \\
 &= \frac{a^*(s_1) a(s_2) \langle \psi(s_1) | \psi(s_2) \rangle}{a^*(s_2) a(s_2) \langle \psi(s_2) | \psi(s_2) \rangle} \exp \left( - \int_{s_1}^{s_2} ds \frac{\langle \psi(s) | \dot{\psi}(s) \rangle}{\langle \psi(s) | \psi(s) \rangle} \right) \frac{a(s_1)}{a(s_2)} \\
 &= \frac{|a(s_1)|^2 \langle \psi(s_1) | \psi(s_2) \rangle}{|a(s_2)|^2 \langle \psi(s_2) | \psi(s_2) \rangle} \exp \left( - \int_{s_1}^{s_2} ds \frac{\langle \psi(s) | \dot{\psi}(s) \rangle}{\langle \psi(s) | \psi(s) \rangle} \right) \\
 &= \mathcal{X} \quad \text{if } a(s_1) = a(s_2) = 1.
 \end{aligned} \tag{1.2.76}$$

Since this is a complex quantity we can separate the real and the imaginary part to obtain

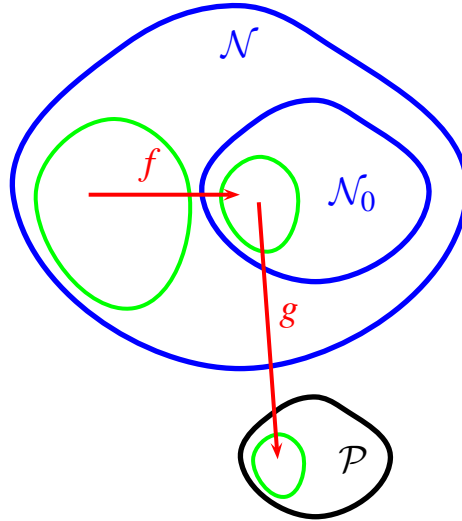


Figure 1.10: Map of the curve from  $\mathcal{N}$ , the state space comprising all vectors, to  $\mathcal{N}_0$  the space of normalised vectors and finally into ray space  $\mathcal{P}$ .

two real invariants:

$$\text{Im } \mathcal{X} = \arg \langle \psi(s_1) | \psi(s_2) \rangle - \text{Im} \int_{s_1}^{s_2} ds \frac{\langle \psi(s) | \dot{\psi}(s) \rangle}{\langle \psi(s) | \psi(s) \rangle} \tag{1.2.77}$$

$$\text{Re } \mathcal{X} = \frac{|\langle \psi(s_1) | \psi(s_2) \rangle|}{|a(s_2)|^2 \langle \psi(s_2) | \psi(s_2) \rangle} \exp \left( \text{Re} \int_{s_1}^{s_2} ds \frac{\langle \psi(s) | \dot{\psi}(s) \rangle}{\langle \psi(s) | \psi(s) \rangle} \right). \tag{1.2.78}$$

For normalised vectors  $|\psi(s)\rangle \in \mathcal{N}_0$  we obtain the trivial invariant  $\text{Re } \mathcal{X} = 1$ .

The definition of the geometric phase for non-unitary evolution follows from the imaginary part,

$$\phi_g[\tilde{\mathcal{C}}_0] = \text{Im } \mathcal{X} = \Phi[\mathcal{C}] - \phi_d[\mathcal{C}] \quad (1.2.79)$$

$$\Phi[\mathcal{C}] = \text{total phase of } \mathcal{C} = \arg\langle\psi(s_1)|\psi(s_2)\rangle \quad (1.2.80)$$

$$\phi_d[\mathcal{C}] = \text{dynamical phase of } \mathcal{C} = \text{Im} \int_{s_1}^{s_2} ds \frac{\langle\psi(s)|\dot{\psi}(s)\rangle}{\langle\psi(s)|\psi(s)\rangle}. \quad (1.2.81)$$

Under the scaling  $|\psi(s)\rangle \mapsto r(s)|\psi(s)\rangle$  both  $\Phi[\mathcal{C}]$  and  $\phi_d[\mathcal{C}]$  are separately invariant for real and positive  $r(s)$ . Consequently,  $\phi_g[\tilde{\mathcal{C}}_0]$  is also invariant under a scale transformation. By an appropriate choice of  $r(s)$  the curve  $\mathcal{C}$  in  $\mathcal{N}$  can be projected to  $\mathcal{C}_0$  in  $\mathcal{N}_0$ . Afterwards the  $U(1)$  gauge invariance can be used to project  $\mathcal{C}_0$  to the curve  $\tilde{\mathcal{C}}_0$  in ray space  $\mathcal{P}$  so that the geometric phase is determined again by the projected curve in  $\mathcal{P}$  as in the unitary case. “As an example, for two-level systems, whether the evolution is unitary or not, the geometric phase can always be analysed on the Poincaré-Bloch sphere  $S^2$ .” [MS93, p. 259].

### 1.3 Experiments on the geometric phases

The huge amount of experiments on the geometric phase makes it hardly possible to keep track of all of them - a thorough listing would go beyond the scope of this thesis. For this reason I will just mention a few tests of the geometric phase with the main focus on experiments involving neutrons.

The first experimental verification with explicit mention of Berry’s phase is due to Tomita and Chiao [TC86] using an helically wound optical fibre to examine the polarisation change of linearly polarised light extending a similar experiment by Ross [Ros84] to non-uniformly wound fibres. The entrance and exit direction of the fibre are equal such that the path in momentum space is closed. The rotation of the plane of polarisation is attributed to Berry’s phase proportional to the solid angle enclosed in momentum space. Note, however, that this setup is somewhat different to Berry’s phase since it is not the polarisation vector itself that is transported around a closed loop by variation of some parameters of the Hamiltonian, but the state in momentum space is changed, which can be understood fully classically [Hal87, Ber87] and resembles the example given in Section 1.1.

In neutron science, Bitter and Dubbers [BD87] were the first who used the spin degree of freedom of neutrons to demonstrate the geometric phase. Polarised neutrons are sent through an helically wound Helmholtz-like coil (c.f. Section 5, Figure 5.10) such that their spin polarisation vector is adiabatically rotated following the rotation of the magnetic field in the neutron’s reference frame. Additional to the dynamical phase due to the Larmor precession they observed Berry’s phase as a constant offset in the total phase which increases when the field strength is increased. Soon afterwards stored ultra cold neutrons served as probes for Berry’s phase factor [RKGL88]. In this setup - which will be discussed and adapted in Section 5 and in the Appendix D to test the stability of the geometric phase -

neutrons are stored in an appropriate vessel. Three perpendicular pairs of Helmholtz coils are arranged around the vessel to produce a magnetic field in an arbitrary direction and enables an adiabatic rotation of the neutrons' spin.

Neutron interferometry has been used first by Allman *et al.* [AKW<sup>+</sup>97] to spot the effects of the geometric phase. In their experiment the evolution was not adiabatic anymore and constitutes already a realisation of the more general non-adiabatic geometric phase. Static coils have been inserted in the interferometer beam paths to implement  $\pi$  spin-flip operations in both arms, whereas the two flipper axes enclose a non-zero opening angle  $\Delta\beta$ . The geometric phase is a function only of  $\Delta\beta$  since a change in the opening angle changes the path from the initial to the flipped state (c.f. Figure 5.9).

Further examples of neutron experiments on topological effects can be found in Refs. [WB90, WRFI98, Bha99, WBR<sup>+</sup>00, HZR96, HLB<sup>+</sup>01, HLB<sup>+</sup>02].

A demonstration of Berry's phase, although highly unwanted, is the experiment on the electric dipole moment of neutrons [HBG<sup>+</sup>99, BDG<sup>+</sup>06]. The electric dipole moment if it exists should result in a different phase whether it is align or anti-aligned with the magnetic field, but since neutrons are moving freely in the magnetic field region they experience temporal magnetic field variations in their moving reference frame. Consequently, their spin traces out some path which in turn gives rise to geometric phase contributions [PHS<sup>+</sup>04].

A recent experiment in NMR considers the possible application of the geometric phase for quantum computation [JVEC00]. Using two weakly coupled spins of a heteronuclear system a conditional Berry phase is applied to one of the spins, i. e. the phase shift of one system depends on the state of the of the other system, which is a imperatively necessary for the implementation of a universal set of quantum gates [NC00].

## 1.4 Facts to remember

In conclusion, the evolution of a state of a quantum system is accompanied in general by a change of the phase of the system. In particular, for an adiabatic and cyclic evolution the initial state is equal to the final state up to a phase factor. This phase factor can be separated into a dynamical and a geometric part, where the former comprises all the dependence on the dynamics like the evolution time and the energy of the system. The latter is only dependent on the geometry of the state space in which the evolution takes place. The curvature of the subjacent state space determines the geometric phase. This behaviour is not restricted to an adiabatic process, but can be generalised to all kinds of processes, where the focus is then shifted to the path in state space rather than in parameter space as for Berry's phase. This can also be regarded as a distinction between Berry's adiabatic phase and the more general geometric phase.

The geometric phase is a property of projective Hilbert space which is constructed by taking all states differing only by a phase factor as equivalent. The purpose in doing so is that in quantum mechanics a global phase factor does not have physical relevance, it is only relative phases that can be measured. That the geometric phase belongs to this projective

Hilbert space expresses the fact that physically it must not matter whether the instantaneous states along the evolution path are multiplied by an additional phase factor, that is, gauge transformed. It is a gauge invariant quantity, otherwise it would not be measurable. There exists then a specific *parallel* path in Hilbert space for which the dynamical phase vanishes. Along such a path two neighbouring states are *in-phase*, their relative phase difference vanishes.

Reparametrisation invariance is another important feature of the geometric phase. Since we are claiming that it is a property only of the path in the projective Hilbert space, or - by Stokes's theorem - proportional to the surface area enclosed by the path, a change of the rate of traversal must be immaterial.

To obtain the enclosed surface area also for an open curve a prescription is needed which curve has to be employed to connect the final with the initial state. This turns out to be a geodesic, i. e. the shortest possible path, which is always defined as long as the states are not orthogonal to each other. In the latter case there is no unique shortest path and, consequently, no unique geometric phase. This observation will bother us in the following chapters, where an *off-diagonal geometric phase* is discussed that discloses information on the geometry also in such situations.

As an outlook to the last chapter, note, that it is believed that the geometric phase is widely insusceptible to disturbances because of its independence of the dynamics.



# Chapter 2

## Geometric Phase For Mixed States

Is the geometric phase concept only applicable to pure states? What happens if the system is not prepared in a particular pure state but in a mixture of pure states? In the following, mixed states are introduced and it will be demonstrated that the notion of the geometric phase can be extended to include mixed states as well.

### 2.1 Mixed states

Suppose that we have maximal knowledge of the state of our quantum system, a complete set of quantum numbers is known. An example of such a situation is a neutron beam with definite momentum and spin polarisation. The representation is then usually by a state - ket,

$$|\Psi\rangle = |k\rangle \otimes |s\rangle, \quad (2.1.1)$$

constructed as a tensor product of the different state spaces,  $|k\rangle$  for the momentum space and  $|s\rangle$  for the internal spin space. For each other degree of freedom another Hilbert space has to be added, for example to describe the internal quark structure, but such additional degrees of freedom will not be considered in the following.

$|k\rangle$  is an eigenvector to the momentum operator  $\hat{p} = \hbar\hat{k}$ ,  $\hat{k}|k\rangle = k|k\rangle$ , and  $|s\rangle$  is an eigenvector to some linear combination of Pauli matrices  $\vec{n} \cdot \vec{\sigma}|s\rangle = |s\rangle$ .  $\vec{n}$  is a unit vector in  $\mathbb{R}^3$  and  $\vec{\sigma} = (\sigma_x, \sigma_y, \sigma_z)^T$  denotes the vector of the usual Pauli matrices. The state as it stands comprises just a single wave vector  $k$ , it represents a plane monochromatic wave and one might question the physical relevance of such an idealised description. A real beam always has a - whatever small but - non-zero momentum spread and also a wave-length distribution. To a certain degree one can save the day by introducing a superposition of momenta,

$$|k\rangle \mapsto \int a(k)|k\rangle dk, \quad \int |a(k)|^2 dk = 1, \quad (2.1.2)$$

for example to be able to localise the neutron somewhere in space in contrast to the odd property of a plane wave that it is spread over the whole space at the same time. What we get

is a superposition state with well defined phase relations between the different constituting partial waves, a *coherent superposition*.

Such states are usually not an adequate description of an experiment since adverse conditions are always against coherent superpositions - *dephasing* or - more generally *decoherence* - destroys the phase relation among the partial waves. It is only if the system is completely separated from its environment (*closed system*) that superpositions can be kept for an arbitrarily long time. In reality, it is only the degree of decoherence that the experimenter can affect by elaborate techniques, but not its presence. In the recent past the quest for the quantum computer has put forth numerous ideas and techniques how to fight decoherence. For example, the possibility to store ions for as long as 20 seconds [HSKH<sup>+</sup>05] in a superposition state has been demonstrated in Innsbruck, or, it has become feasible to send entangled photons as long as 600 meters through the atmosphere as shown in Zeilinger's group [UJA<sup>+</sup>04]. But sooner or later, decoherence takes over and what is called a *pure state* is turned into a *mixed state*. Since the experimenter cannot keep track of all the environmental interactions, the full information about the state is lost. Such states deserve another notation than pure state, they are represented by *density operators* (or *density matrices*) instead of state vectors in Hilbert space. The simplest density operator is a pure state projection operator,  $|\psi\rangle \mapsto |\psi\rangle\langle\psi| \equiv P_\psi$  that has the defining projector property  $P_\psi = P_\psi^2$ . It is an element of the projective Hilbert space as we have already learnt in Section 1.2.2. A linear combination of  $P_\psi$ 's denotes a mixed state and can be regarded as mixing several pure states with different weights,

$$\rho = \sum_k p_k |\psi_k\rangle\langle\psi_k|, \quad \sum_k p_k = 1, \quad (2.1.3)$$

where  $|\psi_k\rangle$  are arbitrary vectors in Hilbert space and need not constitute a set of basis vectors.

$$\rho = \sum p(v) |\psi(v)\rangle\langle\psi(v)| dv, \quad \int p(v) dv = 1, \quad (2.1.4)$$

denotes the continuous version. The sum over all possible states of the system must be unity by the laws of probability. Unlike the pure superposition state in (2.1.2), for instance, the phase relation between the constituting  $|\psi_i\rangle\langle\psi_i|$  is not maintained, it is an *incoherent* sum and  $\rho \neq \rho^2$ .

A proper density matrix  $\rho$  has to be Hermitian and positive, otherwise the interpretation as a (incoherent) sum of pure states (2.1.3) which occur with a specific probability fails. In addition normalisation is maintained by demanding the trace of  $\rho$  to be unity. In summary,

$$\rho = \rho^\dagger \quad (2.1.5)$$

$$\rho > 0 \quad (2.1.6)$$

$$\text{Tr} \rho = 1. \quad (2.1.7)$$

**Example of a mixed state** Let us continue with the neutron beam example. The concept of mixed states is best illustrated by the spin part of the wave function (2.1.1), since the

finite dimensionality of the spin space allows for a more elegant approach than the in principle<sup>1</sup> infinite dimension of momentum space. Suppose that you want to measure the spin polarisation of a beam prepared in the  $|s\rangle$ -state and you find an apparatus that perfectly enables you to measure the polarisation along the  $\vec{n}$ -axis. Since the state  $|s\rangle$  is an eigenstate to the polarisation measurement operator  $s = \vec{n}_s \cdot \vec{\sigma}$  a definite measurement direction  $\vec{n}_s$  can be found, such that all neutrons are in the positive eigenstate. If the apparatus can discriminate between positive and negative polarised neutrons, all neutrons will be in the positive and no single one in the negative channel. In practice, such a situation will not be encountered since it would require a perfectly polarised neutron beam by either a perfectly polarised source or a perfect selection mechanism. As example, take a Stern-Gerlach apparatus [GS22] oriented in direction  $\vec{n}_s$ , which spatially separates the neutrons according to their polarisation due to a magnetic field gradient. Dismissing one of these separated beams, the state  $|s\rangle$  can be prepared. Unfortunately, it is for instance not possible to have a constant magnetic field gradient all over the beam cross section and the experimenter is left with the maybe dissatisfying situation of either improving the accuracy of the field gradient or inserting smaller and smaller apertures. In the former it is (at least in the beginning) a time and money issue to improve the homogeneity of the field over the beam cross section and keeping at the same time the cross section, i. e. the intensity, constant. In the latter, one gains better polarisation but loses drastically intensity. One has to find a trade-off somewhere in between, but things won't get perfect, the resulting state will be a *mixture* of neutrons passing the apparatus at different places and therefore having slightly different spin directions in the end.

The density matrix consists of the differently polarised spin states

$$\rho = p_1 |\uparrow\rangle\langle\uparrow| + p_2 |\downarrow\rangle\langle\downarrow|, \quad (2.1.8)$$

with  $p_1 + p_2 = 1$ . The eigenvalues  $p_1$  and  $p_2$  denote the probability to detect either a  $|\uparrow\rangle$  or  $|\downarrow\rangle$  polarised neutron, respectively. In the following it will be sometimes convenient to parametrise the state by the *degree of polarisation*  $r$ ,

$$\rho = \frac{1+r}{2} |\uparrow\rangle\langle\uparrow| + \frac{1-r}{2} |\downarrow\rangle\langle\downarrow|. \quad (2.1.9)$$

$r = 0$  denotes a totally mixed state with eigenvalues  $1/2$ . For a pure state,  $|r| = 1$  and we either have a beam polarised in  $|\uparrow\rangle$  or  $|\downarrow\rangle$  direction. The further evolution of  $\rho$  can then be either unitary so that the degree of polarisation does not change, or non-unitary yielding finally a totally mixed state.

**Coupling to the environment** Theoretically, decoherence is explained by the coupling of the system to its environment and this interaction generates a superposition state between system and environment. Forgetting subsequently the further evolution of the environment and focusing only on the system itself a transformation from the formerly pure to a mixed

---

<sup>1</sup>Compactifying the state space by introducing periodic boundary conditions cures this “defect”. The basis is then again finite and calculations are simpler, but still the two dimensions of spin are easier to deal with.

state is noticed. In the language of quantum mechanics, the initial state  $|\Psi\rangle = |\psi\rangle \otimes |\alpha\rangle$  is a product state of the system ( $|\psi\rangle$ ) and the environment ( $|\alpha\rangle$ ), each of them being pure<sup>2</sup>. It is an element of the *extended Hilbert space*  $\mathcal{H}_E = \mathcal{H}_S \otimes \mathcal{H}_A$ . The advantage of including the environment into the theoretical description of the system is that one can always find a unitary operator describing the evolution of the system plus environment (e. g. [NC00, p. 357 ff.]),

$$|\Psi\rangle \mapsto |\Psi_t\rangle = U_E |\Psi\rangle. \quad (2.1.10)$$

The  $U_E$  can in general not be factorised, i. e. written as a tensor product  $U_E = U_S \otimes U_A$  with  $U_S$  acting only on the system and  $U_A$  only on the environment. Only if the coupling between system and environment vanishes we have  $U_E = U_S \otimes U_A$  and the system stays in a pure state. Consequently, in general,  $|\Psi_t\rangle$  cannot be factorised either.

“Forgetting” what happened to the environment amounts to “tracing out the environment” in the quantum mechanical calculus and is denoted by the *partial trace*  $\text{Tr}_A$ ,

$$\text{Tr}_A [|\psi_1\rangle\langle\psi_2| \otimes |\alpha_1\rangle\langle\alpha_2|] \equiv |\psi_1\rangle\langle\psi_2| \text{Tr}[|\alpha_1\rangle\langle\alpha_2|], \quad (2.1.11)$$

where  $\text{Tr}$  denotes the usual trace operation. This definition is made complete by demanding the linearity of  $\text{Tr}_A$  in its arguments.

Given a pure state in the total Hilbert space that has evolved from the initial state according to the unitary evolution Eq. 2.1.10,

$$|\Psi_t\rangle = \sum_{ij} c_{ij} |\psi_i\rangle \otimes |\alpha_j\rangle \quad (2.1.12)$$

the partial trace operation tells us what happens to the state of the system if the environment is neglected,

$$\begin{aligned} \text{Tr}_A [|\Psi_t\rangle\langle\Psi_t|] &= \text{Tr}_A \left[ \sum_{ij,kl} c_{ij} c_{kl}^* |\psi_i\rangle\langle\psi_k| \otimes |\alpha_j\rangle\langle\alpha_l| \right] \\ &= \sum_{ik} |\psi_i\rangle\langle\psi_k| \text{Tr} \left[ \sum_{jl} c_{ij} c_{kl}^* |\alpha_j\rangle\langle\alpha_l| \right] = \sum_{ijk} |\psi_i\rangle\langle\psi_k| c_{ij} c_{kj}^* = \rho, \end{aligned} \quad (2.1.13)$$

where it has been assumed that the basis vectors of the ancilla<sup>3</sup> (environmental) Hilbert space  $|\alpha_i\rangle$  are orthonormal.

$\rho_\Psi$ , the pure state in the total Hilbert space  $\mathcal{H}_E$ , or, more precisely of the operator algebra

---

<sup>2</sup>Whether the environment is in a pure state or not is rather a technical question. Literally, it is inconsistent to speak of environment and denote its state as a pure state since this implies that we know everything about it and this is in opposition to the terminus “environment”. For a model environment, however, a pure state approximation will do.

<sup>3</sup>“Ancilla” and “environment” will be used on equal footing, since it is not necessary to distinguish between an ancilla system that is usually a second particle of the same kind and an environment with lots of other particles.

## 2. GEOMETRIC PHASE FOR MIXED STATES

---

of the extended Hilbert space  $\mathcal{O}(\mathcal{H}_E)$  [Haa96], is mapped onto a state  $\rho \in \mathcal{O}(\mathcal{H}_S)$ ,

$$\text{Tr}_E : \mathcal{O}(\mathcal{H}_E) \mapsto \mathcal{O}(\mathcal{H}_S).$$

$\rho$  is in general a density operator denoting a mixed state ( $\rho \neq \rho^2$ ). The transition from a pure to a mixed state represents the loss of information when forgetting about the environmental degrees of freedom.

The partial trace can be most easily explained on the example of a fully entangled state,  $|\Psi\rangle = 1/\sqrt{2}(|0\rangle_S \otimes |0\rangle_A + |1\rangle_S \otimes |1\rangle_A) \in \mathcal{H}_E$ , where both the system and the ancilla are two-dimensional with basis states  $\{|0\rangle, |1\rangle\}$ , also called a *Bell-state* after John S. Bell and his paper [Bel64] on the Einstein-Podolsky-Rosen paradox [EPR35]. In density matrix notation the same state reads

$$\begin{aligned} |\Psi\rangle\langle\Psi| &= \frac{1}{2}(|0\rangle\langle 0| \otimes |0\rangle\langle 0| + |1\rangle\langle 1| \otimes |1\rangle\langle 1| \\ &\quad + |1\rangle\langle 0| \otimes |1\rangle\langle 0| + |0\rangle\langle 1| \otimes |0\rangle\langle 1|) \in \mathcal{O}(\mathcal{H}_E) \end{aligned} \quad (2.1.14)$$

and performing the partial trace over the environmental degrees of freedom means that we keep only terms with diagonal elements  $|0\rangle \otimes \langle 0|$  or  $|1\rangle \otimes \langle 1|$  in the ancilla. We are left with a totally mixed state of the system,

$$\rho = \text{Tr}_A [|\Psi\rangle\langle\Psi|] = \sum_i^{\dim \mathcal{H}_A} {}_A \langle i | \Psi \rangle \langle \Psi | i \rangle_A = \frac{1}{2}(|0\rangle\langle 0| + |1\rangle\langle 1|) \in \mathcal{O}(\mathcal{H}_S), \quad (2.1.15)$$

hence, the name *totally entangled state*. It can be regarded as if the system is in the state  $|0\rangle$  with probability one half and with same probability in the state  $|1\rangle$ .

**Non-unitary evolution** More generally, suppose the system is initially in the state  $|\Psi\rangle = |\psi_1\rangle \otimes |\alpha_1\rangle$ , or, in density matrix notation,  $P_\Psi(0) = |\Psi\rangle\langle\Psi| = |\psi_1\rangle\langle\psi_1| \otimes |\alpha_1\rangle\langle\alpha_1|$ . The time evolution is determined by the unitary operator  $U_E$ , and therefore

$$P_\Psi(t) \equiv |\Psi_t\rangle\langle\Psi_t| = U_E |\Psi\rangle\langle\Psi| U_E^\dagger. \quad (2.1.16)$$

Taking the partial trace we find

$$\begin{aligned} \rho_t &= \text{Tr}_A P_\Psi(t) = \text{Tr}_A [U_E |\Psi\rangle\langle\Psi| U_E^\dagger] = \text{Tr}_A [(U_E |\psi_1\rangle \otimes |\alpha_1\rangle)(\langle\psi_1| \otimes \langle\alpha_1| U_E)] \\ &= \sum_\mu \langle \alpha_\mu | U_E | \alpha_1 \rangle \rho \langle \alpha_1 | U_E^\dagger | \alpha_\mu \rangle \\ &\equiv \sum_\mu M_\mu \rho M_\mu^\dagger, \end{aligned} \quad (2.1.17)$$

which is called the *operator sum representation* [Pre98] or *Kraus representation* [Kra83].

$\rho_t$  is in general a mixed state,

$$\rho_t = \sum_{\mu} M_{\mu} |\psi_1\rangle \langle \psi_1| M_{\mu}^{\dagger} \neq \rho_i^2.$$

The operators  $M_{\mu}$  satisfy the relation  $\sum_{\mu} M_{\mu} M_{\mu}^{\dagger} = 1$ , which follows from the unitarity of  $U_E$ . But given a specific evolution of the system the choice of the  $M_{\mu}$ 's is not unique. One can choose another bases in the ancilla Hilbert space  $\{|\alpha'_{\mu}\rangle\}$  that is unitarily connected to the  $|\alpha_{\mu}\rangle$ ,  $|\alpha'_{\mu}\rangle = V|\alpha_{\mu}\rangle$ , resulting in different

$$M'_{\mu} = \langle \alpha'_{\mu} | U_E | \alpha'_{\mu} \rangle = \langle \alpha_{\mu} | V^{\dagger} U_E V | \alpha_{\mu} \rangle \neq \langle \alpha_{\mu} | U | \alpha_{\mu} \rangle = M_{\mu}.$$

## 2.2 Geometric Phase for Mixed States

A geometric phase for mixed states has to fulfil the same criteria as its pure state analogue. That is, it has to be gauge invariant such that it is not possible to dispose of it by a different choice of phases of the eigenstates. Furthermore, it must be reparametrisation invariant in order to be independent of the rate at which the system is transported. It must be a property of the path in the state of density matrices only. It is not difficult to imagine that things get more complicated in the mixed state case. Indeed, we will notice that there are several possibilities to define a mixed state geometric phase that are in general incompatible. Furthermore, the fact that mixed states have to be represented by matrices instead of vectors leads to non-abelian, matrix-valued ‘‘phase factors’’.

I will draw a demarcation line, albeit artificial, between two different kinds of geometric phases and its connection to mixed states: As indicated in the previous section, when mentioning mixed states one is automatically lead to questions about decoherence and the stability of quantum systems under influence of perturbations from the environment. Much importance is attributed to this issue, especially, when it comes to quantum information technology and it is augured that the geometric phase may be more robust compared to e. g. the dynamical phase. Constructing a quantum gate, say, a phase transformation, one can choose a unitary operator that yields a particular output state such that the input state is parallel transported and the transformation is then called a *geometric quantum gate*. Perturbations in the gate parameters bring about slightly perturbed paths and, consequently, different output states dependent on the actual perturbation. The ensemble of output states has to be described by a mixed state and one is tempted to talk already about a mixed state geometric phase. However, the measured mixed state phase at the end is in general not a purely geometric phase. It is dependent on the dynamics of the perturbations and may not fulfil some kind of parallel transport condition, hence, it is rather vague to term the resulting quantity a geometric phase.

In contrast, in this section I will discuss ‘‘genuine’’ definitions of a mixed state geometric phase in terms of parallel transports in the space of density operators. The role of the geometric phase in decoherence will be postponed to Chapter 5.

As in the pure state case, the geometric phase is associated to the path of a state in its subjacent state space. The prescription how the state has to evolve in order to produce only a geometric phase is given by the *parallel transport law* (Eq. 1.2.48). The generalisation of this parallel transport law to the mixed state case is however not unique. On the one hand side one can demand the parallel transport of the eigenstates of the mixed state. This approach is particularly suited for the unitary evolution of an initially non-degenerate mixed state in an interferometer [SPE<sup>+</sup>00]. It has been generalised later to degenerate mixed states [STB<sup>+</sup>03] and finally to non-unitary evolutions by a kinematic approach by Tong *et al.* [TSKO04]. Besides, Ericsson *et al.* [ESB<sup>+</sup>03] – and independently Peixoto *et al.* [dFdTPN03] – proposed the extension of the to non-unitary evolutions by introducing an ancilla Hilbert space and replacing the unitary evolution by a Kraus map [Kra83]<sup>4</sup>.

On the other hand side, the possibility to represent a mixed state as a vector in a higher dimensional Hilbert space suggests the definition of a geometric phase via such a *purification*. A rigorous treatise of this approach has been put forward by Uhlmann [Uhl86, Uhl95] and it works for both for unitary and non-unitary processes [TS03]. Another approach taken by Chaturvedi *et al.* [CEM<sup>+</sup>04] uses methods from differential geometry to obtain a mixed state geometric phase.

We notice, that there is still a large diversity in possible definition of a mixed state geometric phase, however, with respect to off-diagonal generalisations to be presented later I will mainly focus on the interferometric approach by Sjöqvist [SPE<sup>+</sup>00] and Uhlmann's definition [Uhl86].

## 2.3 Interferometric mixed state geometric phase

In Section 1 the pure state geometric phase has been defined as the phase difference between an initial state  $|\psi_i\rangle$  and a final state  $|\psi_f\rangle = U^\parallel|\psi_i\rangle$  for a parallel transporting unitary map  $U^\parallel$ . An obvious way to test such a phase difference is by means of interferometry, where the system in one arm is manipulated by the unitary operation denoted by  $U^i$  and leads to the intensity

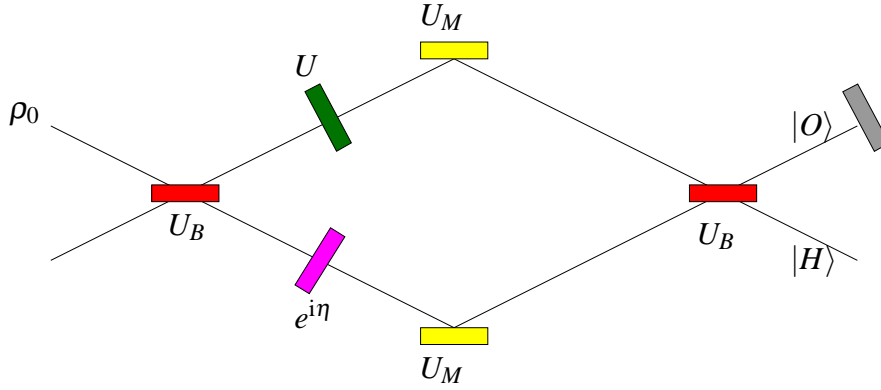
$$I \propto 1 + |\langle\psi_i|U^i|\psi_i\rangle| \cos(\eta + \arg\langle\psi_i|U^i|\psi_i\rangle).$$

A natural extension to mixed states is to replace the pure input state  $|\psi\rangle$  by a mixed input state  $\rho_0$ , for example a neutron beam with a portion  $p_1$  of spin-up polarised and  $p_2$  spin-down polarised neutrons, and look once more at the phase shift of the interference pattern (Figure 2.1).

The input state  $\rho_0 = \sum_k p_k |\psi_k\rangle\langle\psi_k|$  describes the internal state of the incident particle, e. g. the spin state of the neutron; or the polarisation state of a light beam. The internal Hilbert space  $\mathcal{H}_S$  is spanned by the vectors  $|\psi_k\rangle$ ,  $k = 1, 2, \dots, \dim \mathcal{H}_S$ . Applying  $U^i$  – which acts only on  $\mathcal{H}_S$  like for example a magnetic field interacting with the neutrons' spin – in one path and a phase shift operator  $U_{PS}(\chi) = e^{i\eta}$  in the other path the intensity  $I_\rho = \text{Tr}[P_O\rho_{out}]$

---

<sup>4</sup>Their approaches have the disadvantage that the Kraus representation of a particular map is not unique.


 Figure 2.1: Mach-Zehnder Interferometer with mixed input state  $\rho_0$ .

of the output state can be calculated. The output state is

$$\rho_{out} = P_O U_B U_M U_{PS}(\chi) U^i U_B \rho_0 U_B^\dagger U^{i\dagger} U_{PS}^\dagger(\chi) U_M^\dagger U_B^\dagger P_O, \quad (2.3.1)$$

where  $U_B$  represents a beam splitter,  $U_M$  is a mirror and  $P_O$  is the projection to the output beam, taken to be  $|O\rangle$ . Consequently, the output intensity  $I_\rho$  is given by

$$I_\rho \propto 1 + |\text{Tr}(U^i \rho_0)| \cos[\eta - \arg \text{Tr}[U^i \rho_0]]. \quad (2.3.2)$$

One arrives at this equation either by calculating explicitly the density operator in (2.3.1) or, more intuitively, by summing up all the contributions of the different orthogonal state incoherently,

$$I = \sum_k I_k \propto \sum_k p_k (1 + |\langle \psi_k | U^i | \psi_k \rangle| \cos(\eta - \arg \langle \psi_k | U^i | \psi_k \rangle)). \quad (2.3.3)$$

(2.3.2) and (2.3.3) are equivalent which can be seen by using the harmonic addition theorem [Wei].

The definition of the mixed state geometric phase  $\phi_\rho$  must obviously be associated to the additional shift  $\arg \text{Tr}[U^i \rho_0]$  of the intensity pattern. Indeed, for parallel transporting unitarities  $U^i = U^\parallel$ , the geometric phase for mixed states is defined by [SPE<sup>+</sup>00]

$$\phi_\rho \equiv \arg \text{Tr}[U^\parallel \rho_0] = \arg \left( \sum_k p_k v_k e^{i\beta_k} \right), \quad (2.3.4)$$

where  $v_k = |\langle \psi_k | U^\parallel | \psi_k \rangle|$  is the visibility factor and  $\beta_k = \arg \langle \psi_k | U^\parallel | \psi_k \rangle$  the phase contribution of a single basis state  $|\psi_k\rangle$ .  $\phi_\rho$  reduces to the Pancharatnam phase difference  $\arg \langle \psi_0 | U | \psi_0 \rangle$  for a pure input state  $\rho_0 = |\psi_0\rangle \langle \psi_0|$ .

What is the parallel transport condition in the mixed state case?  $U^\parallel$  has to fulfil the

parallel transport conditions

$$\langle \psi_j | U^{\parallel \dagger}(t) \dot{U}^{\parallel}(t) | \psi_j \rangle = 0, \quad 1 < j < \dim \rho, \quad (2.3.5)$$

where the dot denotes the derivative with respect to the continuous parameter  $s$  of  $U = U(s)$ . This means that each eigenstate must be parallel transported, which in turn guarantees vanishing dynamical phase

$$\phi_d = -\frac{1}{\hbar} \int_{s_1}^{s_2} ds \operatorname{Tr}[\rho(s) H(s)] = -i \int_{s_1}^{s_2} ds \operatorname{Tr}[\rho(s) U^\dagger(s) \dot{U}(s)].$$

Then, the mixed state geometric phase  $\phi_\rho$  does not depend on the dynamics but merely on the geometry of the (open) unitary path in the space of density operators traced out by  $\rho(s) = U^{\parallel}(s) \rho_0 U^{\parallel \dagger}(s)$ ,  $s \in [s_1, s_2]$ .

Experimental tests of this concept has been carried out using nuclear magnetic resonance [DZS<sup>+</sup>03, GK06], photons [EAB<sup>+</sup>05] and neutrons [KSH<sup>+</sup>05].

### 2.3.1 Parallel transport

Equation (2.3.5) denotes the parallel transport condition imposed on the basis states of the Hilbert space on which the density operator  $\rho_0$  is defined. In contrast to the pure state case the parallel transport involves the complete set of orthonormal basis vectors. It requires that the phase difference between two adjacent basis states vanishes. To see the connection to the pure state parallel transport condition (Eq. 1.2.48) let us formulate the parallel transport condition in terms of the instantaneous basis  $|\psi_k(s)\rangle = U(s)|\psi_k\rangle$ , where  $U(s)$  is a continuous one-parameter family  $\{U(s), s \in [s_1, s_2] | U(s_1) = \mathbb{1}\}$  of unitarities.  $U(s)$  maps any initial complete orthonormal basis  $\{|\psi_k\rangle\}$  of a Hilbert space  $\mathcal{H}$  of dimension  $N$  to a continuous set of complete orthonormal bases  $\{|\psi_k(s)\rangle\}$  of the same  $\mathcal{H}$ . Inserting  $|\psi_k\rangle = U^{-1}(s)|\psi_k(s)\rangle = |\psi_k(0)\rangle$  into Eq. (2.3.5) leads to

$$\langle \psi_k(s) | \left( \frac{d}{ds} U(s) \right) U^\dagger(s) | \psi_k(s) \rangle = 0. \quad (2.3.6)$$

The unitary evolution operator  $U(s)$  stems from the according (time-dependent) Schrödinger equation and has to fulfil

$$i\dot{U}(s) = H(s)U(s), \quad (2.3.7)$$

which entails

$$\langle \psi_k(s) | H(s) | \psi_k(s) \rangle = i\hbar \langle \psi_k(s) | \frac{d}{ds} | \psi_k(s) \rangle = 0, \quad \forall k. \quad (2.3.8)$$

The local accumulation of phase along the unitary path has to vanish for each instantaneous basis state  $|\psi_k(s)\rangle$  in accordance with the pure state parallel transport condition (1.2.48). Any parallel transporting unitarity is denoted by  $U^{\parallel}$  in the following. Moreover, an instantaneous non-degenerate density operator whose eigenvectors coincide with the basis  $\{|\psi_k(s)\rangle\}$  is said

to be parallel transported by  $U^{\parallel}$  if Eq. (2.3.8) is satisfied.

### 2.3.2 Gauge invariance

With the condition (2.3.5) the parallel transporting unitarity  $U^{\parallel}$  is completely specified and the resulting phase shift in the interference pattern (2.3.2) is purely geometric. However, if  $U(s)$  does not fulfil the parallel transport condition additional dynamical phase contributions are accumulated and  $\arg \text{Tr}[U(s)\rho_0]$  is not purely geometric anymore. To construct a gauge invariant quantity for a general unitary evolution, note, that such a unitary can be multiplied by an element

$$g_N(s) = \sum_{n=1}^N e^{i\theta_n(s)} |\psi_n\rangle\langle\psi_n| \in \underbrace{U(1) \times U(1) \times \dots \times U(1)}_N \quad (2.3.9)$$

from the right. Such a transformation leaves the path of the density matrix invariant [STB<sup>+</sup>03],

$$\rho(s) = U(s)g_N(s)\rho_0g_N^\dagger(s)U(s) = U(s)\rho_0U^\dagger(s), \quad (2.3.10)$$

since  $\rho_0$  is diagonal in the bases  $\{|\psi_n\rangle\}$ . The  $\theta_n$ 's are real time-dependent parameters such that  $\theta_n(0) = 0$ . The unitary

$$\tilde{U}(s) = U(s)g_N(s) = U(s) \sum_{n=1}^N e^{i\theta_n(s)} |\psi_n\rangle\langle\psi_n| \quad (2.3.11)$$

can be used to satisfy the parallel transport condition by choosing the  $\theta_n$ 's appropriately. Inserting  $\tilde{U}(s)$  into Eq. (2.3.5) we obtain the condition

$$\theta_n(s) = \theta_n^{\parallel}(s) = i \int_{s_1}^{s_2} \langle\psi_n|U^\dagger(s')\dot{U}(s')|\psi_n\rangle ds' \quad (2.3.12)$$

and

$$U^{\parallel}(s) = U(s) \sum_{n=1}^N e^{i \int_{s_1}^{s_2} \langle\psi_n|U^\dagger(s')\dot{U}(s')|\psi_n\rangle ds'} |\psi_n\rangle\langle\psi_n|. \quad (2.3.13)$$

The total geometric phase  $\phi_\rho$  with the parallel transporting unitary  $U^{\parallel}(s)$  is

$$\phi_\rho = \arg \text{Tr} [\rho_0 U^{\parallel}(s)] = \arg \left\{ \sum_n p_n \langle\psi_n|U(s)|\psi_n\rangle e^{i\theta_n(s)} \right\} \quad (2.3.14)$$

which is a gauge invariant property of the path of the density operator for  $\theta_n = \theta_n^{\parallel}$ . Explicitly, the mixed state geometric phase is

$$\phi_g \equiv \arg \left\{ \sum_n [p_n \langle\psi_n|U(s)|\psi_n\rangle e^{-\frac{i}{\hbar} \int_0^s ds' \langle\psi|U(s')^\dagger \dot{U}(s')|\psi\rangle}] \right\} \quad (2.3.15)$$

as proposed by Singh *et al.* [STB<sup>+</sup>03] and constitutes the extension of Eq. (2.3.5) to arbitrary unitarities.

### 2.3.3 Degenerate density matrices

For degenerate systems one has to pay attention that in the degenerate subspace the unitary  $U$  can be multiplied with an element of the unitary group  $U(K)$ ,  $K$  being the dimension of the degenerate subspace, without changing the path of  $\rho$ . Indeed, if the eigenvalues  $p_k$ ,  $k = 1, \dots, K$  are degenerate and  $p_i$ ,  $i = K + 1, \dots, N$  are non-degenerate, one can multiply the unitary evolution operator  $U$  with an additional (unitary) matrix

$$V(s) = \begin{pmatrix} \alpha(s) & & & \\ & e^{i\beta_{K+1}(s)} & & \\ & & \dots & \\ & & & e^{i\beta_N(s)} \end{pmatrix}. \quad (2.3.16)$$

$V(s)$  belongs to the product group  $U(K) \times U(1) \times U(1) \times \dots \times U(1)$  and does not affect the evolution of  $\rho(s)$ ,

$$\rho(s) = U(s)\rho_0U(s)^\dagger = U(s)V(s)\rho_0V(s)^\dagger U(s)^\dagger.$$

This has to be reflected in the parallel transport condition and in the definition of a functional similar to (2.3.15). To completely determine a parallel transporting  $U$  the parallel transport condition (2.3.5) has to be generalised to

$$\langle \psi_i | U^{\parallel\dagger}(s) \frac{d}{ds} U^{\parallel}(s) | \psi_j \rangle = 0, \quad i, j = 1, 2, \dots, K, \quad (2.3.17)$$

$$\langle \psi_k | U^{\parallel\dagger}(s) \frac{d}{ds} U^{\parallel}(s) | \psi_k \rangle = 0, \quad k = K + 1, \dots, N. \quad (2.3.18)$$

Similar to the non-degenerate case the gauge invariant geometric phase is defined by

$$\phi_g \equiv \arg \text{Tr} [\rho_0 U(s) F[U, s_2 - s_1]]. \quad (2.3.19)$$

The functional  $F[U, \Delta s]$  ( $\Delta s \equiv s_2 - s_1$ ) can be written in Block diagonal form,  $F[U, \Delta s] = F_{\mathcal{H}_K} \oplus F_{\mathcal{H}_{K+1}} \oplus F_{\mathcal{H}_{K+1}} \oplus \dots \oplus F_{\mathcal{H}_N}$ , where

$$F_{\mathcal{H}_m} = \langle \psi_i | P \exp \left( -\frac{1}{\hbar} \int_{s_1}^{s_2} ds U(s)^\dagger \dot{U}(s) | \psi_j \right), \quad i, j = 1, 2, \dots, \dim \mathcal{H}_m \quad (2.3.20)$$

if  $\dim \mathcal{H}_m \neq 1$  and

$$F_{\mathcal{H}_m} = \exp \left\{ -\frac{1}{\hbar} \int_{s_1}^{s_2} ds \langle \psi_i | U(s)^\dagger \dot{U}(s) | \psi_j \rangle \right\} \quad (2.3.21)$$

otherwise [STB<sup>+</sup>03]. This functional defines the geometric phase even for degenerate mixed states.

### 2.3.4 Non-unitary evolution

The generalisation to non-unitary evolution has been addressed in Refs. [ESB<sup>+</sup>03, dFdTPN03] in terms of Kraus operators, but it may yield different values of geometric phase when using different Kraus representations. Tong *et al.* [TSKO04] resolved this ambiguity by defining a geometric phase based on the path

$$\mathcal{C} : s \in [s_1, s_2] \mapsto \rho(s) = \sum_{k=1}^N p_k(s) |\psi_k(s)\rangle \langle \psi_k(s)|. \quad (2.3.22)$$

The non-unitary nature of the evolution is expressed by the time-dependent eigenvalues  $p_k(s)$  of the mixed state  $\rho(s)$ . In brief, the geometric phase is found by taking the purification of  $\rho(s)$ ,

$$|\Psi(s)\rangle = \sum_{k=1}^N \sqrt{p_k(s)} |\psi_k(s)\rangle \otimes |a_k\rangle$$

to the pure state  $|\Psi(s)\rangle \in \mathcal{H}_S \otimes \mathcal{H}_A$  in the extended Hilbert space. The phase difference of the initial and final purification defines the geometric phase (for  $V^{\parallel}$  parallel transporting the basis states)

$$\arg \langle \Psi(s_1) | \Psi(s_2) \rangle = \arg \left( \sum_{k=1}^N \sqrt{p_k(s_1)p_k(s_2)} \langle \psi_k(s_1) | V^{\parallel}(s_2) | \psi_k(s_1) \rangle \right).$$

## 2.4 Uhlmann Holonomies

Uhlmann's approach is somewhat different to Sjöqvist's definition of a mixed state geometric phase in that in some way physical intuition is replaced by mathematical rigour. Uhlmann's approach is slightly more general, because its basic definition does not distinguish between unitary and non-unitary evolution, as opposed to the original interferometric definition in Eq. (2.3.4), but its operational meaning is not as straightforward. The main difference is that Uhlmann defines not only a geometric phase factor, but non-abelian holonomy invariants represented by matrices instead of complex numbers. In brief, Uhlmann [Uhl76, Uhl86, Uhl93] proposed a phase holonomy for paths of density operators utilising a purification scheme of mixed into pure states obtained via a certain parallelity condition. The idea is to purify each quantum state, either pure or mixed, to a pure state in an extended Hilbert space. This purification can be represented by an (Hilbert-Schmidt) operator in the extended space and is called an *amplitude*. To each path of density operators a corresponding path of the amplitudes can be constructed which projects down to the original path. The exceptional choice of a path of amplitudes by imposing the parallel transport condition leads to a unique path in the extended Hilbert space which is a property only of the path of the states and serves to define a *holonomy invariant*.

### 2.4.1 Construction of amplitudes

Let us try to construct these amplitudes that represents the states as operators in a higher dimensional Hilbert space starting from pure states and consequently generalising these to mixed states.

The elements of projective Hilbert space ( $\mathcal{P}$ ) have the form of projection operators.  $P_\psi \equiv |\psi\rangle\langle\psi| \in \mathcal{P}$  represents all states  $e^{i\alpha}|\psi\rangle \in \mathcal{H}$  with real  $\alpha$ . Or, the other way round,  $W = e^{i\alpha_0}|\psi\rangle$  is a possible *amplitude* of the state operator  $P_\psi$  since a multiplication of  $W$  and its daggered version  $W^\dagger$  leads back to the state operator,

$$WW^\dagger = e^{i\alpha_0}|\psi\rangle\langle\psi|e^{-i\alpha_0} = |\psi\rangle\langle\psi|.$$

By relaxing the condition that  $P_\psi$  is a projection operator satisfying  $P^2 = P$  the state space is extended to mixed states. These are nothing else than linear combinations of  $P$ 's,

$$\rho = \sum_i a_i P_{\psi_i} \quad (2.4.1)$$

with  $a_i \in \mathbb{R}$  and  $\sum_i a_i = 1$ . We can immediately see that  $\rho^2 \neq \rho$  and that the amplitude  $W$  of  $\rho$  is not simply a sum of kets multiplied by an arbitrary phase factor. The latter can easily be verified by trying the converse and making the ansatz  $W''' = \sum_i b_i |\psi_i\rangle$ ,  $b_i \in \mathbb{C}$ , and multiply with its adjoint  $W'''^\dagger = \sum_j b_j^* \langle\psi_j|$ ,

$$W'''W'''^\dagger = \sum_{i,j} b_i b_j^* |\psi_i\rangle\langle\psi_j| = \sum_i |b_i|^2 |\psi_i\rangle\langle\psi_i| + \sum_{i \neq j} b_i b_j^* |\psi_i\rangle\langle\psi_j|. \quad (2.4.2)$$

If the off-diagonal terms vanished this quantity would resemble the original mixed state  $\rho$ . But the off-diagonal terms  $|\psi_i\rangle\langle\psi_j|$  vanish in general only if all but one  $b_i$  vanish and this is true only for pure states. In this case the choice of  $b_1 = \sqrt{a_1} e^{i\alpha_0}$  yields the pure state  $\rho = a_1 P_{\psi_1}$ . So, this ansatz works only for pure states and their purifications.

To remedy this defect we can choose another form of the amplitude,

$$W'' = \sum_i a_i |\psi_i\rangle \otimes \langle\phi_i|. \quad (2.4.3)$$

We have simply added another other Hilbert space  $\mathcal{H}_A$  of same dimensionality as the systems Hilbert space  $\mathcal{H}_S$ , the *ancilla* Hilbert space, with an orthonormal set of basis vectors  $\langle\phi_j|$ . The amplitude  $W''$  is therefore an operator acting on the extended Hilbert space  $\mathcal{H}_E = \mathcal{H}_S \otimes \mathcal{H}_A$ . This procedure is called *purification*, and it can be shown that every state  $\rho \in \Omega(\mathcal{H})$  has an extension to an operator acting on  $\mathcal{H}_E$  which is pure if the dimension of  $\mathcal{H}_A$  is at least the same as  $\dim \mathcal{H}_S$ . This is the mathematical expression for the fact that an open system where the environmental interactions cannot be neglected is embedded into a larger system comprising also the environment. The subtle difference to the usual purification is that here the density operators are purified again by a operator valued quantity instead of a pure state vector, but these descriptions are equivalent as shown in [Uh191b].

The result justifies this slight complication in (2.4.3): Forming the quantity  $W''W''^\dagger$  we obtain

$$\begin{aligned}
 W''W''^\dagger &= \sum_{i,j} a_i a_j^* (|\psi_i\rangle \otimes \langle \phi_i|) (\langle \psi_j| \otimes \langle \phi_j|) \\
 &= \sum_{i,j} a_i a_j^* |\psi_i\rangle \langle \psi_j| \otimes \underbrace{\langle \phi_i | \phi_j \rangle}_{\delta_{ij}} \\
 &= \sum_i |a_i|^2 |\psi_i\rangle \langle \psi_i|. \tag{2.4.4}
 \end{aligned}$$

The only remaining flaw is the square modulus of the coefficients, which can be corrected by taking the square root of the  $a_i$  to get an amplitude of  $\rho$ ,

$$W' = \sum_i \sqrt{a_i} |\psi_i\rangle \otimes \langle \phi_i|. \tag{2.4.5}$$

Extracting the square root is admissible since the  $a_i$  have to be real according to the requirements on a mixed state (Eq. 2.1.5). Furthermore, a multiplication by a unitary matrix is admissible since it does not alter the state  $\rho$ ,

$$WW^\dagger = W \underbrace{VV^\dagger}_1 W^\dagger.$$

The unitary  $V$  reflects the additional *gauge* degree of freedom similar to the total phase factor  $e^{i\alpha_0}$  from the pure state example. The general form of an amplitude is consequently

$$W = \sum_i \sqrt{a_i} |\psi_i\rangle \otimes \langle \phi_i| V, \tag{2.4.6}$$

with  $V$  denoting a unitary operator. In fact,  $V$  is a partial isometry [RS80] defined on the subspace spanned by the  $\langle \phi_i|$  in the ancilla Hilbert space, but we will assume  $V$  to be unitary unless otherwise noted since we take only density matrices of full rank into account at the moment.

## 2.4.2 Parallellity of states

Until now we have just defined an operator purifying the state of a quantum system. In previous discussions we have learnt that some kind of parallel transport condition is crucial to obtain a notion for an holonomy invariant like the geometric phase. The freedom which is left in the amplitude is the unitary  $V$ . It can be used to define a parallel transport condition for the amplitudes by clarifying the question how  $V$  has to be chosen for two neighbouring states  $\rho_1$  and  $\rho_2$  and their belonging amplitudes  $W_1$  and  $W_2$ .

The parallel transport condition in Section 1.2.3, Eq. (1.2.48) already demonstrated a possible way in that neighbouring states  $|\psi_1\rangle$  and  $|\psi_2\rangle$  are required to be *in-phase*, i. e. their scalar product  $\langle \psi_1 | \psi_2 \rangle$  shall be purely real. For the amplitudes  $W$  a similar condition can be

stated which relies on the transition probability of mixed states. Since we have already seen that any mixed state can be represented by a pure state in a larger system the first guess is to define the transition probability  $\text{tprob}(\rho_1, \rho_2) = |\langle \phi_1 | \phi_2 \rangle|^2$ , where the  $|\phi_i\rangle$  are purifications of the  $\omega_i$ . In terms of amplitudes this translates to  $(\text{Tr}[W_1^\dagger W_2])^2$ . This number, however, depends on the choice of the purification  $W_1$  and  $W_2$ , since

$$\text{Tr}[\tilde{W}_1^\dagger \tilde{W}_2] \equiv \text{Tr}[(W_1 V_1)^\dagger W_2 V_2] = \text{Tr}[W_1^\dagger W_2 V_2 V_1^\dagger] \neq \text{Tr}[W_1^\dagger W_2].$$

Uhlmann defines the transition probability by the supremum over all possible purifications [Uhl76]  $\tilde{W}_1, \tilde{W}_2$  of  $\rho_1, \rho_2$ ,

$$\text{tprob}(\rho_1, \rho_2) \equiv \sup \text{tprob}(\tilde{W}_1, \tilde{W}_2) \quad (2.4.7)$$

A *parallel purification* is then given by the pair of amplitudes  $W_1$  and  $W_2$  which purify  $\rho_1$  and  $\rho_2$  and for which the supremum in Eq. (2.4.7) is attained.

An explicit expression is obtained by writing the *polar decomposition* of the amplitudes,  $W_i = \sqrt{\rho_i} U_i$ . In fact, any (non-singular) operator  $A$  can be decomposed uniquely into a Hermitian  $|A|$  and a unitary  $U$  factor,  $A = |A|U$ . This extends the common polar decomposition of a complex number  $r = |r|e^{i\arg r}$  to operator valued quantities. The modulus  $|A|$  is defined by  $|A| = \sqrt{AA^\dagger}$  [RS80], and the square root operation is defined by taking the square roots of the eigenvalues,  $\sqrt{A} = (\sum_i a_i |\alpha_i\rangle \langle \alpha_i|)^{1/2} = \sum_i \sqrt{a_i} |\alpha_i\rangle \langle \alpha_i|$ , in the diagonal basis. This is unambiguous since  $AA^\dagger$  is real and positive<sup>5</sup> possessing real and positive eigenvalues. Using the polar decomposition the transition probability is

$$\text{tprob}(W_1, W_2) = \left( \text{Tr} [\sqrt{\rho_1} \sqrt{\rho_2} U_2 U_1^\dagger] \right)^2 = \left( \text{Tr} [|\sqrt{\rho_1} \sqrt{\rho_2}| U U_2 U_1^\dagger] \right)^2, \quad (2.4.8)$$

where the polar decomposition  $\sqrt{\rho_1} \sqrt{\rho_2} = |\sqrt{\rho_1} \sqrt{\rho_2}| U$  has been used. Now the product of unitary operators is again unitary and can therefore not exceed the value of one in operator norm. Consequently, the supremum is reached if

$$\text{tprob}(\rho_1, \rho_2) = \left( \text{Tr} |\sqrt{\rho_1} \sqrt{\rho_2}| \right)^2 = \left( \text{Tr} (\sqrt{\rho_2} \rho_1 \sqrt{\rho_2})^{1/2} \right)^2. \quad (2.4.9)$$

Demanding that two adjacent states are in-phase, translates to the requirement that the product of unitary operators in (2.4.8) is the identity operator. In terms of the amplitudes this is equivalent (for a proof see [Uhl76]) to require that for two amplitudes  $W_1$  and  $W_2$  the product  $W_1^\dagger W_2$  is Hermitian and positive,

$$W_1^\dagger W_2 = W_2^\dagger W_1 \geq 0. \quad (2.4.10)$$

---

<sup>5</sup> $AA^\dagger$  is Hermitian due to  $(AA^\dagger)^\dagger = AA^\dagger$  and positive due to  $\langle \psi | AA^\dagger | \psi \rangle = \langle A^\dagger \psi | A^\dagger \psi \rangle = \|A\psi\|^2 \geq 0$ .

**Example of two parallel amplitudes** Given two states  $\rho_1$  and  $\rho_2$ , what are the corresponding parallel amplitudes?  $\rho_1$  is purified by the amplitude  $W_1 = \rho_1^{1/2}$ <sup>6</sup>, where we have set  $U_1 = 1$  without loss of generality. The initial unitary is irrelevant for the question of parallelity. For  $\rho_2$  the requirement of  $UU_2U_1^\dagger = 1$  from Eq. (2.4.8) and the choice  $U_1 = 1$  leads to  $U = U_2^\dagger$  and eventually

$$U_2 = \rho_2^{1/2} \rho_1^{1/2} (\sqrt{\rho_2} \rho_1 \sqrt{\rho_2})^{-1/2}$$

due to  $\rho_2^{1/2} \rho_1^{1/2} = |\sqrt{\rho_1} \sqrt{\rho_2}| U$ . Consequently, the parallel amplitude is  $W_2 = \sqrt{\rho_2} U_2 = \rho_1^{-1/2} (\sqrt{\rho_2} \rho_1 \sqrt{\rho_2})^{1/2}$  where the unitarity of  $U_2$  ( $U_2^{-1} = U_2^\dagger \rightarrow U_2 = (U_2^\dagger)^{-1}$ ) has been used.

### 2.4.3 Parallel transport

With the help of the instructions how to build parallel amplitudes for two given states also a parallel transport from one state to another along a given path can be constructed. Let

$$\mathcal{C} : s \in [0, 1] \mapsto \rho_s \tag{2.4.11}$$

be a path of density operators. A *lift* of  $\mathcal{C}$  is a path

$$\hat{\mathcal{C}} : s \in [0, 1] \mapsto W_s \tag{2.4.12}$$

such that  $\rho_s = W_s W_s^\dagger$  with amplitude  $W_s = \rho_s^{1/2} V_s$  for each  $s$ . The unitary ‘‘phase’’ factors  $V_s$  serve to define a parallel transport via the path  $\hat{\mathcal{C}}$  in extended Hilbert space. Taken each amplitude for itself the choice of  $V_s$  is arbitrary since the projection map  $W_i W_i^\dagger$  is invariant under a change of the  $V_i$ . The lifted path  $\hat{\mathcal{C}}$  is not unique, by a local gauge transformation another path

$$\hat{\mathcal{C}}' : s \mapsto W_s Y_s, \quad 0 \leq s \leq 1, \quad Y_s \text{ unitary,}$$

is obtained that is also a valid lift of  $\mathcal{C}$ . Invoking the parallel transport condition (2.4.10) in its infinitesimal version,

$$W_s^\dagger dW_s = dW_s^\dagger W_s, \tag{2.4.13}$$

the unitary  $V_s$  is determined by the adjacent amplitude  $W_{s-ds}$  for each  $s$ .

The task is to find a quantity that is an invariant property of the path  $\mathcal{C}$  in projective Hilbert space. Such a quantity is realised by the so called *Bargmann invariant* (c. f. Refs. [Bar64, MS93] and Section 1.2.4) defined via a sequence of scalar products.

$$\Delta_n(\psi_1, \psi_2, \dots, \psi_n) \equiv \langle \psi_1 | \psi_2 \rangle \langle \psi_2 | \psi_3 \rangle \dots \langle \psi_n | \psi_1 \rangle \tag{2.4.14}$$

denotes the  $n$ -vertex Bargmann invariant which is a property of the path in ray space since it

---

<sup>6</sup>Note the slight abuse of notation since  $W_1 = \sum_k \sqrt{a_k} |\psi_k\rangle \otimes \langle \phi_k|$  is a map from the ancilla Hilbert space to the system Hilbert space in contrast to  $\rho_1^{1/2} = \sum_k \sqrt{a_k} |\psi_k\rangle \langle \psi_k|$  which acts only in the system’s space.

## 2. GEOMETRIC PHASE FOR MIXED STATES

---

is invariant under an individual  $U(1)$  gauge transformation of each constituent state  $|\psi_i\rangle \mapsto |\psi'_i\rangle = e^{i\alpha_i}|\psi_i\rangle$ . Consider now a subdivisions of  $\mathcal{C}$  into  $m+1$  fractions by discretising the parameter  $s$ ,  $1 > s_1 > s_2 > \dots > s_n > 0$ . To each point there is a specific state  $\rho_{s_i}$  along with its amplitude  $W_{s_i}$ . Similar to the  $n$ -vertex Bargmann invariant the product of the amplitudes can be formed,

$$\xi = (W_1, W_{s_1})(W_{s_1}, W_{s_2}) \dots (W_{s_n}, W_0) \quad (2.4.15)$$

with the definition of the scalar product of Hilbert Schmidt operators,

$$(W_1, W_2) \equiv \text{Tr} [W_1^\dagger W_2]. \quad (2.4.16)$$

The gauge transformation  $\xi \mapsto \tilde{\xi}$  by  $W_j \mapsto W_j Y_j$  yields a different path, while for a unique lift of the original path  $\mathcal{C}$  the parallelity condition (2.4.10) or equivalently  $|(W_{i+1}, W_i)| = \text{Tr}(\rho_i^{1/2} \rho_{i+1} \rho_i^{1/2})^{1/2}$  from (2.4.9) has to be imposed on each scalar product. This is in turn equivalent to find a gauge where  $\xi$  is maximal. The remaining arbitrariness is in a re-gauging  $W_i \mapsto \varepsilon_j U W_i$  by a number  $\varepsilon_j$  of modulus one and a global unitary  $U$ . A gauge invariant quantity can then be formed by multiplication of a factor  $(W_0, W_1)$  to  $\xi$ ,

$$\xi \mapsto \xi(W_0, W_1) = (W_1, W_{s_1})(W_{s_1}, W_{s_2}) \dots (W_{s_n}, W_0)(W_0, W_1).$$

Refining the subdivisions one obtains a gauge invariant linear form,

$$\lim_{n \rightarrow \infty} \xi(W_0, W_1). \quad (2.4.17)$$

In this limit all of the scalar products are real due to the parallel transport condition in its infinitesimal version  $(W, dW) = (dW, W)$  and, furthermore, all of them have to attain their maximum to give maximal  $\xi$  which is unity (for infinitesimally close states). The remaining term defines the *Uhlmann phase*

$$v_{\mathcal{C}} \equiv \arg(W_0, W_1) = \arg \text{Tr} W_0^\dagger W_1 = \arg \text{Tr} \rho_0^{1/2} \rho_1^{1/2} V_1 V_0^\dagger. \quad (2.4.18)$$

The quantity  $V_1 V_0^\dagger$  generalises the geometric phase difference of pure states. The former belongs to the group of  $U(n)$  matrices where  $n$  is the rank of the density matrix whereas the latter is merely a unimodular number element of  $U(1)$ .

In terms of the amplitudes the *holonomy invariant* is a matrix valued quantity that just depends on the path of the density matrix,

$$\mathcal{X}_{\mathcal{C}} \equiv W_1 W_0^\dagger. \quad (2.4.19)$$

and from which the phase  $v_{\mathcal{C}} = \arg \text{Tr} \mathcal{X}_{\mathcal{C}}$  can be deduced.

### Berry's phase factor

For a path of pure states  $\rho_s = |\psi_s\rangle\langle\psi_s|$ ,  $W_s$  is given by  $W_s = |\psi_s\rangle \otimes \langle a| e^{i\alpha_s} \in \mathcal{H} \otimes \mathcal{H}^*$ , where  $a$  can be any element of the dual Hilbert space  $\mathcal{H}^*$  and does not have to be path dependent. The Hilbert Schmidt scalar product between two adjacent purifications

$$\begin{aligned} \text{Tr} \left[ W_s^\dagger \frac{d}{ds} W_s \right] &= \text{Tr} \left[ e^{-i\alpha_s} |a\rangle\langle\psi_s| \frac{d}{ds} \left( |\psi_s\rangle\langle a| e^{i\alpha_s} \right) \right] \\ &= \langle\psi_s| \frac{d}{ds} |\psi_s\rangle + i \frac{d\alpha_s}{ds} \end{aligned} \quad (2.4.20)$$

From the normalisation of  $|\psi_s\rangle$  it follows that  $\langle\psi_s| \frac{d}{ds} |\psi_s\rangle$  is purely imaginary. However, the parallel transport condition states that the trace has to be real and we therefore obtain that  $d\alpha_s/ds = i \langle\psi_s| \frac{d}{ds} |\psi_s\rangle$ . The phase  $\alpha_1$  of the amplitude of the final state is determined by the integral

$$\alpha_1 = i \int \langle\psi_s| \frac{d}{ds} |\psi_s\rangle ds - \alpha_0 \quad (2.4.21)$$

and yields (with  $\alpha_0 = 0$ ) the holonomy invariant

$$\mathcal{X}_C = W_1 W_0^\dagger = |\psi_0\rangle\langle\psi_1| e^{i \int \langle\psi_s| \frac{d}{ds} |\psi_s\rangle ds}. \quad (2.4.22)$$

The argument of its trace  $\nu = \arg \text{Tr} [W_1 W_0^\dagger] = i \int \langle\psi_s| \frac{d}{ds} |\psi_s\rangle ds$  is equal to Pancharatnam's relative phase factor.

### 2.4.4 Hamiltonian motion

In order to discuss the ‘‘all-time highlight’’, a spin-1/2 particle in a magnetic field using Uhlmann's formalism an evolution governed by Schrödinger's equation will be examined in the following [Uhl93]. The time evolution of the density operator is given by the *Liouville-von Neumann* equations with the (in general time-dependent) Hamiltonian

$$i\hbar\dot{\rho} = [H(t), \rho]. \quad (2.4.23)$$

As an evolution equation of the lifted path we can write

$$i\hbar\dot{W} = H(t)W - W\tilde{H}(t) \quad (2.4.24)$$

which can be considered as a kind of Schroedinger equation

$$i\hbar\dot{W} = H^{\text{ext}}(t)W \quad \text{with } H^{\text{ext}}(t) = (L_H - R_{\tilde{H}}), \quad (2.4.25)$$

where  $L_H W \equiv HW$  and  $R_{\tilde{H}} W \equiv W\tilde{H}$ . The strange form of the Hamiltonian acting once from the left and once from the right is due to the use of the dual Hilbert space for the representation of the amplitudes in  $\mathcal{H}^{\text{ext}} = \mathcal{H} \otimes \mathcal{H}^*$ , i. e. the Hamiltonian is split into a tensor product  $H = H \otimes \tilde{H}$ , where  $H$  acts as usual on  $|\psi\rangle \in \mathcal{H}$ , but  $\tilde{H}$  on  $\langle\phi| \in \mathcal{H}^*$ .

## 2. GEOMETRIC PHASE FOR MIXED STATES

---

The discussion is simplified by taking a time-independent Hamiltonian  $H(t) = H$ , where the formal solution reads  $\rho_t = U(t)\rho_0U^\dagger(t)$  with  $U(t) = e^{-\frac{i}{\hbar}tH}$  and the corresponding solution for  $W(t)$  reads [Uhl91a]

$$W(t) = U(t)\rho_0^{1/2}V(t) \quad \text{with } V(t) = e^{\frac{i}{\hbar}t\tilde{H}}. \quad (2.4.26)$$

The gauge invariant quantity of the curve  $t \mapsto W_tW_0^\dagger$  that depends only on  $\rho_t$  can be written as

$$U(t)\rho_0^{1/2}V(t)\rho_0^{1/2}.$$

The parallelity of the lift  $W_t$  demands the hermiticity of  $W^\dagger \frac{dW}{dt}$ ,

$$V^\dagger \rho_0^{1/2} \left[ -\frac{i}{\hbar}H \right] \rho_0^{1/2} V + V^\dagger \rho_0 \left[ \frac{i}{\hbar}\tilde{H} \right] V = \left[ -\frac{i}{\hbar}\tilde{H} \right] V^\dagger \rho_0^{1/2} V + V^\dagger \rho_0^{1/2} \left[ \frac{i}{\hbar}H \right] \rho_0^{1/2} V$$

which simplifies to

$$2\rho_0^{1/2}H\rho_0^{1/2} = \rho_0\tilde{H} + \tilde{H}\rho_0. \quad (2.4.27)$$

If  $\rho_0$  is non-degenerate, i. e. all of its eigenvalues are non-zero, this equation defines  $\tilde{H}$ . For degenerate  $\rho_0$  one may require

$$\langle \psi | \tilde{H} | \psi \rangle = 0 \quad \text{if} \quad \rho_0 | \psi \rangle = 0. \quad (2.4.28)$$

Explicitly, we find for a  $\rho_0 = \sum_m \lambda_m |\psi_m\rangle\langle\psi_m|$  given in terms of eigenvalues and -vectors

$$\tilde{H} = \sum_{m,n} \frac{2\sqrt{\lambda_m\lambda_n}}{\lambda_m + \lambda_n} \langle \psi_m | H | \psi_n \rangle |\psi_m\rangle\langle\psi_n|. \quad (2.4.29)$$

**Neutron in magnetic field** If the neutron's spin is initially perpendicular to the stationary magnetic field pointing, e. g., in the positive  $y$ -direction, the state is denoted by  $\rho_0 = |z+\rangle\langle z+|$  as the eigenstate of the Pauli spin matrix  $\sigma_z$  and the Hamiltonian is given by  $H = -\frac{\hbar\omega_y}{2}\sigma_y$  ( $\omega_y = 2\mu_n B/\hbar$ ). The evolution operator

$$U(t) = \exp \left[ -\frac{i}{\hbar}tH \right] = \begin{pmatrix} \cos \frac{\omega_y t}{2} & \sin \frac{\omega_y t}{2} \\ -\sin \frac{\omega_y t}{2} & \cos \frac{\omega_y t}{2} \end{pmatrix}$$

is parallel transporting the initial state and we expect  $V = \exp[it\tilde{H}/\hbar] = 1$ . Indeed we can calculate  $\tilde{H}$  via (2.4.29) and see that all components are vanishing. Therefore  $V = 1$ .

The holonomy invariant  $W(t)^\dagger W(0) = U(t)\rho_0^{1/2}V(t)\rho_0^{1/2}$  is given by  $U(t)|z+\rangle\langle z+|$  and the geometric phase can be calculated by looking at the argument of the trace of this expression, i. e.

$$\gamma = \arg \text{Tr}[U(t)|z+\rangle\langle z+| \mathbb{1}|z+\rangle\langle z+|] = \arg \langle z+ | U(t) | z+ \rangle,$$

which is 0 or  $\pi$  in this case as expected.

Suppose we have a non-parallel transporting Hamiltonian  $H = -\frac{\hbar\omega_n}{2}\vec{n} \cdot \vec{\sigma}$ , where  $\vec{n} = (\sin\theta, 0, \cos\theta)^T$  is some unit vector lying in the  $x$ - $z$  plane. From (2.4.29) we conclude that the off-diagonal elements of  $\tilde{H}$  vanish since only  $\lambda_1 \neq 0$ . From (2.4.28) we find  $\tilde{H}_{22} = 0$ . The only element left is  $\tilde{H}_{11} = \frac{\hbar\omega_n}{2} \cos\theta$  and therefore,

$$V = \exp\left[\frac{i}{\hbar}t\tilde{H}\right] = e^{i\frac{\omega_n t}{2}\cos\theta}|z+\rangle\langle z+|.$$

The geometric phase follows as above from the functional (2.4.18)

$$\begin{aligned} \gamma \equiv v_C(1) &= \arg \text{Tr}[U(t)|z+\rangle\langle z+|V|z+\rangle\langle z+|] = \\ &= \frac{\omega_n t}{2} \cos\theta + \arg\left[\cos\frac{\omega_n t}{2} - i\cos\theta \sin\frac{\omega_n t}{2}\right] \\ &= \frac{\omega_n t}{2} \cos\theta - \arctan\left[\tan\frac{\omega_n t}{2} \cos\theta\right] \end{aligned} \quad (2.4.30)$$

and – lo and behold – we end up with the usual expression for the geometric phase which equals minus half of the solid angle,  $\gamma = -\Omega/2$ , enclosed by the path traced out by the pure state.

**Mixed states** Things get more interesting if we take a mixed instead of a pure state. A step further is to look at the Uhlmann holonomy for a non-unitary evolution as it has been carefully worked out by Tidström and Sjöqvist [TS03] with reference to Hübner [Hüb93]. Here, however, we stick to a simple unitary example when the initially mixed state  $\rho_0 = \frac{1+r}{2}|z+\rangle\langle z+| + \frac{1-r}{2}|z-\rangle\langle z-|$  evolves to  $\rho_t = U(t)\rho_0U^\dagger(t)$ . For  $U(t)$  we make the same choice as above, viz., a magnetic field in some direction  $\vec{n} = (\sin\theta, 0, \cos\theta)^T$  with Hamiltonian

$$H = -\frac{\hbar\omega_n}{2}\vec{n} \cdot \vec{\sigma} = -\frac{\hbar\omega_n}{2} \begin{pmatrix} \cos\theta & \sin\theta \\ \sin\theta & -\cos\theta \end{pmatrix}.$$

According to Eq. (2.4.29),  $\tilde{H}$  is

$$\begin{aligned} \tilde{H} &= \langle z+|H|z+\rangle|z+\rangle\langle z+| + \langle z-|H|z-\rangle|z-\rangle\langle z-| \\ &\quad + \sqrt{1-r^2}(\langle z+|H|z-\rangle|z+\rangle\langle z-| + \langle z-|H|z+\rangle|z-\rangle\langle z+|) \\ &= -\frac{\hbar\omega_n}{2} \left\{ \cos\theta(|z+\rangle\langle z+| - |z-\rangle\langle z-|) \right. \\ &\quad \left. + \sqrt{1-r^2}(\sin\theta|z+\rangle\langle z-| + \sin\theta|z-\rangle\langle z+|) \right\}. \end{aligned} \quad (2.4.31)$$

In terms of Pauli matrices

$$\tilde{H} = \frac{\hbar\omega_n}{2} \left\{ \sqrt{1-r^2} \sin\theta \sigma_x + \cos\theta \sigma_z \right\}. \quad (2.4.32)$$

## 2. GEOMETRIC PHASE FOR MIXED STATES

---

Introducing the unit vector  $\vec{n}' = (\sqrt{1-r^2} \sin \theta, 0, \cos \theta)^T / \alpha$ ,  $\alpha = (\sqrt{1-r^2 \sin^2 \theta})$  we find

$$V = e^{\frac{i}{\hbar} \tilde{H} t} = e^{\frac{i}{\hbar} \frac{\alpha \omega_n t}{2} \vec{n}' \cdot \vec{\sigma}} = \mathbb{1} \cos \frac{\alpha \omega_n t}{2} + i \vec{n}' \cdot \vec{\sigma} \sin \frac{\alpha \omega_n t}{2}.$$

The holonomy invariant  $\mathcal{X} = U(t) \rho_0^{1/2} V(t) \rho_0^{1/2}$  can then be calculated explicitly although yielding a rather lengthy expression [ESB<sup>+</sup>03]. Here we just note that Uhlmann's phase  $\arg \mathcal{X}$  has a different structure than  $\phi_\rho$ , the interferometric mixed state geometric phase, due to the appearance of  $V(t)$ . Due to the different parallel transport conditions the geometric phases from Sjöqvist and from Uhlmann are in general different, for non-degenerate  $\rho_0$  it is only in the case where  $V(t) = \mathbb{1}$  that  $\arg \text{Tr} \mathcal{X}$  reduces to  $\phi_\rho = \arg \text{Tr} [U(t) \rho_0]$ . Its argument is then equal to the interferometric mixed state geometric phase. However,  $V(t)$  is only the identity if  $\mathcal{H} = 0$  which implies that  $H$  must be zero, if all  $\lambda_m$ 's are non-vanishing and we have neither an evolution in the ancilla nor in the system.



# Chapter 3

## Off-diagonal Geometric Phases

Now that we have discussed different manifestations and extensions of *Berry's* or rather *Pancharatnam's* phase (Section 1) for pure states in different kinds of evolutions (adiabatic, non-adiabatic, noncyclic, non-unitary, ...) and also geometric phase definitions for mixed states (Section 2) it appears on the agenda to look at their nodal points. These are points where the relative phase between two states - either pure or mixed - is not well defined. A first account on this subject has been given by Bhandari in [Bha91, Bha97] for pure states and by the same author also for the interferometric mixed state geometric phase  $\phi_\rho$  (Section 2.3) [Bha02]. Generally speaking, if initial and final state are orthogonal to each other no relative phase can be defined. Naturally, this lead to the idea of an *off-diagonal geometric phase* by Manini and Pistoiesi [MP00] and for non-adiabatic evolutions by Mukunda *et al.* [MACS01] which is well-defined for orthogonal states. Instead, it is undefined for a cyclic evolution, if initial and final state only differ by a phase factor. The synthesis of the latter and the mixed state geometric phase leads to a universal notion comprising the pure state diagonal and off-diagonal as well as the mixed state geometric phase as limiting cases. We distinguish between a version based on the Sjöqvist's interferometric approach presented in Section 3.2 and an extension of Uhlmann's definition (Section 3.3).

### 3.1 Pure state off-diagonal geometric phase

As it has been pointed out in the discussion of Pancharatnam's phase difference between two state vectors  $\arg\langle\psi|\phi\rangle$ , this quantity is undefined for  $|\psi\rangle \perp |\phi\rangle$  (Figure 3.1). For example, a curve is traced out in parameter space by the initial state  $|\psi_j(s_1)\rangle$  under the influence of the adiabatically changing Hamiltonian  $H(s)$  which has (non-degenerate) eigenvectors  $|\psi_j(s)\rangle$ ,  $j = 1, \dots, \dim H$  at all values of the parameter  $s \in [s_1, s_2]$ . In the particular case where the  $j^{\text{th}}$  eigenstate  $|\psi_j(s_1)\rangle$  evolves adiabatically to another eigenstate of  $H(s_1)$ ,  $|\psi_j(s_1)\rangle \rightarrow |\psi_j(s_2)\rangle = e^{i\alpha} |\psi_k(s_1)\rangle$  ( $j \neq k$ ), the scalar product  $\langle\psi_j(s_1)|\psi_j(s_2)\rangle$  vanishes,

$$\langle\psi_j(s_1)|\psi_j(s_2)\rangle = e^{i\alpha} \langle\psi_j(s_1)|\psi_k(s_1)\rangle = 0, \quad (3.1.1)$$

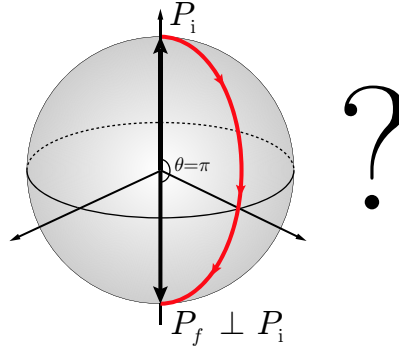


Figure 3.1: For orthogonal states the geometric phase is undefined since the initial state  $P_i = |\psi_i\rangle\langle\psi_i|$  is orthogonal to the final state  $P_f = |\psi_f\rangle\langle\psi_f|$ . Their scalar product  $\langle\psi_f|\psi_i\rangle$  vanishes.

if the eigenstates of  $H(s_1)$  are mutually orthogonal (which is true for Hermitian  $H$ ). The only phase information left is in the cross scalar product  $\langle\psi_j(s_1)|\psi_k(s_2)\rangle$  ( $j \neq k$ ).

Assuming a unitary operator  $U^\parallel$  parallel-transporting *all*  $|\psi_k(s_1)\rangle$  to  $|\psi_k(s_2)\rangle = U^\parallel|\psi_k(s_1)\rangle$  along the paths  $\mathcal{C}_j : s \mapsto |\psi_j(s)\rangle$  in Hilbert space the phase factors of the off-diagonal elements of  $U^\parallel$  are given by

$$\sigma_{jk} \equiv M(U_{jk}) = M[\langle\psi_j(s_1)|U|\psi_k(s_1)\rangle] = M[\langle\psi_j(s_1)|\psi_k(s_2)\rangle], \quad (3.1.2)$$

with  $M(z) \equiv \frac{z}{|z|}$ . The  $\sigma_{jk}$ 's are well-defined phase factors whenever  $|\psi_k(s_2)\rangle = e^{i\alpha}|\psi_k(s_1)\rangle$  ( $\alpha$  real), thus, if  $U^\parallel$  acting on an eigenstate of  $H$  produces an orthogonal eigenstate multiplied by a phase factor.

Unfortunately, the  $\sigma_{jk}$ 's are not invariant under a  $U(1)$  gauge transformation like

$$|\psi_j(s)\rangle \rightarrow e^{i\phi_j(s)}|\psi_j(s)\rangle. \quad (3.1.3)$$

They transform like

$$\sigma_{jk} \rightarrow \sigma_{jk} \exp i[\phi_k(s_1) - \phi_j(s_1)], \quad (3.1.4)$$

hence,  $\sigma_{jk}$  is arbitrary, i. e. non-measurable. An invariant quantity consisting of  $\sigma_{jk}$ 's can be found by combining two of them:

$$\gamma_{jk} \equiv \sigma_{jk}\sigma_{kj}. \quad (3.1.5)$$

$\gamma_{jk}$  is determined by the trajectories  $\mathcal{C}_j$  and  $\mathcal{C}_k$  of  $|\psi_j\rangle$  and  $|\psi_k\rangle$ , respectively. Furthermore it is invariant under the gauge transformation (3.1.3) and consequently measurable.

**Geometric interpretation** For  $\gamma_{jk}$  a nice geometric visualisation can be constructed as depicted in Figure 3.2: As already pointed out above the geometric phase difference can be build up of the phase difference acquired by the parallel evolution of a state  $|\psi(s_1)\rangle$  to

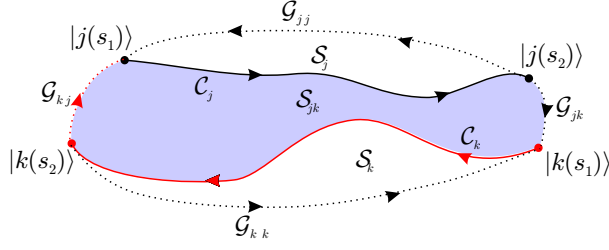


Figure 3.2: Geometric interpretation of the off-diagonal geometric phase  $\gamma_{jk}$ .

$|\psi(s_2)\rangle$  and the phase factor achieved by transporting the final state  $|\psi(s_2)\rangle$  back to the initial state  $|\psi(s_1)\rangle$  on a geodesic line. Consider now two states  $|j(s)\rangle$  and  $|k(s)\rangle$  evolving along  $C_j$  and  $C_k$  (in the projective Hilbert space  $\mathcal{P}$ ) from  $s_1$  to  $s_2$ . Three possibilities to achieve closed loops consisting of the  $C$ 's and geodesic paths  $\mathcal{G}$  emerge:

- (i)  $C_j + \mathcal{G}_{jj}$ ,
- (ii)  $C_k + \mathcal{G}_{kk}$ ,
- (iii)  $C_j + \mathcal{G}_{jk} + C_k + \mathcal{G}_{kj}$ .

(i) and (ii) give the usual geometric phase factors  $\phi_g^j$  and  $\phi_g^k$  respectively, the third loop (iii) corresponds to the off-diagonal geometric phase  $\gamma_{jk}$ . Having this picture in mind  $\gamma_{jk}$  can like before be computed as a surface integral of a two-form, whereas the surface is bounded by the loop (iii).

This approach also explains, why in a two-level system the off-diagonal geometric phase has to be  $\pi$  for all  $U \in U(2)$  parallel-transporting  $|j(s_1)\rangle$  to  $|j(s_2)\rangle$ ; a result that has been experimentally verified in neutron interferometry [HLB<sup>+</sup>01, HLB<sup>+</sup>02]. Representing these states as points on the Bloch sphere, the loop consisting of  $C_j + \mathcal{G}_{jk} + C_k + \mathcal{G}_{kj}$  encloses a half-sphere for every unitary rotation. This is obvious for the simple case of a single rotation about any axis perpendicular to the  $z$  axis (assuming that the initial Bloch vector points in the positive  $z$ -direction) (Figure 3.3(a)): Independent of the rotational angle the loop is closed to the orthogonal state, i. e. to the “south”-pole of the sphere, and because the orthogonal vector evolves exactly in the opposite way the loop encloses a half-sphere, thus the solid angle  $\Omega = 2\pi$  and the phase is  $\gamma_{\downarrow} = \frac{1}{2}2\pi = \pi$ . But the same results holds for any path parallel transporting  $|j(s_1)\rangle$  to  $|j(s_2)\rangle$  and  $|k(s_1)\rangle$  to  $|k(s_2)\rangle$  by the same reasoning (Figure 3.3(b)): the states  $|j(s)\rangle$  and  $|k(s)\rangle$  behave exactly contrarily, the solid angle enclosed by the sum of the paths  $(C_j + \mathcal{G}_{jk} + C_k + \mathcal{G}_{kj})$  does not change and consequently the off-diagonal geometric phase is always equal to  $\pi$ .

**Generalisation** Instead of taking only the evolution of two orthogonal eigenstates of a Hamiltonian  $H$  into consideration the same concept can be generalised to  $n$  orthonormal eigenstates  $|\psi_j(s)\rangle$  of a Hamiltonian  $H$ . Any cyclic product of  $\sigma$ 's is then gauge invariant

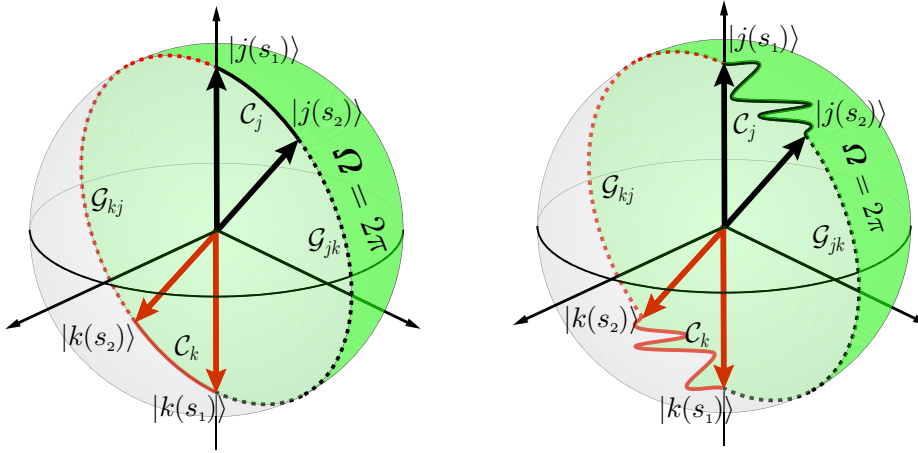


Figure 3.3: Bloch sphere picture of the off-diagonal geometric phase  $\gamma_{jk}$  for a qubit.  $\gamma_{jk}$  is always  $\pi$  since the evolution of the  $|j(s)\rangle$  state is always mimicked by the  $|k(s)\rangle$  state and vice versa so that the enclosed surface area is always same.

under the transformation (3.1.2). The definition (3.1.3) can be extended by defining

$$\gamma_{j_1 j_2 j_3 \dots j_l}^{(l)} \equiv \sigma_{j_1 j_2} \sigma_{j_2 j_3} \dots \sigma_{j_{l-1} j_l} \sigma_{j_l j_1}. \quad (3.1.6)$$

For  $l = 1$  this reduces to the diagonal geometric phase factor  $\phi_g^j$ , for  $l = 2$  we get the quantity  $\gamma_{jk}$  (3.1.5) describing the off-diagonal geometric phase. For  $l > 2$  more complex off-diagonal phase relations between eigenstates can be described.

## 3.2 Off-diagonal Geometric Phase for Mixed States - Interferometric approach

What about the mixed state geometric phase? Is it always well defined or are there similar situations as in the pure state case and is it possible to take an alternative quantity for such nodal points to learn something about the subjacent state space. As Bhandari already noted there are situations where in an interference experiment the contrast between the two sub-beams vanishes also if the input state is mixed [Bha02] and it is explained in the following how to construct and also how to measure an off-diagonal version of the mixed state geometric phase that is well-defined at these nodal points [FS03b, FS03a, SF03].

### 3.2.1 Orthogonality

For pure states the Hilbert space scalar product,  $\langle \psi | \phi \rangle$ , is used to define orthogonality. Vanishing scalar product denotes orthogonal states, for example, two non-overlapping Gaussian states or two anti-parallel spin states are orthogonal. In the mixed state case there is no well-established notion of orthogonality. It is not clear per se what is the equivalent to the scalar

product between pure state vector.

**Trace distance** In a first guess one could take the *trace distance* [NC00] between two density matrices as a measure for orthogonality. It is defined by

$$d_T(\rho_\psi, \rho_\phi) \equiv \text{Tr} |\rho_\psi - \rho_\phi|, \quad |X| \equiv \sqrt{X^\dagger X} \quad (3.2.1)$$

which defines a metric on the space of quantum states with  $0 \leq d_T \leq 2$  [GLN05]<sup>1</sup>. The maximum distance of  $d_T^{\text{max}}(\rho_\psi, \rho_\phi) = 2$  is, however, only reached for orthogonal pure states, since  $\text{Tr}[\rho_\psi, \rho_\phi] = 0$  must hold<sup>2</sup>. Explicitly, positivity implies that given a certain state  $A$  it is in general not possible to find a state  $B$  which is at maximal distance ( $\text{Tr}[AB] = 0$ ):

$$\text{Tr}[AB] = \text{Tr}\left[\left(\sum_i \alpha_i |a_i\rangle\langle a_i|\right)\left(\sum_{jk} \beta_{jk} |a_j\rangle\langle a_k|\right)\right] = \sum_i \alpha_i \beta_{ii} > 0,$$

unless the diagonal entries  $\beta_{ii}$  of the matrix  $B$  vanish. But this is impossible if  $B$  denotes a valid density matrix with  $\text{Tr}[B] \neq 0$ . Only if  $A$  has not full rank  $B$  can be chosen such that  $\text{Tr}[AB] = 0$ .  $B$  must “live” in a different subspace of state space and must not be of full rank either.

**Hilbert-Schmidt distance** Another choice could be the *Hilbert-Schmidt distance*, which is defined slightly different, viz.

$$d_{HS}(\rho, \rho^\perp) \equiv \sqrt{\text{Tr}[(\rho - \rho^\perp)^2]} = \sqrt{2 - 2\text{Tr}[\rho_\psi \rho_\phi]}, \quad (3.2.2)$$

where the last equality follows from the normalisation of the  $\rho$ 's. Furthermore, from the positivity of the  $\rho$ 's it follows that  $d_{HS}(\rho_\psi, \rho_\phi)$  is always less or equal than 2, whereas the maximum is reached again just for orthogonal pure states due to the same reasons as above.

**Bures distance** A third option is the *Bures distance* [Bur69] being a worst case measure of distinguishability between  $\rho$  and  $\rho'$  [Joz94]. The distance between two states is in this metric defined by

$$d_B[\rho_\psi, \rho_\phi] = 2\sqrt{1 - \text{Tr}\sqrt{\sqrt{\rho_\psi}\rho_\phi\sqrt{\rho_\psi}}}. \quad (3.2.3)$$

The Bures distance is according to Uhlmann [Uhl76] connected to the *transition probability* between mixed states. In the previous chapter we have already derived (c. f. Equation 2.4.9) that the Hilbert-Schmidt-norm in the space of purifications of density operators induces a norm on the space of density operators itself which is connected to the Bures distance above.

---

<sup>1</sup>The factor 1/2 is skipped in our definition to fit to the subsequent distance measures.

<sup>2</sup>From  $|\rho_\psi - \rho_\phi| = (\rho_\psi^\dagger \rho_\psi + \rho_\phi^\dagger \rho_\phi - \rho_\psi^\dagger \rho_\phi - \rho_\phi^\dagger \rho_\psi)^{1/2}$  and noting that  $\rho_\psi$  and  $\rho_\phi$  are positive we observe that the last two terms must vanish to achieve a maximum.

**Interferometric orthogonality** All of them have in common that for general density matrices the maximum distance  $d^{max} = 2$  is not reached. In order to define an orthogonal state  $\rho^\perp$  for a given  $\rho$  we have to be content with a  $\rho^\perp$  that maximises any of these distance. We will see later on that this is possible for the qubit case (two-dimensional Hilbert space), however, in higher dimensions this becomes a tedious task and a simpler definition of orthogonality is highly wanted. In the spirit of Pancharatnam the interference between two states provides the clue to a possible solution: Let us first recall the interferometric setup where two unitarily connected pure states,  $|\psi\rangle$  and  $|\phi\rangle = U|\psi\rangle$ , are brought to interference. Assuming further, that  $|\psi\rangle$  is exposed to the variable  $U(1)$  shift  $e^{i\eta}$ , the resulting interference pattern is determined by the intensity

$$I \propto \left| e^{i\eta}|\psi\rangle + |\phi\rangle \right|^2 = 2 + 2|\langle\psi|\phi\rangle| \cos[\eta - \arg\langle\psi|\phi\rangle], \quad (3.2.4)$$

which oscillates as a function of  $\eta$ . The key point here is to note that  $\psi$  and  $\phi$  are orthogonal if and only if  $I$  is independent of  $\eta$  so that the interference oscillations disappear. This feature translates naturally to the mixed state case. Consider a pair of isospectral non-degenerate density operators

$$\rho_\psi = \sum_k \lambda_k |\psi_k\rangle\langle\psi_k| \text{ and } \rho_\phi = \sum_k \lambda_k |\phi_k\rangle\langle\phi_k|, \quad (3.2.5)$$

where each  $|\phi_k\rangle = U|\psi_k\rangle$  for some unitarity  $U$ . The physical assumption we make is that each pair of state vectors  $|\psi_k\rangle$  and  $|\phi_k\rangle$  are coherent, i. e. able to interfere with each other, while there is no interference between different  $|\psi_k\rangle$  and  $|\phi_j\rangle$  ( $j \neq k$ ). Each such orthonormal pure state component of the density operator contributes to the interference according to Eq. (3.2.4). Thus, the total intensity profile becomes [SPE<sup>+</sup>00]

$$I \propto \sum_k \lambda_k \left| e^{i\eta}|\psi_k\rangle + |\phi_k\rangle \right|^2 = 2 + 2 \sum_k \lambda_k |\langle\psi_k|\phi_k\rangle| \cos[\eta - \arg\langle\psi_k|\phi_k\rangle], \quad (3.2.6)$$

where we have used that the eigenvalues  $\lambda_k$  sum up to unity. Following the above pure state case, we say that  $\rho_\psi$  and  $\rho_\phi$  are orthogonal if and only if  $I$  is independent of  $\eta$  for all eigenstates  $\{|\psi_k\rangle\}$  and  $\{|\phi_k\rangle\}$  of  $\rho_\psi$  and  $\rho_\phi$ , respectively. It follows that  $\rho_\psi$  and  $\rho_\phi$  are orthogonal if and only if  $\langle\psi_k|\phi_k\rangle = 0, \forall k$ .

**N-dimensional orthogonality** For an  $N$  dimensional Hilbert space  $\mathcal{H}$ , we may generate a set of  $N$  mutually orthogonal density operators as follows. Assume  $\rho_1 = \sum_k \lambda_k |\psi_k\rangle\langle\psi_k|$  is non-degenerate and introduce a unitary operator  $U_g$  such that  $|\psi_n\rangle = (U_g)^{n-1} |\psi_1\rangle, n = 1, \dots, N$ . Thus, we may write

$$U_g = |\psi_1\rangle\langle\psi_N| + |\psi_N\rangle\langle\psi_{N-1}| + \dots + |\psi_2\rangle\langle\psi_1| \quad (3.2.7)$$

and it follows that

$$\rho_n = (U_g)^{n-1} \rho_1 (U_g^\dagger)^{n-1}, \quad n = 1, \dots, N \quad (3.2.8)$$

is a set of mutually orthogonal density operators.

Explicitly, this entails that

$$\begin{aligned}
 \rho_1 &= \lambda_1 |\psi_1\rangle\langle\psi_1| + \lambda_2 |\psi_2\rangle\langle\psi_2| + \dots + \lambda_N |\psi_N\rangle\langle\psi_N|, \\
 \rho_2 &= \lambda_1 |\psi_2\rangle\langle\psi_2| + \lambda_2 |\psi_3\rangle\langle\psi_3| + \dots + \lambda_N |\psi_1\rangle\langle\psi_1|, \\
 &\dots, \\
 \rho_N &= \lambda_1 |\psi_N\rangle\langle\psi_N| + \lambda_2 |\psi_1\rangle\langle\psi_1| + \dots + \lambda_N |\psi_{N-1}\rangle\langle\psi_{N-1}|.
 \end{aligned} \tag{3.2.9}$$

Notice here, that different sets of mutually orthogonal mixed states may be generated by permuting the  $\psi_n$ 's in  $U_g$ . For clarification take a three-level system specified by

$$\rho = \lambda_0 |0\rangle\langle 0| + \lambda_1 |1\rangle\langle 1| + \lambda_2 |2\rangle\langle 2|.$$

Application of (3.2.7) yields

$$\rho^\perp = \lambda_0 |1\rangle\langle 1| + \lambda_1 |2\rangle\langle 2| + \lambda_2 |0\rangle\langle 0|$$

or

$$\rho^\perp = \lambda_0 |2\rangle\langle 2| + \lambda_1 |0\rangle\langle 0| + \lambda_2 |1\rangle\langle 1|.$$

**2-dimensional example** In the qubit case it is an easy task to find the set of orthogonal density matrices, viz. for

$$\rho = \sum_{k=1}^2 \lambda_k |\varphi_k\rangle\langle\varphi_k| = \begin{pmatrix} \lambda_1 & 0 \\ 0 & \lambda_2 \end{pmatrix}$$

the orthogonal counterpart is

$$\rho^\perp = \begin{pmatrix} \lambda_2 & 0 \\ 0 & \lambda_1 \end{pmatrix}.$$

Furthermore, it is also not difficult to calculate the orthogonal state  $\rho^\perp$  by maximising the distance. Indeed, for the Hilbert-Schmidt distance in Eq. (3.2.2) one finds that  $\text{Tr}[\rho\rho^\perp]$  must be a minimum. We demand that  $\rho$  and  $\rho^\perp$  are unitarily connected,  $\rho^\perp = U\rho U^\dagger$ . The general form of  $U \in U(2)$  is

$$U(\theta, \alpha, \beta, \gamma) = e^{i\gamma} \begin{pmatrix} \cos \frac{\theta}{2} - i \sin \frac{\theta}{2} \cos \alpha & -i \sin \frac{\theta}{2} \sin \alpha e^{-i\beta} \\ -i \sin \frac{\theta}{2} \sin \alpha e^{i\beta} & \cos \frac{\theta}{2} + i \sin \frac{\theta}{2} \cos \alpha \end{pmatrix}. \tag{3.2.10}$$

The calculation of the trace of the product  $\rho\rho^\perp = \rho U\rho U^\dagger$  yields

$$\text{Tr}[\rho\rho^\perp] = \frac{1}{2}(\lambda_1^2 + \lambda_2^2)(1 + \cos \theta + \cos^2 \alpha \sin^2 \frac{\theta}{2}) + 2\lambda_1\lambda_2 \sin^2 \alpha \sin^2 \frac{\theta}{2} \tag{3.2.11}$$

which is minimal for  $\alpha = (2n + 1)\pi/2$  and  $\theta = (2n + 1)\pi$ ,  $n$  integer. A unitary  $U_g$  generating an orthogonal state is therefore,

$$U_g = \begin{pmatrix} 0 & 1 \\ 1 & 0 \end{pmatrix}, \quad (3.2.12)$$

where  $\beta$  and  $\gamma$  are chosen such that the components of  $U_g$  are real. Applying  $U_g$  to  $\rho$  corresponds to an exchange of the eigenvalues like in the interferometric approach.

Using Bures distance we find the same orthogonal state  $\rho^\perp$ , the maxima of both distances are equal:

$$d_{HS}(\rho, \rho^\perp) \max \leftrightarrow d_B(\rho, \rho^\perp) \max.$$

due to the fact that we can rewrite the transition probability in the Bures distance (3.2.3)  $\text{Tr} \left[ \underbrace{(\sqrt{\rho}\rho^\perp\sqrt{\rho})}_{A}^{1/2} \right]$  to  $\text{Tr}[\sqrt{A}] = \text{Tr}[V\sqrt{AV^\dagger}] = \text{Tr}[\sqrt{VAV^\dagger}]$  for unitary  $V$ . The last equality follows from

$$(VXV^\dagger)^2 = VXV^\dagger VXV^\dagger = VX^2V^\dagger = VAV^\dagger$$

when taking the square root. The square root is defined by  $X = \sqrt{A}$  if and only if  $X^2 = A$ . By a particular choice of  $V$ ,  $VAV^\dagger \equiv D$  is diagonal and for a diagonal matrix the square root is found simply by taking the square root of the eigenvalues,  $\sqrt{D} = \sqrt{\sum_k \delta_k |d_k\rangle\langle d_k|} = \sum_k \sqrt{\delta_k} |d_k\rangle\langle d_k|$ . But then  $\text{Tr}[\sqrt{D}] = \sqrt{\delta_1} + \sqrt{\delta_2}$ , which is minimal if  $\delta_1 + \delta_2$  is minimal,

$$\text{Tr}[\sqrt{D}] \min. \leftrightarrow \text{Tr}[D] \min.$$

Since  $D = VAV^\dagger$ , finding a minimum of  $\text{Tr}[D]$  amounts to finding a minimum of  $\text{Tr}[A] = \text{Tr}[\sqrt{\rho}\rho^\perp\sqrt{\rho}] = \text{Tr}[\rho^\perp\rho]$  by definition and using the cyclic property of the trace. In conclusion, we have explicitly shown that a minimum of  $\text{Tr}[\rho^\perp\rho]$  is also a minimum of  $\text{Tr} \left[ (\sqrt{\rho}\rho^\perp\sqrt{\rho})^{1/2} \right]$ , so that states orthogonal with respect to the Hilbert-Schmidt norm are also orthogonal in the Bures norm.

This result can be nicely visualised on the Bloch sphere. A mixed qubit state is parametrised by  $\rho = \frac{1}{2}(\mathbb{1} + \vec{r} \cdot \vec{\sigma})$ , where the norm of the vector  $\vec{r}$ ,  $r = \|\vec{r}\|$  indicates the degree of mixedness.  $r = 0$  denotes a totally mixed state,

$$\rho(r=0) = \begin{pmatrix} 1/2 & 0 \\ 0 & 1/2 \end{pmatrix},$$

whereas for  $r = 1$  the state is pure. We can always rotate the coordinate system so that  $\vec{r}$  points in the  $z$ -direction thus  $r = r_z$  and we get

$$\rho = \frac{1+r}{2} |0\rangle\langle 0| + \frac{1-r}{2} |1\rangle\langle 1|,$$

i. e. the eigenvalues of  $\rho$  are  $\lambda_0 = (1+r)/2$  and  $\lambda_1 = (1-r)/2$ . The orthogonal density

matrix is given by

$$\rho^\perp = \frac{1}{2} \left( \mathbb{1} + \vec{r}^\perp \cdot \vec{\sigma} \right) = \frac{1-r}{2} |0\rangle\langle 0| + \frac{1+r}{2} |1\rangle\langle 1|.$$

The polarisation vectors are related as  $\vec{r} = -\vec{r}^\perp$  (Figure 3.4). For a pure state ( $r = \pm 1$ )

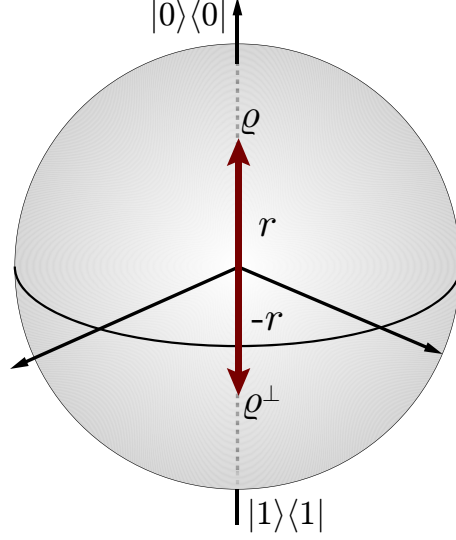


Figure 3.4: In the qubit case the orthogonal state can be visualised on the Bloch sphere. The polarisation vectors  $\vec{r}$  and  $\vec{r}^\perp$  point in opposite direction

equation (3.2.11) reduces to the Hilbert space scalar product  $Tr[\rho\rho^\perp] = |\langle 0|1\rangle|^2$ , which vanishes as  $|0\rangle \perp |1\rangle$ . For an arbitrarily mixed state ( $r \neq 1$ ) equation (3.2.11) yields  $Tr[\rho\rho^\perp] = (1 - r^2)/2$  for orthonormalised basis states  $|0\rangle, |1\rangle$ . It is easy to see that these states can be associated with Bloch vectors pointing in the opposite direction.

### 3.2.2 Consistency and normalisation

The final step towards a definition of an off-diagonal mixed state geometric phase is to determine how to construct a quantity comprising mutually orthogonal density operators that is gauge invariant and reduces to the Manini-Pistoiesi off-diagonal geometric phase in the limit of pure states.

We first notice that the Manini-Pistoiesi expression [MP00] may be written in terms of pure state projectors  $P_{j_k} = |\psi_{j_k}\rangle\langle\psi_{j_k}|$  as

$$\gamma_{P_{j_1} P_{j_2} \dots P_{j_l}}^{(l)} \equiv M \left[ \text{Tr} \left( U^\parallel P_{j_1} U^\parallel P_{j_2} \dots U^\parallel P_{j_l} \right) \right], \quad (3.2.13)$$

where  $M[z] = z/|z|$  for any complex number  $z$ . Each of these projectors is now replaced by the function  $F^{(l)}(\rho_{j_k})$ , where, for reason of permutation symmetry of the indexes  $j_1, j_2, \dots, j_l$ , the form of the function  $F^{(l)}$  may only depend on  $l$ . To assure consistency with Ref. [MP00]

we further require that  $F^{(l)}(\rho_{j_k}) \rightarrow P_{j_k}$  in the pure state limit. We take the simplest nontrivial choice fulfilling this requirement, which is  $F^{(l)}(\rho_{j_k}) = \rho_{j_k}^{p/q}$ ,  $p = p(l)$  and  $q = q(l)$  integers<sup>3</sup>. Notice that  $\rho_{j_k}^{p/q}$  is well-defined since  $\rho_{j_k} \geq 0$ .

Next, from  $(P_k)^l = P_k$ , we obtain the normalisation condition

$$\begin{aligned} \text{Tr}(U_g^\dagger P_k U_g^\dagger P_{(k+1) \bmod N} \cdots U_g^\dagger P_{(k+l) \bmod N}) = \\ \text{Tr}((U_g^\dagger)^l P_k) = \delta_{lN}, \quad \forall k \in [1, N], \end{aligned} \quad (3.2.14)$$

where we have used  $U_g^\dagger$  defined in Eq. (3.2.7),  $P_{(k+n) \bmod N} = (U_g)^{n-1} P_k (U_g^\dagger)^{n-1}$  and  $(U_g^\dagger)^N = 1$ .

This normalisation structure shall be preserved also in the mixed state case: After the replacement  $P_{j_k} \rightarrow \rho_{j_k}^{p/q}$ , we similarly have

$$\begin{aligned} \text{Tr}(U_g^\dagger \rho_k^{p/q} U_g^\dagger \rho_{(k+1) \bmod N}^{p/q} \cdots U_g^\dagger \rho_{(k+l) \bmod N}^{p/q}) = \\ \text{Tr}((U_g^\dagger)^l \rho_k^{lp/q}) = \delta_{lN} \text{Tr}(\rho_k^{lp/q}), \quad \forall k \in [1, N], \end{aligned} \quad (3.2.15)$$

where we have used that  $(U_g \rho U_g^\dagger)^{p/q} = U_g \rho^{p/q} U_g^\dagger$ . Thus, only  $p(N) = 1$  and  $q(N) = N$  assures the desired kind of normalisation in the mixed state case. Since  $p$  and  $q$  are functions of  $l$  only, it follows that  $p = 1$  and  $q = l$ . This choice may also be understood from the following simple convergence arguments in the  $N \rightarrow \infty$  case.  $\rho^{lp/q}$  typically involves factors of the form  $\lambda^{lp/q}$ ,  $0 \leq \lambda \leq 1$ . If  $lp/q < 1$  ( $lp/q > 1$ ) then the trace diverges (goes to zero) when  $l \rightarrow \infty$ . Thus, only for  $lp/q = 1$  the  $N \rightarrow \infty$  limit is finite and well-defined.

Note, however, that we are only interested in a phase factor the norm of the trace does not play a fundamental role and we could also skip the normalisation condition.  $F^{(l)}(\rho_{j_k})$  is then simply the density matrix itself,  $F^{(l)}(\rho_{j_k}) = \rho_{j_k}$ .

### 3.2.3 Off-diagonal mixed state geometric phase

As a consequence of the preceding results the off-diagonal mixed state phase for an ordered set of  $l \leq N$  mutually orthogonal non-degenerate density operators  $\rho_{j_k}$ ,  $k = 1, \dots, l$ , parallel transported by  $U^\parallel$  is given by

$$\gamma_{\rho_{j_1} \rho_{j_2} \dots \rho_{j_l}}^{(l)} \equiv M \left[ \text{Tr} \left( U^\parallel \sqrt{\rho_{j_1}} U^\parallel \sqrt{\rho_{j_2}} \dots U^\parallel \sqrt{\rho_{j_l}} \right) \right]. \quad (3.2.16)$$

---

<sup>3</sup>Nothing prevents us to consider more complicated  $F^{(l)}$ 's. For example, one may add a function  $G^{(l)}(\rho)$  to  $\rho^{p/q}$  provided it converges for any  $\rho$  and  $G^{(l)}(P) = 0$  for any projector  $P$ . Although considerations of such alternative definitions may have some mathematical interest, from a physical point of view, this is the most natural, as it turns out to be reducible to the mixed state phase of Ref. [SPE<sup>+</sup>00] for  $l = 1$  (see Eq. (3.2.17)) and it can be realised experimentally, at least for  $l \leq 2$  (see Section 3.2.8).

This is manifestly gauge invariant and independent of cyclic permutations of the indexes  $j_1, j_2, \dots, j_l$ . The diagonal mixed state geometric phase factor

$$\gamma_{\rho_{j_1}}^{(1)} = M[\text{Tr}(U^{\parallel} \rho_{j_1})] \quad (3.2.17)$$

may be seen as a natural consequence of this general framework if we put  $l = 1$ . It can be assigned an operational meaning in terms of a purification lift that can be experimentally tested using a two-arm Franson-type interferometer. In Section 3.2.8 we propose experimental realisations of the first ( $l = 1$ ) and second order ( $l = 2$ ) phases, the latter being defined by

$$\gamma_{\rho_{j_1} \rho_{j_2}}^{(2)} = M[\text{Tr}(U^{\parallel} \sqrt{\rho_{j_1}} U^{\parallel} \sqrt{\rho_{j_2}})]. \quad (3.2.18)$$

For  $\rho$ 's characterising pure states ( $\lambda_i = 1, \lambda_{j \neq i} = 0$ ) we automatically fall back to the pure state off-diagonal geometric phase definition in (3.1.5). Furthermore, it is gauge invariant under the  $U(1)$  transformation of the basis vectors  $|\varphi_k\rangle$ ,

$$|\varphi_k\rangle \rightarrow |\varphi_k'\rangle = e^{i\alpha_k} |\varphi_k\rangle, \quad (3.2.19)$$

The nodal point structure, i. e. the distribution of points in parameter space where the diagonal mixed state geometric phase vanishes, will be discussed for the most important qubit case. In this case it can be shown explicitly that the nodal points of the diagonal and the off-diagonal phase do not coincide (Section 3.2.6).

### 3.2.4 Computation of off-diagonal mixed state phases

In the qubit case  $N = 2$ , consider the unitarity

$$U^{\parallel} = U_{11}^{\parallel} |\psi_1\rangle\langle\psi_1| + U_{12}^{\parallel} |\psi_1\rangle\langle\psi_2| + U_{21}^{\parallel} |\psi_2\rangle\langle\psi_1| + U_{22}^{\parallel} |\psi_2\rangle\langle\psi_2| \quad (3.2.20)$$

that parallel transports some orthonormal basis  $\{|\psi_1\rangle, |\psi_2\rangle\}$ . The matrix elements of  $U^{\parallel}$  fulfil  $U_{11}^{\parallel} = (U_{22}^{\parallel})^* = v e^{-i\Omega/2}$  and  $U_{12}^{\parallel} U_{21}^{\parallel} = -\det U^{\parallel} + U_{11}^{\parallel} U_{22}^{\parallel} = -1 + v^2$  as  $U^{\parallel} \in SU(2)$ . Here,  $v = |\langle\psi_1|U^{\parallel}|\psi_1\rangle|$  is the pure state visibility and  $\Omega$  is the solid angle enclosed by the path traced out by the basis vectors  $\{|\psi_1\rangle, |\psi_2\rangle\}$  and the shortest geodesic connecting its end points on the Bloch sphere.

Now,  $U^{\parallel}$  in Eq. (3.2.20) parallel transports the mutually orthogonal density operators  $\rho_1 = \lambda_1 |\psi_1\rangle\langle\psi_1| + \lambda_2 |\psi_2\rangle\langle\psi_2|$  and  $\rho_2 = \lambda_1 |\psi_2\rangle\langle\psi_2| + \lambda_2 |\psi_1\rangle\langle\psi_1|$ , for which we obtain

$$\begin{aligned} \text{Tr}(U^{\parallel} \rho_1) &= \text{Tr}(U^{\parallel} \rho_2)^* = v(\lambda_1 e^{-i\Omega/2} + \lambda_2 e^{i\Omega/2}), \\ \text{Tr}(U^{\parallel} \sqrt{\rho_1} U^{\parallel} \sqrt{\rho_2}) &= -1 + v^2 + 2v^2 \sqrt{\lambda_1 \lambda_2} \cos \Omega = -1 + v^2 + v^2 \sqrt{\mathcal{F}_B[\rho_1, \rho_2]} \cos \Omega, \end{aligned} \quad (3.2.21)$$

where we have used the Bures fidelity  $\mathcal{F}_B[\rho_1, \rho_2] = [\text{Tr} \sqrt{\sqrt{\rho_1} \rho_2 \sqrt{\rho_1}}]^2 = 4\lambda_1 \lambda_2$ . Notice that  $\mathcal{F}_B[\rho_1, \rho_2] = 0$  for pure states and  $\mathcal{F}_B[\rho_1, \rho_2] = 1$  in the maximally mixed state case.

In the non-degenerate mixed state case  $\lambda_1 \neq \lambda_2$ , the  $l = 1$  phases are indeterminate only

for  $v = 0$ , for which the  $l = 2$  phase is well-defined since  $\text{Tr}(U^\parallel \sqrt{\rho_1} U^\parallel \sqrt{\rho_2}) = -1$ . In the degenerate case  $\lambda_1 = \lambda_2$ , the density operators  $\rho_1$  and  $\rho_2$  become identical and spherically symmetric, so that no specific basis is singled out by the parallel transport condition and the mixed state geometric phase factors  $\gamma_\rho^{(1)}$  and  $\gamma_{\rho\rho^\perp}^{(2)}$  become undefined. Still, there is a unique notion of relative phase in this case with additional nodal points, as discussed in [Bha02]. For a generic  $U = e^{-i\delta\vec{n}\cdot\vec{\sigma}}$ ,  $\vec{n}$  denoting a unit vector, we obtain for  $l = 1$  nodal points at  $\text{Tr}(U\rho_1) = \text{Tr}(U\rho_2) = \cos\delta = 0$  at which  $\delta$  we have  $\text{Tr}(U\sqrt{\rho_1}U\sqrt{\rho_2}) = \cos 2\delta = -1$ . This shows that the  $l = 1$  and  $l = 2$  phases never become indeterminate simultaneously and thus provide a complete phase characterisation of the qubit case.

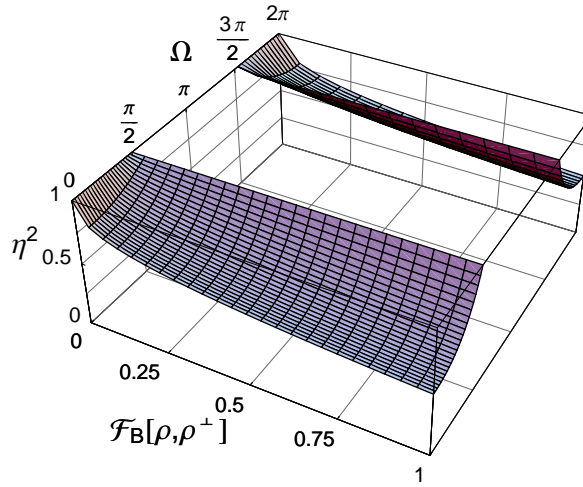


Figure 3.5: Nodal surfaces of the off-diagonal mixed state geometric phase for a qubit with the solid angle  $\Omega$  in steradians. For Bures fidelity  $\mathcal{F}_B = [\text{Tr} \sqrt{\sqrt{\rho_1}\rho_2\sqrt{\rho_1}}]^2 > 0$  (mixed states), there are nodes also for paths with pure state visibility  $v = |\langle \psi_1 | U^\parallel | \psi_1 \rangle|^2 \neq 1$  at various solid angles.

The off-diagonal mixed state geometric phase in the qubit case has a nontrivial nodal structure that arises due to the nonvanishing Bures fidelity. This can be seen by putting the left-hand side of Eq. (3.2.22) to zero and solving for  $v^2$  yielding

$$v^2 = (1 + \sqrt{\mathcal{F}_B[\rho_1, \rho_2]} \cos \Omega)^{-1}, \quad (3.2.22)$$

which has solutions at  $v < 1$  for  $\mathcal{F}_B[\rho_1, \rho_2] \cos \Omega > 0$ . Thus, the off-diagonal mixed state geometric phase factor may change sign across the nodal surfaces in the parameter space  $(\mathcal{F}_B[\rho_1, \rho_2], v, \Omega)$  defined by the solutions of Eq. (3.2.22), as shown in Figure 3.5. Thus, the corresponding off-diagonal mixed state geometric phase can take both values 0 and  $\pi$ , contrary to the corresponding pure state phase, which can only be  $\pi$ .

This discussion can be generalised to arbitrary Hilbert space dimensions  $N$ . In [FS03a] a method is introduced that allows for the computation of mixed state geometric phases to any order  $l \leq N$  for unitarities under which the parallel transported eigenbasis  $\{|\psi_1\rangle, \dots, |\psi_N\rangle\}$

of the mutually orthogonal  $\rho$ 's is divided into two parts: one part where each basis vector undergoes cyclic evolution and one part where all basis vectors are permuted among each other.

### 3.2.5 Projection phase

Since the definition of the off-diagonal geometric mixed state phase claims to be reducible to the pure state off-diagonal geometric phase, the question arises if there is a connection to the experimental verification of the latter performed by Hasegawa *et al.* [HLB<sup>+</sup>01, HLB<sup>+</sup>02]. This has to be answered in the negative, since in this experiment the evolution of the orthogonal state is implemented as a projection operator, which is by definition equivalent to a pure state. The resulting intensity is given by

$$I \propto \text{Re Tr}[U\rho U^\dagger P] + |\text{Tr}[U\rho UP]| \cos(\arg \text{Tr}[U\rho UP] + \eta), \quad (3.2.23)$$

where  $P$  represents the projection operator to a specific spin state and  $\eta$  is an additional phase shift.

The shift in the interference pattern given by the additional phase factor

$$\gamma_{\rho P} \equiv M[\text{Tr}(U\rho UP)], \quad M[z] = \frac{z}{|z|}, \quad (3.2.24)$$

could be used as a definition of the off-diagonal geometric mixed state phase, if the unitarity  $U$  describing the evolution inside the interferometer is parallel transporting the eigenvectors of the non-degenerate  $\rho$ . Parallel transport is for example fulfilled in the Hasegawa *et al.* experiment if the incident spinor is polarised in a plane perpendicular to the direction of the magnetic field.

In the two dimensional case relevant for the Hasegawa *et al.* experiment with input  $\rho = \lambda_1 |\psi_1\rangle\langle\psi_1| + \lambda_2 |\psi_2\rangle\langle\psi_2|$ ,  $\lambda_1 > \lambda_2$ , we can write Eq. (3.2.24) as

$$\text{Tr}[U\rho UP] = \lambda_1(-1 + v^2) + \lambda_2 v^2 e^{-2i\alpha}. \quad (3.2.25)$$

Here,  $U \in SU(2)$  with the diagonal matrix elements  $U_{11} = U_{22}^* = v e^{i\alpha}$  is not necessarily fulfilling the parallel transport condition with respect to  $\{|\psi_1\rangle, |\psi_2\rangle\}$ . In the pure state limit  $\lambda_1 = 1, \lambda_2 = 0$  the off-diagonal phase is always  $\pi$  since  $\text{Tr}[U\rho UP]_{\lambda_1=1} = -1 + v^2$  is real and negative, irrespective of whether  $U$  parallel transports  $|\psi_1\rangle, |\psi_2\rangle$  or not. For a mixed input state  $\rho$  the  $\lambda_2$ -term does not vanish and we obtain additional geometric and/or dynamical phase contributions. These can be considered to originate in the subjacent geometry only if  $U$  is a parallel transporting unitarity, but not for arbitrary  $U$ .

To show the consistency with the experiment performed by Hasegawa *et al.* we calculate the phase  $\phi_{\rho P} = \arg \text{Tr}[U\rho UP]$ . In the left panel of Figure 3.6 we show  $\phi_{\rho P}$  for a mixed input state with  $\lambda_1 = 0.87, \lambda_2 = 0.13$ , in accordance with the experimental degree of polarisation in [HLB<sup>+</sup>01, HLB<sup>+</sup>02], and the spin polarisation angle  $\theta = \pi/6$  relative to the magnetic

field in the upper arm of the interferometer (see Figure 2 of Ref. [HLB<sup>+</sup>02]). The calculated curve matches with the experimental and theoretical results presented in Figure 5(d) of Ref. [HLB<sup>+</sup>02]. Note that in this case  $U$  is not parallel transporting the incident spinor.

Another interesting fact is that due to the impurity of the input state we expect phase jumps for  $\theta = \pi/2$  for  $\delta = 2 \arccos \sqrt{\lambda_1}$  and  $\delta = 2\pi - 2 \arccos \sqrt{\lambda_1}$ , see right panel of Figure 3.6, where  $\delta$  is the precession angle of the incident spinor about the direction of the magnetic field. Here, we have a parallel transporting  $U = U^{\parallel}$ , thus these jumps have their origin in the subjacent geometry of state space.

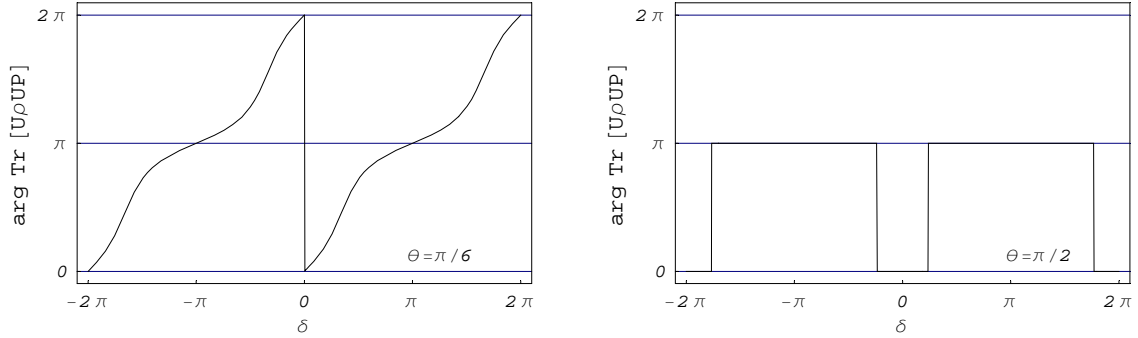


Figure 3.6: The projection off-diagonal mixed state geometric phase  $\arg \text{Tr}[U \rho U P]$  in radians modulus  $2\pi$  for the Hasegawa setup with  $\lambda_1 = 0.87, \lambda_2 = 0.13$  and  $\theta = \pi/6$  or  $\theta = \pi/2$ , respectively.  $\delta$  is the precession angle in radians of the incident spinor about the direction of the magnetic field.

The projection off-diagonal geometric phase factor  $\gamma_{\rho P}$  is invariant under phase transformations of the eigenvectors of  $\rho$ , it reduces to the corresponding  $l = 2$  phase factor  $\gamma_{ij}$  in the pure state limit, and it has the advantage that it can be observed in single particle experiments. The drawbacks are that it is less symmetric than that in Eq. (3.2.18), one cannot easily state a generalisation like in Eq. (3.2.16), and vice versa it cannot be regarded as an off-diagonal generalisation of the mixed state geometric phase in Ref. [SPE<sup>+</sup>00] as  $\rho$  and  $P$  are not unitarily connected. These features suggest that the mixed state geometric phase factor in Eq. (3.2.18) is to be preferred over  $\gamma_{\rho P}$ .

### 3.2.6 Explicit calculations for a simple path

In this section I present an explicit example of a parallel transported mixed state  $\rho_0$  in contrast to the more general discussion in the previous Section 3.2.4.

The initial mixed state  $\rho_0$  is given by

$$\rho_0 = \frac{1}{2} \begin{pmatrix} 1+r & 0 \\ 0 & 1-r \end{pmatrix} \quad (3.2.26)$$

in the orthonormal eigenbasis  $|0\rangle, |1\rangle$  of  $\rho_0$  and  $r$  denotes the degree of polarisation. The

### 3. OFF-DIAGONAL GEOMETRIC PHASES

orthogonal state under the definition (3.2.11) is then

$$\rho_0^\perp = \frac{1}{2} \begin{pmatrix} 1-r & 0 \\ 0 & 1+r \end{pmatrix}. \quad (3.2.27)$$

To gain information about the geometric phase we have to choose a unitary operator  $U$  such that it fulfils the parallel transport condition. For the sake of simplicity we choose an evolution that comprises two subsequent rotations, first by an arbitrary angle  $\beta$  about the  $y$ -axis, and second, by an angle  $\gamma$  about an axis  $\vec{n}$  such that the state vector is again parallel transported.

The 2<sup>nd</sup> the rotation axis  $\vec{n}$  has to be chosen orthogonal to the Bloch vector after the first rotation  $(\sin \beta, 0, \cos \beta)^T$ , where  $\beta$  is the angle to the  $z$ -axis, to guarantee a parallel transport. The orthogonal plane through the origin is spanned by the two vectors

$$\vec{a} = \begin{pmatrix} 0 \\ 1 \\ 0 \end{pmatrix} \quad \text{and} \quad \vec{b} = \begin{pmatrix} -\cos \beta \\ 0 \\ \sin \beta \end{pmatrix},$$

which is evident from Figure (3.7). The rotational axis is now singled out by the choice of

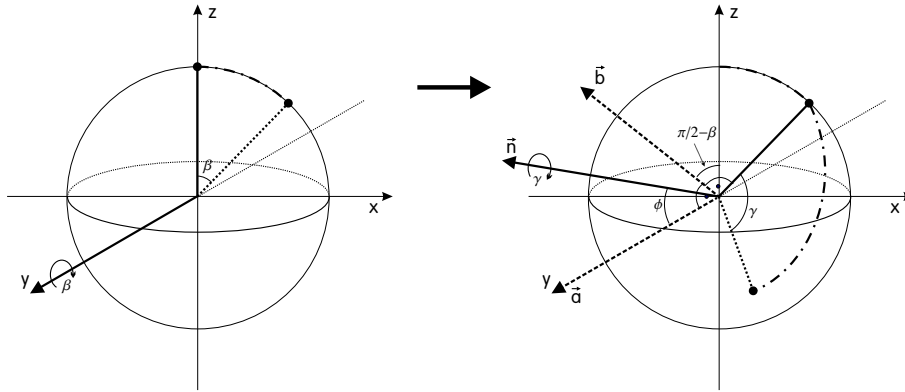


Figure 3.7: Rotation of mixed states

the coefficients of the linear sum of these vectors and can be specified by a single parameter  $\phi$ :

$$\vec{n} = \cos \phi \vec{a} + \sin \phi \vec{b} = \begin{pmatrix} -\sin \phi \cos \beta \\ \cos \phi \\ \sin \phi \sin \beta \end{pmatrix}. \quad (3.2.28)$$

A rotation around the axis  $\vec{n}$  by an angle  $\gamma$  on the Bloch sphere is given by

$$\begin{aligned}
 U_{\vec{n}}(\phi, \gamma) &= e^{-i\frac{\gamma}{2}\vec{n}\cdot\vec{\sigma}} \\
 &= \mathbb{1} \cos \frac{\gamma}{2} - i \sin \frac{\gamma}{2} \sum_k n_k \sigma_k \\
 &= \mathbb{1} \cos \frac{\gamma}{2} - i \sin \frac{\gamma}{2} \begin{pmatrix} \sin \phi \sin \beta & -\sin \phi \cos \beta - i \cos \phi \\ -\sin \phi \cos \beta + i \cos \phi & -\sin \phi \sin \beta \end{pmatrix}.
 \end{aligned} \tag{3.2.29}$$

The total rotation can now be written as

$$\begin{aligned}
 U(\phi, \gamma, \beta) &= U_{\vec{n}}(\phi, \gamma) U_y(\beta) = \\
 &= \begin{pmatrix} \cos(\frac{\gamma}{2}) - i \sin(\frac{\gamma}{2}) \sin \phi \sin \beta & i \sin(\frac{\gamma}{2}) [\sin \phi \cos \beta + i \cos \phi] \\ i \sin(\frac{\gamma}{2}) [\sin \phi \cos \beta - i \cos \phi] & \cos(\frac{\gamma}{2}) + i \sin(\frac{\gamma}{2}) \sin \phi \sin \beta \end{pmatrix} \begin{pmatrix} \cos(\frac{\beta}{2}) & -\sin(\frac{\beta}{2}) \\ \sin(\frac{\beta}{2}) & \cos(\frac{\beta}{2}) \end{pmatrix}.
 \end{aligned} \tag{3.2.30}$$

Using  $U(\gamma, \phi, \beta)$  guarantees parallel transport throughout the whole evolution, so that one can be sure to get a geometric phase factor without any dynamical contribution.

### Nodal structure of the diagonal geometric phase of mixed states $\phi_\rho$

First we look at the nodal structure of the diagonal phase for mixed states  $\phi_\rho \equiv \arg \text{Tr}[U\rho_0]$ . The phase information is lost when  $|\text{Tr}[U\rho_0]|$  vanishes. Explicit calculation using (3.2.30) yields

$$\begin{aligned}
 |\text{Tr}[U\rho_0]| &= |(\cos \frac{\beta}{2} \cos \frac{\gamma}{2} - \cos \phi \sin \frac{\beta}{2} \sin \frac{\gamma}{2}) + ir \sin \frac{\beta}{2} \sin \frac{\gamma}{2} \sin \phi| = \\
 &= \sqrt{(\cos \frac{\beta}{2} \cos \frac{\gamma}{2} - \cos \phi \sin \frac{\beta}{2} \sin \frac{\gamma}{2})^2 + r^2 \sin^2 \frac{\beta}{2} \sin^2 \frac{\gamma}{2} \sin^2 \phi}.
 \end{aligned} \tag{3.2.31}$$

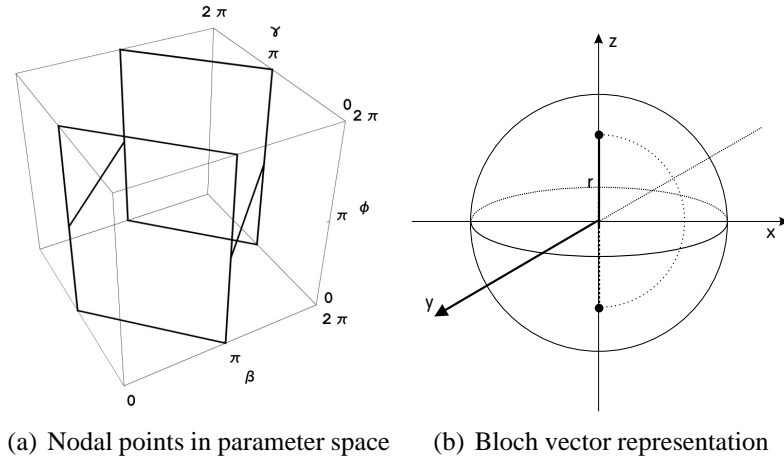
**Mixed and pure states  $r \neq 0$**  For mixed states with  $r \neq 0$  the expression (3.2.31) vanishes whenever

$$(\beta + \gamma) = (2n + 1)\pi, \quad \phi = 2n'\pi \quad \vee \tag{3.2.32a}$$

$$(\beta - \gamma) = (2n + 1)\pi, \quad \phi = (2n' + 1)\pi, \tag{3.2.32b}$$

for  $n, n' = 0, 1, 2, \dots$  (see Figure 3.8(a)). In both cases, (3.2.32a) and (3.2.32b), these conditions for a nodal point can be regarded as a rotation of the original Bloch vector to the Bloch vector pointing in the opposite direction, or for  $r = 1$  - thus for pure states - as the rotation to the orthogonal pure state. The difference is only the choice of the  $2^{nd}$  rotational axis between the positive y-axis in (3.2.32a) and the negative y-axis in (3.2.32b).

**Totally mixed state  $r = 0$  [Bha02, ASP<sup>+</sup>01]** For a totally mixed state (3.2.31) vanishes for numerous combinations of  $\beta$ - $\gamma$ - $\phi$  values comprising the values in (3.2.32), but also for


 Figure 3.8: Nodal structure of  $|\text{Tr}[U\rho_0]|$ ,  $r \neq 0$ 

combinations when the single remaining term in (3.2.31) vanishes,

$$\cos\left(\frac{\beta}{2}\right)\cos\left(\frac{\gamma}{2}\right) - \cos\phi \sin\left(\frac{\beta}{2}\right)\sin\left(\frac{\gamma}{2}\right) = 0,$$

which produces a richer nodal structure than for  $r \neq 0$ . The nodal points of  $|\text{Tr}[U\rho_0]|$  are shown in Figure (3.9).

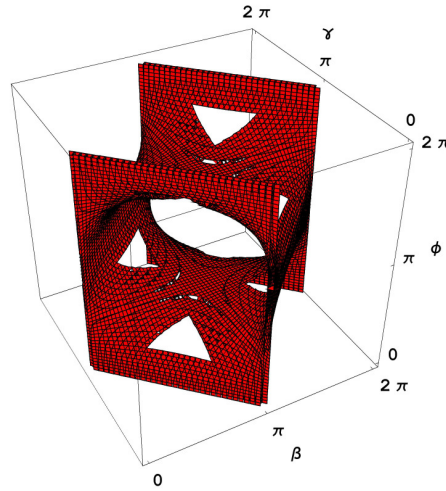


Figure 3.9: Nodal structure of  $|\text{Tr}[U\rho_0]|$ ,  $r = 0$ . The holes in the plot are only numerical artifacts.

### Nodal structure of the off-diagonal geometric phase for mixed states $\phi_{\rho\rho^\perp}$

Let us investigate now the behaviour of the off-diagonal geometric phase for mixed states  $\phi_{\rho\rho^\perp} \equiv \arg \text{Tr}[U\sqrt{\rho_0}U\sqrt{\rho_0^\perp}]$ . This quantity becomes undefined if the modulus of  $\text{Tr}[U\sqrt{\rho_0}U\sqrt{\rho_0^\perp}]$  vanishes. Explicit calculation using the unitary transformation (3.2.30)

results in the expression

$$\begin{aligned} \text{Tr}[U\sqrt{\rho_0}U\sqrt{\rho_0^\perp}] &= \frac{1}{2}(-1 + \cos\beta\cos\gamma - \cos\phi\sin\beta\sin\gamma + \sqrt{1-r^2} \times \\ &\times [\cos^2\phi(1 + \cos\beta\cos\gamma) + \sin^2\phi(\cos\beta + \cos\gamma) - \cos\phi\sin\beta\sin\gamma]). \end{aligned} \quad (3.2.33)$$

**Pure states** For  $r = 1$ , the right hand side of Eq. (3.2.33) is negative for all values of  $\phi$ ,  $\beta$  and  $\gamma$ , because the term comprising  $\sqrt{1-r^2}$  vanishes and the other terms can only be smaller or equal to zero. Thus, no sign change happens -  $\phi_{\rho\rho^\perp}$  is equal to  $\pi$  for every unitary evolution - in correspondence to the off-diagonal phase for pure states discussed in [MP00]. In detail, we get nodal points of  $|\text{Tr}[U\sqrt{\rho_0}U\sqrt{\rho_0^\perp}]|$  for the following scenarios (see Figure 3.10(c)):

$$\phi = (2n + 1)\pi, \quad \beta - \gamma = 2n\pi, \quad (3.2.34a)$$

$$\phi = 2n\pi, \quad \beta + \gamma = 2n\pi, \quad (3.2.34b)$$

$$\phi \text{ arbitrary}, \quad \beta = \gamma = n\pi. \quad (3.2.34c)$$

All three cases represent a rotation of the initial (pure) state back to itself.

**Mixed states** For  $r \neq 1$  (3.2.33) is not a purely negative function anymore - we get sign changes for different choices of  $r$  - see Figures (3.10(a)) and (3.10(b)). In these plots the nodal points of  $|\text{Tr}[U\sqrt{\rho_0}U\sqrt{\rho_0^\perp}]|$  are shown and it is remarkable that contrary to the pure state case the surface indicates also a sign change of this expression. For this reason  $\phi_{\rho\rho^\perp} = \arg \text{Tr}[U\sqrt{\rho_0}U\sqrt{\rho_0^\perp}]$  can take the values 0 or  $\pi$ .

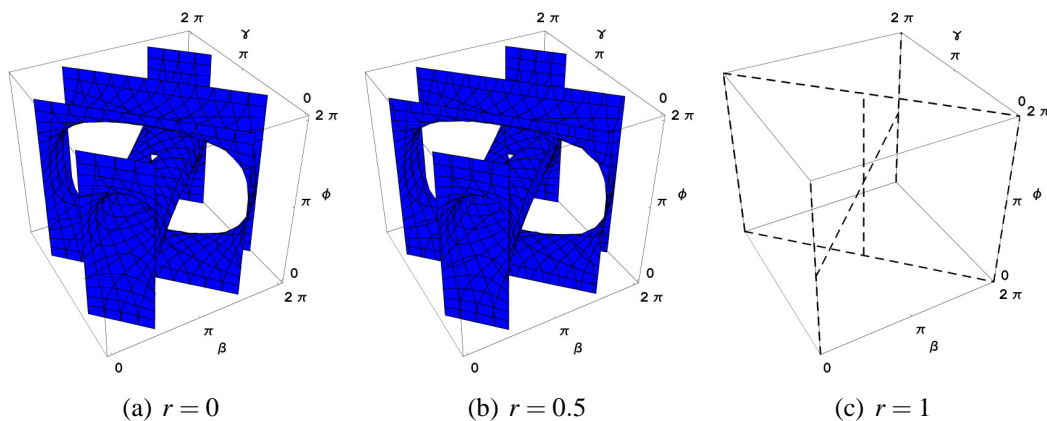


Figure 3.10: Nodal structure of  $|\text{Tr}(U\sqrt{\rho_0}U\sqrt{\rho_0^\perp})|$

### Comparison of the diagonal and the off-diagonal geometric phase

Now we only have to check that the nodal points of the diagonal ( $\phi_\rho$ ) and the off-diagonal geometric phases ( $\phi_{\rho\rho^\perp}$ ) do not coincide, otherwise we would have failed to construct an expression carrying information about the subjacent geometry, when the diagonal geometric phase is undefined in the mixed state case. Comparing the nodal structures of  $\phi_\rho$  and  $\phi_{\rho\rho^\perp}$  we can see that both expressions vanish at distinct points in the parameter space for  $r = 0$  (Figure 3.11(a)). For  $r \neq 0$  the nodal structure of  $\phi_\rho$  is independent of  $r$  and by comparing Figure 3.8(a) with the Figures 3.10(b)-3.10(c) it is obvious that the nodal points of  $\phi_\rho$  and  $\gamma_{\rho\rho^\perp}$  do not coincide (see Figure 3.11(b)).

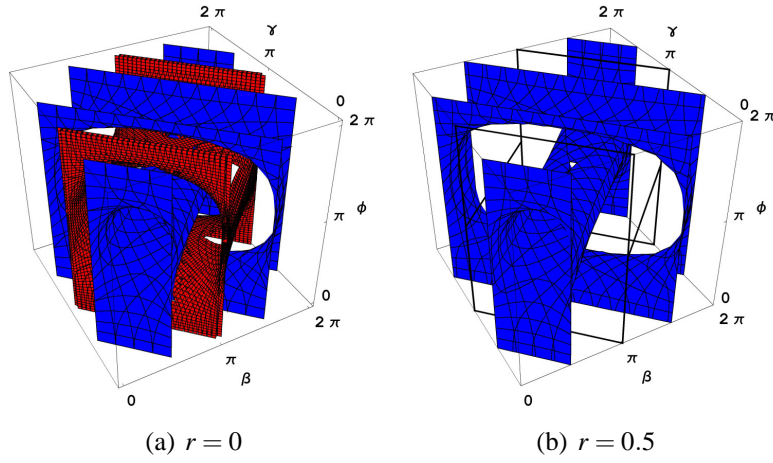


Figure 3.11: Comparison of nodal points between  $\gamma_{\rho\rho^\perp}$  and  $\phi_\rho$

### 3.2.7 Kinematic approach to off-diagonal geometric phases

Similar to the extension of the diagonal geometric phase  $\phi_\rho$  to general not parallel transporting unitarities the same procedure can be applied to the off-diagonal geometric phase. Essentially by subtracting the dynamical phase from the contribution of each eigenstate to the total phase (c. f. Eq. 2.3.15) a gauge invariant quantity is obtained. For the off-diagonal mixed state geometric phase in the non-degenerate case, the parallel transport conditions are still given by Eq. (2.3.5) and  $U^\parallel(t)$  by Eq. (2.3.13). Substituting  $U^\parallel(t)$  into Eq. (3.2.16), we obtain the kinematic expression for the off-diagonal geometric phase factors for mixed states with the evolution operator  $U(s)$  ( $s \in [0, T]$ ) as

$$\gamma_{\rho_{j_1 \dots j_l}}^{(l)} = M \left[ \sum_{i_1, \dots, i_l=1}^N \sqrt{\lambda_{i_1-j_1+1} \dots \lambda_{i_l-j_l+1}} \langle \psi_{i_1} | U(T) | \psi_{i_2} \rangle \langle \psi_{i_2} | U(T) | \psi_{i_3} \rangle \dots \langle \psi_{i_l} | U(T) | \psi_{i_1} \rangle \right] \times \exp \left( - \int_0^T \sum_{a=1}^l \langle \psi_{i_a} | U^\dagger(s) \dot{U}(s) | \psi_{i_a} \rangle ds \right), \quad (3.2.35)$$

where  $\lambda_{-p} = \lambda_{N-p}$ ,  $p = 0, \dots, N-1$ . One may verify that the phase factors  $\gamma_{\rho_{j_1} \dots \rho_{j_l}}^{(l)}$  are gauge invariant in that they are independent of the choice of  $U(s)$  as long as they transport  $\rho$  along the same path.

For degenerate mixed states one has to account for the different parallel transport conditions (Eq. 2.3.17), but the scheme works similar to the formalism for the diagonal geometric phase for degenerate mixed states. There is only a subtle complication in that the functional  $F_{\mathcal{H}_m}$  (2.3.20) guaranteeing the gauge invariance is not the same for the different orthogonal states, if their degeneracy structure changes. That means, when the permutation of the basis-vectors exchanges the basis of different degenerate subspaces the  $F_{\mathcal{H}_m}$ 's are different for each orthogonal state. For a more detailed examination the reader is referred to [TSF<sup>+</sup>05] where we also stated an example for further clarification.

### 3.2.8 Experimental verification

When we consider possible experimental realisations of the off-diagonal mixed state phases we immediately encounter a problem: how do we experimentally implement the  $l$ -th root of density operators? Fortunately, this may be resolved in the  $l = 2$  case in the sense of purification, i.e., by adding an ancilla system in a certain way. Here, we propose a physical scenario for the qubit case in terms of polarisation-entangled two-photon interferometry.

We first show how to realise the  $l = 1$  and  $l = 2$  phases via purification. For an  $N$  dimensional Hilbert space  $\mathcal{H}$ , consider the non-degenerate density operator

$$\rho_1 = \sum_{k=1}^N \lambda_k |\psi_k\rangle \langle \psi_k|. \quad (3.2.36)$$

A purification of this  $\rho_1$  is any pure state  $|\Psi_1\rangle$  obtained by adding an ancilla system  $a$  to the considered system  $s$  such that  $\rho_1 = \text{Tr}_a |\Psi_1\rangle \langle \Psi_1|$ . Thus, we may write

$$|\Psi_1\rangle = \sum_{k=1}^N \sqrt{\lambda_k} |\psi_k\rangle \otimes |\phi_k\rangle, \quad (3.2.37)$$

where  $\{|\phi_k\rangle\}$  is an orthonormal set of vectors in the ancilla Hilbert space  $\mathcal{H}_a$ . Consequently, any orthogonal density operator  $\rho_n = (U_g)^{n-1} \rho_1 (U_g^\dagger)^{n-1}$  has a purification of the form

$$|\Psi_n\rangle = (U_g)^{n-1} \otimes \tilde{U}_a |\Psi_1\rangle \quad (3.2.38)$$

for any unitarity  $\tilde{U}_a$  acting on  $\mathcal{H}_a$ . In the following, we assume  $\dim \mathcal{H}_a = N$  and put  $|\phi_k\rangle = |\psi_k\rangle$ .

Let  $U_s \otimes U_a |\Psi_1\rangle$  and  $V_s \otimes V_a |\Psi_1\rangle$  be two Hilbert space representatives of a pair of purifications of  $U_s \rho_1 U_s^\dagger$  and  $V_s \rho_1 V_s^\dagger$ . The coincidence interference pattern obtained in superposition

is determined by the interference profile

$$I \propto \left| U_s \otimes U_a |\Psi_1\rangle + V_s \otimes V_a |\Psi_1\rangle \right|^2 = 2 + 2\text{Re} \left[ \text{Tr} (U_s^\dagger V_s \otimes U_a^\dagger V_a |\Psi_1\rangle \langle \Psi_1|) \right]. \quad (3.2.39)$$

By choosing  $U_s = e^{i\eta} (U_g)^{j_1-1}$ ,  $V_s = U^\parallel (U_g)^{j_1-1}$ , and  $U_a = V_a = I$ , we obtain the  $l = 1$  phase factors  $\gamma_{\rho_{j_1}}^{(1)} = \phi_\rho$  by variation of the  $U(1)$  phase  $\eta$  since

$$\begin{aligned} M \left[ \text{Tr} (U_s^\dagger V_s \otimes U_a^\dagger V_a |\Psi_1\rangle \langle \Psi_1|) \right] &= e^{-i\eta} M \left[ \text{Tr} ((U_g^\dagger)^{j_1-1} U^\parallel (U_g)^{j_1-1} \otimes I |\Psi_1\rangle \langle \Psi_1|) \right] \\ &= e^{-i\eta} M \left[ \text{Tr} (U^\parallel \rho_{j_1}) \right], \end{aligned} \quad (3.2.40)$$

where we have used that  $\text{Tr}_a [(U_g)^{j_1-1} |\Psi_1\rangle \langle \Psi_1| (U_g^\dagger)^{j_1-1}] = \rho_{j_1}$ . Similarly, the  $l = 2$  phase factors  $\gamma_{\rho_{j_1} \rho_{j_2}}^{(2)}$  are obtained by letting  $U_s = e^{i\eta} (U_g)^{j_2-1}$ ,  $V_s = U^\parallel (U_g)^{j_1-1}$ ,  $U_a = (U_g)^{j_2-1}$ , and  $V_a = (U^\parallel)^T (U_g)^{j_1-1}$ ,  $T$  being transpose with respect to the ancilla basis  $\{|\psi_k\rangle\}$ , since

$$\begin{aligned} M \left[ \text{Tr} (U_s^\dagger V_s \otimes U_a^\dagger V_a |\Psi_1\rangle \langle \Psi_1|) \right] &= e^{-i\eta} M \left[ \text{Tr} ((U_g^\dagger)^{j_2-1} U^\parallel (U_g)^{j_1-1} \right. \\ &\quad \left. \otimes (U_g^\dagger)^{j_2-1} (U^\parallel)^T (U_g)^{j_1-1} |\Psi_1\rangle \langle \Psi_1|) \right] \\ &= e^{-i\eta} M \left[ \text{Tr} (U^\parallel \sqrt{\rho_{j_1}} U^\parallel \sqrt{\rho_{j_2}}) \right], \end{aligned} \quad (3.2.41)$$

where the last equality may be obtained by explicit use of  $|\Psi_1\rangle$  in Eq. (3.2.37) with  $|\phi_k\rangle = |\psi_k\rangle$ ,  $\forall k$ .

Let us discuss a physical purification scenario for the  $l = 1$  and  $l = 2$  phases in the qubit case. Consider the two-photon Franson-type [Fra89] setup in Figure 3.12. A source that in the horizontal-vertical ( $h - v$ ) basis produces polarisation-entangled photon states of the form

$$|\Psi_1\rangle = \sqrt{\frac{1}{2}(1+r)} |h\rangle \otimes |h\rangle + \sqrt{\frac{1}{2}(1-r)} |v\rangle \otimes |v\rangle \quad (3.2.42)$$

has been demonstrated in Ref. [KWW<sup>+</sup>99]. Considered as subsystems both photons are in a mixed linear polarisation state  $\rho_1$  with polarisation degree  $r$ . The desired superposition of  $U_s \otimes U_a |\Psi_1\rangle$  and  $V_s \otimes V_a |\Psi_1\rangle$  is obtained by requiring a sufficiently short coincidence window so that detection occurs only when the photons took both either the shorter path or the longer path [HS00]. A purification of the orthogonal density operator  $\rho_2 = U_g \rho_1 U_g^\dagger$  may be achieved by flipping the polarisations of the photons, yielding

$$|\Psi_2\rangle = U_g \otimes U_g |\Psi_1\rangle = \sqrt{\frac{1}{2}(1+r)} |v\rangle \otimes |v\rangle + \sqrt{\frac{1}{2}(1-r)} |h\rangle \otimes |h\rangle. \quad (3.2.43)$$

To demonstrate the  $l = 1$  and  $l = 2$  geometric phases in this scenario, it is sufficient to consider unitarities that rotate linear polarization states along great circles an angle  $\beta$  on the

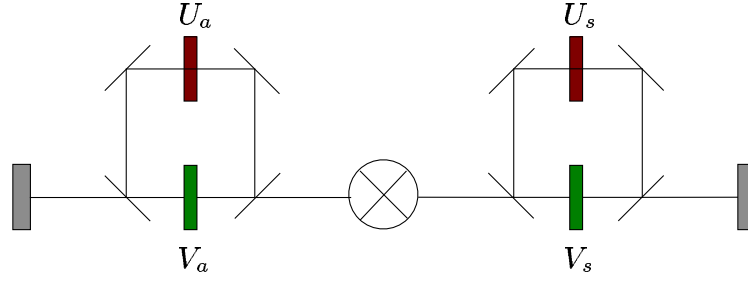


Figure 3.12: Franson setup for polarisation-entangled photon pairs. In the longer arms, the system and ancilla photons are exposed to the polarisation affecting unitarities  $U_s$  and  $U_a$ , respectively, and similarly  $V_s$  and  $V_a$  in the shorter arms.

Poincaré sphere, see Figure 3.13. This amounts to

$$U(\beta, \theta) = \exp\left(-i\frac{\beta}{2}\left[\cos\theta(|h\rangle\langle v| + |v\rangle\langle h|) + \sin\theta(-i|h\rangle\langle v| + i|v\rangle\langle h|)\right]\right), \quad (3.2.44)$$

which fulfils the parallel transport condition (2.3.8) with respect to the  $h-v$  basis. In practice,  $U(\beta, \theta)$  may be implemented by appropriate  $\lambda$ -plates, the thickness and orientation of which correspond to the parameters  $\beta$  and  $\theta$ , respectively. For example,  $U_g = U(\pi, \pi/2)$  acts on the linear polarisation states as a polarisation flip and thus connects  $\rho_1$  and  $\rho_2$ . It is achieved by a  $\lambda/2$  plate with half axis making an angle  $45^\circ$  to the vertical ( $v$ ) direction. Furthermore,  $\theta = 0$  and  $\beta = \pi/2$ , corresponding to a  $\lambda/4$  plate oriented along the vertical direction, takes  $h$  and  $v$  into the right ( $R$ ) and left ( $L$ ) circular polarisation states, respectively.

The phase factors  $\gamma_{\rho_n}^{(1)} = \phi_{\rho_n}$ ,  $n = 1, 2$ , are obtained from the coincidence intensity by setting  $U_s = e^{i\eta}(U_g)^{n-1}$ ,  $V_s = U(\beta, \theta)(U_g)^{n-1}$ , and  $U_a = V_a = I$ . Explicit calculation for  $U(\beta, \theta)$  in Eq. (3.2.44) yields  $\text{Tr}(\rho_1 U(\beta, \theta)) = \text{Tr}(\rho_2 U(\beta, \theta)) = \cos(\beta/2)$ , which entails that  $\gamma_{\rho_1}^{(1)}$  and  $\gamma_{\rho_2}^{(1)}$  are real-valued and changes sign at  $\beta = (2j+1)\pi$ ,  $j$  integer, corresponding to a sequence of phase jumps of  $\pi$ . Furthermore, the choice  $U_s = e^{i\eta}U_g$ ,  $V_s = U(\beta, \theta)$ ,  $U_a = U_g$ , and  $V_a = U^T(\beta, \theta) = U(\beta, -\theta)$ , yields  $\gamma_{\rho_1\rho_2}^{(2)}$  and we may compute the expected output as  $\text{Tr}(\sqrt{\rho_1}U(\beta, \theta)\sqrt{\rho_2}U(\beta, \theta)) = \sqrt{1-r^2}\cos^2(\beta/2) - \sin^2(\beta/2)$ , which is independent of  $\theta$  and can be positive and negative for  $r \neq 1$  depending upon  $\beta$ .  $\gamma_{\rho_1\rho_2}^{(2)}$  changes sign at  $\beta = 2\pi j + 2\arctan\sqrt[4]{1-r^2}$ . Note that  $0 \leq \arctan\sqrt[4]{1-r^2} \leq \pi/4$ , modulus  $\pi$ , which assures that the  $l = 1$  and  $l = 2$  phases never become indeterminate for the same  $\beta$  value, and thus provide a complete experimental phase characterisation of the qubit case in the sense of purification.

**Off-diagonal geometric phase measurement with a neutron interferometer** Why is it not possible to use a neutron interferometer to test the off-diagonal mixed state geometric phase? For the pure state case this was possible since in order to measure  $\sigma_{jk}\sigma_{kj} = M[\langle\psi_j|U|\psi_k\rangle\langle\psi_k|U|\psi_j\rangle]$  the projection operator  $|\psi_k\rangle\langle\psi_k|$  between the two unitarities  $U$  can

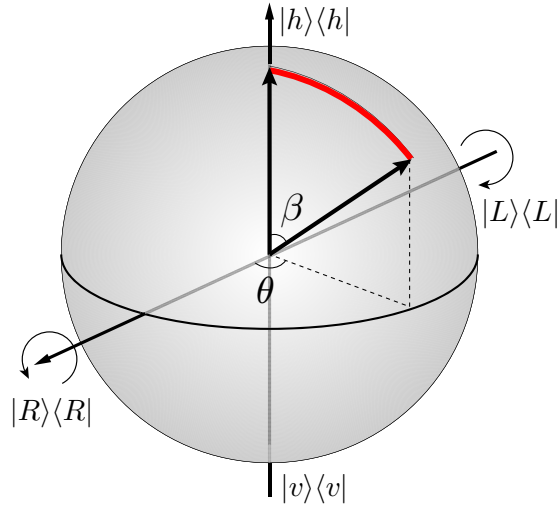


Figure 3.13: Effect of the unitarity  $U(\beta, \theta)$  on the Poincaré sphere. The horizontal polarisation state  $|h\rangle$  at the north pole is taken into a new polarisation state at spherical polar angles  $(\beta, \theta)$ .

be implemented by a spin projection measurement. In the mixed state case this does not work since it leads to an asymmetric definition of the off-diagonal mixed geometric phase (Eq. 3.2.24). Instead of a projective measurement one could also think of using a more generalised measurement, a positive operator-valued measurement (POVM) [NC00]. But for this one usually needs an ancilla Hilbert space. Generally speaking, a POVM behaves analogous to the purification of a mixed state by means of an extra Hilbert space, or like the possibility to represent any non-unitary operation as a unitary transformation in an extended Hilbert space. A normal projective (von Neumann-type) measurement in the extended Hilbert space yields a POVM in the system's Hilbert space. But for neutrons there is no other degree of freedom than spin for the construction of an extended Hilbert space.

Unfortunately, a scheme similar to the Franson-type interferometer introduced above does not work either, although the topology of the interferometer could possibly be mimicked by building a three-loop interferometer as further extension to the two-loop interferometer utilised in Chapter 4. But, there are no entangled neutrons available. The interference of neutrons is a single-particle effect, each of them interacts with itself, and even if there is a slight probability to find two neutrons in a small time-window, they are totally uncorrelated. So, it seems that for neutrons there is only the projective mixed state geometric phase at hand, which has been measured in [HLB<sup>+</sup>02].

### 3.3 Off-diagonal holonomies following Uhlmann's definition

The Uhlmann holonomy defined in Section 2.4 is a further candidate to spot its nodal points and attempt to find an off-diagonal extension. It is given by the expression (c. f. Eq. 2.4.19)

$$\mathcal{X}_{\mathcal{C}} = W_1 W_0^\dagger$$

and the task is now to find points where this expression becomes undefined. In particular, we say that a point is a nodal point whenever the functional  $v_{\mathcal{C}} = \text{Tr } \mathcal{X}_{\mathcal{C}}$  from Eq. (2.4.18) vanishes. Furthermore, a comparison with previous definitions of off-diagonal geometric phases for pure and mixed states is carried out and, finally, examples are given to show the relevance of this extension.

#### 3.3.1 Nodal points of Uhlmann holonomies

In the pure state limit,  $v_{\mathcal{C}}$  has nodal points (i. e., is undefined) for orthogonal initial and final states. In general, let  $\mathcal{H}_1 \oplus \mathcal{H}_2 \oplus \dots \oplus \mathcal{H}_n$  be an orthogonal sum decomposition of the Hilbert space  $\mathcal{H}$  of the system, where  $n \leq \dim \mathcal{H}$  with equality for the pure state case. Then, if the initial state  $\rho(0)$  with support in  $\mathcal{H}_k$  ( $\rho(0) \in \mathcal{O}(\mathcal{H}_k)$ ) evolves to the state  $\rho(T)$  with support in  $\mathcal{H}_l$  ( $l \neq k$ ),  $v_{\mathcal{C}}$  is undefined since the trace vanishes. If this happens  $\rho(0)$  and  $\rho(T)$  are said to be orthogonal.

#### 3.3.2 Definition of off-diagonal quantum holonomies

Like in the previous sections (and [MP00, FS03b, FS03a]) we wish to obtain geometric information about the path even in the special case of orthogonal initial and final states. Suppose we have a set of initial density operators  $\rho_k(0)$ ,  $k = 1, \dots, n$ , each of which with support in the corresponding Hilbert space  $\mathcal{H}_k$ . Then, we can define the *off-diagonal quantum holonomy invariants* as [FS05]

$$\begin{aligned} \mathcal{X}_{j_1 \dots j_l}^{(l)}[\mathcal{C}_{j_1} \dots \mathcal{C}_{j_l}] &\equiv W_{j_1}(T) W_{j_1}^\dagger(0) W_{j_2}(T) W_{j_2}^\dagger(0) \dots W_{j_l}(T) W_{j_l}^\dagger(0) \\ &= \mathcal{X}_{j_1}^{(1)}[\mathcal{C}_{j_1}] \mathcal{X}_{j_2}^{(1)}[\mathcal{C}_{j_2}] \dots \mathcal{X}_{j_l}^{(1)}[\mathcal{C}_{j_l}], \end{aligned} \quad (3.3.1)$$

where  $l = 1, \dots, n$ . Evidently,  $\mathcal{X}_{j_k}^{(1)}[\mathcal{C}_{j_k}]$ ,  $k = 1, \dots, n$  is the Uhlmann holonomy invariant for the path of a single density matrix,  $\mathcal{C}_{j_k} : t \in [0, \tau] \rightarrow \rho_{j_k}(t)$ , and each  $\mathcal{X}_{j_k}^{(1)}[\mathcal{C}_{j_k}]$  comprises a relative phase factor  $\tilde{V}_{j_k}$  depending only on the path  $\mathcal{C}_{j_k}$ .

$\mathcal{X} \equiv \mathcal{X}_{j_1 \dots j_l}^{(l)}[\mathcal{C}_{j_1} \dots \mathcal{C}_{j_l}]$  can be decomposed either as  $\mathcal{X} = (\mathcal{X} \mathcal{X}^\dagger)^{1/2} \mathcal{U}_R$  (right polar decomposition) or as  $\mathcal{X} = \mathcal{U}_L (\mathcal{X}^\dagger \mathcal{X})^{1/2}$  (left polar decomposition), where the left (right) support of the partial isometry<sup>4</sup>  $\mathcal{U}_R$  ( $\mathcal{U}_L$ ) is required to be equal to the right (left) support of

---

<sup>4</sup>Here, the polar decomposition comprises a partial isometry instead of a unitary operator since the density

the positive Hermitian part of the left (right) polar decomposition of  $\mathcal{X}$ . The holonomies  $\mathcal{U}_L$  or  $\mathcal{U}_R$  defined via the left or right polar decomposition, respectively, are Uhlmann analogues to the off-diagonal geometric phase factors defined in Ref. [MP00] for pure states and Refs. [FS03b, FS03a] for mixed states.

Orthogonal supports of the positive Hermitian parts of the left and right polar decomposition is a sufficient condition for a nodal point of the generalised functional

$$v_{\mathcal{C}_{j_1} \dots \mathcal{C}_{j_l}}^{(l)} \equiv \arg \text{Tr} [W_{j_1}(T)W_{j_1}^\dagger(0)W_{j_2}(T)W_{j_2}^\dagger(0) \dots W_{j_l}(T)W_{j_l}^\dagger(0)]. \quad (3.3.2)$$

This can be seen by noting at first that the left and right support of the operator  $\mathcal{X}$  is given by the support of  $\mathcal{X}\mathcal{X}^\dagger$  and  $\mathcal{X}^\dagger\mathcal{X}$ , respectively, and in addition that the trace of  $\mathcal{X}$  vanishes for non-overlapping left and right support. Since  $\mathcal{X}\mathcal{X}^\dagger$  and  $\mathcal{X}^\dagger\mathcal{X}$  appear in the positive Hermitian parts of the polar decomposition the nodal points of  $v_{\mathcal{C}_{j_1} \dots \mathcal{C}_{j_l}}^{(l)}$  are necessary for orthogonal left and right supports of  $\mathcal{X}$ .

Let us have a detailed look at the right and left support of  $\mathcal{X}$ . The left support is given by

$$\begin{aligned} \mathcal{X}\mathcal{X}^\dagger &= \rho_{j_1}^{1/2}(T)\tilde{V}_{j_1}(T)\rho_{j_1}^{1/2}(0)\rho_{j_2}^{1/2}(T)\tilde{V}_{j_2}(T) \dots \rho_{j_l}^{1/2}(T)\tilde{V}_{j_l}(T) \\ &\quad \times \rho_{j_l}(0)\tilde{V}_{j_l}^\dagger(T) \dots \rho_{j_1}^{1/2}(0)\tilde{V}_{j_1}^\dagger(T)\rho_{j_1}^{1/2}(T) \end{aligned} \quad (3.3.3)$$

and the right support

$$\begin{aligned} \mathcal{X}^\dagger\mathcal{X} &= \rho_{j_l}^{1/2}(0)\tilde{V}_{j_l}^\dagger(T)\rho_{j_l}^{1/2}(T) \dots \rho_{j_1}^{1/2}(0)\tilde{V}_{j_1}^\dagger(T) \\ &\quad \times \rho_{j_1}(T)\tilde{V}_{j_1}(T)\rho_{j_1}^{1/2}(0)\rho_{j_2}^{1/2}(T)\tilde{V}_{j_2}(T) \dots \rho_{j_l}^{1/2}(T)\tilde{V}_{j_l}\rho_{j_l}^{1/2}(0). \end{aligned} \quad (3.3.4)$$

These are apparently only orthogonal in the case that  $\rho_{j_1}(T)$  and  $\rho_{j_l}(0)$  have orthogonal support and this in turn can be avoided by a proper choice of initial states. These choices of the  $\rho_{j_k}(0)$ ,  $k = 1, \dots, l$  are evidently not unique, one can take any state  $\rho_{j_l} \in \mathcal{O}(\mathcal{H}_{j_l})$  for a given  $\rho_{j_1}$  with the minimal requirement that  $\rho_{j_k}(T)$  has overlapping support at least with  $\rho_{j_{k-1}}(0)$  where the indices  $k$  have to be considered modulo  $n$ . This is equivalent to non-vanishing transition probability from  $\rho_{j_k}(T)$  to  $\rho_{j_{k-1}}(0)$  [Uhl76].

To assure that the off-diagonal quantum holonomy invariants  $\mathcal{X}_{j_1 \dots j_l}^{(l)}[\mathcal{C}_{j_1} \dots \mathcal{C}_{j_l}]$  fulfil all necessary criteria, we note that the  $\mathcal{X}_{j_1 \dots j_l}^{(l)}[\mathcal{C}_{j_1} \dots \mathcal{C}_{j_l}]$ 's are only dependent upon the paths  $\mathcal{C}_{j_k}$  by the same reasoning as for the  $l = 1$  case. In fact, the final amplitude  $W_{j_k}(t)$  of each initial state  $\rho_{j_k}(0)$  is determined by the parallel transport condition in Eq. (2.4.13) up to a  $t$ -independent partial isometry  $S$ . This latter global gauge leaves  $\mathcal{X}_{j_1 \dots j_l}^{(l)}[\mathcal{C}_{j_1} \dots \mathcal{C}_{j_l}]$  invariant even for distinct choices  $S = S_{j_k}$  for the different constituent initial states.

**Unitary evolution** We now rewrite the parallel transport mechanism in the particular case of mixed states undergoing unitary evolution. The standard purification of a mixed state  $\rho(0) = \sum \lambda_j |\psi_j\rangle\langle\psi_j|$  with  $\sum_j \lambda_j = 1$  and  $|\psi_j\rangle$  being a basis diagonalising  $\rho(0)$  is

---

matrix may not have support in the total Hilbert space but only in a subspace.

$W(0) = \sum_j \sqrt{\lambda_j} |\psi_j\rangle \langle \phi_j|$ , i. e.,  $\mathcal{H}$  is extended by an ancilla Hilbert space  $\mathcal{H}' = \mathcal{H}^*$ , where the  $\langle \phi_j| \in \mathcal{H}^*$  form a basis in the ancilla part. Subjected to the unitary evolution  $\rho(0) \mapsto \rho(t) = U(t)\rho(0)U^\dagger(t)$ ,  $t \in [0, T]$ , the path of the purifications  $t \mapsto W(t)$  has to fulfil the parallelity condition (2.4.13). This latter path can be described by applying a partial isometry  $B(t) \in \mathcal{O}(\mathcal{H}')$  resulting in

$$W(t) = U(t)\rho^{1/2}(0)B(t), \quad (3.3.5)$$

where  $B(t) = U^\dagger(t)V(t)$  and  $U(t)$  are related via the parallel transport condition Eq. (2.4.13). Inserting (3.3.5) into (2.4.13) we get the parallel transport condition

$$2\rho^{1/2}(0)U^\dagger(t)\dot{U}(t)\rho^{1/2}(0) = B(t)\dot{B}^\dagger(t)\rho(0) - \rho(0)\dot{B}(t)B^\dagger(t), \quad (3.3.6)$$

where the dot denotes the derivative with respect to the parameter  $t$ . If  $\rho(0)$  is pure,  $\rho(0) = |\psi_j\rangle \langle \phi_j|$ , Eq. (3.3.6) simplifies to

$$\langle \psi_j|U^\dagger(t)\dot{U}(t)|\psi_j\rangle = \langle \phi_j|B^\dagger(t)\dot{B}(t)|\phi_j\rangle. \quad (3.3.7)$$

To verify that Eq. (3.3.1) is consistent with known results we consider the pure unitary case from Section 3.1. Having a set of initial pure states  $|\psi_k\rangle$ ,  $k = 1, \dots, n$ , the defining quantity from Eq. (3.3.1) can be written as

$$\begin{aligned} & W_{j_1}(T)W_{j_1}^\dagger(0)W_{j_2}(T)W_{j_2}^\dagger(0) \dots W_{j_l}(T)W_{j_l}^\dagger(0) \\ &= U(T)|\psi_{j_1}\rangle \langle \phi_{j_1}|B(T)|\phi_{j_1}\rangle \langle \psi_{j_1}|U(T)|\psi_{j_2}\rangle \langle \phi_{j_2}|B(T)|\phi_{j_2}\rangle \\ & \quad \times \langle \psi_{j_2}|\dots \langle \psi_{j_{m-1}}|U(T)|\psi_{j_l}\rangle \langle \phi_{j_l}|B(T)|\phi_{j_l}\rangle \langle \psi_{j_l}|, \end{aligned} \quad (3.3.8)$$

where we have used the purified states  $|\psi_k\rangle \langle \phi_k|$ . If  $U(t) = U^\parallel(t)$  is already parallel transporting the basis states, i. e.,  $\langle \psi_j|U^\parallel(t)\dot{U}^\parallel(t)|\psi_j\rangle = 0$ ,  $B(t)$  may be chosen to be the identity and Eq. (3.3.8) simplifies to

$$\begin{aligned} & W_{j_1}(T)W_{j_1}^\dagger(0)W_{j_2}(T)W_{j_2}^\dagger(0) \dots W_{j_l}(T)W_{j_l}^\dagger(0) \\ &= U^\parallel(T)|\psi_{j_1}\rangle \langle \psi_{j_1}|U^\parallel(T)|\psi_{j_2}\rangle \langle \psi_{j_2}|\dots \langle \psi_{j_{m-1}}|U^\parallel(T)|\psi_{j_l}\rangle \langle \psi_{j_l}|. \end{aligned} \quad (3.3.9)$$

It is straightforward to write down the off-diagonal phase factors corresponding to this quantity using  $v_{\mathcal{C}_{j_1 \dots j_l}}^{(l)}$  to see the equivalence to the pure state off-diagonal geometric phase.

What is even more noteworthy is the naturally arising generalisation of the latter to non-parallel transporting unitarities  $U(t)$ . A proper choice of  $B(t)$  according to Eq. (3.3.7) yields a parallel lift and therefore a well-defined invariant of the paths  $\mathcal{C}_i$  of the amplitudes  $W_i$ 's.

### 3.3.3 Comparison with the interferometric off-diagonal geometric phase

The interferometric off-diagonal geometric phase for mixed phase in its simplest form is given by (recall Section 3.2)

$$\gamma_{\rho_{j_1}\rho_{j_2}\dots\rho_{j_l}}^{(l)} \equiv M \left[ \text{Tr} \left( U(T) \sqrt[l]{\rho_{j_1}} U(T) \sqrt[l]{\rho_{j_2}} \dots U(T) \sqrt[l]{\rho_{j_l}} \right) \right] \quad (3.3.10)$$

with  $M[z] \equiv z/|z|$  for any complex number  $z$ , the  $\rho_{j_k}$ 's only differing by permutations of their eigenstates, and  $U(t)$ ,  $t \in [0, T]$ , fulfilling parallel transport for each common eigenstate of the  $\rho_{j_k}$ 's. For  $l = 1$  this reduces to the geometric mixed state phase in [SPE<sup>+</sup>00] that has in general been shown to be distinct from the trace of the  $l = 1$  holonomy factor [ESB<sup>+</sup>03]. The question is therefore, how the previously defined off-diagonal geometric phase definition for mixed states  $\gamma_{\rho_{j_1}\rho_{j_2}\dots\rho_{j_l}}^{(l)}$  relates to the off-diagonal generalisation of the Uhlmann phase factor. Using the same scheme as above to compensate dynamical effects in the system by an appropriate choice of unitary operator  $B(t) \in \mathcal{O}(\mathcal{H}')$ , we get

$$\begin{aligned} & W_{j_1}^\dagger(0) W_{j_2}(T) W_{j_2}^\dagger(0) \dots W_{j_l}(T) W_{j_l}^\dagger(0) W_{j_1}(T) \\ &= \rho_{j_1}^{1/2}(0) U(T) \rho_{j_2}^{1/2}(0) B(T) \rho_{j_2}^{1/2}(0) \dots U(T) \rho_{j_l}^{1/2}(0) B(T) \\ & \quad \times \rho_{j_l}^{1/2}(0) U(T) \rho_{j_1}^{1/2}(0) B(T), \end{aligned} \quad (3.3.11)$$

where the  $\rho_{j_k}$ 's are those of Eq. (3.3.10).

In a first guess one could think to obtain a similar form like  $\gamma_{\rho_{j_1}\rho_{j_2}\dots\rho_{j_l}}^{(l)}$  with a unitarity  $U(t)$  parallel transporting all eigenstates of the  $\rho_{j_k}$ 's, so that the  $B(t)$  can be chosen to be time independent. But this procedure fails since the parallel transport condition behind the  $\gamma_{\rho_{j_1}\rho_{j_2}\dots\rho_{j_l}}^{(l)}$ 's is much weaker than the parallel transport condition in Eq. (3.3.6). In the former parallel transport is required for the state vectors  $|\psi_k\rangle$  diagonalising the initial  $\rho = \sum_k \lambda_k |\psi_k\rangle \langle \psi_k|$ , i. e.,  $\langle \psi_k | U^\dagger(t) \dot{U}(t) | \psi_k \rangle = 0$ , whereas in the latter case putting  $B(t)$  constant amounts to vanishing matrix elements of  $U^\dagger(t) \dot{U}(t)$  in the support of  $\rho(0)$ . This means that the left hand side of Eq. (3.3.6) can only vanish for unitarities  $U(t)$  that leave all the  $\rho_{j_k}$ 's appearing in  $\mathcal{X}_{j_1\dots j_l}^{(l)}[\mathcal{C}_{j_1} \dots \mathcal{C}_{j_l}]$  unaffected or, in other words that Eq. (3.3.6) is trivially fulfilled for no evolution at all. However, the two approaches are on equal footing in the limit of pure states.

### 3.3.4 Examples

As our first example, let us consider the qubit (two-level) case for which  $\mathcal{H} = \mathcal{H}_1 \oplus \mathcal{H}_2$ ,  $\dim \mathcal{H}_1 = \dim \mathcal{H}_2 = 1$ , is the only form of orthogonal sum decomposition of Hilbert space. Let  $\rho_1(0) = |0\rangle \langle 0|$  and  $\rho_2(0) = |1\rangle \langle 1|$  have support in  $\mathcal{H}_1$  and  $\mathcal{H}_2$ , respectively, and consider the paths  $\mathcal{C}_1, \mathcal{C}_2 : t \in [0, T] \rightarrow \rho_1(t), \rho_2(t)$  in state space. Assume  $\tilde{V}_1(t), \tilde{V}_2(t)$  are solutions of the parallel transport equation Eq. (2.4.13), computed for example according to the prescrip-

tion given by Hübner [Hüb93]. The  $l = 1$  holonomy invariants read

$$\begin{aligned}\mathcal{X}_1^{(1)}[\mathcal{C}_1] &= \rho_1^{1/2}(T)\tilde{V}_1(T)|0\rangle\langle 0|, \\ \mathcal{X}_2^{(1)}[\mathcal{C}_2] &= \rho_2^{1/2}(T)\tilde{V}_2(T)|1\rangle\langle 1|\end{aligned}\tag{3.3.12}$$

with resulting left and right positive parts

$$\begin{aligned}\mathcal{X}_1^{(1)}\left(\mathcal{X}_1^{(1)}\right)^\dagger &= \rho_1^{1/2}(T)\tilde{V}_1(T)|0\rangle\langle 0|\tilde{V}_1^\dagger(T)\rho_1^{1/2}(T), \\ \left(\mathcal{X}_1^{(1)}\right)^\dagger\mathcal{X}_1^{(1)} &= |0\rangle\langle 0|\langle 0|\tilde{V}_1^\dagger(T)\rho_1(T)\tilde{V}_1(T)|0\rangle, \\ \mathcal{X}_2^{(1)}\left(\mathcal{X}_2^{(1)}\right)^\dagger &= \rho_2^{1/2}(T)\tilde{V}_2(T)|1\rangle\langle 1|\tilde{V}_2^\dagger(T)\rho_2^{1/2}(T), \\ \left(\mathcal{X}_2^{(1)}\right)^\dagger\mathcal{X}_2^{(1)} &= |1\rangle\langle 1|\langle 1|\tilde{V}_2^\dagger(T)\rho_2(T)\tilde{V}_2(T)|1\rangle.\end{aligned}\tag{3.3.13}$$

The essential point here is that these equations display nodal points if  $\rho_1(T) \in \mathcal{O}(\mathcal{H}_2)$  and  $\rho_2(T) \in \mathcal{O}(\mathcal{H}_1)$ , which is equivalent to say that  $\rho_1(T) = |1\rangle\langle 1|$  and  $\rho_2(T) = |0\rangle\langle 0|$ . For this case we obtain the  $l = 2$  holonomy invariant with its right and left positive parts as

$$\begin{aligned}\mathcal{X}_{12}^{(2)}[\mathcal{C}_1\mathcal{C}_2] &= \mathcal{X}_1^{(1)}[\mathcal{C}_1]\mathcal{X}_2^{(1)}[\mathcal{C}_2] = |1\rangle\langle 1|\langle 1|\tilde{V}_1(T)|0\rangle\langle 0|\tilde{V}_2(T)|1\rangle, \\ \mathcal{X}_{12}^{(2)}\left(\mathcal{X}_{12}^{(2)}\right)^\dagger &= \left(\mathcal{X}_{12}^{(2)}\right)^\dagger\mathcal{X}_{12}^{(2)} = |1\rangle\langle 1|\left|\langle 1|\tilde{V}_1(T)|0\rangle\langle 0|\tilde{V}_2(T)|1\rangle\right|^2.\end{aligned}\tag{3.3.14}$$

Clearly,  $\mathcal{X}_{12}^{(2)}[\mathcal{C}_1\mathcal{C}_2]$  is well-defined unless  $\langle 1|\tilde{V}_1(T)|0\rangle\langle 0|\tilde{V}_2(T)|1\rangle$  vanishes. If the paths  $\mathcal{C}_1 : |0\rangle\langle 0| \rightarrow |1\rangle\langle 1|$  and  $\mathcal{C}_2 : |1\rangle\langle 1| \rightarrow |0\rangle\langle 0|$  are unitary, then we may choose the corresponding  $U(t)$  to be parallel transporting and put  $B_{1,2}(t) = U^\dagger(t)\tilde{V}_{1,2}(t) = 1$ . Thus,  $\tilde{V}_{1,2}(T) \equiv U(T)$  are purely off-diagonal and thus  $\left|\langle 1|\tilde{V}_1(T)|0\rangle\langle 0|\tilde{V}_2(T)|1\rangle\right|^2 = 1$ . In the non-unitary case, there might exist exceptional paths for which at least one of  $\tilde{V}_{1,2}(T)$  is diagonal making  $\mathcal{X}_{12}^{(2)}[\mathcal{C}_1\mathcal{C}_2]$  to vanish. In the worst case, one may envisage situations where both  $\tilde{V}_1(T)$  and  $\tilde{V}_2(T)$  are diagonal so that none of the holonomies is defined.

For higher dimensional Hilbert spaces, we may envisage evolutions of generally non-pure states that both start and end in orthogonal subspaces. Taking  $\dim \mathcal{H} = 3$  an initial pure state can evolve to a mixed state or vice versa. For a mixed state with rank two the states may have support in different subspaces. Because of the change in the rank both cases are only possible for non-unitary evolutions in general.

However, for the sake of simplicity, we will increase the dimensionality of the Hilbert space under consideration to four. In a four dimensional Hilbert space we may encounter evolutions, where the rank of the density matrix representing the state  $\rho_1$  does not change, and nonetheless the supports of the initial and the final state are non-overlapping.

Suppose that the Hilbert space  $\mathcal{H}$  can be decomposed as  $\mathcal{H} = \mathcal{H}_1 \oplus \mathcal{H}_2$  with  $\dim \mathcal{H}_1 = \dim \mathcal{H}_2 = 2$ . The initial state  $\rho_1(0)$  has support exclusively in  $\mathcal{H}_1$  evolving to a state  $\rho_1(T)$  in  $\mathcal{H}_2$ . For this scenario, we may for instance consider the unitarity  $U(t)$  causing the transport

$t \mapsto W_1(t) = U(t)W_1(0)B_1(t) = \rho_1^{1/2}(t)\tilde{V}_1(t)$  with the amplitude  $W_1(0) = \rho_1^{1/2}(0) \in \mathcal{O}(\mathcal{H}_1)$  of the initial state.  $U(t)$  and  $B_1(t) = U^\dagger(t)\tilde{V}_1(t)$  are related via the parallel transport condition Eq. (3.3.6). If the final amplitude  $W_1(T) = U(T)W_1(0)B_1(T)$  has support exclusively in  $\mathcal{H}_2$ , clearly the functional  $v_{\mathcal{C}_1}^{(1)} = \arg \text{Tr}[W_1(T)W_1^\dagger(0)]$  is undefined since the left and right support of the holonomy invariant  $\mathcal{X}_1^{(1)}[\mathcal{C}_1]$ , denoted as l-supp  $\mathcal{X}_1^{(1)}[\mathcal{C}_1]$  and r-supp  $\mathcal{X}_1^{(1)}[\mathcal{C}_1]$ , respectively, are orthogonal:

$$\begin{aligned}
 \text{l-supp } \mathcal{X}_1^{(1)} &= \text{supp } \mathcal{X}_1^{(1)}(\mathcal{X}_1^{(1)})^\dagger = \text{supp } \rho_1^{1/2}(T)\tilde{V}_1\rho_1(0)\tilde{V}_1^\dagger\rho_1^{1/2}(T) = \mathcal{H}_2 \\
 \text{r-supp } \mathcal{X}_1^{(1)} &= \text{supp } (\mathcal{X}_1^{(1)})^\dagger\mathcal{X}_1^{(1)} = \text{supp } \rho_1^{1/2}(0)\tilde{V}_1^\dagger\rho_1(T)\tilde{V}_1\rho_1^{1/2}(0) = \mathcal{H}_1.
 \end{aligned}$$

However, the generalised  $l = 2$  holonomy invariant  $\mathcal{X}_{12}^{(2)}[\mathcal{C}_1\mathcal{C}_2]$  can be used to construct a holonomy invariant of the given evolution by utilising  $W_2(t)$  as the amplitude of another state  $\rho_2(t)$  which has support in  $\mathcal{H}_2$  at  $t = 0$ , i. e.  $\text{supp } \rho_2(0) = \mathcal{H}_2$ , and  $\text{supp } \rho_2(T) = \mathcal{H}_1$  for the final state. In particular, we have

$$\begin{aligned}
 \mathcal{X}_{12}^{(2)}[\mathcal{C}_1\mathcal{C}_2] &= W_1(T)W_1^\dagger(0)W_2(T)W_2^\dagger(0) \\
 &= \rho_1^{1/2}(T)\tilde{V}_1\rho_1^{1/2}(0)\rho_2^{1/2}(T)\tilde{V}_2\rho_2^{1/2}(0).
 \end{aligned} \tag{3.3.15}$$

The right and left support of  $\mathcal{X}_{12}^{(2)}[\mathcal{C}_1\mathcal{C}_2]$  are overlapping and therefore the holonomy invariant  $\mathcal{X}_{12}^{(2)}[\mathcal{C}_1\mathcal{C}_2]$  is well-defined in the nodal points of  $\mathcal{X}_i^{(1)}[\mathcal{C}_i]$  for the states  $\rho_i$ ,  $i = 1, 2$ .

Notwithstanding the conceptual allure of Uhlmann's holonomy invariants and the consequent off-diagonal holonomies it is doubtful whether a physical implementation of the latter by some kind of experiment is possible. An experiment to test the diagonal Uhlmann holonomy is proposed in [EPS<sup>+</sup>03] where the explicit control over the ancilla Hilbert space is essential to ensure the parallel transport of the state. The ancilla Hilbert space remains no longer a theoretical concept, but is also manifest in the experiment. Even in this proposal it is only the complex valued functional  $v_{\mathcal{C}}^{(1)}$  (Eq. 3.3.2) that is measured instead of the matrix valued holonomy invariant  $\mathcal{X}^{(1)}$  and it remains an open question how to measure the latter.

### 3.3.5 Spin Flip Operation on a Mixture of Bell States

One explicit example of an evolution that leads to orthogonal initial and final mixed states is a spin plus phase flip operation applied to a mixture of Bell states. For the initial state

$$\rho_1(0) = \frac{1}{1+\varepsilon}(|\Psi^-\rangle\langle\Psi^-| + \varepsilon|\Psi^+\rangle\langle\Psi^+|), \quad \varepsilon \geq 0, \tag{3.3.16}$$

we obtain by spin- and phase-flipping the first qubit, i.e.,  $U_{\text{sf}} : (|0\rangle, |1\rangle) \mapsto (|1\rangle, -|0\rangle)$  or  $U_{\text{sf}} = |\Phi^+\rangle\langle\Psi^-| + |\Psi^+\rangle\langle\Phi^-| - |\Psi^-\rangle\langle\Phi^+| - |\Phi^-\rangle\langle\Psi^+|$ , the final state

$$\rho_1(\tau) = \frac{1}{1+\varepsilon}(|\Phi^+\rangle\langle\Phi^+| + \varepsilon|\Phi^-\rangle\langle\Phi^-|), \tag{3.3.17}$$

where we have denoted the Bell states by  $|\Psi^\pm\rangle = 2^{-1/2}(|01\rangle \pm |10\rangle)$  and  $|\Phi^\pm\rangle = 2^{-1/2}(|00\rangle \pm |11\rangle)$ . A simple implementation of such an operation is given by the time-independent Hamiltonian  $H_s = \sigma_y \otimes 1_2$  so that the path  $\mathcal{C}_1 : t \in [0, T] \mapsto \rho_1(t) = U_s(t)\rho_1(0)U_s^\dagger(t)$  with  $U_s(t) = e^{-itH_s}$  is traced out in state space. Inserting  $U_s(t)$  into Eq. (3.3.6) yields a vanishing left-hand side, so that we can choose  $B_{s1}(t) = 1_1 \otimes 1_2$  to fulfil the parallel transport condition. For  $T = \pi/2$  we obtain the amplitude  $W_1(T) = U_s(T)\rho_1^{1/2}(0) = U_{\text{sf}}\rho_1^{1/2}(0)$  and the  $l = 1$  holonomy invariant reads

$$\begin{aligned} \mathcal{X}_1^{(1)}[\mathcal{C}_1] &= W_1(T)W_1^\dagger(0) = U_{\text{sf}}\rho_1(0) \\ &= \frac{1}{1+\varepsilon} (|\Phi^+\rangle\langle\Psi^-| - \varepsilon|\Phi^-\rangle\langle\Psi^+|), \end{aligned} \quad (3.3.18)$$

which has nonoverlapping right and left support and is therefore undefined. In particular, the trace functional  $v_{\mathcal{C}}^{(1)} = \arg \text{Tr}[U_{\text{sf}}\rho_1(0)]$ , which in this special case is equal to the diagonal geometric phase for mixed states (Eq. 2.3.4), vanishes. The  $l = 2$  off-diagonal holonomy invariant can be formed by choosing the reference state  $\rho_2(0) = \rho_1(T)$ , which evolves to  $\rho_2(T) = \rho_1(0)$  along the path  $\mathcal{C}_2 : t \mapsto \rho_2(t) = U_s(t)\rho_2(0)U_s^\dagger(t)$ . Again, we can set  $B_{s2}(t) = 1_1 \otimes 1_2$  and obtain  $\mathcal{X}_2^{(1)}[\mathcal{C}_2] = W_2(T)W_2^\dagger(0) = U_{\text{sf}}\rho_2(0)$ , which also has nonoverlapping left and right support. These considerations result in

$$\begin{aligned} \mathcal{X}_{12}^{(2)}[\mathcal{C}_1\mathcal{C}_2] &= W_1(T)W_1^\dagger(0)W_2(T)W_2^\dagger(0) = U_{\text{sf}}\rho_1(0)U_{\text{sf}}\rho_2(0) \\ &= -\frac{1}{(1+\varepsilon)^2} [|\Phi^+\rangle\langle\Phi^+| + |\Phi^-\rangle\langle\Phi^-|], \end{aligned} \quad (3.3.19)$$

the left and right support of which are overlapping and  $\mathcal{X}_{12}^{(2)}$  is therefore well-defined at this particular nodal point of  $\mathcal{X}_i^{(1)}[\mathcal{C}_i]$ . The Hamiltonian  $H_s$  above is not a unique choice for a spin-flip implementation, this task can also be performed, e.g., by the time-dependent Hamiltonian  $H_r(t) = [u_z\sigma_z + u_{xy}(\sigma_x \cos \omega t + \sigma_y \sin \omega t)] \otimes 1_2$  similar to the Hamiltonian for a resonance spin-flipper (on the first particle). The unitary time evolution operator corresponding to  $H_r(t)$  can be written as  $U_r(t) = U_{\text{rot}}U_{\text{eff}} = e^{-i\omega t\sigma_z/2}e^{-itH_{\text{eff}}} \otimes 1_2$  with  $H_{\text{eff}} = (u_z + \omega/2)\sigma_z + u_{xy}\sigma_x$ . By the particular choice of the parameters  $u_z = -u/2$  and  $\omega = -2u_{xy} = -2u_z$ , one can verify that for  $t = \frac{\pi}{\omega}$  we have implemented the same spin-flipping unitary as in the static case, i.e.,  $U_r(\pi/\omega) = U_s(\pi/2) = U_{\text{sf}}$ . Inserting  $U_r$  on the left-hand side of Eq. (3.3.6) we obtain

$$\begin{aligned} B_{r1}(t) &= \cos \gamma(t) [|\Psi^+\rangle\langle\Psi^+| + |\Psi^-\rangle\langle\Psi^-|] \\ &\quad - i \sin \gamma(t) [|\Psi^+\rangle\langle\Psi^-| + |\Psi^-\rangle\langle\Psi^+|], \\ \gamma(t) &= \frac{\sqrt{\varepsilon}\omega t}{1+\varepsilon}. \end{aligned} \quad (3.3.20)$$

This gives us the  $l = 1$  holonomy invariant for the path  $\tilde{\mathcal{C}}_1 : t \in [0, T] \mapsto \rho_1(t) = U_r(t)\rho_1(0)U_r^\dagger(t)$  as

$$\begin{aligned}\mathcal{X}_1^{(1)}[\tilde{\mathcal{C}}_1] &= W_1(T)W_1^\dagger(0) = U_{\text{sf}}\rho_1^{1/2}(0)B_{r1}(T)\rho_1^{1/2}(0) \\ &= \frac{1}{1+\varepsilon} \left[ \cos \gamma(T) (|\Phi^+\rangle\langle\Psi^-| - \varepsilon|\Phi^-\rangle\langle\Psi^+|) \right. \\ &\quad \left. + i\sqrt{\varepsilon} \sin \gamma(T) (-|\Phi^+\rangle\langle\Psi^+| + |\Phi^-\rangle\langle\Psi^-|) \right],\end{aligned}\quad (3.3.21)$$

which has nonoverlapping left and right supports and is therefore undefined. Similarly, by again taking  $\rho_2(0) = \rho_1(T)$  from Eq. (3.3.17), the  $l = 1$  holonomy invariant associated with the path  $\tilde{\mathcal{C}}_2 : t \in [0, T] \mapsto \rho_2(t) = U_r(t)\rho_2(0)U_r^\dagger(t)$  becomes

$$\begin{aligned}\mathcal{X}_2^{(1)}[\tilde{\mathcal{C}}_2] &= W_2(T)W_2^\dagger(0) = U_{\text{sf}}\rho_2^{1/2}(0)B_{r2}(T)\rho_2^{1/2}(0) \\ &= \frac{1}{1+\varepsilon} \left[ \cos \gamma(T) (\varepsilon|\Psi^+\rangle\langle\Phi^-| - |\Psi^-\rangle\langle\Phi^+|) \right. \\ &\quad \left. + i\sqrt{\varepsilon} \sin \gamma(T) (|\Psi^-\rangle\langle\Phi^-| - |\Psi^+\rangle\langle\Phi^+|) \right]\end{aligned}\quad (3.3.22)$$

with nonoverlapping left and right support.

We may use Eqs. (3.3.21) and (3.3.22) to obtain the  $l = 2$  holonomy invariant

$$\begin{aligned}\mathcal{X}_{12}^{(2)}[\tilde{\mathcal{C}}_1\tilde{\mathcal{C}}_2] &= W_1(T)W_1^\dagger(0)W_2(T)W_2^\dagger(0) \\ &= U_{\text{sf}}\rho_1^{1/2}(0)B_{r1}(T)\rho_1^{1/2}(0)U_{\text{sf}}\rho_2^{1/2}(0)B_{r2}(T)\rho_2^{1/2}(0) \\ &= \frac{1}{(1+\varepsilon)^2} \left[ -(\cos^2 \gamma(T) + \varepsilon \sin^2 \gamma(T)) (|\Phi^+\rangle\langle\Phi^+| + \varepsilon|\Phi^-\rangle\langle\Phi^-|) \right. \\ &\quad \left. + i\sqrt{\varepsilon}(1-\varepsilon) \sin \gamma(T) \cos \gamma(T) (|\Phi^+\rangle\langle\Phi^-| - |\Phi^-\rangle\langle\Phi^+|) \right],\end{aligned}\quad (3.3.23)$$

which has overlapping right and left support and is therefore well-defined at this particular nodal point of  $\mathcal{X}_i^{(1)}[\tilde{\mathcal{C}}_i]$ . The difference between  $\mathcal{X}_{12}^{(2)}[\mathcal{C}_1\mathcal{C}_2]$  from the Hamiltonian  $H_s$  and  $\mathcal{X}_{12}^{(2)}[\tilde{\mathcal{C}}_1\tilde{\mathcal{C}}_2]$  from  $H_r(t)$  reflects the path dependence of the off-diagonal holonomy.

## 3.4 Conclusions

Recent investigations in geometric phases in quantum systems have led to cases where the standard definitions breaks down. In this chapter the concept of the off-diagonal geometric phase by Manini and Pistolesi has been taken up and applied to the mixed state case. For the evolution of density matrices, there are points in parameter space for which the standard mixed state geometric phase  $\phi_\rho$  cannot be defined in the usual way since the initial and final state are orthogonal to each other leading to a break down of the contrast in the interferometric approach. If this happens there remain still off-diagonal geometric phases of higher order which are probably well-defined and which are independent of the particular dynamics. Besides a general discussion on possible values also a simple example of a trajectory on the

Bloch-sphere for a two-level system is presented which visualises the complementarity between the diagonal and the off-diagonal geometric phase. In the qubit case the off-diagonal mixed state phase can be fully qualified both from the theoretical and from the experimental point of view. But it has to be mentioned that the measurement seems to require control and measurement of one or more ancilla systems although the off-diagonal mixed state phases are properties of the system alone, since the constituting set of density operators pertains solely to the system. Explicitly, a Franson interferometer setup for the qubit case has been presented illustrating the nontrivial sign change property of the off-diagonal phase connected to the mixed state case. The apparent need for control over an ancilla system seems to suggest that the proposed concept of off-diagonal mixed state geometric phase is a nonlocal and/or contextual property of the unitary evolution of a quantum system.

Furthermore, basically motivated by possible nodal points occurring in Uhlmann's concept of relative phase for some particular paths of mixed quantum states we have extended the original notion to off-diagonal quantum holonomy invariants. Utilizing these generalised quantities the problem of undefined relative Uhlmann phase for initial and final state with orthogonal supports can be overcome in line with the introduction of off-diagonal geometric phases for pure states. The definition of the holonomy invariants is equivalent to the Manini-Pistolesi approach in the pure state limit, moreover it provides us with a natural extension of the latter to nonparallel-transporting unitary evolutions. Besides other examples, we have explicitly demonstrated by means of the evolution of a Bell state mixture the necessity to resort to off-diagonal quantum holonomies to obtain information about the geometry of state space.

When comparing these holonomy invariants with the former off-diagonal mixed state geometric phases  $\gamma_{\rho\rho^\perp}$  we have detected a general discrepancy for these two approaches related to a fundamental difference in the treatment of parallel transport of quantum states. In general, the interferometric off-diagonal geometric phase and the Uhlmann holonomies are incompatible as long as we are not dealing with pure states. Both of them, however, allow for a further characterisation of the geometry of the state space of density operators in case of undefined mixed state geometric phase.

## Chapter 4

# Spatial Geometric Phase - A Neutron Interferometry Experiment

The geometric phase manifests itself not only in the spin degrees of freedom of a neutron. It is a property of the underlying Hilbert space no matter which particular physical property is represented. Hence, we expect to find a geometric phase not only connected to the internal spin angular momentum of a particle but also to its kinematics in ordinary space-time. In one of the earlier experiments on the geometric phase Tomita and Chiao [TC86] investigated the change of the plane of polarisation of linearly polarised light after transmission along a mono-mode optical fibre wound helically around a cylinder. In this experiment the geometric phase arises due to the (parallel) transport of the polarisation vector along a path in momentum space similar to the situation encountered in the classical example in the introductory Section 1.1.

To examine a quantum geometric phase originating from the shape of momentum space itself independent of internal degrees of freedom like spin for neutrons or the polarisation for light we use a interferometric setup with totally unpolarised incident neutrons [RW00]. The possible states are restricted to a two-dimensional subspace of the total continuous momentum space. A neutron with a specific momentum incident onto a (perfect) beam splitter has only the possibility of being either transmitted or reflected, the subjacent two-dimensional Hilbert space is spanned by the two possible paths in the interferometer. The neutron is after the beam splitter in a superposition state of these alternatives and the evolution of the state can be manipulated by phase shifters and absorbers. Due to this evolution the state obtains a phase and by carefully eliminating the dynamical phase the resulting phase is purely geometric, i. e. it is independent of the particular neutron's momentum (wavelength). One proposal to verify the spatial geometric phase is discussed by Sjöqvist [Sjö01] using polarised neutrons and reversing the rôles of the magnetic field and the spatial degrees of freedom.

An experiment by Hasegawa *et al.* [HZR96] follows another approach to verify the special case of a *cyclic* spatial geometric phase, where a phase shift of an integer multiple of  $2\pi$  is exerted between the transmitted and the reflected path. The interpretation of this experiment, viz. to ascribe a geometric phase to this particular state evolution, has however met

severe criticism [Wag99]. A more detailed examination is necessary to settle this conflict. In the following the extension to *non-cyclic* evolutions proves advantageous to manifest the correctness of the interpretation of the previous experiment by means of an explicit calculation of the non-cyclic geometric phase in terms of paths on the Bloch-sphere. The theoretical treatment, which comprises the cyclic geometric phase as a special case, is then confirmed by an experiment [FHLR05b, FHLR05a].

## 4.1 Neutron Interferometry

Neutron interferometry is now a well established technique for measurements of various quantum mechanical effects. It resembles closely a Mach-Zehnder widely used in light optics, but the huge difference is that massive particles are brought to interference. The first interference fringes have been sighted in 1974 by Rauch, Treimer and Bonse [RTB74] and the wave-like nature of neutrons – as proposed by *de Broglie* – could therewith be shown.

A neutron interferometer consists of a single silicon perfect-crystal (Figure 4.1) cut in such a way that the incoming neutrons are split by Bragg diffraction at the net planes of the first plate and finally recombined at the last plate.

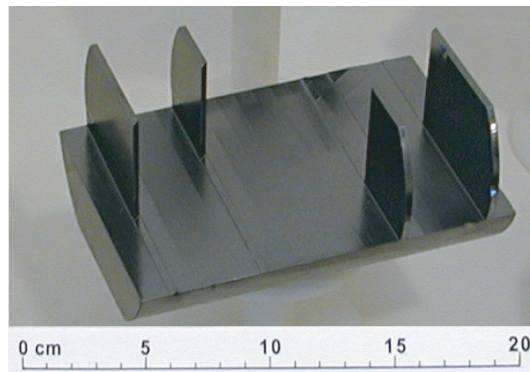


Figure 4.1: (Skew-symmetric) single crystal neutron interferometer.

Many beautiful experiments on the fundamentals of quantum mechanics have been conducted since: Besides showing the existence of coherent neutron matter waves [RTB74], one year later the verification of the  $4\pi$ -spinor symmetry followed [RZB<sup>+</sup>75]. The influence of gravitation of the earth on the wavefunction [COW75] or the spin superposition law that the superposition of two coherent beams with (orthogonal) spin polarisation results in a polarised beam again [SBRK82, BRS83] are further examples. Recently, a test of Bell's inequalities [Bel64, FS04b, FS04a] has been performed using the spatial degree of freedom in the interferometer to generate a “*bi-partite*” Bell-State [HLB<sup>+</sup>03]. Worth mentioning is also the experiment on a confinement induced phase shift [RLBL02] where the neutrons experience a wall potential when going through narrow channels. Due to energy conservation their longitudinal momentum decreases which in turn gives rise to a phase shift. The geometric phase associated to the spin evolution has been tested by use of a neutron interferometer

where static spin flippers are put in both arms [WRS<sup>+</sup>97]. For a more thorough review of fundamental neutron optics experiments the reader is referred to [RW00, Rau04].

In our case the interferometer features a double-loop geometry [ZBLR02]. This particular shape enables us to measure the spatial geometric phase associated with the evolution of neutrons in the second loop giving rise to a phase shift relative to the reference beam from the first loop. The same instrument has been used, e. g., for first attempts in reconstructing the neutron state [BRS03]. Like for all other types of neutron interferometers the monolithic property is crucial since the individual beam-splitting plates have to be arranged with a precision comparable to the lattice parameter. The basic principle is relatively simple: Before falling onto the skew-symmetric interferometer, the incident neutron beam is collimated and monochromatised by the 220-Bragg reflection of a Si perfect crystal monochromator placed in the thermal neutron guide. In our case the wavelength has been tuned to give a mean value of  $\lambda = 2.715 \text{ \AA}$ . The interferometer is then aligned such that the net planes of the interferometer plates are parallel to the net planes of the monochromator (non-dispersive arrangement). The surface of the plates is perpendicular to the reflecting net planes which is called *Laue-geometry*. The incident beam is split into a transmitted and a reflected beam, if the interferometer is aligned with the monochromator, and these beams have a well-defined phase relation to each other - otherwise there would be no interference. In terms of state vectors the situation can be described by

$$|\Psi_i\rangle \mapsto t|\Psi_t\rangle + r|\Psi_r\rangle, \quad (4.1.1)$$

where  $|\Psi_i\rangle$  denotes the incident beam,  $|\Psi_t\rangle$  and  $|\Psi_r\rangle$  the transmitted and the reflected beam, respectively. The complex factors  $t$  and  $r$  ( $|t|^2 + |r|^2 = 1$  for a non-absorptive beam splitter) describe the ratio of transmission ( $t$ ) and reflection ( $r$ ) and the phase relation between the outgoing beam. In the following we will assume a 50:50 beam-splitter ( $t = r = 1/\sqrt{2}$ ) with zero phase difference. This can be justified a posteriori since in an interferometer all beam paths exhibit the same number of reflections and transmissions and, furthermore, the intrinsic phase shift of the beam splitting slabs remains immaterial since it is constant throughout the measurement process. Unfortunately, this last assumption is merely wishful thinking, temperature gradients and other environmental influences causes a sometimes non-negligible phase drift as can be noticed in the final interference fringes.

Putting now several beam splitting plates together such that the partial waves are finally recombined behind the interferometer and adding an additional slab that produces an adjustable phase shift the relative phase difference between the beams taking different paths in the apparatus can be monitored (see Figure 4.2).

Since the number of reflections and transmissions is same for both beams the amplitude of the beams is of equal magnitude in the forward (O) detector. The state leaving the interferometer at the beam splitter BS4 is given by

$$|\psi_O\rangle = a(|\psi_I\rangle + e^{i\Delta\chi}|\psi_{II}\rangle), \quad (4.1.2)$$

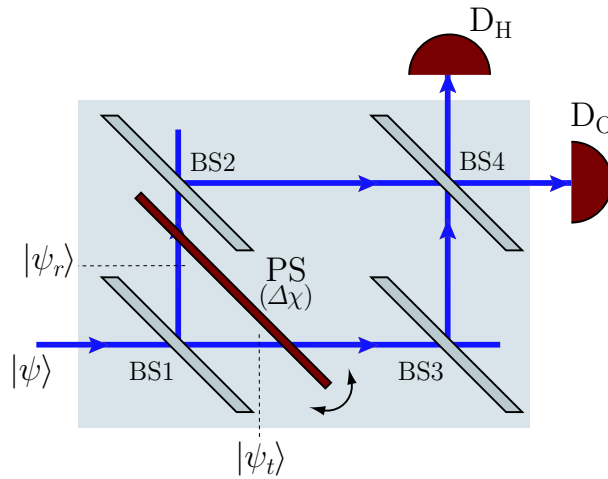


Figure 4.2: (Skew-symmetric) neutron interferometer where the incident beam  $|\psi\rangle$  is split at the first beam splitter BS1 and recombined at BS4 into a transmitted ( $|\psi_t\rangle$ ) and a reflected beam ( $|\psi_r\rangle$ ). The phase shifter PS induces a relative phase difference between the two beam paths which give rise to interference fringes detector ( $D_O$ ) in the forward direction.

where  $a \in \mathbb{C}$  denotes the amplitude of the outgoing wave and comprises also a global phase factor. This global phase factor is immaterial at first, because it does not show up in the interference fringes of the intensity

$$I = \langle \psi_O | \psi_O \rangle = 2|a|^2(1 + \cos \Delta\chi). \quad (4.1.3)$$

Later on this phase will be of crucial importance for the measurement of the spatial geometric phase. By adding another loop to the interferometer we can measure the phase of the coefficient  $a$  and it will be associated to the geometric phase arising from the evolution of the wave in a single interferometer loop.

Equation (4.1.3) is valid only if the states  $|\psi_I\rangle$  and  $|\psi_{II}\rangle$  are fully overlapping and coherent, i. e.  $\langle \psi_I | \psi_{II} \rangle = 1$ , otherwise an additional visibility (or contrast) factor  $v \equiv |\langle \psi_I | \psi_{II} \rangle| \in [0, 1]$  appears that reduces the amplitude of the interference fringes (Figure 4.3). Adding additionally a sample into one beam path producing a phase shift of  $\Phi$  the intensity finally reads

$$I \propto 1 + v \cos(\Delta\chi + \Phi). \quad (4.1.4)$$

### Neutrons with spin

Neutrons are fermions with spin 1/2. Consequently the state vector comprises in addition a factor for the spin degrees of freedom, usually written in terms of basis states of the Pauli spin matrices ( $\sigma_x, \sigma_y, \sigma_z$ ) discussed in Section 1.2.1. The spin state is represented as a vector element of a complex two dimensional Hilbert space and the transformation from one state to another is state is via a two dimensional unitary matrix element of  $U(2)$ . Evidently, the

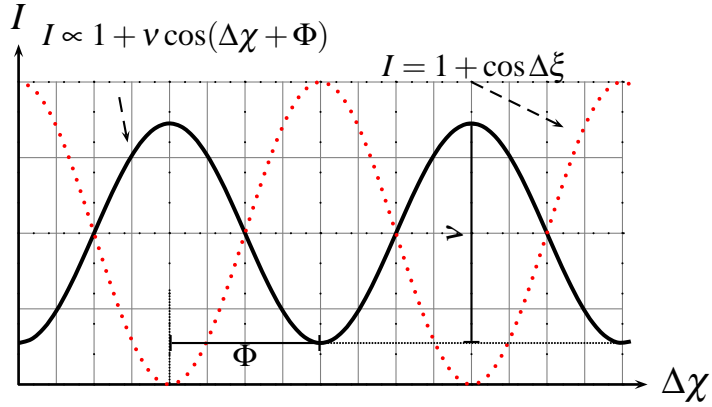


Figure 4.3: Interference fringes due to rotation of the phase shifter. A shift of the interference fringes is caused by an additional phase difference  $\Phi$  between the two interferometer paths. Partial overlap of the states leads to a reduction of the contrast  $v$ .

interference pattern is sensitive to changes of the spin state provided that these are different for the different interferometer paths. In terms of equations, the initial state is given by

$$|\psi^0\rangle = |\psi_x\rangle \otimes |\psi_s\rangle, \quad (4.1.5)$$

where  $|\psi_x\rangle$  denotes the initial translational and  $|\psi_s\rangle$  the initial spin part. The beam splitter acts on the first factor and produces the state

$$|\psi^0\rangle \xrightarrow{BS1} |\psi^1\rangle = 1/\sqrt{2}(|\psi_t\rangle + |\psi_r\rangle) \otimes |\psi_s\rangle. \quad (4.1.6)$$

If we switch on some magnetic field ( $B$ ) in the transmitted beam path, say, the spin part will change and we get the state

$$|\psi^1\rangle \xrightarrow{B} |\psi^2\rangle = 1/\sqrt{2}(|\psi_t\rangle \otimes U_B|\psi_s\rangle + |\psi_r\rangle \otimes |\psi_s\rangle), \quad (4.1.7)$$

where  $U_B$  denotes the interaction between spin and magnetic field. This is called an *entangled state* [Sch35, Sch36] since it cannot be written in product form. Such states have formed in recent years the germ of a vast new branch of physics, *Quantum Information*, with the sublime aim to build once a quantum computer. Here, we note this just in passing and head on to calculate the interference fringes. Like before we add a phase shifter and obtain

$$|\psi^2\rangle \xrightarrow{PS} |\psi^3\rangle = 1/\sqrt{2}(|\psi_t\rangle \otimes U_B|\psi_s\rangle + e^{i\Delta\chi}|\psi_r\rangle \otimes |\psi_s\rangle). \quad (4.1.8)$$

The recombination of the beams by means of beam-splitters BS2, BS3 and BS4 modifies only the spatial state:

$$|\psi^3\rangle \xrightarrow{BS} |\psi^4\rangle = 1/2(|\psi_{trr}\rangle - |\psi_{trt}\rangle) \otimes U_B|\psi_s\rangle + e^{i\Delta\chi}(|\psi_{rrt}\rangle + |\psi_{rrr}\rangle) \otimes |\psi_s\rangle, \quad (4.1.9)$$

where each beam splitter adds a subscript to the state indicating a transmission (t) or a reflection (r). We are just interest in the intensity in the O detector and can therefore skip the parts which are travelling towards the H detector ( $|\psi_{trt}\rangle$  and  $|\psi_{rrr}\rangle$ ). Consequently, the intensity in the O-detector is given by

$$\begin{aligned} I &\propto ||\psi_{trr}\rangle \otimes U_B|\psi_s\rangle + e^{i\Delta\chi}|\psi_{rrt}\rangle \otimes |\psi_s\rangle|^2 \\ &= 2 + 2|\langle\psi_{trr}|\psi_{rrt}\rangle||\langle\psi_s|U_B^\dagger|\psi_s\rangle|\cos(\Delta\chi + \Phi_x + \Phi_s) \end{aligned} \quad (4.1.10)$$

when using  $\Phi_x \equiv \arg\langle\psi_{trr}|\psi_{rrt}\rangle$  and  $\Phi_s \equiv \arg\langle\psi_s|U_B^\dagger|\psi_s\rangle$ . We notice that the interference fringes are reduced by the *visibility* factor

$$v = v_x v_s \equiv |\langle\psi_{trr}|\psi_{rrt}\rangle||\langle\psi_s|U_B^\dagger|\psi_s\rangle| \quad (4.1.11)$$

comprising a translatorial ( $v_x$ ) and a spin component ( $v_s$ ). The former describes the overlap of the states in phase space, whereas the latter depends only on the spin part. However, for the present setup the spin part of the wave function can be neglected since there is no magnetic field interaction involved and  $\langle\psi_s|U_B^\dagger|\psi_s\rangle = 1$ . Hence, the spin part of the wave function will be omitted.

### 4.1.1 Phase Shifter

As phase shifters we use parallel-sided aluminium slabs of different thicknesses which have a high transmission rate for neutrons. The phase shift  $\chi = N_{Al}b_c\lambda d_{eff}$  depends on the wavelength  $\lambda = 2.715 \times 10^{-10}m$ , the coherent scattering length of aluminium  $b_{cAl} = 3.449(5) \times 10^{-15}m$ , the particle density of aluminium  $N_{Al} = 6.0264 \times 10^{28}$  atoms per cubic meter and the effective thickness  $d_{eff}$ .

#### Calculation of the phase shift

Let us revise the principles of refraction of a (matter) wave at an aluminium slab which acts dominantly as a phase shifter for neutrons with negligible absorptive losses. The time-independent Schrödinger equation is the starting point:

$$\left(-\frac{\hbar^2}{2m}\Delta + V(\vec{r})\right)\psi(\vec{r}) = E\psi(\vec{r}), \quad (4.1.12)$$

where the potential  $V(\vec{r})$  is given by the sum over all nucleonic scattering centres sitting at  $\vec{r}_i$ ,

$$V(\vec{r}) = \frac{2\pi\hbar^2 b_{cAl}}{m_n} \sum_i \delta(\vec{r} - \vec{r}_i). \quad (4.1.13)$$

$m_n$  is the mass of the neutron. The solution of this equation is issue of *dynamical diffraction theory* and is thoroughly discussed in [RP76a, RP76b]. A transformation of the Schrödinger



possess kinetic energy of about 0.02 eV which is orders of magnitude larger than typical values of  $V_F$  typically in the nano-electronvolts regime (e. g. for aluminium  $V_F \approx 50$  neV). The situation changes drastically for ultra-cold neutrons with energies in the same order of magnitude (e. g.  $\approx 130$  neV for a neutron velocity of 5 m/s). In such situations the reflected beam cannot be omitted, but it becomes dominant. By virtue of their low energy ultra-cold neutrons can be stored in bottles made of appropriate materials with high  $V_F$ , for example beryllium with  $V_F = 250$  neV. This technique is of potential use for measuring decoherence phenomena as will be discussed later in Section 5.

For the moment we stick to thermal neutrons. When the reflected beam is neglected we have energy conservation and the Schrödinger equation for the free neutron with momentum  $\vec{k}$  provides a value for the kinetic energy  $E = \hbar^2 k^2 / (2m)$ .

$$K^2 = k^2 [1 - V_F/E] \quad (4.1.17)$$

follows from Eq. (4.1.16). Using again  $V_F/E \ll 1$  we can extract the root in Eq. (4.1.17) and approximate the right hand side to first order in  $V_F/E$  to obtain

$$K \approx k \left( 1 - \frac{V_F}{2E} \right). \quad (4.1.18)$$

Recalling Eq. (4.1.15) we can write

$$V_F/(2E) = \frac{2\pi\hbar^2 b_c N_{Al}}{m} \frac{2m}{2\hbar^2 k^2} = 2\pi b_c N_{Al}/k^2 = \lambda^2 \frac{N_{Al} b_c}{2\pi} \quad (4.1.19)$$

and obtain the refractive index

$$n \equiv \frac{K}{k} \approx 1 - \frac{V(0)}{2E} = 1 - \lambda^2 \frac{N_{Al} b_c}{2\pi}. \quad (4.1.20)$$

Note, that for most materials used as phase-shifters (e. g. aluminium or silicon)  $V_F > 0$  since the coherent scattering length  $b_c > 0$  leads to a refractive index slightly smaller than one ( $n < 1$ ). Due to the additional potential energy the kinetic energy is lowered, 'the neutron passes the potential more slowly'. An exceptions is for example titanium with a negative scattering length  $b_c$  which can therefore be used to compensate the phase shift called *phase echo* [CKW<sup>+</sup>91].

The direction of the beam  $\vec{K}$  is obtained by requiring the continuity of the tangential component  $\vec{k}_{\parallel} = \vec{K}_{\parallel}$ , defined by the vanishing scalar product with the surface normal  $\vec{n}_s \cdot \vec{k}_{\parallel} = 0$ . Accordingly, we find with (4.1.17)

$$\begin{aligned} K^2 &= K_{\perp}^2 + K_{\parallel}^2 = K_{\perp}^2 + k_{\parallel}^2 = k^2 \left( 1 - \frac{V_F}{E} \right) \\ &= k_{\parallel}^2 + k_{\perp}^2 - k^2 \frac{V(0)}{E} \end{aligned} \quad (4.1.21)$$

and it follows for the perpendicular component  $K_{\perp}$  that

$$\begin{aligned} K_{\perp} &= \sqrt{k_{\perp}^2 - k^2 \frac{V_F}{E}} \approx k_{\perp} \left( 1 - \frac{1}{2} \frac{k^2 V_F}{k_{\perp}^2 E} \right) \\ &= k_{\perp} \left( 1 - \frac{1}{2} \frac{1}{\cos^2 \gamma} \frac{V_F}{E} \right). \end{aligned} \quad (4.1.22)$$

Using  $k_{\perp} = \vec{k} \cdot \vec{n}_s = k \cos \alpha$  we can finally write

$$\vec{K} = \vec{k} - \frac{k}{\cos \alpha} \frac{V_F}{2E} \vec{n}_s. \quad (4.1.23)$$

Now it is easy to calculate the phase shift  $X$  induced by a phase shifter of thickness  $d$ . The phase shift at a point  $\vec{r}$  relative to the origin is given by  $\vec{k} \cdot \vec{r}$ . A comparison of the phase difference between the refracted wave  $\vec{K}$  and the incident wave  $\vec{k}$  at the surface characterised by  $\vec{n}_s \cdot \vec{r} = d$  yields

$$X \equiv (\vec{k} - \vec{K}) \cdot \vec{r} = \frac{k}{\cos \alpha} \frac{V_F}{2E} d = \lambda^2 \frac{N_{Al} b_{cAl} k d}{2\pi \cos \alpha} = N_{Al} b_{cAl} \lambda \underbrace{d / \cos \alpha}_{d_{eff}}. \quad (4.1.24)$$

It turns out useful to write the phase shift of the wave-packet as the wave vector  $\vec{k}$  times a spatial displacement  $\vec{\Delta}$ ,

$$X = \vec{\Delta} \cdot \vec{k} \quad (4.1.25)$$

with

$$\vec{\Delta} = (1 - n) d \vec{n}_s = \lambda^2 \frac{N_{Al} b_c}{2\pi} d \vec{n}_s$$

Since  $X$  is wavelength-dependent the phase shifter induces dephasing if the incident has non-vanishing momentum spread. This leads to the concept of *coherence* which will be discussed in Section 4.8.1.

### 4.1.2 Induced phase shift

The adjustable parameter is the effective thickness  $d_{eff} = d / \cos \alpha$  in the forward direction of the beam which is proportional to the inverse cosine of the enclosed angle  $\alpha$  according to Eq. (4.1.24). It can be changed by a rotation of the phase shifter

The phase shifter is aligned at an angle of  $\alpha_0 = 45^\circ$  and the rotation is about  $\pm 2^\circ$  so that the inverse cosine can be approximated by a Taylor expansion up to first order at  $\alpha_0 = \pi/4$ ,

$$\frac{1}{\cos(\alpha_0 + \xi)} = \frac{1}{\cos \alpha_0} + \frac{\sin \alpha_0}{\cos^2 \alpha_0} \xi + \mathcal{O}(\xi^2) \approx \sqrt{2}(1 + \xi). \quad (4.1.26)$$

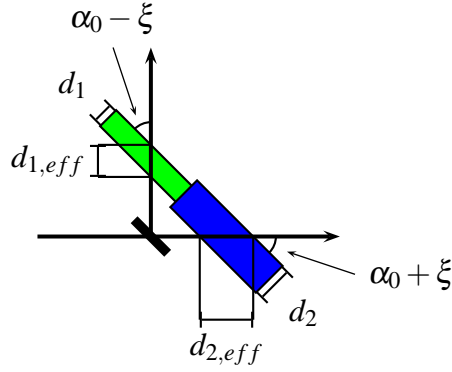


Figure 4.5: Beam incident on a phase shifting slab.

Consequently, the phase shift

$$X = \sqrt{2}dN_{Al}b_{cAl}\lambda(1 + \xi) \quad (4.1.27)$$

comprises a constant term  $\chi^0 \equiv \sqrt{2}DN_{Al}b_{cAl}\lambda$  and a variable term  $\chi \equiv \sqrt{2}DN_{Al}b_{cAl}\lambda\xi$ , i. e.

$$X = \chi^0 + \chi. \quad (4.1.28)$$

The superposition of the transmitted and reflected beam  $|\psi\rangle \propto |\psi_1\rangle + |\psi_2\rangle$  after a beam-splitter is changed by a phase shifter covering both beams (Figure 4.5) to  $|\psi\rangle \mapsto e^{iX_1}|\psi_1\rangle + e^{iX_2}|\psi_2\rangle = e^{iX_1}(|\psi_1\rangle + e^{i(X_2-X_1)}|\psi_2\rangle)$ . The global factor  $e^{iX_1}$  can be neglected as usual and the rotation angle  $\xi$  determines the variable relative phase difference between the two beams  $\Delta X \equiv X_2 - X_1$ ,

$$\begin{aligned} \Delta X &\equiv X_2 - X_1 \\ &= \sqrt{2}N_{Al}b_{cAl}\lambda [d_2(1 + \xi) - d_1(1 - \xi)] \\ &= \sqrt{2}N_{Al}b_{cAl}\lambda [(d_2 - d_1) + \xi(d_2 + d_1)] \\ &\equiv \Delta\chi^0 + \Delta\chi(\xi) \end{aligned} \quad (4.1.29)$$

where the subscripts denote the different beams. The rotation direction has been chosen counter-clockwise so that increasing  $\xi$  yields an increase (decrease) of the phase shift  $\chi_2$  ( $\chi_1$ ) and  $d_2$  ( $d_1$ ) denotes the thickness of the plate in the transmitted (reflected) beam.

### 4.1.3 Absorber

The process of absorption can be described by the imaginary part of the *coherent scattering length*  $b_c$  which defines the *total attenuation cross section*  $\sigma_t = \frac{4\pi}{k} \text{Im} b_c$  [Sea89, p.45].  $\sigma_t$  is the average number of incident neutrons that are scattered or absorbed per unit time per unit incident flux. The complex phase shift  $\beta = \beta' + i\beta''$  of a neutron wave going through a material slab,  $|\psi_0\rangle \mapsto e^{i\beta}|\psi_a\rangle$ , consists therefore of a term including the coherent scattering length  $\beta' = X = Nb_c\lambda d_{eff}$  and a term proportional to the total attenuation cross section  $\sigma_t$ ,

$\beta'' = N\sigma_t d_{eff}/2$  [RW00, p. 67].

The incident wave function obtains an exponential damping factor due to the absorption and the scattering,

$$|\psi_a\rangle = e^{-iX} e^{-\sigma_t N D_{eff}/2} |\psi_0\rangle$$

or in terms of the intensity the beam is attenuated according to

$$I = \langle \psi_a | \psi_a \rangle = I_0 e^{-\sigma_t N D_{eff}}.$$

In the following the exponential absorption term will be denoted by the *transmission coefficient*  $T \equiv e^{-\sigma_t N D_{eff}}$  and consequently

$$|\psi_a\rangle = e^{-iX} \sqrt{T} |\psi_0\rangle.$$

For aluminium  $\sigma_t$  is negligible, 1 mm aluminium absorbs about 1% of the incident neutrons. On the other hand gadolinium has a large absorption cross section and by mixing with deuterium (almost no absorption) the absorption rate can be tuned to the desired value by changing the concentration. Such a solution has been prepared in a quartz-cuvette and put into one of the beams.

An interesting issue has been discussed by Summhammer [RS84]: The absorption process in the form mentioned above involves unpredictable probabilities whether the neutron is absorbed or not. It is not possible to predict for a single neutron if it will be absorbed or not, quantum mechanics just tells us the probability in the form of the amplitude of the state vector. This situation changes drastically if one replaces the static absorptive material by a time-dependent chopper so that it becomes possible to dismiss a certain fraction of neutrons “manually”. The knowledge of the time of transmission or absorption results in a different behaviour of the interference fringes, viz. the contrast is either proportional to the square root of the transmission probability for the former setup, or linearly dependent thereupon in the latter case.

The difference should also be seen in the geometric phase. The results presented here are for the static case, whereas for the latter we would have to weight the geometric phase contributions stemming either from total absorption or a total transmission.

## 4.2 Description of the setup

Being confident that the short introduction to the vast field of neutron interferometry will do, we can proceed to the measurement of the spatial geometric phase that shows up due to the neutron’s motion through the interferometer loop:

As noticed by Feynman [FVH57] the description of any two-level quantum system is equivalent to the description of a spin-1/2 particle. Exploiting this equivalence there is in principle no difference between manipulations in the spin space of neutrons with the orthogonal basis  $\{|\uparrow\rangle, |\downarrow\rangle\}$  as eigenstates of the Pauli matrix  $\sigma_z$  representing a neutron in spin up

or spin down state, respectively, and momentum space with  $\{|k\rangle, |k'\rangle\}$  as orthogonal basis vectors. The latter corresponds to two directions of the neutron beam in an interferometer. In both cases one can assign a geometric phase to the particular evolution of the initial state. An even more appropriate description for the interferometric case for the forthcoming discussion is in terms of “which-way” basis states  $\{|p\rangle, |p^\perp\rangle\}$ , namely, if the neutron is found in the upper beam path after a beam-splitting plate it is said to be in the state  $|p\rangle$ , or in the state  $|p^\perp\rangle$ , if found in the lower beam path. The operators measuring the path of the neutrons are denoted by  $P_p \equiv |p\rangle\langle p|$  and  $P_{p^\perp} \equiv |p^\perp\rangle\langle p^\perp|$ , respectively. The complementary operator which corresponds to measuring the interference instead of the path is denoted by  $P_q \equiv |q\rangle\langle q| = (1 + |p\rangle\langle p^\perp| + |p^\perp\rangle\langle p|)/2$  (and  $P_{q^\perp} = 1 - P_q = |q^\perp\rangle\langle q^\perp|$ ) with eigenvector  $|q\rangle = 1/\sqrt{2}(|p\rangle + |p^\perp\rangle)$  ( $|q^\perp\rangle = 1/\sqrt{2}(|p\rangle - |p^\perp\rangle)$ ) as a superposition of the path eigenstates.

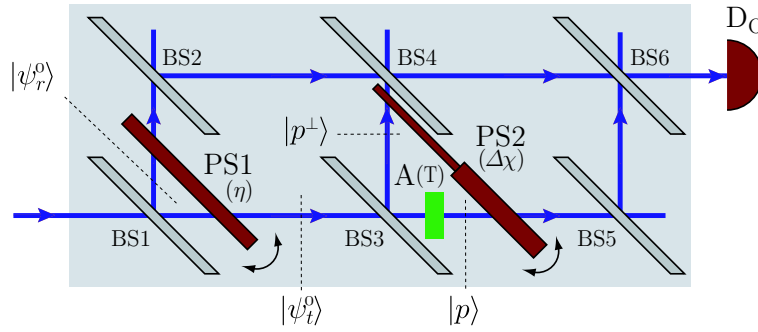


Figure 4.6: Double-loop interferometer used for the measurement of the spatial geometric phase.

For testing the spatial geometric phase we use a double-loop interferometer (c. f. Figure 4.6), where the incident unpolarised neutron beam  $|\psi\rangle$  is split up into a diffracted reference beam  $|\psi_r^0\rangle$  and a transmitted beam  $|\psi_t\rangle$  by means of the first beam splitting plate BS1. The double-loop geometry is needed to have a well-defined phase reference at our disposal in order to measure the phase of the state evolution in the second loop. In fact, recalling equation (4.1.3) a global phase factor  $\Phi$  of the evolution  $|\psi\rangle \mapsto t|\psi_1\rangle + r|\psi_2\rangle \mapsto e^{i\Phi}|\psi\rangle$  cannot be measured in a single loop interferometer, it is only the phase difference between  $|\psi_1\rangle$  and  $|\psi_2\rangle$  that is measurable. One has to resort to an additional reference beam with respect to which the phase difference can be measured. Hence, the double loop geometry is essential.

The reflected beam at the first beam splitter BS1,  $|\psi_r^0\rangle$ , is used as a reference with adjustable phase  $\eta$  relative to  $|\psi_t^0\rangle$  from the phase shifter PS1. The latter beam is defined to be in the state  $|\psi_t^0\rangle \equiv |p\rangle$  before falling onto the beam splitter BS3, since it is clearly localised as seen from the second loop. Behind BS3 there are two possible orthogonal paths  $|p\rangle$  and  $|p^\perp\rangle$  spanning a two-dimensional Hilbert space.  $|p\rangle$  denotes the state of the transmitted beam and  $|p^\perp\rangle$  the state of the reflected beam, respectively. Having a 50:50 beam splitter  $|\psi_t^0\rangle$  is transformed into a superposition of the basis vectors  $|p\rangle$  and  $|p^\perp\rangle$ :  $|\psi_t^0\rangle \mapsto |q\rangle \equiv (|p\rangle + |p^\perp\rangle)/\sqrt{2}$ .

The beam  $|\psi_t^0\rangle$  is subjected to further evolution in the second loop of the interferometer by use of beam-splitters (BS4 and BS5), an absorber (A) with transmission coefficient  $T$  and the phase shifter (PS2) generating a phase shift of  $e^{i\chi_1}$  on the upper and  $e^{i\chi_2}$  on the lower beam path, respectively, yielding the final state  $|\psi_f\rangle = U|\psi_t^0\rangle$ . The unitary matrix  $U = U(T, \chi_1, \chi_2)$  comprises all the manipulations in the second loop:

$$\begin{aligned} |\psi_t^0\rangle &\xrightarrow{\text{BS}} \frac{1}{\sqrt{2}}(|p^\perp\rangle + |p\rangle) \xrightarrow{\text{A}} \frac{1}{\sqrt{2}}(|p^\perp\rangle + \sqrt{T}|p\rangle) \\ &\xrightarrow{\text{PS2}} \frac{1}{\sqrt{2}}(e^{i\chi_1}|p^\perp\rangle + \sqrt{T}e^{i\chi_2}|p\rangle) \equiv U|\psi_t^0\rangle = |\psi_f\rangle. \end{aligned} \quad (4.2.1)$$

The geometric phase is usually extracted from the argument of the complex valued scalar product between the initial and the final state  $\arg\langle\psi_t^0|\psi_f\rangle$  (when removing dynamical contributions as will be discussed later). This is where the reference beam comes into play:  $|\psi_r^0\rangle$  is not subjected to any further evolution, but is stationary apart from adding a phase factor  $e^{i\eta}$  by use of the phase-shifter PS1<sup>1</sup>,  $|\psi_r^0\rangle \mapsto |\psi_{ref}\rangle = e^{i\eta}|\psi_r^0\rangle$ .  $|\psi_{ref}\rangle$  propagates towards the beam-splitter BS2 from the upper path, thus, we can assert it to be in the state  $e^{i\eta}|p\rangle$ . By varying  $\eta$  one can measure the shift of the interference fringes reflecting the phase difference between  $|\psi_{ref}\rangle$  and  $|\psi_f\rangle$ .

The two beams  $|\psi_f\rangle$  and  $|\psi_{ref}\rangle$  are recombined at the beam-splitter BS2 and finally detected at the detector  $D_O$  in the forward beam. This step can be described by the application of the projection operator  $|q\rangle\langle q| = 1/2(|p\rangle + |p^\perp\rangle)(\langle p| + \langle p^\perp|)$  to  $|\psi_f\rangle$  as well as to  $|\psi_{ref}\rangle$ :

$$\begin{aligned} |\psi'_f\rangle &= |q\rangle\langle q|\psi_f\rangle = K(e^{i\chi_1} + \sqrt{T}e^{i\chi_2})|q\rangle \\ |\psi'_{ref}\rangle &= |q\rangle\langle q|\psi_{ref}\rangle = K|q\rangle, \end{aligned} \quad (4.2.2)$$

where  $K$  is some scaling constant.

The intensity  $I$  measured in the detector  $D_O$  is proportional to the absolute square of the superposition  $|\psi'_f\rangle + e^{i\eta}|\psi'_{ref}\rangle$ :

$$\begin{aligned} I &\propto |(e^{i\eta} + e^{i\chi_1} + \sqrt{T}e^{i\chi_2})|q\rangle|^2 = \langle\psi'_{ref}|\psi'_{ref}\rangle + \langle\psi'_f|\psi'_f\rangle + \\ &+ 2|\langle\psi'_{ref}|\psi'_f\rangle|\cos(\eta - \arg\langle\psi'_{ref}|\psi'_f\rangle). \end{aligned} \quad (4.2.3)$$

We notice a phase shift of the interference pattern by  $\arg\langle\psi'_{ref}|\psi'_f\rangle$ . This phase shift corresponds to the Pancharatnam connection [Pan56] between the state  $|\psi'_f\rangle$  and the state  $|\psi'_{ref}\rangle$  from which we can extract the geometric phase. Explicitly we obtain

$$\begin{aligned} \Phi &= \arg\langle\psi'_{ref}|\psi'_f\rangle \\ &= \frac{\chi_1 + \chi_2}{2} - \arctan\left[\tan\left(\frac{\Delta\chi}{2}\right)\left(\frac{1 - \sqrt{T}}{1 + \sqrt{T}}\right)\right], \end{aligned} \quad (4.2.4)$$

<sup>1</sup>In fact, a phase shift of  $\eta/2$  is – as usual – imposed on the reflected and  $-\eta/2$  on the transmitted beam yielding a phase difference of  $\eta$  and a neglected overall phase.

where  $\Delta\chi \equiv \chi_2 - \chi_1$ .

Note, that in the considerations above we have omitted both the phase shifts of the empty interferometer (without phase shifters and absorber) and the constant phase shift for parallel phase shifters  $\Delta\chi^0$  as defined in Eq. (4.1.29).

The geometric phase is defined as [MS93]

$$\phi_g \equiv \arg\langle \psi'_{ref} | \psi'_f \rangle - \phi_d, \quad (4.2.5)$$

where  $\phi_d$  denotes the dynamical part and we have to remove first the dynamical phase before we can claim that the quantity to be measured is purely geometric.

### 4.3 Dynamical contribution

According to the theory presented in Section 1.2.3 the dynamical phase can be made to vanish by imposing a parallel transport condition on the evolution, namely, that adjacent states are in phase,  $\langle \psi(\xi) | \psi(\xi + \delta) \rangle \in \mathbb{R}$ . To this end we denote the state in the second loop with its explicit dependence on the rotation angle  $\xi$  of the phase shifter PS2:

$$|\psi(\xi)\rangle = e^{i\chi_1(\xi)}|p^\perp\rangle + \sqrt{T}e^{i\chi_2(\xi)}|p\rangle, \quad (4.3.1)$$

where  $\chi_1(\xi) = -Cd_1\xi$  and  $\chi_2 = Cd_2\xi$  with  $C = \sqrt{2}N_{AI}b_{cAI}\lambda$  according to (4.1.27). The constant phase shift  $\chi^0$  is omitted. A rotation of PS2 by the angle  $\delta$  changes the state to

$$|\psi(\xi + \delta)\rangle = e^{-iCd_1(\xi+\delta)}|p^\perp\rangle + \sqrt{T}e^{iCd_2(\xi+\delta)}|p\rangle. \quad (4.3.2)$$

From the imaginary part of the scalar product between two infinitesimally close states

$$\langle \psi(\xi) | \psi(\xi + \delta) \rangle = (e^{-iCd_1\delta} + Te^{iCd_2\delta}) \quad (4.3.3)$$

we obtain the parallel transport condition

$$-\sin(Cd_1\delta) + T \sin(Cd_2\delta) = 0 \quad (4.3.4)$$

or

$$d_1 = Td_2 \text{ for small } \delta. \quad (4.3.5)$$

If the parallel transport condition is not fulfilled the integral of all the infinitesimal contributions, divided by the norm of the state, defines the dynamical phase,

$$\phi_d \equiv \int_{-\xi/2}^{\xi/2} \frac{C(-d_1 + Td_2)s}{\langle \psi(s) | \psi(s) \rangle} ds = \sqrt{2}N_{AI}b_{cAI}\lambda \frac{(Td_2 - d_1)\xi}{1 + T} = \frac{\chi_1 + T\chi_2}{1 + T}. \quad (4.3.6)$$

The division by the norm is due to the definition of the geometric phase for non-unitary state vectors in Section 1.2.4.

Up to now we have assumed that there is only absorption in the lower beam bath. In view of the experimental realisation the in reality non-zero absorption coefficient of the path  $p^\perp$  can immediately be taken into account by multiplying  $d_1$  with a transmission coefficient  $T_1$ . With the (obvious) replacement  $T \mapsto T_2$  we obtain

$$\phi_d = \frac{T_1\chi_1 + T_2\chi_2}{T_1 + T_2}. \quad (4.3.7)$$

The dynamical phase part stemming from the phase shifter PS2 is given by a weighted sum of the phase shifts  $\chi_1$  and  $\chi_2$  with the weights depending on the transmission coefficient  $T_1$  and  $T_2$ , respectively.

It is now an easy task to adapt the experimental setup such that the dynamical phase vanishes. By selecting a phase shifter with unequal thickness in the beam paths the ratio can be adjusted to meet the requirement

$$d_1T_1 = d_2T_2 \quad \text{or} \quad \frac{d_1}{d_2} = \frac{T_2}{T_1}.$$

## 4.4 Paths on Bloch-sphere - A geometrical interpretation

The shift of the interference pattern in Eq. (4.2.3) with a properly adjusted ratio of  $T_1/T_2$  to avoid dynamical contributions should be equal to the (oriented) surface area enclosed by the paths of the state vectors on the Bloch sphere, or, equivalently, to the solid angle traced out by the state vectors as seen from the origin of the sphere.

The two dimensional Hilbert space is here spanned by the orthogonal paths  $|p\rangle$  and  $|p^\perp\rangle$  instead of the spin eigenstates  $|\uparrow\rangle$  and  $|\downarrow\rangle$  as in Figure 1.4. The north and south pole of the sphere are identified with states with well-defined path, i. e. an eigenstate of the observables  $|p^\perp\rangle\langle p^\perp|$  and  $|p\rangle\langle p|$ , respectively. All equally weighted superposition of path eigenstates are located on the equatorial line. An excess of  $|p^\perp\rangle$  contributions, i. e. if the neutron is more likely to take the upper path, displaces the state into the upper hemisphere and the lower hemisphere is populated with neutrons taking the lower path (Figure 4.7(a)). Note, that the particular point on the equator which denotes the state after the beam-splitter BS3 is arbitrary due to the arbitrary choice of the phases of the basis vectors. The absorber changes the weights of the superposed basis states. In particular, for the extremal values of  $T$  parameterised by the angle  $\theta$  with  $T = \tan^2 \theta/2$  we end up either again with an equally weighted superposition for no absorption ( $T = 1$  or  $\theta = \pi/2$ ) or the state is situated at the north pole for total absorption ( $T = 0$  or  $\theta = 0$ ), since in the latter scenario we know that the particle has taken the upper path when detecting a neutron in  $D_O$ . For  $T \in (0, 1)$  the state is encoded as a point on the geodesic from the north pole to the equatorial line.

The phase shifter PS2 generates a relative phase shift between the superposing states of  $\Delta\chi = \chi_2 - \chi_1$ :

$$(|p^\perp\rangle + \sqrt{T}|p\rangle) \mapsto (|p^\perp\rangle + e^{i\Delta\chi}\sqrt{T}|p\rangle). \quad (4.4.1)$$

This can be depicted as an evolution along a circle of latitude on the Bloch sphere with periodicity  $2\pi$ .

The recombination at BS2 followed by the detection of the forward beam in  $D_O$  is represented as a projection to the starting point on the equatorial line, i. e. we have to close the curve associated with the evolution of the state by a geodesic to the point  $|q\rangle\langle q|$  on the sphere as discussed for non-cyclic paths in Section 1.2.3. As for the reference state  $|\psi_r\rangle$  we note that the phase shift of  $\eta$  has no impact on the position of the state on the Bloch sphere, it stays at the north pole. Due to the recombination at BS2 and the detection this state is also projected to  $|q\rangle\langle q|$  contributing to the forward beam incident to the detector  $D_O$ .

The paths are depicted in Figure 4.7 in detail for cyclic (a) as well as non-cyclic evolution (b). For a relative phase difference greater than  $\pi/2$  we have to take the direction of the loops into account. In 4.7(b) the first loop is transversed clockwise, whereas the second loop is transversed counter-clockwise yielding a positive or negative contribution to the geometric phase, respectively. We expect that this sign is reflected in the measured phase shift as well, i. e. there should be a change of the behaviour at the point  $\Delta\chi = \pi/2$ .

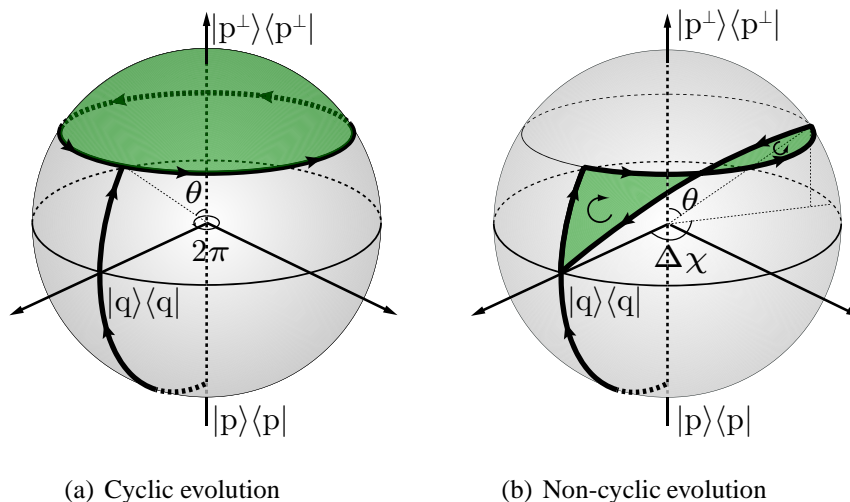


Figure 4.7: Paths on the Bloch-sphere corresponding to the evolution of the state in the split-beam experiment.

#### 4.4.1 Calculation of the surface integrals

From what has been said before about the geometric phase we know that it is proportional to the surface area enclosed by the path traced out by the state in state space. In our case this surface area can be calculated easily since the state space (or better the ray space) is isomorphic to the two-dimensional sphere  $S^2$ . To obtain the area  $\mathcal{F}$  enclosed by the curve  $C$  ( $\mathcal{F} = \partial\mathcal{C}$ ) we just have to calculate the integral

$$\Omega = \int_{\mathcal{F}} d\Omega = \int_{\mathcal{F}} \sin\theta d\theta d\phi, \quad (4.4.2)$$

where we denote the polar angle by  $\theta \in [0, \pi]$  and the azimuthal angle by  $\phi \in [0, 2\pi]$ . To evaluate the integral (4.4.2) we have to parameterise  $\mathcal{C}$ . We can immediately identify three different regions and write  $\mathcal{C} = \mathcal{C}_1 + \mathcal{C}_2 + \mathcal{C}_3$  (Figure 4.8). The first part connects the point  $p_1$  on the equator (whose azimuthal angle can be chosen arbitrarily and can therefore be set to zero since it just amounts to another equivalent choice of basis vectors) to some point  $p_2$  on the meridian to the north pole of the sphere and is defined by constant  $\phi$  ( $\mathcal{C}_1 : \phi \text{ const.}$ ).  $p_2$  and  $p_3$  lie then on the same circle of latitude ( $\mathcal{C}_2 : \theta \text{ const.}$ ). The curve  $\mathcal{C}_3$  between  $p_3$  and  $p_1$  is more involved since it is a geodesic, i. e. the shortest possible path, between these points. In the Appendix B (Eq. B.25) an explicit formula for this curve is given. We only have to adapt this equation to the initial values of the curve  $\mathcal{C}_3$ ,  $p_1 = (\theta_1, \phi_1) = (\pi/2, 0)$  and the point  $p_3 = (\theta_3, \phi_3)$ . Inserting these points into Eq. (B.25) we get

$$\frac{\pi}{2} = \arctan(A^{-1}) \rightarrow A = 0 \quad (4.4.3)$$

$$\theta_3 = \arctan\left(\frac{1}{B \sin \phi_3}\right) \rightarrow \frac{\cot \theta_3}{\sin \phi_3} = B \quad (4.4.4)$$

and consequently

$$\theta(\phi) = \arctan\left[\frac{\sin \phi_3}{\sin \phi} \tan \theta_3\right]. \quad (4.4.5)$$

The surface area can be calculated via the integral

$$\Omega = \int_0^{\phi_3} d\phi \int_{\theta(\phi)}^{\theta_3} d\theta \sin \theta. \quad (4.4.6)$$

In general a great circle intersects a circle of latitude twice. This means that the geodesic  $\theta(\phi)$  given in Eq. (B.25) forms either the lower bound or the upper bound in the integration over  $\phi$  and we would suspect the necessity to divide the integration into two regions,  $\theta(\phi) < \theta_3$  and  $\theta(\phi) > \theta_3$  to add the absolute values of both surface areas. However, the quantity of interest in our case is the oriented surface area and therefore the sign change inherent to the different regions reflects exactly the different orientation of the surface areas.

Integrating first over  $\theta$  in Eq. (4.4.6) and setting  $\xi_3 \equiv \sin \phi_3 \tan \theta_3$  we get

$$\begin{aligned} \Omega &= \int_0^{\phi_3} d\phi \left(-\cos \theta\right)_{\arctan(\xi_3/\sin \phi)}^{\theta_3} \\ &= \int_0^{\phi_3} d\phi \left\{-\cos \theta_3 + \cos \arctan(\xi_3/\sin \phi)\right\} \\ &= \int_0^{\phi_3} d\phi \left\{-\cos \theta_3 + \left(1 + (\xi_3/\sin \phi)^2\right)^{-\frac{1}{2}}\right\} \end{aligned} \quad (4.4.7)$$

The last integration over  $\phi$  can be performed numerically. For  $\phi_3 > \pi$  one has to keep in mind that the geodesic curve  $\theta(\phi)$  from Eq. (4.4.5) does not represent the correct boundary of the enclosed surface for values of  $\phi < \pi$ . In this region it is rather the circle of latitude at  $\theta_3$  that limits the integration. The easiest way to take this fact into account is to calculate the

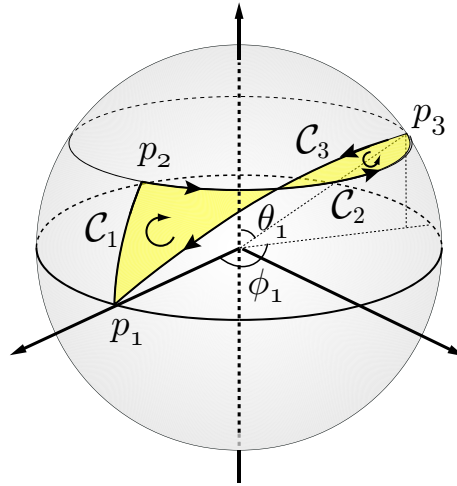


Figure 4.8: Integration path to calculate the solid angle enclosed by the path of the state vector on the Bloch sphere.

same integral as in the region  $\phi_3 < \pi$  and add the surface of the spherical cap limited by  $\theta_3$  towards the equator that is given by

$$\int_0^{2\pi} d\phi \int_0^{\theta_3} d\theta \sin \theta = 2\pi(1 - \cos \theta_3), \quad (4.4.8)$$

Finally, we obtain the graph shown in Figure 4.9, where we notice as expected the increase of the solid angle  $\Omega$  up to the point  $\phi = \pi/2$  followed by a decrease up to  $\phi = 3\pi/2$ . This nicely reveals the dependence of the geometric phase on the orientation of the path, i. e. whether the surface area is enclosed clockwise or anti-clockwise.

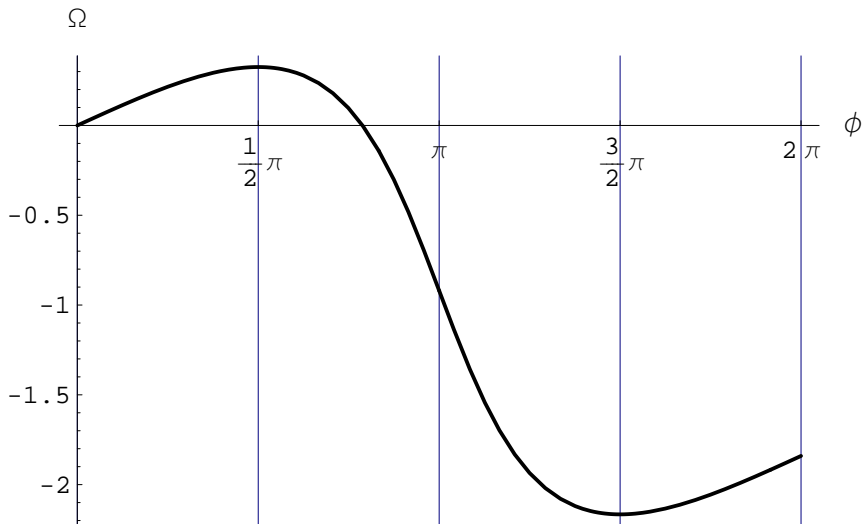


Figure 4.9: Solid angle of the path shown in Figure 4.7 for  $\theta = \pi/4$ .

The same behaviour we also expect from the spatial geometric phase measured with the

double-loop interferometer. The values derived here only by geometric means will turn out to be equal to the values obtained by calculating the interference pattern of the three beams. This manifests the purely geometric character of the measured phase.

**Non-unitary evolution** The question is definitely justified, whether the use of an attenuator in our setup and therefore the transition from properly normalised to non-normalised states spoils the geometric visualisation of the state path on the Bloch sphere. However, recalling the discussion in Section 1.2.4, the path of non-unit vectors can be mapped onto a path in  $\mathcal{N}_0$ , the space of normalised states, and finally again to the projective Hilbert space  $\mathcal{P}$  which is in our case the Bloch-sphere. In conclusion, the geometric phase is determined by the path on the unit Bloch sphere even for non-unitary evolutions.

### 4.5 Measurement procedure

The common technique to measure a phase shift in neutron interferometry is to record the interference fringes due to the relative phase imposed by the rotation of a phase shifter in the beam path first for the empty interferometer. After insertion of the sample (or turning on the magnetic field or quite generally changing the quantity to be measured) again the interference fringes are measured and a phase shift shows up as a shift in the pattern (Figure 4.3).

As for the double-loop setup we have two phase-shifters at our disposal both producing interference fringes if rotated. The geometric phase to be measured is adjusted in the second loop by tuning the transmission coefficient of the absorber and the phase difference between the beams  $|p\rangle$  and  $|p^\perp\rangle$ . Consequently, by rotating the phase shifter PS1 in the first loop an interference pattern is recorded for a particular geometric phase. A change in the second loop results in a shifted interference pattern and possibly also with another value for the contrast. It is mainly the phase that is of further interest for the current experiment. In Figure 4.10 the interference pattern produced by a rotation of PS1 is shown whereas the different oscillations are for different positions of the phase shifter in the second loop PS2.

In fact the measurement procedure was not to rotate PS1 for each position of PS2, but the other way round. To prevent massive errors due to unpredictable phase drifts in the interferometer one step of PS1 ( $\eta$ ) is followed by a rotation of PS2 for slightly more than one period. This approach guarantees that relatively slow intrinsic phase drifts do not affect the measurement of the phase  $\Phi$  between second loop and reference beam. Such phase drifts are mainly caused by temperature gradients [May03], but also vibrations and stray magnetic fields can influence the phase stability of the interferometer.

### 4.6 Experimental results

In the experiment we have used four different settings of the thicknesses of the aluminium slabs of PS2. We have chosen one 4.1 mm thick slab in the transmitted beam ( $|p\rangle$ ) resulting

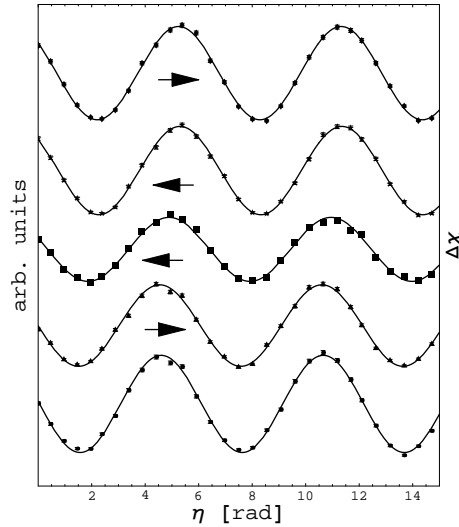


Figure 4.10: Interference pattern produced by a rotation of PS1. The shift indicated by the arrows is the phase shift  $\phi$  caused by the different positions of PS2.

in the phase shift  $\chi_2$  and in the reflected beam ( $|p^\perp\rangle$ ) plates 0.5 mm, 1 mm, 2 mm and 4.1 mm in thickness giving the phase shift  $\chi_1$ . The relative phase difference  $\Delta\chi$  is proportional to these ratios. For all setups the phase shifter in the first loop is rotated to give a relative phase difference of approximately two periods and in the second loop slightly more than one period has been measured by the rotation of PS2.

#### 4.6.1 Thickness ratio $d_1/d_2 \approx 1/8$

First we have chosen a phase shifting slab of 0.5 mm thickness in path  $|p^\perp\rangle$  to obtain a ratio of  $d_1/d_2 = 0.5/4.1 \approx 0.122$  between the thicknesses of PS2. In order to have vanishing dynamical phase contributions (Equation 4.3.6) the absorber in path  $|p\rangle$  has to be chosen to reduce the neutron intensity to  $I = 0.5/4.1I_0$  ( $I_0$  is the non attenuated flux in the lower path). This is achieved by using a gadolinium solution with appropriate concentration. The transmission coefficients  $T_1$  and  $T_2$  for beam  $|p^\perp\rangle$  and  $|p\rangle$ , respectively, has been measured to

$$T_1 = 0.985 \pm 0.004 \quad \text{and} \quad T_2 = 0.118 \pm 0.005. \quad (4.6.1)$$

$T_1$  comprises the contribution from 0.5 mm aluminium oriented in an angle of  $45^\circ$  with respect to the forward direction of the beam and the contribution from a 5 mm silicon slab compensating the transversal shift of the beam due to the refraction at the phase shifter (c. f. Section 4.8). Hence, the transmission ratio is  $T_1/T_2 = 0.120 \pm 0.005$ .

### Fitting the data

In the general discussion we have found an expression for the phase shift of the second loop with respect to the reference beam  $|\psi_r\rangle$  (Eq. 4.2.4),

$$\phi = \frac{\chi_1 + \chi_2}{2} - \arctan \left[ \tan \left( \frac{\chi_2 - \chi_1}{2} \right) \left( \frac{1 - \sqrt{T}}{1 + \sqrt{T}} \right) \right].$$

This equation is valid only for the abstract perfect theory, but it can be tailored to our needs by introducing a few more parameters. First the small, but non-vanishing absorption due to the aluminium slabs in the beam path  $|p^\perp\rangle$  is taken into account by insertion of a transmission coefficient  $T_1$  for this beam as well. Furthermore, as will be demonstrated in Section 4.8.1 at length, the phase shift has a bothersome side effect in that for a divergent poly-chromatic beam the interference fringes vanish for large phase shifts. The partial waves from each beam do not overlap anymore. This unfortunately also affects the relative phase between the reference beam  $|\psi_{ref}\rangle$  and the two sub-beams  $|p\rangle$  and  $|p^\perp\rangle$ . In short, this can be shown by considering the wavefunction at the interferometer output,

$$|\Psi_f\rangle \propto (A_0 e^{i\eta} + A_1 e^{i\chi_1} + A_2 e^{i\chi_2})|O\rangle, \quad (4.6.2)$$

where the real coefficients  $A_i$  denote any norm reducing influences. For the intensity  $I = \langle \Psi_f | \Psi_f \rangle$  we get

$$\begin{aligned} I &= \sum A_i^2 + 2A_1 A_2 \cos(\chi_2 - \chi_1) \\ &\quad + 2A_0 A_1 \cos(\eta - \chi_1) + 2A_0 A_2 \cos(\eta - \chi_2) \\ &\propto \frac{1}{2A_0} \sum A_i^2 + \frac{A_1 A_2}{A_0} \cos(\chi_2 - \chi_1) \\ &\quad + A_1 \cos(\eta - \chi_1) + A_2 \cos(\eta - \chi_2) \end{aligned} \quad (4.6.3)$$

For fixed  $\chi_1$  and  $\chi_2$  (fixed position of PS2) the intensity consists only of a linear superposition of two oscillations with the same argument  $\eta$ ,

$$I = C + A_1 \cos(\eta - \chi_1) + A_2 \cos(\eta - \chi_2) \quad (4.6.4)$$

and can be simplified to

$$I = C + v \cos(\eta + \Phi), \quad (4.6.5)$$

$$v = (A_1^2 + A_2^2 + 2A_1 A_2 \cos(\chi_2 - \chi_1))^{1/2} \quad (4.6.6)$$

$$\Phi = \arctan \left[ \frac{\sin \chi_1 + A_2/A_1 \sin \chi_2}{\cos \chi_1 + A_2/A_1 \cos \chi_2} \right]. \quad (4.6.7)$$

From the last equation it becomes apparent that the amplitudes of the superposition of the cosine functions influence the phase of the resulting sinusoidal interference fringes. Not fully

overlapping sub-beams gives a contribution to the measured phase shift, except at points where the arctan- term vanishes. In fact,  $\Phi$  is equivalent to the expression for the phase difference in Eq. (4.2.4). From the latter we can read off that at the points  $\Delta\chi = n\pi$ ,  $n$  integer,  $\tan(\Delta\chi/2) = 0$  and therefore  $\Phi$  is independent of the  $A$  coefficients. Here, the overlap of the sub-beams is immaterial. This result can be appreciated in the graphs of the experimental data below (Figures 4.11, 4.13, 4.15 and 4.17): The measured data curve is flattened with respect to the theoretical predicted curve which is a consequence of the merely partial overlap of the different subbeams except at the points where  $\Delta\chi$  is an integer multiple of  $\pi$ . From  $\Phi$  in (4.6.7) it becomes evident that an additional fit parameter  $C = A_1/A_2$  is necessary taking all contrast reducing influences into account. The fit function reads then

$$\mathcal{F}(\xi; C) = \frac{\chi_1(\xi) + \chi_2(\xi)}{2} - \arctan \left[ \tan \frac{\Delta\chi(\xi)}{2} \frac{\sqrt{T_1} - C\sqrt{T_2}}{\sqrt{T_1} + C\sqrt{T_2}} \right]. \quad (4.6.8)$$

But this is still not the whole truth, since we have to include possible dynamical phase contributions as well. It is in the dynamical phase's nature (c. f. Eq. 4.3.6) that it depends linearly on the rotation angle  $\xi$  and for this reason we simply include a linear term in the fit function,

$$\mathcal{F}(\xi; C, D) = \frac{\chi_1(\xi) + \chi_2(\xi)}{2} - \arctan \left[ \tan \frac{\Delta\chi(\xi)}{2} \frac{\sqrt{T_1} - C\sqrt{T_2}}{\sqrt{T_1} + C\sqrt{T_2}} \right] + D\xi. \quad (4.6.9)$$

Figure 4.11 shows finally the measured phase shifts fitted with the function  $\mathcal{F}(\xi; C, D)$ .

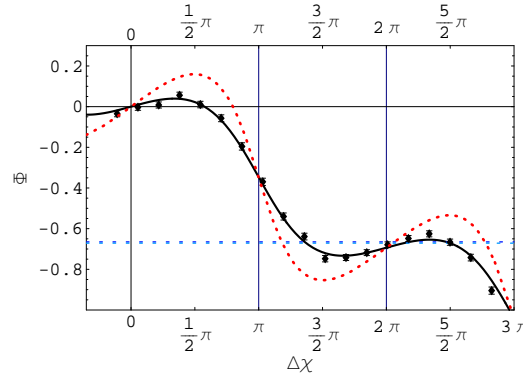


Figure 4.11: Measured phase shift of the intensity pattern by an induced phase shift of  $\Delta\chi$  due to rotation of PS2.

The fit results in values of  $C = 0.57 \pm 0.02$  and  $D = -0.6 \pm 0.6$ . The contributions to the dynamical phase reflected in non-zero  $D$ -coefficient are mainly due to a deviation in the precise  $d_1/d_2$  thickness ratio and in a misalignment of the phase shifter PS2. This issue will be discussed below.

**Cyclic evolution** The foregoing theory predicts that the geometric phase at  $\Delta\chi = n\pi$  is not affected by the disturbances subsumed in the fit parameter  $C$  since at these points the

tangent in (4.6.9) vanishes. The distance between the curve fitted to the measured data and the theoretical curve in Figure 4.11 should be zero for these values. This provides us with a further check of the theory. We already see that the differences between the measured values and the theoretical results are minimal at these points, however, in order to quantify such a statement we have to embark on another strategy for fitting the data, because the fit function in Eq. (4.6.9) automatically gives us the correct value for the geometric phase at  $\Delta\chi = n\pi$ : As already indicated at these points  $\tan\Delta\chi/2 = 0$  and only the sum  $(\chi_1(\xi) + \chi_2(\xi))/2$  along with the term referring to the dynamical phase term  $D\xi$  is left.

Explicitly, the dynamical phase can be rewritten as

$$\phi_d = \frac{T_1\chi_1 + T_2\chi_2}{T_1 + T_2} = \frac{\chi_1 + \chi_2 \tan^2 \frac{\theta}{2}}{1 + \tan^2 \frac{\theta}{2}} = \chi_1 \cos^2 \frac{\theta}{2} + \chi_2 \sin^2 \frac{\theta}{2} = \frac{\chi_1 + \chi_2}{2} - \frac{\Delta\chi}{2} \cos \theta, \quad (4.6.10)$$

where we have used  $T = \tan^2 \theta/2$ . Subtracting this term from the fit function in (4.6.9) and bearing in mind that the arctan term is either 0 or  $\pi$  for a half rotation ( $\Delta\chi = \pi$ ) or a full rotation ( $\Delta\chi = 2\pi$ ), respectively, we find

$$\mathcal{F} = \begin{cases} \frac{\pi}{2} \cos \theta & \Delta\chi = \pi \\ \pi(\cos \theta - 1) & \Delta\chi = 2\pi. \end{cases} \quad (4.6.11)$$

There is by definition of  $\mathcal{F}$  no free parameter left to take the measurement results into account, the transmission coefficients determines the fit function  $\mathcal{F}$  completely at these points. So, by design of the fit function at these points when subtracting the dynamical phase  $D\xi$  we obtain exactly the theoretical result for the geometric phase, which is not what we want. We would rather like to have a more objective approach to the geometric phase also for  $\Delta\chi = n\pi$ .

**Trigonometric fit** To find a remedy we proceed by fitting the data values with a sum of trigonometric functions plus a linear term

$$\mathcal{F}'(\xi) = A + B\xi + \sum_{j=0}^N \{C_j \cos(j\omega_{d_1/d_2} \xi) + D_j \sin(j\omega_{d_1/d_2} \xi)\}. \quad (4.6.12)$$

Eq. (4.1.29) provides the oscillation period  $\omega_{d_1/d_2} = \sqrt{2}N_{AI}b_{cAI}\lambda(d_1 + d_2)$ , in particular,  $\omega_{0.5/4} = 367.1$  rad/s. The maximal value of  $N$  is given by the number of data points in that the number of fit parameters must not exceed the number of data points. Here we have 19 points, hence  $N < 9$ . The exact number for  $N$  can be found by looking at the *reduced  $\chi$ -square* value [Leo94] of the fit that is given by the sum over the weighted squared residuals

$$\chi_r^2 = \frac{1}{\nu} \sum_{i=1}^n \left( \frac{x_i - \mu_i}{\sigma_i} \right)^2, \quad (4.6.13)$$

where  $x_i$  is the  $i^{th}$  measured value,  $\mu_i$  is the value predicted by the fit function,  $\sigma_i$  denotes the variance and  $\nu$  the degrees of freedom of the fit ( $\nu = \text{number of data points} - \text{number of parameters}$ ).

If  $\chi_r^2 \approx 1$ , we can be satisfied with the fit function. Indeed, we take the fit with  $N$  as small as possible and  $\chi_r^2$  close to one in order to avoid over-fitting. A reduced chi-square value  $\chi_r = 1.47$  is found for  $N = 1$  and  $\nu = 15$ . The probability to obtain a larger chi-square  $\chi^2 \equiv \nu\chi_r^2$  than the chi-square from the fit  $S$ ,  $P(\chi^2 \geq S)$ , serves also an indicator for the goodness of the fit. For acceptance it should be greater than 5%. Here,  $P(\chi^2 \geq S) = 10\%$ . Figure 4.12 shows this trigonometric fit along with the measured data.

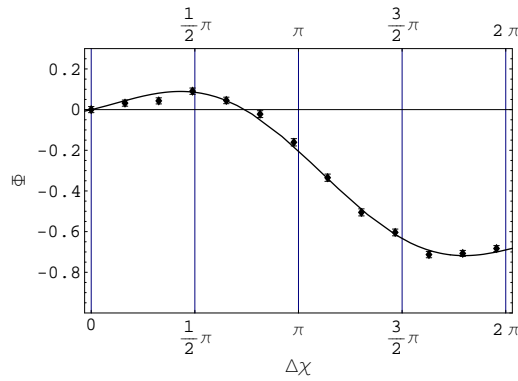


Figure 4.12: Trigonometric fit with  $N = 1$ .

At the point  $\Delta\chi = 2\pi$  the measured value from the trigonometric fit is  $\Phi = -0.689 \pm 0.015 \text{ rad}$ . The dynamical phase contribution is determined by the fit parameter  $D$  in  $\mathcal{F}(\xi; C, D)$  from Eq. (4.6.9)<sup>2</sup>,

$$\phi_d(2\pi) = \frac{D2\pi}{N_{AI}b_{cAI}\lambda\sqrt{2}(d_1 + d_2)} = -0.01 \pm 0.01 \text{ rad}, \quad (4.6.14)$$

where we have assumed that the wavelength spread  $\Delta\lambda/\lambda \approx 1\%$  and the error in the thicknesses  $\Delta d_i \approx 0.05 \text{ mm}$ . The resulting geometric phase is

$$\phi_g \equiv \Phi - \phi_d = -0.68 \pm 0.02 \text{ rad} \quad (4.6.15)$$

which is in good agreement with the theoretical value  $\phi_g^{th} = -0.671 \text{ rad}$ .

### Causes of spurious dynamical phase contributions

In the derivation of the geometric phase from the measured values we have omitted a discussion on the origin of the dynamical phase contributions.

<sup>2</sup>Note, that  $\phi_d$  cannot be determined from  $B$  of the trigonometric fit  $\mathcal{F}'(\xi)$ , since for this fit we did not make any assumption on the separation of the dynamical and the geometric phase.

**Ratio mismatch** First, there is a small contribution from the mismatch of the ratios  $d_1/d_2$  and  $T_2/T_1$ . For the present setup we have found  $T_2/T_1 \approx 0.120$  and  $d_1/d_2 \approx 0.122$  which adds a dynamical phase component of

$$\phi_d(\Delta\chi) = \frac{(-d_1T_1 + d_2T_2)}{T_1 + T_2} \frac{\Delta\chi}{(d_1 + d_2)} \approx -0.002\Delta\chi. \quad (4.6.16)$$

At  $\Delta\chi = 2\pi$  we have already accumulated a dynamical phase of  $\phi_d \approx -0.011$  which explains the deviations found above.

**Parallel position** Secondly, a misalignment of the phase shifter PS2 can give also rise to a dynamical phase. If the phase shifter is not inserted precisely parallel the ratio of the mean effective thicknesses changes as well. Recalling the discussion in Section 4.1.2, the phase shift of the neutron wave is  $X_i = N_{Al}b_{cAl}\lambda d_i / \cos \alpha$  with  $d_{i,eff} = d / \cos \alpha$  the effective thickness. For small  $\alpha$  the series expansion of the inverse cosine  $(\cos^{-1}(\alpha \pm \xi))|_{\alpha_0=\pi/4} = \sqrt{2}(1 \pm \xi)$  determines the effective thickness  $d_{eff} = d\sqrt{2}$  relating the rotation about  $\xi$  to the phase shift  $\chi = N_{Al}b_{cAl}\lambda d_{eff}\xi$ . But for an expansion about  $\alpha_0 = \pi/4 \pm \delta$ , corresponding to a slight misalignment  $\delta$  we obtain

$$X_i = N_{Al}b_{cAl}\lambda d_i\sqrt{2}(1 \pm \xi \pm \delta + 3\delta\xi + \mathcal{O}(\delta)^2 + \mathcal{O}(\xi)^2) \quad (4.6.17)$$

for small  $\delta$  and small  $\xi$ . Note, that terms proportional to  $\xi^2$  are not included although they are of the same order as the terms proportional to  $\xi\delta$  since we just want to estimate the order of magnitude of the error contributions. The terms of order  $\delta^2$  contribute only to a constant offset for varying  $\xi$  and are therefore also not included. The variable phase shift is then

$$\chi_i = N_{Al}b_{cAl}\lambda \underbrace{d\sqrt{2}(3\delta \pm 1)}_{d'_{eff}} \xi. \quad (4.6.18)$$

The effective thickness has changed by an amount  $(3\delta \pm 1)$  leading to a modified phase shift ratio

$$\frac{d_1}{d_2} \mapsto \frac{d'_1}{d'_2} = \frac{d_1}{d_2} \frac{3\delta - 1}{3\delta + 1}.$$

Recalling the parallel transport condition from Eq. (4.3.5) we notice that a misalignment of the initial position contributes to the dynamical phase and inevitably spoils the ideal parallel transport even for properly adapted thickness vs. transmission ratios.

Why does this effect usually not bother in standard neutron interferometry? To answer this question let us consider again a phase-shifter with plates of different thickness. The relative phase shift is according to the above

$$\begin{aligned} \Delta\chi &= \chi_2 - \chi_1 = \sqrt{2}N_{Al}b_{cAl}\lambda (d_2\xi(3\delta + 1) - d_1\xi(3\delta - 1)) \\ &= \sqrt{2}N_{Al}b_{cAl}\lambda ((d_2 + d_1) + 3(d_2 - d_1)\delta)\xi. \end{aligned} \quad (4.6.19)$$

From the last expression one immediately realises that the term proportional to  $\delta$  vanishes for  $d_2 = d_1$  which is usually the case. This term becomes only important for differently thick slabs in the different beam paths. For the present setup the misalignment  $\delta$  causes an additional dynamical phase contribution of

$$\phi_d(\Delta\chi) = \frac{(d_1(1-3\delta)T_1 + d_2(1+3\delta)T_2)}{T_1 + T_2} \frac{\Delta\chi}{(d_1(1-3\delta) + d_2(1+3\delta))} \quad (4.6.20)$$

when replacing  $d_j$  with  $d'_j = d_j((-1)^j + 3\delta)$  in Eq. (4.6.16). For an otherwise perfectly adjusted setup ( $d_1/d_2 = T_2/T_1 \rightarrow \phi_d = 0$ ) the additional contribution to the dynamical phase from a misaligned phase shifter amounts to

$$\phi_d(\Delta\chi) = \frac{6d_2T_2\delta}{(T_1 + T_2)(d_1 + d_2 + 3\delta(d_2 - d_1))}. \quad (4.6.21)$$

For example  $\delta = 1^\circ$  gives rise to  $\phi_d(\Delta\chi) = -0.096\Delta\chi$  in the 4.1/0.5 setting, i. e. for a  $2\pi$  rotation  $\approx -0.05$  rad. It becomes evident that the parallel adjustment has even more influence on the dynamical phase as the errors in the adjustment of the phase shifter thickness.

#### 4.6.2 Thickness ratio $d_1/d_2 \approx 1/4$

In the next experiment we have chosen a ratio of 1 mm vs. 4.1 mm between the aluminium slabs of the phase shifter PS2. The transmission rate of the absorber in the beam denoted by  $|p\rangle$  has again been adjusted to reflect the same ratio between the intensities in  $|p\rangle$  and  $|p^\perp\rangle$ ,

$$T_1 = 0.984 \pm 0.010 \quad \text{and} \quad T_2 = 0.240 \pm 0.011, \quad (4.6.22)$$

where  $T_1$  comprises the absorption of 1 mm aluminium at an angle of  $45^\circ$  relative to the forward direction plus the 5 mm silicon plate inserted to compensate for the beam deflection (Section 4.8). Altogether, this yields a transmission ratio of  $T_2/T_1 = 0.244 \pm 0.011$  which is in good agreement with the ratio of the thicknesses  $d_1/d_2 = 1/4.1 = 0.244$  aimed for.

A fit of the data using the function in Eq. (4.6.9) shows again the good qualitative agreement with the theoretical prediction (Figure 4.13). The fit parameters have values of  $C = 0.463 \pm 0.015$  and  $D = 8.51 \pm 0.75$  and the deviations from the theoretical curve can be explained in the same manner as above (Section 4.6.1).

Again, we fit the data with a sum of trigonometric functions (4.6.12) to obtain the geometric phase  $\phi_g$  at  $\Delta\chi = 2\pi$  with an oscillation period  $\omega_{1/4} = 407.0$  rad/s. Here,  $N = 2$  yields the best fit with  $S_r = 0.35$  shown in Figure 4.14. The confidence level  $P(\chi^2 \geq S) = 96.7\%$ .

Let us here as well identify the cyclic spatial geometric phase at  $\Delta\chi = n\pi$ : There is no deviation from these points stemming from the partial overlaps of the sub-beams, but there is a contribution from the dynamical phase coming mainly from the misalignment of the phase shifter. At the point  $\Delta\chi = 2\pi$  we obtain a measured value of  $\Phi = -1.10 \pm 0.013$  rad. From

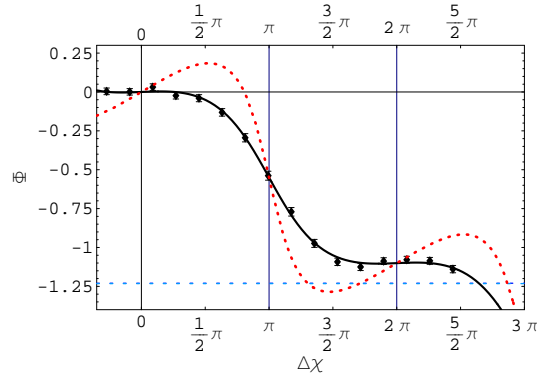


Figure 4.13: Measured phase shift of the intensity pattern by an induced phase shift of  $\Delta\chi$  due to rotation of PS2 with thickness 1 mm and 4.1 mm, respectively. The fit parameters for the fitted (solid) curve are  $C = 0.463 \pm 0.015$  and  $D = 8.51 \pm 0.75$ . The dotted curve shows the theoretical curve disregarding the effects of different contrast values, i. e. for  $C = 1$ .

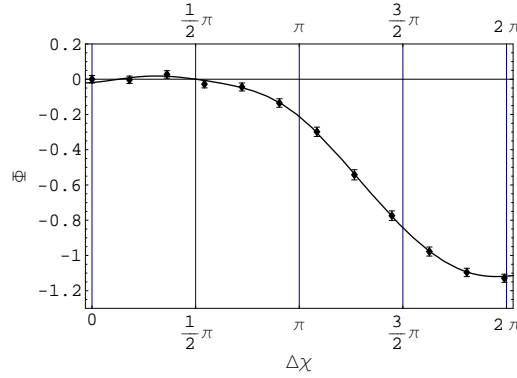


Figure 4.14: Trigonometric fit with  $N = 2$ .

the fit parameter  $D$  we can estimate the contribution of the dynamical phase,

$$\phi_d(2\pi) = \frac{D2\pi}{N_A |b_{cA}| \lambda \sqrt{2}(d_1 + d_2)} = 0.131 \pm 0.012 \text{ rad} \quad (4.6.23)$$

and therefore the geometric phase reads

$$\phi_g \equiv \Phi - \phi_d = -1.230 \pm 0.018 \text{ rad} \quad (4.6.24)$$

This is to be compared with a theoretical value of  $\phi_g^{th} = -1.232 \text{ rad}$ .

### 4.6.3 Thickness ratio $d_1/d_2 \approx 1/2$

For the setting of 2 mm vs. 4.1 mm phase shifting slabs at PS2 we have obtained the following results: The transmission coefficients have been determined to  $T_1 = 0.97 \pm 0.004$  and  $T_2 = 0.45 \pm 0.017$  yielding a transmission ratio of  $T_2/T_1 = 0.47 \pm 0.017$  which has to be compared with the ratio of the thickness of the phase shifting slabs  $d_1/d_2 = 2/4.1 \approx 0.488$ .

The measured phase shifts are shown in Figure 4.15 where the fit parameters for the fit functions are  $C = 0.68 \pm 0.025$  and  $D = 14.3 \pm 2.5$ , i. e. there is a quite large dynamical phase contribution.

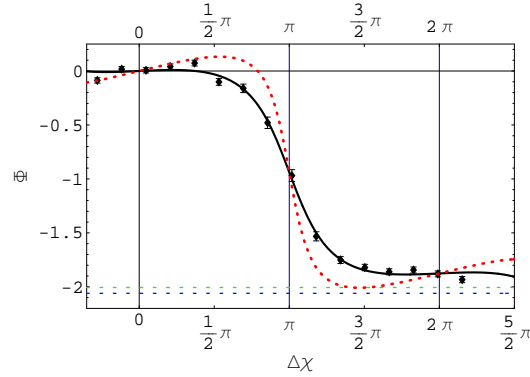
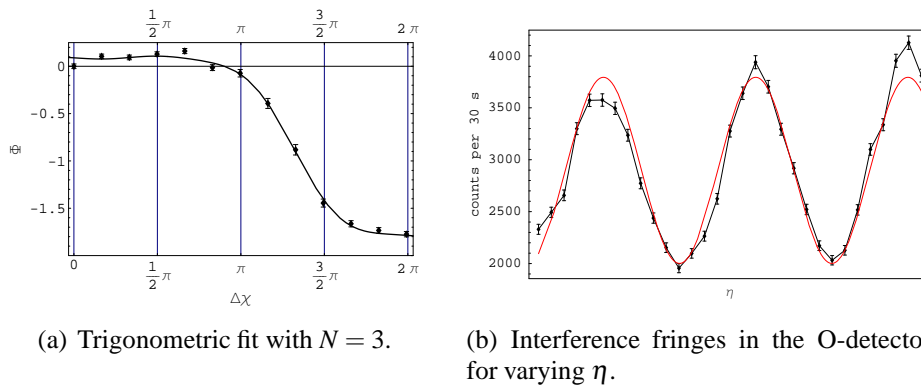


Figure 4.15: Measured phase shift of the intensity pattern by an induced phase shift of  $\Delta\chi$  due to rotation of PS2 with thickness 2 mm and 4.1 mm, respectively. The fit parameters for the fitted (solid) curve are  $C = 0.68 \pm 0.025$  and  $D = 14.3 \pm 2.5$ .

From a trigonometric fit with  $\omega_{2/4} = 486.8$  rad/s,  $N = 3$  and  $S_r = 37.6$  we obtain the value  $\Phi = -1.876 \pm 0.07$  rad at  $2\pi$  (Figure 4.6.3). Note that  $S_r$  is extraordinarily large and also the confidence level is very low  $P(\chi^2 \geq S) = 8 \times 10^{-6}$ . The fit to the measured data or even the measured data is questionable. The malfunction of the fit procedure may result from very large intrinsic phase shifts during the measurement process that is already visible in the fits of the interference patterns. They look quite distorted (Figure 4.16(b)) - the reason might be large temperature drifts. Nevertheless we will present the data.



(a) Trigonometric fit with  $N = 3$ .

(b) Interference fringes in the O-detector for varying  $\eta$ .

Figure 4.16: Due to parasitic influences the measured values are not that great for this setup.

The dynamical phase at the point  $2\pi$  can be estimated from the fit parameter  $D$  to  $\phi_d = 0.18 \pm 0.03$  rad and the geometric phase evaluates therefore to

$$\phi_g = \Phi - \phi_d = -2.06 \pm 0.08 \text{ rad.} \quad (4.6.25)$$

Despite of the bad data this is quite close to the theoretical value of  $\phi_g^{th} = 2.006$  rad.

#### 4.6.4 Thickness ratio $d_1/d_2 = 1$

Finally, we want to discuss the simple situation with no absorber attached and therefore equally thick phase shifting slabs of PS2. The transmission coefficients in both beam paths  $|p\rangle$  and  $|p^\perp\rangle$  are determined only by the absorption cross section of the 4.1 mm thick aluminium slabs,  $T_1 = T_2 = 0.96 \pm 0.001$ , and is moreover irrelevant since they are same in both beams.

For the fit function shown in Figure 4.17 together with the collected experimental data the parameters are  $C = 0.925 \pm 0.022$  and  $D = 0.0 \pm 4.2$ . Note, that there is one point in between the step-like function with a very large error-bar. This is due to the vanishing contrast in this case and can be interpreted also geometrically: At this point the initial and the final state on the equatorial line are exactly opposite and therefore there is no unique geodesic connecting these two points. The geometric phase is therefore undefined at this point.

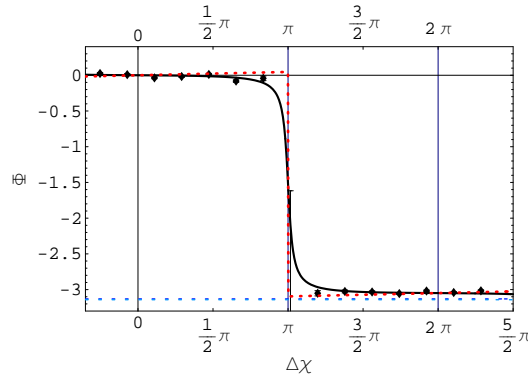


Figure 4.17: Measured phase shift of the intensity pattern by an induced phase shift of  $\Delta\chi$  due to rotation of PS2 with thickness 4.1 mm and 4.1 mm, respectively. The fit parameters for the fitted (solid) curve are  $C = 0.925 \pm 0.022$  and  $D = -0.0 \pm 4.2$ .

To obtain an estimate of the measured value at  $\Delta\chi = 2\pi$  we forbear from applying a trigonometric fit to the measured values. We fit the left part of the data points that are close to zero separately from the right part (close to  $-\pi$ ) with the constant functions  $D_l(\xi) = A_l$  and  $D_r(\xi) = A_r$ . The relative phase difference is then just the difference  $\Phi = A_r - A_l$ . The parameters turn out to

$$A_l = -0.077 \pm 0.016 \text{ rad} \quad \text{and} \quad A_r = -3.11 \pm 0.006 \text{ rad}$$

resulting in  $\Phi = -3.04 \pm 0.02 \text{ rad}$ .

The dynamical contribution is estimated as  $\phi_d(2\pi) = 0. \pm 0.04 \text{ rad}$  for  $\Delta\chi = 2\pi$  and the geometric phase is therefore

$$\phi_g = \Phi - \phi_d = -3.04 \pm 0.05 \text{ rad}. \quad (4.6.26)$$

Clearly, for this setup we expect a geometric phase of  $\pi$  since the evolution is along the equator and therefore half of the enclosed solid angle is  $\pi$ . The deviation from the theoret-

ical value is here not due to dynamical contributions, since we have already argued that the misalignment is immaterial for phase shifting slabs of equal thickness. The source of the discrepancy must be ascribed to the linear fitting procedure, because it does not take into account the phase shift due to the different contrast values in the different loops of the beams subsumed in the fit parameter  $C$ . Although there is no deflection of the beams due to differently thick phase shifters, there are still interferometer intrinsic imperfections that reduce the contrast and lead to  $C \neq 1$ .

#### 4.6.5 Cyclic geometric phase

In Figure 4.18 the measured geometric phases  $\phi_g$  are plotted over the solid angle  $\Omega$  enclosed by the path on the Bloch sphere. We notice that in comparison to the cyclic spatial geometric phase recorded in the antecedent experiment in [HZR96] the deviation from the theoretical curve is smaller. This is because we have corrected for the dynamical phase, whereas in the other experiment additional dynamical contributions are still included in the plotted phase.

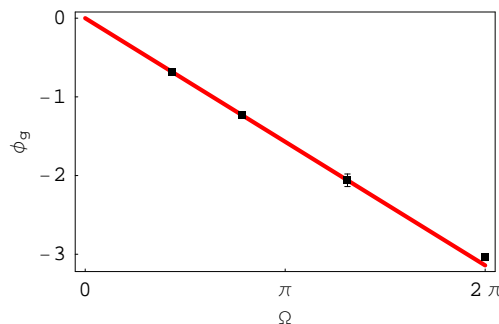


Figure 4.18: Measured geometric phase  $\phi_g$  values over the solid angle  $\Omega$ . The theoretical value of  $\phi_g$  is indicated by the solid line.

The values of the measured  $\phi_g$  along with the theoretical predictions and the transmission ratio is presented in Table 4.1.

$\phi_g^m$ [rad]	$\phi_g^{th}$ [rad]	$T_2/T_1$	$d_1/d_2$	$\phi_d$ [rad]
$-0.68 \pm 0.02$	$-0.671$	$0.120 \pm 0.005$	$0.5/4.1 = 0.122$	$-0.01 \pm 0.01$
$-1.23 \pm 0.02$	$-1.232$	$0.244 \pm 0.011$	$1/4.1 = 0.244$	$0.13 \pm 0.01$
$-2.06 \pm 0.08$	$-2.006$	$0.47 \pm 0.017$	$2/4.1 = 0.488$	$0.18 \pm 0.03$
$-3.04 \pm 0.04$	$-\pi$	1	1	$0.0 \pm 0.04$

Table 4.1: Measured cyclic spatial geometric phase values  $\phi_g^m$  along with the theoretical predictions  $\phi_g^{th}$  for the various transmission and thickness ratios.

## 4.7 Wagh’s critical comments

In measuring the non-cyclic spatial geometric phase the qualitative and also - when taking systematic effects into account - quantitative agreement between theory and experiment has been verified and the way is paved to turn back to the critical comments by Wagh [Wag99] on the antecedent experiment on the cyclic spatial geometric phase. In his comment Wagh put forward some arguments against a geometrical interpretation of the experiment. He argues that the observed phase is only due to  $U(1)$  evolutions, i. e. it is a scalar phase shift and therefore cannot be of geometric origin. A comparison with a measurement of the geometric phase using the neutron’s spin serves him as indicator that the observed phase is only dynamical. His argument relies on the orthogonality of the spin eigenstates states, where the scalar product  $\langle \uparrow | \downarrow \rangle$  vanishes. This is in contrast to the superposition of the different beams after the last beam splitter BS6, which are admittedly in the same momentum eigenstate, and he concludes that placing the states  $|p\rangle$  and  $|p^\perp\rangle$  “at opposite poles on the two-sphere ray space amounts to a conceptual error”. To dismiss such criticism it is essential to stress that  $|p\rangle$  and  $|p^\perp\rangle$  are definitely not in the same state, it is not until their recombination and their recombination with the reference beam  $|\psi_{ref}\rangle$  that they differ only in phase. It is immaterial whether the final superposed partial beams are in the same state, the geometric phase is imprinted in the global phase obtained from the evolution in the second loop.

That the “density operator remains stationary in ray space throughout the evolution” can be refuted by the same argument: It is evident that the beams in the second interferometer loop do not overlap and are therefore orthogonal to each other. Therefore, in the simplest description we have at least a two dimensional Hilbert space. A phase shifter in the second loop generates different states in this two dimensional space and the density operator does definitely not remain stationary. Otherwise, we would not see a change in the contrast as shown in Figure 4.19.

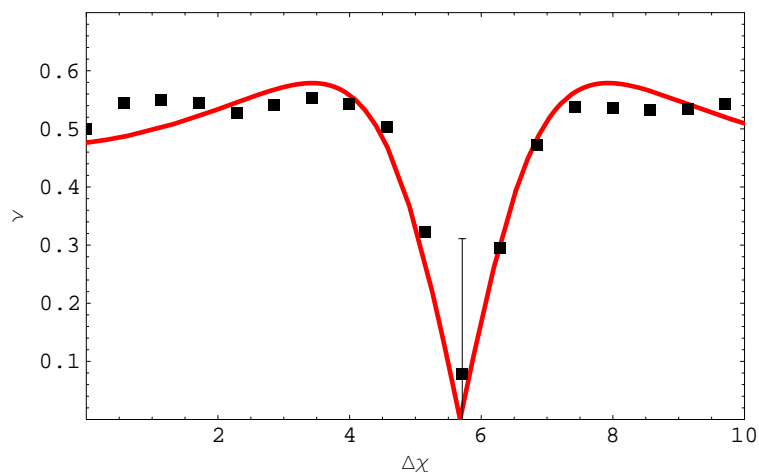


Figure 4.19: Contrast  $v = |\langle \psi'_{ref} | \psi'_f \rangle|$  for different values of the phase difference  $\Delta\chi$  for the  $d_1/d_2 = 1$  setup.

The results presented endorse this interpretation by explicitly showing that the geometric

phase is observed with “an appropriately reduced interference contrast due to the noncyclic-ity” as asked for by Wagh. Therefore, I believe that this experiment provides a proper test of the spatial geometric phase.

## 4.8 Systematic deviations due to partial overlap

The last point to settle is the origin of the flattening of the experimental curves in Figures 4.11, 4.13, 4.15 and 4.17, which we attributed above to the not 100% overlap of the sub-beams.

If phase shifters are put into the beam paths in the interferometer a reduction of the contrast will in general be recognised also if these phase shifters are perfectly transmissive. In analogy to geometrical optics this effect can be depicted as a spatial translation of the beam in the same way as a light ray is deflected at the boundary between two media with different refractive index. The unaffected and the translated beam are just partially overlapping. In the argument leading to the correct fitting parameter in Section 4.6.1 we have already encountered an additional phase shift due to the imperfect overlap of the three sub-beams which finally distorts the curve of the geometric phase. Usually this effect is compensated by placing the phase shifting slab such that it covers both beam paths. Then, each of the beams is shifted approximately by the same amount and just the small difference in the effective thickness due to a slight tilt causes the relative phase shift. However, in our case the phase shifter PS2 is of unequal thickness and therefore the beams are not fully overlapping anymore.

### 4.8.1 Coherence properties

In neutron interferometry single neutrons are counted after making their way through the interferometer. The outgoing beams at the two output ports (O- and H- beam) are in a superposition of having taken either one or the other path. Interference fringes are induced by a phase shifter described above which shifts the wavefunction in one path by  $\chi$  (Eq. 4.1.24). The *order of the interference* is determined by the number of interference maxima passing by when increasing  $\chi$  continuously starting from zero. The relative phase between the contribution from either path sweeps the intensity between the O- and H- beam. For a plane wave with a single wave vector  $\vec{k}_0$  the amount of the phase shift  $\chi$  is immaterial, the interference pattern will be visible for any interference order, yet, in reality the beam contains a multitude of wavelengths and each partial wave obtains now a different phase factor. In turn, the contributions from different monochromatic waves with slightly different wavelength lead to different periodicities. The resulting interference pattern is the sum over all such contributions and with increasing phase shift their addition will lead to a less and less well-defined interference pattern because the maxima will get more and more out of step. The vanishing of the interference pattern defines the *coherence length* of the beam. In fact, the phase shift  $X$  produced by a typical phase shifting slab can be denoted by the scalar product  $X = \vec{\Delta} \cdot \vec{k}$

with  $\vec{\Delta} = (\Delta_x, \Delta_y, \Delta_z)^T$  as the spatial displacement vector (Eq. 4.1.25) and serves to distinguish between the coherence lengths in different directions. Qualitatively,  $\Delta_x^c$  is the amount of displacement of the wave in direction  $x$  (and equally for  $y$  and  $z$ ) for which the interference pattern vanishes. The *coherence volume* [Gla63, RWK<sup>+</sup>96, RW00, Pet87] is defined as the product of these coherence lengths,  $v_c = \Delta_x^c \Delta_y^c \Delta_z^c$ . Specific to neutron interferometry are the large differences in the coherence lengths due to the restrictions on the wavelength distribution imposed by the Bragg-diffraction at the perfect crystal silicon plates in one direction ( $\Delta_y \gg \Delta_x, \Delta_z$ , where  $y$  is perpendicular to the reflecting lattice planes of the interferometer).

As an expedient example we consider an incident Gaussian wave packet

$$|\psi\rangle = \int d\vec{k} f(\vec{k}) |\vec{k}\rangle.$$

The momentum distribution function  $f(\vec{k})$  can be written as a product of the individual distribution function,  $f(\vec{k}) = f(k_x, k_y, k_z) = f(k_x)f(k_y)f(k_z)$  with

$$f(k_i) = e^{-\left[\frac{k_i - \bar{k}_i}{2(\delta k_i)}\right]^2} (2\pi(\delta k_i)^2)^{-1/4}.$$

$\bar{k}_i$  denotes the mean momentum and  $\delta k_i$  the momentum spread in the corresponding direction. The superposition of the wave-packet  $|\psi\rangle$  with a phase shifted copy of itself

$$|\psi_\Delta\rangle = \int d\vec{k} f(\vec{k}) e^{i\vec{\Delta} \cdot \vec{k}} |\vec{k}\rangle$$

enables the measurement of the autocorrelation function. The superposition  $|\psi\rangle + |\psi_\Delta\rangle$  corresponds to the output of a neutron interferometer with a phase shift  $\vec{\Delta} \cdot \vec{k}$  in one of the beams. We assume that the spatial displacement  $\vec{\Delta}$  does not depend explicitly on the momentum  $k$  which is justified if the momentum spread  $\delta k$  is small so that the difference in the refractive index can be neglected. The superposition leads to the intensity

$$\begin{aligned} I &= ||\psi\rangle + |\psi_\Delta\rangle|^2 \\ &= \langle\psi|\psi\rangle + \langle\psi_\Delta|\psi_\Delta\rangle + 2|\langle\psi|\psi_\Delta\rangle| \cos \arg \langle\psi|\psi_\Delta\rangle. \end{aligned} \quad (4.8.1)$$

Due to the normalisation the first two terms are both unity. The cross product  $\langle\psi|\psi_\Delta\rangle$  can be calculated to

$$\begin{aligned} \langle\psi|\psi_\Delta\rangle &= (2\pi(\delta k_i))^{-1/2} \prod_i \iint dk_i dk'_i e^{-\left[\frac{(k_i - \bar{k}_i)}{2(\delta k_i)}\right]^2} e^{-\left[\frac{(k'_i - \bar{k}_i)}{2(\delta k_i)}\right]^2} e^{i\Delta_i k'_i} \underbrace{\langle k_i | k'_i \rangle}_{\delta_{k_i, k'_i}} \\ &= (2\pi(\delta k_i))^{-1/2} \prod_i \int dk_i e^{-\frac{(k_i - \bar{k}_i)^2}{2(\delta k_i)^2}} e^{i\Delta_i k_i} \\ &= \prod_i e^{i\Delta_i \bar{k}_i} e^{-\frac{(\Delta_i \delta k_i)^2}{2}}, \end{aligned} \quad (4.8.2)$$

and inserting this expression into Eq. (4.8.1) we obtain

$$I = 2 \left( 1 + e^{-\frac{\sum_i (\Delta_i \delta k_i)^2}{2}} \cos\left(\sum_i \bar{k}_i \Delta_i\right) \right), \quad (4.8.3)$$

i. e. the interference oscillations are damped by an exponential term depending on the wave-length spread  $\delta k$ .

Looking at the contribution of a single direction a phase shift of

$$\Delta_i^c = \sqrt{2}/\delta k_i \quad (4.8.4)$$

causes a reduction of the amplitude of the oscillations by a factor  $1/e$ . Equation (4.8.4) serves as a possible definition for the coherence length  $\Delta_i^c$ . Other definitions differing by some constant factors can be found as well, for example a definition of the coherence length via the Heisenberg uncertainty relation by Rauch and Werner [RW00],

$$\Delta_i^H \delta k_i = 1/2. \quad (4.8.5)$$

In this case the coherence function decays to a value of  $e^{-1/8}$  for a displacement of the wave-packet by  $\Delta_i^H$ .

## 4.8.2 Correlation Function approach

For the sake of completeness I want to mention that the classical approach above is somewhat outdated today since it does not describe effects on the quantum level. Photonic and electronic *anti-bunching* are typical effects which cannot be formulated in this classical framework. The first experiment on bunching effects has been performed by Hanbury-Brown and Twiss [BT57, BT58]. They looked at the intensity correlations of two detectors and found out that photons are more likely to arrive bunched in pairs rather than separately due to their bosonic nature. The coincidence rate of clicks in the detectors is the interesting quantity in such experiments, where only events are taken into account when a particle is found in one detector and  $\tau$  seconds later another one in the other detector. Varying  $\tau$  leads to the so-called second-order correlation function  $G^{(2)}(\vec{r}_1, t; \vec{r}_2, t + \tau)$  as defined by Glauber [Gla63]. This function is different for different types of particles, or more generally for different types of quantum states. For fermions one expects to find a different behaviour as for bosons since the *Pauli exclusion principle* tells that two fermions are not allowed to bunch, but rather to repel each other. For electrons this anti-bunching has been already verified [KRH02] and recently Iannuzzi *et al.* claim to have measured the corresponding effect for neutrons [IOS<sup>+</sup>06]. Photons though being bosons can also be found anti-bunched under special circumstances [KDM77] and it is in particular this phenomenon that can only be described by quantum electrodynamics, whereas the photon bunching can be described classically in terms of the fluctuations of a classical field [Pur56]. It was finally Glauber who presented a quantum theory of coherence [Gla63] which accounts for the quantum effects of light by use

of field operators instead of complex valued intensity functions.

Since the neutron density is usually rather low the neutron beam consists in the mean of just one neutron at a time and the fermionic nature of neutrons in interferometry experiments can safely be neglected for almost all cases. Therefore, the neutron beam can also be thought of a quantum field and its coherence properties described in the quantum optical framework [RW00, RWK<sup>+</sup>96].

I will not go into further detail since the results are equivalent to what we have obtained in Section 4.8.1, since we do not pay attention to particular quantum features of the beam. However, it is important to note the close analogy between neutron and general quantum optics, i. e. between matter and photon waves.

### 4.8.3 Coherence volume in a neutron interferometer

In neutron interferometry the coherence lengths  $\Delta_i^C$  in different directions (Eq. 4.8.4) differ by some orders of magnitude. This property is due to the Bragg reflexion at the perfect crystal monochromator and the crystal structure of the interferometer itself. The beam incident on the first interferometer plate which has same coherence length in  $x$  and  $y$  direction (if the effect of the monochromator is neglected) is depicted in Figure 4.20. The Bragg condition

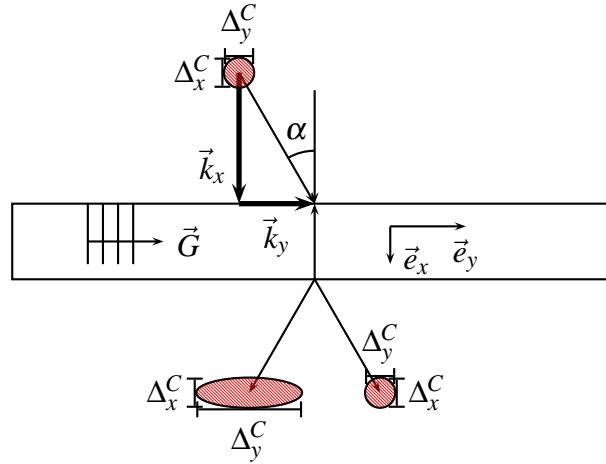


Figure 4.20: Perfect crystal silicon plate of the neutron interferometer.  $\vec{G}$  denotes the reciprocal lattice vector perpendicular to the lattice planes. The incident beam has equal coherence length in all spatial directions (neglecting the monochromator), whereas the reflected beam shows a larger coherence length in the direction  $\vec{G}$ .

$$\vec{k}' - \vec{k} = \vec{G}, \quad (4.8.6)$$

relates the incident beam  $\vec{k}$  to the reflected beam  $\vec{k}'$  via the reciprocal lattice vector  $\vec{G}$  pointing in the  $\vec{e}_y$  direction. The distribution of  $k_y$  is restricted to a narrow interval much smaller than the distribution of  $k_x$  (and  $k_z$ ) where the Laue diffraction does not have any influence and therefore the reflected beam exhibits a larger coherence length  $\Delta_y^C$ .

#### 4.8.4 Three Beam superposition

Let us continue with the double-loop interferometer where three beams are interfering. We can calculate the reduction of the visibility leading to an additional phase shift by adapting Eq. (4.8.1) to the three beam situation:

$$\begin{aligned}
 I &= \left| \langle \psi_{\tilde{H}_-} \rangle + \langle \psi_{\tilde{H}_+ + \tilde{X}_1} \rangle + \langle \psi_{\tilde{H}_+ + \tilde{X}_2} \rangle \right|^2 \\
 &= \langle \psi_{\tilde{H}_-} | \psi_{\tilde{H}_-} \rangle + \langle \psi_{\tilde{H}_+ + \tilde{X}_1} | \psi_{\tilde{H}_+ + \tilde{X}_1} \rangle + \langle \psi_{\tilde{H}_+ + \tilde{X}_2} | \psi_{\tilde{H}_+ + \tilde{X}_2} \rangle \\
 &\quad + 2 \langle \psi_{\tilde{H}_-} | \psi_{\tilde{H}_+ + \tilde{X}_1} \rangle \cos \arg \langle \psi_{\tilde{H}_-} | \psi_{\tilde{H}_+ + \tilde{X}_1} \rangle \\
 &\quad + 2 \langle \psi_{\tilde{H}_-} | \psi_{\tilde{H}_+ + \tilde{X}_2} \rangle \cos \arg \langle \psi_{\tilde{H}_-} | \psi_{\tilde{H}_+ + \tilde{X}_2} \rangle \\
 &\quad + 2 \langle \psi_{\tilde{H}_+ + \tilde{X}_2} | \psi_{\tilde{H}_+ + \tilde{X}_1} \rangle \cos \arg \langle \psi_{\tilde{H}_+ + \tilde{X}_2} | \psi_{\tilde{H}_+ + \tilde{X}_1} \rangle.
 \end{aligned} \tag{4.8.7}$$

The tilde in the subscript denotes the spatial displacements of the wave-packets,  $\tilde{X}_{1,2} = 2\pi X_{1,2}/\bar{\lambda}$  (and similarly for  $\tilde{H}$ ,  $\tilde{\eta}$  and  $\tilde{\chi}$ ) with the mean wavelength  $\bar{\lambda}$ .  $\tilde{H}_{\pm} = \tilde{\eta}^0 \pm \tilde{\eta}/2$  denotes the spatial shift (4.1.25) of the wave-packet imposed by PS1 comprising the constant term plus the variable positive or negative term (Eq. 4.1.28) for the reflected and the transmitted beam, respectively. The choice of the sign corresponds to an anti-clockwise rotation.  $\tilde{X}_{1,2} = \tilde{\chi}_{1,2}^0 + \tilde{\chi}_{1,2}$  are the spatial displacements induced by PS2. Inserting Eq. (4.8.2) into Eq. (4.8.7) we obtain

$$\begin{aligned}
 I_3 &= 3 + 2 \left[ e^{-\frac{(\tilde{\eta} + \tilde{X}_1)^2 (\delta k)^2}{2}} \cos(\eta + X_1) + e^{-\frac{(\tilde{\eta} + \tilde{X}_2)^2 (\delta k)^2}{2}} \cos(\eta + X_2) \right. \\
 &\quad \left. + e^{-\frac{(\tilde{X}_1 - \tilde{X}_2)^2 (\delta k)^2}{2}} \cos(X_1 - X_2) \right].
 \end{aligned} \tag{4.8.8}$$

For the moment we skip the transmission coefficients  $\sqrt{T_1}$  and  $\sqrt{T_2}$  for the beams  $|\psi_{\tilde{H}_+ + \tilde{X}_1}\rangle$  and  $|\psi_{\tilde{H}_+ + \tilde{X}_2}\rangle$  to simplify the notation. Since the phase-shifter is aligned perpendicular to the reflecting net planes (dispersive direction) it is the *longitudinal coherence length* ( $\Delta_x^C$ ) that is of importance in our case. It is typically about 200 Å, much smaller than the *transversal coherence length* ( $\Delta_y^C \approx 10 \mu\text{m}$ ) [RWK<sup>+</sup>96].

The amplitudes of the cosine oscillations are damped exponentially and also to a different degree. The first two terms describing the oscillations between the reference beam and the two beams from the second loop are reduced proportional to the squared thicknesses  $d_1^2$  and  $d_2^2$ , whereas the last term depends on the squared difference  $(d_1 - d_2)^2$  of the thicknesses. The necessity to introduce an additional compensating phase shifter in the beam with the thinner phase shifting slab becomes now more comprehensible.

The quantity of interest is basically the change in the interference pattern when rotating the phase shifter PS2, i. e. for changing  $\tilde{X}_1$  and  $\tilde{X}_2$ . However, these oscillations are damped by the exponential term  $e^{-\frac{(\tilde{X}_2 - \tilde{X}_1)^2 (\delta k)^2}{2}}$ . For large differences in  $\tilde{X}_2$  and  $\tilde{X}_1$  there won't be any oscillations left so we have to insert a compensating phase shift  $\tilde{S}$  behind BS4 as shown in Figure 4.21. This silicon phase shifting slab (COMP) is 5 mm in thickness and is tilted by

#### 4. SPATIAL GEOMETRIC PHASE

an angle between  $30^\circ$  and  $60^\circ$  from the beam forward direction, depending on the various phase shifting plates. Also without the explicit calculation one could already guess from Figure 4.21 that to compensate the phase shift of the thick plate of PS2 one has to place a phase shifter of approximately the same thickness in both other beam paths in order to induce roughly the same displacement of the wave packets in all beams.

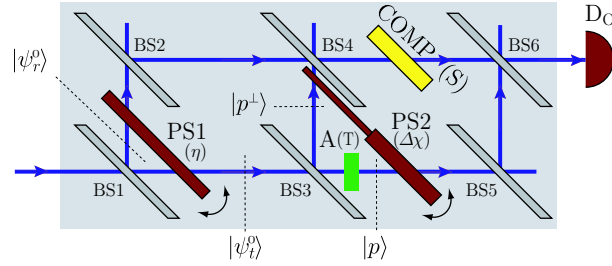


Figure 4.21: Double-loop interferometer setup with an additional silicon phase shifter COMP placed behind BS4 to compensate for the differences in the overall phase shifts exceeding the transversal coherence length.

The intensity pattern in Eq. (4.8.8) is altered accordingly,

$$I_3^S = 3 + 2 \left[ e^{-\frac{(\tilde{\eta} + \tilde{\chi}_1)^2 (\delta k)^2}{2}} \cos(\eta + X_1) + e^{-\frac{(\tilde{\eta} + \tilde{\chi}_2 - \tilde{S})^2 (\delta k)^2}{2}} \cos(\eta + X_2 - S) + e^{-\frac{(\tilde{\chi}_1 - \tilde{\chi}_2 + \tilde{S})^2 (\delta k)^2}{2}} \cos(X_1 - X_2 + S) \right]. \quad (4.8.9)$$

If  $S$  is approximately equal the difference of the constant phase shifts of PS2 ( $S \approx \chi_2^0 - \chi_1^0$ ) we obtain

$$I_3^S \approx 3 + 2 \left[ e^{-\frac{(\tilde{\chi}_1 \delta k)^2}{2}} \cos(\eta - \chi_1) + e^{-\frac{(\tilde{\chi}_2 \delta k)^2}{2}} \cos(\eta + \chi_2 - \chi_1^0) + \cos \Delta \chi \right]. \quad (4.8.10)$$

Here we have omitted the contributions  $\eta$  and  $\chi_{1,2}$  to the exponential terms since these are the terms originating in the rotation of the phase shifters and therefore rather small ( $\eta, \chi_{1,2} \ll \chi_{1,2}^0, \eta^0$ ). This equation demonstrates, that a suitable compensator enables us to reduce the loss of contrast. Only the thinner phase shifter in the  $|p^\perp\rangle$  beam affects now the coherence of the partial beams.

What effects are to be expected for the phase shift between the state in the second loop and the reference beam? For fixed  $\Delta \chi$  Eq. (4.8.10) has the same structure as Eq. (4.6.4) with the identification

$$A_1 = A_2 = e^{-\frac{(\tilde{\chi}_1 \delta k)^2}{2}}. \quad (4.8.11)$$

From Eq. (4.6.7) we notice that there should not be any additional phase changes for ideally adapted compensator. Nevertheless, the experimental results show deviations since the compensator does not work perfectly. Moreover, there are still intrinsic phase differences

across the beam cross section in the two loops, for example due to inhomogeneities in the beam splitting plates, which cannot be compensated for.

### Experimental consequences

Just for a qualitative estimate let us insert some numbers into the equations above. The intensity pattern including again the transmission coefficients  $T_1$  and  $T_2$  and omitting the constant term  $\chi_1^0$  reads finally

$$I_3 = 1 + T_1 + T_2 + 2 \left[ \sqrt{T_1} e^{-\frac{(\tilde{\eta} + \tilde{X}_1)^2 (\delta k)^2}{2}} \cos(\eta - \chi_1) + \sqrt{T_2} e^{-\frac{(\tilde{\eta} + \tilde{X}_2)^2 (\delta k)^2}{2}} \cos(\eta - \chi_2) + \sqrt{T_1 T_2} e^{-\frac{(\tilde{X}_1 - \tilde{X}_2)^2 (\delta k)^2}{2}} \cos \Delta \chi \right] \quad (4.8.12)$$

without compensating phase shifter COMP. With compensator the intensity is given by

$$I_3^S \approx 1 + T_1 + T_2 + 2 \left[ \sqrt{T_1} e^{-\frac{(\tilde{X}_1 \delta k)^2}{2}} \cos(\eta - \chi_1) + \sqrt{T_2} e^{-\frac{(\tilde{X}_2 \delta k)^2}{2}} \cos(\eta - \chi_2) + \sqrt{T_1 T_2} \cos \Delta \chi \right]. \quad (4.8.13)$$

In Figure 4.22 the coherence function  $e^{-\frac{(\tilde{X}(d) \delta k)^2}{2}}$  with  $\tilde{X}(d) = b_{cAl} N_{Al} \frac{\lambda^2}{2\pi} d$  for varying thickness  $d$  is shown. The curve is in good approximation also valid for the silicon phase shifter since the product  $b_{cSi} N_{Si} \approx b_{cAl} N_{Al}$ .

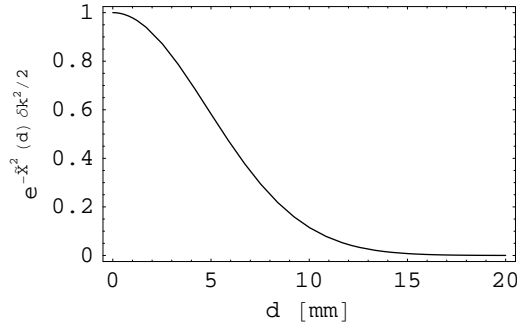


Figure 4.22: The exponential damping factor  $e^{-\frac{(\tilde{X}(d) \delta k)^2}{2}}$  is plotted over the thickness of an aluminium phase shifter.

The amplitude of the cosine oscillations is damped by a factor 1/2 approximately for a slab 5 mm in thickness, where we have assumed that the wavelength spread  $\Delta \lambda / \lambda \approx 1\%$  for  $\lambda = 2.715 \times 10^{-10}$ . So one might argue that there should be still contrast left if we insert one of the phase shifters with thickness  $d_2 = 0.5, 1, 2$  or 4.1 mm. However, we must not neglect the transmission coefficient  $T_2$  which diminishes the contrast in any case. For the experiments with a small transmission coefficient  $T_2 < 1$  and consequently  $\tilde{X}_1 - \tilde{X}_2 > 0$  the compensator has to be utilised in order to obtain the contributions from all the cosine terms.

In the case where PS2 comprises equally thick slabs in both beams there is no need for the compensator. Although the exponential damping of the first two cosine terms in Eq. (4.8.12) is largest for this setup since  $d_1 = d_2 = 4.1$  mm, the transmission coefficients  $T_1 = T_2 \approx 1$ .

## 4.9 Dephasing effects

Apart from the phase drift due to the finite coherence lengths and the consequent spatial displacement of the wave-packets another main contribution comes from dephasing processes. For instance, the surface roughness of the interferometer plates causes a modification of the phase relation between the different beam paths depending on the impinging point. In the particular case of the double-loop interferometer the relative phases between the reference beam and the beams in state  $|p\rangle$  and  $|p^\perp\rangle$  exhibits a position dependence.

Putting this position dependence into the phases of the state  $|\psi_t\rangle$  in the second interferometer loop right after BS3 we get (neglecting normalisation factors)

$$|\psi_t(\vec{x})\rangle = e^{i\alpha_1(x)}|p^\perp\rangle + e^{i\alpha_2(x)}|p\rangle, \quad (4.9.1)$$

where  $\alpha_{1,2}(\vec{x})$  denote the randomly distributed phases across the beam cross-section.  $\vec{x}$  is a vector to a point in the beam cross-section. At the end, the contributions to the intensity from each point have to be added incoherently. Each of these states generates an intensity pattern

$$I_x \propto \left| e^{i\eta} + \sqrt{T_1} e^{i\chi_1} e^{i\alpha_1(\vec{x})} + \sqrt{T_2} e^{i\chi_2} e^{i\alpha_2(\vec{x})} \right|^2$$

according to Eq. (4.2.3).  $\eta$  is independent of  $\vec{x}$  as all relevant information is contained already in the  $\alpha_{1,2}(\vec{x})$ . A remaining global phase factor is immaterial.

The phase shifts  $\chi_1$  and  $\chi_2$  are not taken to be dependent on the position, because these deviations are also already incorporated into the additional phases  $\alpha_1$  and  $\alpha_2$ , respectively. One might argue that this is not admissible since variations in  $\chi_{1,2}$  yield a position dependent evolution of the state that must be reflected in the map  $\tilde{U} : |\psi_t\rangle \mapsto |\psi'_f\rangle$  transporting the state in the second loop, i. e.  $\tilde{U} \mapsto \tilde{U}(\vec{x})$ . However, on a closer look we have defined in Eq. (4.1.28)  $\chi_{1,2}$  to comprise only the terms proportional to the rotation angle  $\xi$  and not the constant offsets  $\chi_{1,2}^0$ . Consequently,  $\tilde{U}$  is also to a good approximation only a function of  $\xi$  and not of  $\vec{x}$ . The change in the spatial phase distribution when rotating the phase shifter PS2 can be neglected with a clear conscience.

The total output intensity has to be understood as an incoherently weighted average of the pure state interference profiles,

$$I = \int p_\alpha(\vec{x}) I_x d^2x.$$

$p_\alpha(\vec{x}) = p_{\alpha_1}(\vec{x}) p_{\alpha_2}(\vec{x})$  is the product of the (independent) distributions of the phase in path

$|p^\perp\rangle$  or  $|p\rangle$ , respectively, with zero mean<sup>3</sup>. According to Equation (4.2.2),

$$I_x = \langle \psi'_{ref} | \psi'_{ref} \rangle + \langle \psi'_f(\vec{x}) | \psi'_f(\vec{x}) \rangle + 2 \underbrace{|\langle \psi'_{ref} | \psi'_f(\vec{x}) \rangle|}_{v_x} \cos(\eta - \underbrace{\arg \langle \psi'_{ref} | \psi'_f(\vec{x}) \rangle}_{\Phi_x}).$$

Averaging over the phase distributions leads to

$$I \propto A + 2 \int d^2x p_\alpha(\vec{x}) v_x \cos(\eta - \Phi_x) = A + 2\bar{v} \cos(\eta - \bar{\Phi}) \quad (4.9.2)$$

with the identifications

$$\bar{v} = \left| \int d^2x p_\alpha(\vec{x}) v_x e^{i\Phi_x} \right|, \quad (4.9.3)$$

$$\bar{\Phi} = \arg \left( \int d^2x p_\alpha(\vec{x}) v_x e^{i\Phi_x} \right) \quad (4.9.4)$$

and where  $A$  denotes the terms independent of  $\alpha_{1,2}$ . Inserting  $v_x e^{i\Phi_x} = \langle \psi'_{ref} | \psi'_f(\vec{x}) \rangle = \langle \psi'_{ref} | \tilde{U} | \psi_t(\vec{x}) \rangle$  we obtain

$$\bar{\Phi} = \arg \int d^2x p_\alpha(\vec{x}) \langle \psi'_{ref} | \tilde{U} | \psi_t(\vec{x}) \rangle \quad (4.9.5)$$

The integration over the phase distribution across the beam cross-section can be executed and yields

$$\begin{aligned} \int d^2x p_\alpha(\vec{x}) |\psi_t(\vec{x})\rangle &= \int d^2x p_\alpha(\vec{x}) \left( e^{i\alpha_1(\vec{x})} |p^\perp\rangle + e^{i\alpha_2(\vec{x})} |p\rangle \right) \\ &= e^{-\Gamma_1} |p^\perp\rangle + e^{-\Gamma_2} |p\rangle, \end{aligned} \quad (4.9.6)$$

if the  $\alpha_{1,2}$  are – for the sake of simplicity – taken to be Gaussian distributed with zero mean and  $\sigma_\alpha^2$  variance, hence  $\Gamma_{1,2} = -\sigma_{\alpha_{1,2}}^2/2$ . By renaming the basis vectors,  $|p_1\rangle \equiv |p^\perp\rangle$  and  $|p_2\rangle \equiv |p\rangle$ , Eq. (4.9.5) can be rewritten as

$$\begin{aligned} \bar{\Phi} &= \arg \langle \psi'_{ref} | \tilde{U} \sum_k e^{-\Gamma_k} |p_k\rangle \rangle = \arg \left[ \left( \sum_l \langle p_l | \right) \tilde{U} \sum_k e^{-\Gamma_k} |p_k\rangle \right] \\ &= \arg \left[ \sum_{l,k} \langle p_l | \tilde{U} e^{-\Gamma_k} |p_k\rangle \right] = \arg \text{Tr} \tilde{U} \left[ \sum_{l,k} e^{-\Gamma_k} |p_k\rangle \langle p_l | \right]. \end{aligned} \quad (4.9.7)$$

Recalling Eq. (4.2.1) for the unitary evolution operator  $\tilde{U} = \sqrt{T_1} e^{i\chi_1} |p_1\rangle \langle p_1| +$

---

<sup>3</sup>Actually, an average phase offset can be put into the definition of the basis states  $|p^\perp\rangle$  and  $|p\rangle$ .

$\sqrt{T_2}e^{i\chi_2}|p_2\rangle\langle p_2|$ , yields

$$\bar{\Phi} = \arg(\sqrt{T_1}e^{i\chi_1}e^{-\Gamma_1} + \sqrt{T_2}e^{i\chi_2}e^{-\Gamma_2}). \quad (4.9.8)$$

The phase distribution has the same effects as the spatial displacement discussed above. Both produce an exponential term to the individual beam contributions. The significant difference between the discussion on the spatial displacement above and the present discussion is the use of either of a coherent superposition (pure state) for the former, or an incoherent superposition (mixed state) for the latter. The visibility vanishes in any case, but the spatial displacement does not derogate the pure state nature. That the partial waves of the beams are still perfectly coherent is demonstrated by looking at the still existent interference fringes in the momentum spectrum - “[...] interference in phase space has to be considered rather than the simple wavefunction overlap criterion [...]” [RW00, p. 141]. In contrast, dephasing reduces the visibility more generally and it is not feasible to compensate this effect. In our stationary experiment, however, we cannot distinguish between these fundamentally different effects, since just neutrons with the same wavelength interfere, cross correlations between different partial waves of a pure state get washed out when averaging over the measurement time [Gab56]. Therefore, two quite distinct causes give rise to the same observed effect, a shift in the measured phase, hence, both are subsumed into the single fit coefficient  $C$  for the fits shown in Figures 4.11, 4.13, 4.15 and 4.17.

**Mixed state geometric phase** Can this additional phase shift be associated with the Sjöqvist’s mixed state geometric phase

$$\phi_\rho = \arg \text{Tr}[U\rho_0] = \arg \sum_k p_k \langle \psi_k | U | \psi_k \rangle, \quad \text{for } \rho_0 = \sum_k p_k \langle \psi_k | | \psi_k \rangle \quad (4.9.9)$$

as defined in [SPE<sup>+</sup>00]?

At least there is a similarity, but certainly not an equivalence. This similarity can be observed by comparing Eq. (4.9.9) with (4.9.7) which are structurally equal. The term  $\sum_{l,k} e^{-\Gamma_k} |p_k\rangle\langle p_l|$  in the latter can even be thought of a (not normalised) density matrix since it is positive and Hermitian, however, the physical meaning remains unclear. The decisive difference to the mixed state geometric phase is the final comparison with the reference state  $|\psi'_{ref}\rangle$  rather than a proper copy of the initial state. Sjöqvist *et al.* defined the mixed state geometric phase by assuming an interferometer with a mixed input state and an evolution of the internal degrees of freedom, whereas here the mixedness stems from the path degrees of freedom. In the former the Hilbert space of the system comprises a spatial as well as a spin part  $\mathcal{H} = \mathcal{H}_{spatial} \otimes \mathcal{H}_{spin}$ , but in the latter the spin part plays no role at all. It is only the dimension of  $\mathcal{H}_{spatial}$  that is enlarged to  $\dim \mathcal{H}_{spatial} = 3$  due to the double-loop geometry in contrast to the tensor product structure of the former with  $\dim \mathcal{H} = 2 \times 2 = 4$ . It is therefore not surprising that the comparison fails and that we find only a formal equivalence.

## 4.10 Conclusions

In summary, we have shown that one can ascribe a geometric phase not only to spin evolutions of neutrons, but also to evolutions in the path degrees of freedom of neutrons in an interferometric setup. This equivalence is evident from the description of both cases via state vectors in a two dimensional Hilbert space. However, there have been arguments contra the experimental verification in [HZR96] which we believe can be settled in favour of a geometric phase appearing in the setup described above. The twofold calculations of the geometric either in terms of a shift in the interference fringes or via surface integrals in an abstract state space allows for a geometric interpretation of the obtained phase shift.

The main difficulty that came up during the experiment was the loss of contrast when using differently thick phase shifting plates for PS2. The rather small coherence length impeded the measurement of the relative phase differences. The different spatial displacements of the different beams together with the attenuator in one beam suppressed the interference oscillations and asked for a further compensating phase shifter. Furthermore, due to the same reasons we have found out that the precise parallel alignment of the phase shifter PS2 in the second loop is important in order to keep dynamical phase contributions minimal. It is only for the exact parallel position that the demanded relation  $d_1/d_2 = T_2/T_1$  is satisfied and deviations will lead to a dynamical phase. Mainly the setups with  $d_1 = 1$  mm and 2 mm suffer from this requirement.

This systematic deviations have been taken into account in the data fits leading to a good agreement of the measured phase with the theoretical prediction for the spatial geometric phase. The flattening of the curve fitted to the measured data compared to the theoretical predictions is on the one hand side the result of the spatial displacement of the poly-chromatic incident wave which cannot be compensated perfectly. On the other hand side there are also contributions from dephasing due to a non-uniform phase distribution across the area on the beam-splitting plates illuminated by the neutron beam.

Apart from the unpleasant discrepancies between theoretical and experimental results the flattened curve might also be useful in future since it forms a stable “platform”: Around the points  $\Delta\chi = \pi/4$  and  $3\pi/4$  a change of the rotation angle  $\xi$  does not have much effect on the phase difference and as we have seen the form of this platform can easily be changed by willingly modifying the visibility, for instance by adding phase shifters to spatially displace the wave-packet.

## Chapter 5

# Geometric phase and adiabatic fluctuations

What happens to the geometric phase, if the evolution of the state gets perturbed by some outer influences? This question has already been addressed in Chapter 2. There, two approaches to define a mixed state geometric phase have been introduced that are valid for unitary as well as non-unitary evolutions. With different kinds of parallel transport laws a geometric phase or, generally speaking, matrix-valued holonomy invariants have been defined that are properties of the path of the density matrices in their respective state spaces only.

In the following, we will turn our attention towards more realistic systems to study the influence of external influences on the geometric phase. This is motivated in that in all realistic situations the system under investigation is – however weak – coupled to the environment. This approach is distinct from the former, more “holistic in nature” [KCS04], in that it uses pure state geometric phases and employ either a quantum trajectory analysis [CFGSV03, NSM02] or solve a Master equation [GW88, GF89, KCS04] to get insight into the behaviour of the geometric phase influenced by some perturbations.

The big “hype” about the geometric phase for open systems has been ignited by investigations in geometric phase gates as basic blocks for the future (or futuristic) quantum computer [NC00]. The main aim of investigations in both decoherence and geometric phases at present seems to be their amalgamation to form robust quantum gates. Zanardi and Rasetti suggested that the Wilczek-Zee non-abelian holonomies [WZ84] could be of potential use to implement *holonomic quantum computation* [ZR99]. A conditional Berry (adiabatic) phase gate has been issue of an NMR-experiment conducted by Jones *et al.* [JVEC00] and Duan *et al.* [DCZ01] proposed a scheme for the implementation of a set of universal geometric quantum gates for the manipulation of trapped ions. Falci *et al.* [FFP<sup>+</sup>00] suggested a method to use a superconducting nanocircuit to design gates for quantum computation, and Ekert *et al.* [EEH<sup>+</sup>00] showed how to implement a conditional geometric phase between two spins.

Intuitively, the geometric phase might be a good candidate for the implementation of quantum gates resilient against environmental influences, since it is not dependent on dy-

---

namical quantities, but is based purely on geometry. This for itself clearly does not ensure its pertinence, but for particular quantum operations and particular noise sources this feature could be of interest. In the recent past numerous analytical and numerical studies have been conducted with predictions sometimes promising, sometimes not.

To name a few, Carollo *et al.* [CFGSV03] conclude that the geometric phase for a spin-1/2 particle is stable under dephasing, i. e. when the phase of the spin states makes some jumps during an otherwise smooth evolution, but not for general decoherence processes. The same authors investigated also the influence of a quantum instead of a classical field [CFGSV04] reasoning that in the adiabatic case the geometric phase is more stable than in a non-adiabatic setup. Zhu and Zanardi [ZZ05] compared dynamical and geometric quantum gates and found out that geometric gates are more robust. On the other hand side, similar quantum gates have been investigated by Nazir *et al.* [NSM02] numerically. They, in contrast, conclude that using an (adiabatic) geometric quantum gate instead of a dynamical one does not bring any advantages since in order to ensure adiabaticity the operation time of the former is much longer and noise has more time to take effect. Also Blais and Tremblay [BT03] pointed out that the cyclic, but non-adiabatic geometric phase is not more robust than a purely dynamical quantum gate for noise in the control parameters. However, both of the latter do not strictly separate dynamical from geometric phase contributions to decoherence and their conclusions are only valid if one is not able to compensate the dynamical phase along with its variations due to the noise. Sarandy and Lidar [SL06], in contrast, derived that the adiabatic geometric is stable both for dephasing and spontaneous emission processes and noted that there is a distinct time-scale for which the geometric phase remains stable.

Eventually, De Chiara and Palma [CP03] calculated the adiabatic geometric phase along with its variance of a spin-1/2 particle subjected to fluctuating magnetic fields for weak noise fluctuations (first-order approximation). Such a situation is ideally suited for an experimental demonstration of the robustness of Berry's (adiabatic) phase with neutrons and we will discuss this example in more detail. Although it is not decoherence in the strict sense in that the quantum system couples to a classical magnetic field and not to a quantum environment (modelled preferably as a bath of quantum harmonic oscillators), it is of particular interest for practical implementations using neutrons and magnetic fields. They conclude with the promising result that for long evolution times the fluctuations in the magnetic field (the environment) do not show up as fluctuation of the geometric phase, under the restriction that everything is sufficiently adiabatic. Whitney *et al.* [WMSG05] extend these results by considering higher-order terms giving rise to a shift of the geometric phase. This behaviour also appears in numerical simulations on the basis of the De Chiara-Palma setup as will be pointed out below.

In summary, the geometric phase seems to be robust for certain configurations, preferably for adiabatic evolutions. However, up to now there is no experimental evidence. To find a remedy I present in the following considerations to a possible experimental setup that can be used to test the predictions in [CP03]. First, the theory behind is set forth and specific calculations on the spin-evolution of neutrons are presented. Second, numerical simulations

are shown giving a hint of the feasibility of such an experiment. The planned experiment is finally discussed in Appendix D.

## 5.1 Spin-1/2 in a fluctuating magnetic field

A spin-1/2 particle, say, a neutron is subjected to a stochastically fluctuating magnetic field. The changes in the magnetic field are slow so that one can use the adiabatic approximation. If the particle is in an eigenstate of the Hamiltonian initially it will stay in an instantaneous eigenstate for all times - the transition probability to another state is sufficiently close to zero. It has been calculated that the geometric phase is more stable than its dynamical counterpart since its variance tends to zero proportional to the inverse evolution time while the variance of the latter increases linearly in time. However, it has to be mentioned that the assumption of adiabaticity all along the evolution also comprises the noise fluctuations. The calculations are not valid for arbitrary non-adiabatic noise, but just for noise with a small bandwidth compared to the Zeeman splitting of the energy levels in the magnetic field.

Let us assume, the spin-1/2 particle is initially polarised along the direction of a magnetic field  $\vec{B}(0) = (0, 0, B_3)^T$  pointing in  $z$ -direction. The magnetic field changes adiabatically so that the spin of the particle stays latched to  $B$  over the total evolution time and obtains a phase relative to the initial state. This phase can be measured by means of interference of the initial and the final state. The geometric part of this phase is not dependent on the strength of the magnetic field, but only on the path in parameter space. So far nothing new. Let us assume an additional noisy component of the magnetic field,  $\vec{B}(t) = \vec{B}_0(t) + \vec{K}(t)$ .  $\vec{K}(t)$  fluctuates around zero leading to instantaneous modifications of the magnetic field direction and - recalling that we only allow adiabatic changes - the polarisation vector as well. In the following we will assume that the deviations from zero mean are Gaussian distributed.

This noise field clearly contributes to the phase observed, but the geometric and dynamical part are affected differently: While the variance of the dynamical part grows linearly with the time spent in the magnetic field, the variance of the geometric part vanishes. The experimental problem is to separate the two parts. For the ideal situation without noise contributions there are several methods available, for example spin-echo or choosing a particular Hamiltonian such that the dynamical phase vanishes. But for the noisy case neither of these approaches work out since the Hamiltonian can neither be chosen such that the dynamical phase vanishes nor does a spin-echo approach guarantee the cancellation of all dynamical terms in the Hamiltonian if the noise is not same for both the first evolution and its “echo”.

For a *proof-of-principle* experiment we can nevertheless resort to the spin-echo principle, if *artificial* noise fluctuations are generated, recorded and applied to the echo as well, so that we have the really exactly the same evolution twice. The dynamical phase and its contributions to decoherence should vanish and the remaining dephasing is only due to the geometric phase.

### 5.1.1 Theoretical considerations

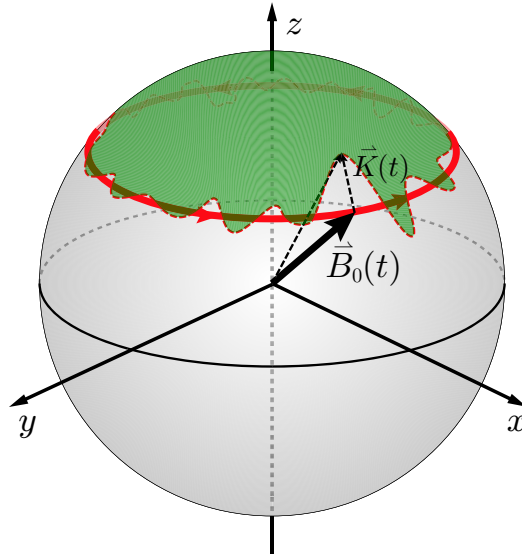


Figure 5.1: Magnetic field vector tracing out a path in parameter space. In the adiabatic domain the polarisation vector of the neutron stays latched to the magnetic field direction throughout the whole evolution.

The Hamiltonian of the magnetic field is given by

$$H(t) = -\vec{\mu} \cdot \vec{B}(t), \quad (5.1.1)$$

where  $\vec{B}(t) = B(t)\vec{n}(t)$  with magnitude  $B(t) \equiv |\vec{B}(t)|$  and the unit vector is parametrised by  $\vec{n}(t) = (\sin \vartheta(t) \cos \varphi(t), \sin \vartheta(t) \sin \varphi(t), \cos \vartheta(t))^T$ .  $\vec{\mu} = \mu_n \vec{\sigma}$  is as usual the magnetic moment  $\mu_n$  times the vector of Pauli matrices (see also Section 1.2.1). If  $\vec{B}(t)$  is varied adiabatically the spin state follows the instantaneous energy eigenstates of the magnetic field pointing in direction  $\vec{n}(t)$ .

To fulfil the adiabaticity condition (c. f. Appendix C) the Zeeman energy splitting of the neutron in the magnetic field which determines the *Larmor frequency*  $\omega_L = 2\mu|B|/\hbar$  has to be much larger than the typical rate of change of  $\vec{B}(t)$ . The instantaneous eigenvectors are given by

$$\begin{aligned} |\uparrow_n(t)\rangle &= \cos \frac{\vartheta(t)}{2} |\uparrow\rangle + e^{i\varphi(t)} \sin \frac{\vartheta(t)}{2} |\downarrow\rangle \\ |\downarrow_n(t)\rangle &= \sin \frac{\vartheta(t)}{2} |\uparrow\rangle - e^{i\varphi(t)} \cos \frac{\vartheta(t)}{2} |\downarrow\rangle. \end{aligned} \quad (5.1.2)$$

Note, that the choice of the phases is different compared to the studies in [CP03]. There, the eigenstates are multiplied by a factor  $e^{-i\varphi(t)/2}$  with the decisive disadvantage that this choice of eigenvectors is not single-valued and therefore not particularly suited for a discussion of Berry's phase. Changing the azimuthal angle of the magnetic field  $\varphi_0$  by  $2\pi$ , the eigenstates

should be equal, whereas the eigenstates chosen in [CP03] change sign. As Berry noted [Ber84], “any choice of phases can be made, provided that  $|\uparrow_n(t)\rangle$  is *single valued* in a parameter domain that includes the circuit C.”

As discussed in Section 1.2 for a cyclic time evolution  $(\vec{B}(T) = \vec{B}(0))$  the state after the evolution can be written as

$$|\uparrow_n(T)\rangle = e^{i\phi_d} e^{i\phi_g} |\uparrow_n(0)\rangle \quad (5.1.3)$$

with the dynamical part  $\phi_d = \frac{\mu}{\hbar} \int_0^T B(t) dt$ . The Berry phase can be expressed in terms of the *Berry connection*  $\phi_g = \oint \vec{A}^\uparrow d\vec{\lambda}$  with  $\vec{A}^\uparrow = i\langle \uparrow_n | \nabla_\lambda | \uparrow_n \rangle$ .  $\vec{\lambda} = \vec{\lambda}(t) = (\vartheta(t), \varphi(t))$  is the set of control parameters. The components of  $\vec{A}^\uparrow$  are easily calculated,

$$A_\varphi^\uparrow = i\langle \uparrow_n | \partial / \partial \varphi | \uparrow_n \rangle = -\frac{1}{2}(1 - \cos \vartheta(t)) \quad (5.1.4)$$

$$A_\varphi^\downarrow = i\langle \downarrow_n | \partial / \partial \varphi | \downarrow_n \rangle = -\frac{1}{2}(1 + \cos \vartheta(t)) \quad (5.1.5)$$

$$A_\vartheta^\uparrow = -A_\vartheta^\downarrow = i\langle \uparrow_n | \partial / \partial \vartheta | \uparrow_n \rangle = 0. \quad (5.1.6)$$

Consequently, Berry’s phase  $\phi_g$  without noise contributions is given by

$$\phi_g^\uparrow = \int_0^{2\pi} A_\varphi^\uparrow d\varphi = -\pi(1 - \cos \vartheta_0) = -\phi_g^\downarrow \quad (5.1.7)$$

for constant  $\vartheta(t) = \vartheta_0$  and varying azimuthal angle  $\varphi(t) \in [0, 2\pi]$  (c. f. Figure 5.1).  $\phi_g^\uparrow$  indicates the geometric phase accumulated by the spin-up state and  $\phi_g^\downarrow$  for the spin-down state. It is only dependent on the path traced out by the state in state space or, equivalently, by the magnetic field vector in parameter space in the adiabatic case.

Now we turn our attention to a fluctuating magnetic field  $\vec{B}(t) = \vec{B}_0(t) + \vec{K}(t)$  (dashed line in Figure 5.1) with Hamiltonian

$$H(t) = -\mu_n \vec{B} \cdot \vec{\sigma} = -\mu_n [\vec{B}_0(t) + \vec{K}(t)] \cdot \vec{\sigma}. \quad (5.1.8)$$

The components of the fluctuating field  $\vec{K}$  are random processes (c. f. Appendix A) with zero average and small amplitude. To assure adiabaticity throughout the operation time also the fluctuations must not violate the adiabaticity assumption in the same way as the rate of change of  $B_0(t)$  itself. Both the connection  $\vec{A}$  and the path are changed. Let  $\vartheta_0, \varphi_0$  be the spherical coordinates denoting the direction of the unperturbed field  $\vec{B}_0$  and  $\vartheta$  and  $\varphi$  stand for the directions of the perturbed magnetic field  $\vec{B}$ . A series expansion of the gauge potential  $\vec{A}$  about the polar angle  $\vartheta_0$  yields

$$A_\varphi^\uparrow(\vartheta) \simeq A_\varphi^\uparrow(\vartheta_0) + \frac{\partial A_\varphi^\uparrow}{\partial \vartheta} \delta \vartheta \Big|_{\vartheta_0} = \frac{1}{2} ((\cos \vartheta_0 - 1) - \sin \vartheta_0 \delta \vartheta). \quad (5.1.9)$$

For the corrections to the path we note that there is no component  $A_\vartheta$ , thus we can restrict

our attention to the  $\varphi$  component of the line element  $d\vec{\lambda}$ :

$$d\lambda_\varphi = \dot{\varphi} dt = \frac{d\varphi(t)}{dt} dt = \frac{d(\varphi_0 + \delta\varphi)}{dt} dt = (\dot{\varphi}_0 + \delta\dot{\varphi}) dt. \quad (5.1.10)$$

Here  $\dot{\varphi}_0 = 2\pi/T \equiv \omega_r$  is the angular velocity of the unperturbed field  $\vec{B}_0$ , while  $\delta\dot{\varphi}$  is the first order correction due to  $\vec{K}$ . The noise-influenced Berry phase  $\tilde{\phi}_g$  (omitting in the following the subscript  $\uparrow$  to simplify the notation) can now be expressed as

$$\begin{aligned} \tilde{\phi}_g &= \int_0^T [A_\varphi(\vartheta_0) + \delta A_\varphi] (\dot{\varphi}_0 + \delta\dot{\varphi}) dt \\ &\simeq \phi_g + \frac{2\pi}{T} \int_0^T \delta A_\varphi dt + A_\varphi(\vartheta_0) \int_0^T \delta\dot{\varphi} dt \\ &= \phi_g - \frac{\pi}{T} \int_0^T \sin \vartheta_0 \delta\vartheta dt + A_\varphi(\vartheta_0) \delta\varphi(T) \end{aligned} \quad (5.1.11)$$

with  $\phi_g$  denoting the mean geometric phase (Eq. 5.1.7). We have assumed that there is no initial deviation,  $\delta\varphi(0) = 0$ , and we have neglected the second-order contributions from  $\delta A_\varphi \delta\dot{\varphi}$ . The last term  $A_\varphi(\vartheta_0) \delta\varphi(T)$  vanishes for a magnetic field returning exactly to its initial position. In general this is not the case and one has to use the definition of Samuel and Bhandari [SB88] of the non-cyclic geometric phase. However, it is not difficult to verify that this contribution is of second-order in  $\delta\varphi(T)$ <sup>1</sup> and we neglect this term as well. Finally, we obtain

$$\tilde{\phi}_g = \phi_g - \frac{\pi}{T} \int_0^T \sin \vartheta_0 \delta\vartheta dt. \quad (5.1.12)$$

A Taylor series expansion yields

$$\cos(\vartheta_0 + \delta\vartheta) \simeq \cos \vartheta_0 - \sin \vartheta_0 \delta\vartheta = \frac{B_{0,3}}{B_0} + \frac{K_3}{B_0} - \frac{B_{0,3}}{B_0^3} \vec{B}_0 \cdot \vec{K}, \quad (5.1.13)$$

where the last part follows from expanding

$$\frac{B_3}{B} = \frac{B_{0,3} + K_3}{|\vec{B}_0 + \vec{K}|} = \frac{B_{0,3} + K_3}{\sqrt{B_0^2 + K^2 - 2\vec{B}_0 \cdot \vec{K}}}$$

for small  $\vec{K}$ .  $B_3$ ,  $B_{0,3}$  and  $K_3$  denote the  $z$ -components of the respective field components. Therefore,

$$-\sin \vartheta_0 \delta\vartheta = \frac{K_3}{B_0} - \frac{B_{0,3}}{B_0^3} \vec{B}_0 \cdot \vec{K}.$$

---

<sup>1</sup>The enclosed surface area determines the geometric phase. If the path does not return to its initial point but rather ends within an  $\varepsilon$ -vicinity off this point the error in the geometric phase is of the order of the area of the disk with radius  $\varepsilon$ , i. e. the error in the geometric phase is of second-order in  $\delta\varphi(T)$ .

Inserting Eq. (5.1.13) into (5.1.12) we find

$$\tilde{\phi}_g = \phi_g + \frac{\pi}{T} \int_0^T \left[ \frac{K_3}{B_0} - \frac{B_{0,3}}{B_0^3} \vec{B}_0 \cdot \vec{K} \right] dt \quad (5.1.14)$$

and we can calculate the probability distribution of  $\phi_g$  once that for  $K_i$  is known. Higher order terms are neglected here although these become important for stronger noise. They induce a change of the mean geometric phase as shown in Section 5.6.3.

Assuming, that the components  $K_i(t)$  are the trajectories of an Ornstein-Uhlenbeck process (Gaussian, stationary and Markovian - c. f. Appendix A), the distribution of  $\tilde{\phi}_g$  is found out to be Gaussian with mean value  $\phi_g$ . Its variance  $\sigma_{\phi_g}^2$  is given by

$$\begin{aligned} \sigma_{\phi_g}^2 = & 2P_{12}^2 \left( \frac{\pi \cos \vartheta_0 \sin \vartheta_0}{T \omega_L} \right)^2 \left[ \frac{(e^{-\Gamma_{12}T} - 1)(\Gamma_{12}^2 - \omega_r^2)}{(\Gamma_{12}^2 + \omega_r^2)^2} + \frac{\Gamma_{12}T}{\Gamma_{12}^2 + \omega_r^2} \right] \\ & + 2P_3^2 \left( \frac{\pi \sin^2 \vartheta_0}{T \omega_L} \right)^2 \left[ \frac{\Gamma_3 T - 1 + e^{-\Gamma_3 T}}{\Gamma_3^2} \right], \end{aligned} \quad (5.1.15)$$

which can be derived by use of (A.4.3) for the  $z$ -component and by combining (A.4.6) and (A.4.7) for the  $x$  and  $y$ -component.

$\Gamma_{12}$  denote the bandwidths of the Lorentzian noise spectrum ( $\Gamma = 1/\tau$  is the inverse of the relaxation time) in  $x$ - and  $y$ -direction and  $\Gamma_3$  the bandwidth of the noise in  $z$ -direction. In order to compare the different energy and time scales involved, all magnetic fields will be given by their according Larmor frequency. That is,  $\omega_L = 2\mu_n B_0/\hbar$  denotes the rotating magnetic guide-field, and  $P_{12}^2$  ( $P_3^2$ ) is the mean power of the noise process  $K_{12}$  ( $K_3$ ) in radians per second (Eq. A.1.10). In the following we will often use the signal-to-noise ratio which we define as

$$s_r \equiv \left| \frac{\omega_L}{P_3} \right|, \quad (5.1.16)$$

the ratio between the strength of the guide field  $B_0$  and the mean power of the stochastic process.

For large enough  $T$  ( $T \gg 1/\Gamma$ ) we can approximate the variance of  $\phi_g$  by

$$\sigma_{\phi_g}^2 = 2P_{12}^2 \left( \frac{\pi \cos \vartheta_0 \sin \vartheta_0}{\omega_L} \right)^2 \frac{1}{\Gamma_{12}T} + 2P_3^2 \left( \frac{\pi \sin^2 \vartheta_0}{\omega_L} \right)^2 \frac{1}{\Gamma_3 T} \quad (5.1.17)$$

and recognise that it tends to zero for  $(\Gamma T)^{-1} \rightarrow 0$ . A typical plot of the variance  $\sigma_{\phi_g}^2$  is shown in Figure 5.2.

The geometric phase does not contribute to dephasing if the evolution time  $T$  is long enough which leads to the rather paradoxical situation that the (geometric) phase difference between final and initial state is more and more exact the longer the spin-1/2 particle is exposed to the noise. Also, we can observe from Figure 5.2 that the contribution of the geometric phase to the dephasing is in general rather small. For a perturbation strength one order of magnitude smaller than the guide-field strength the variance is in the order of 0.1

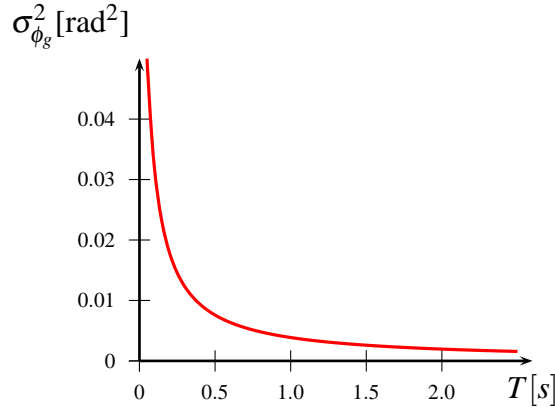


Figure 5.2: Typical plot of the variance  $\sigma_{\phi_g}^2$  for a magnetic guide-field with Larmor frequency  $\omega_L = 10^4$  rad/s ( $\approx 0.5$  Gauss) and an average noise power of  $P_3 = 10^3$  rad/s corresponding to a signal-to-noise ratio of  $s_r = 10$ . The noise bandwidth is  $\Gamma = 50$  rad/s and the field rotates in the equatorial plane ( $\vartheta_0 = \pi/2$ ).

radians yielding a relative error of  $\approx 0.1/2\pi = 1\%$ .

### 5.1.2 Region of applicability of the first-order approximation

It is important to know for what parameter ranges the curve plotted in Figure 5.2 is valid. What fluctuations are allowed such that the adiabaticity assumption is not violated? If the adiabatic condition is not fulfilled the spin state will not follow the direction of the magnetic field and the results derived above have to be modified. On the other hand side, for a strong noise coupling the first-order approximation and consequently the conclusion that the mean geometric phase is not affected by the noise are clearly invalid as will be exemplified in the numerical simulations later on.

**Time scales** There are different time scales involved in this problem,  $\tau_L = \frac{2\pi}{\omega_L}$  is associated to the (mean) Larmor frequency ( $\omega_L = 2\mu_n B_0/\hbar$ ) of the magnetic guide-field,  $\tau_r = \frac{2\pi}{\omega_r}$  is the time needed for the execution of one cycle, and  $\tau_n = 1/\Gamma$  is the relaxation time of the noise associated to the bandwidth of the involved noise frequencies. We definitively demand that

$$\tau_r, \tau_n \gg \tau_L \quad (5.1.18)$$

to ensure adiabaticity. Furthermore, the fluctuating field should have time enough to make many uncorrelated oscillations during the cyclic evolution ( $\tau_n \ll \tau_r$ ) so that we end up with

$$\tau_L \ll \tau_n \ll \tau_r, \quad (5.1.19)$$

or (with  $\omega_n = 2\pi\Gamma$ ),

$$\omega_L \gg \omega_n \gg \omega_r \quad (5.1.20)$$

in terms of the angular frequencies.

**Low-frequency behaviour** For the sake of completeness we can state the behaviour for low frequency noise ( $\tau_r \ll \tau_n$ ) where the noise fluctuations do not oscillate during the evolution. In each run of the experiment the noise is approximately constant and varies only for the different runs. In this case Eq. (5.1.15) is

$$\sigma_{\phi_g}^2 = 4P_{12}^2 \left( \frac{\pi \cos \vartheta_0 \sin \vartheta_0}{\omega_L} \right)^2 \frac{\Gamma_{12} T}{(2\pi)^2} + 2P_3^2 \left( \frac{\pi \sin^2 \vartheta_0}{\omega_L} \right)^2 \left[ \frac{1}{2} - \frac{\Gamma_3 T}{6} \right]. \quad (5.1.21)$$

to first order in  $\Gamma T$ . The leading term is  $P_3^2 (\pi \sin^2 \vartheta_0 / B)^2$  is independent of  $\omega_n$  and  $\omega_r$  and the variance over  $T$  is approximately constant in this range (Figure 5.3) but tends to zero for small fluctuations (small  $\vartheta_0$ ).

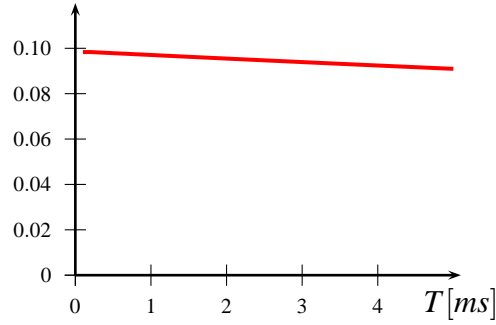


Figure 5.3: For much shorter evolution times as in Figure 5.2, but same parameters in all other respects ( $P_3 = 10^3$  rad/s,  $\omega_L = 10^4$  rad/s,  $\omega_n = 50$  rad/s,  $\vartheta_0 = \pi/2$ ) the variance  $\sigma_{\phi_g}^2$  is approximately constant.

**How much less than the Larmor frequency?** What is left to clarify is the meaning of the statement ‘much less than the Larmor frequency’ (‘ $\ll$ ’). As a rule of thumb there should be approximately one order of magnitude difference. In Figures 5.4 (a)-(d) the polar angle  $\vartheta_B$  of the magnetic field  $\vec{B}$  is plotted along with the angle  $\theta_\psi$  of the instantaneous state of the spin-1/2 particle parametrised by  $|\psi(t)\rangle = \cos(\theta_\psi/2)|\uparrow\rangle + e^{i\phi} \sin(\theta_\psi/2)|\downarrow\rangle$ . The signal-to-noise ratio is fixed ( $s_r = 1.5 \times 10^3$ ) and the noise is in  $z$ -direction ( $\Gamma_{1,2} = 0$ ). The noise frequency bandwidth is varied from  $\omega_n = 10^2$  rad/s (a) to  $\omega_n = 10^4$  rad/s (d). We notice that the state does not follow the magnetic field anymore for higher frequencies. The wiggles in  $\theta_\psi$  are due to the Larmor frequency of the guide field with approximately  $10^4 / (2\pi) \approx 1.6$  kHz. For stronger noise ( $s_r \approx 4.5 \times 10^2$ ) the deviations are even more striking (c. f. Figure 5.5).

### 5.1.3 Dynamical Contribution

As shown above, the fluctuations do not influence the geometric phase in the long run, but there is still the dynamical phase left which contributes significantly to the variance of the

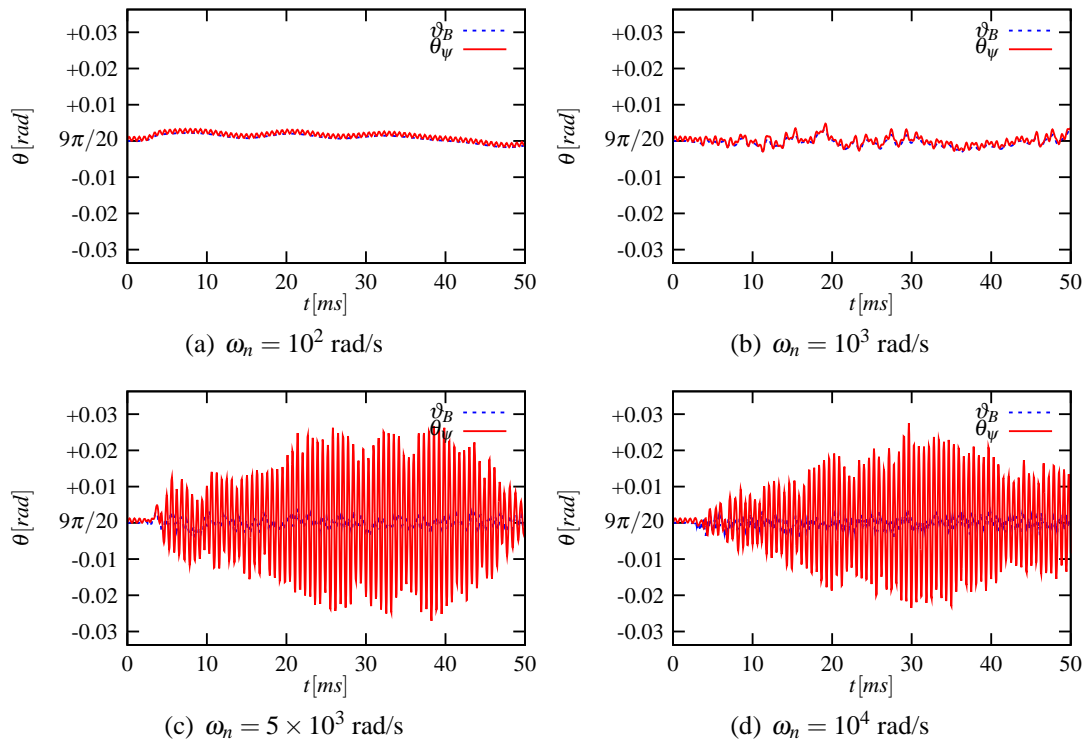


Figure 5.4: The polar angle of the magnetic field  $\vartheta_B$  is plotted along with the polar angle of the state  $\theta_\psi$ . For higher noise frequencies the state does not follow the field adiabatically anymore.

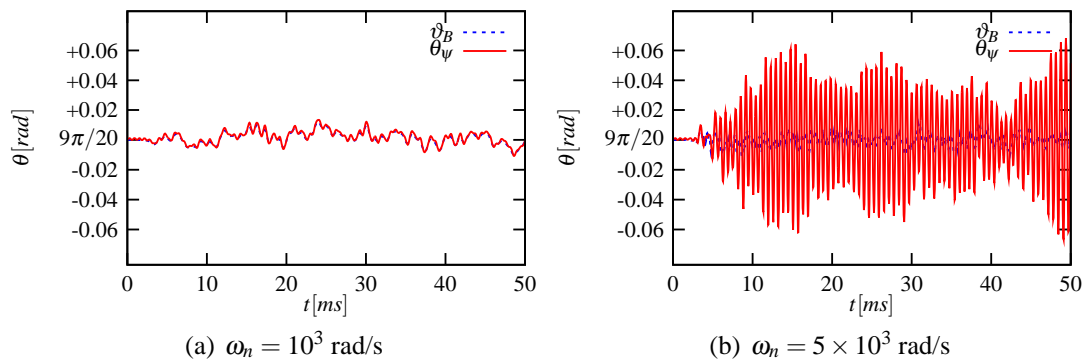


Figure 5.5: The polar angle of the magnetic field  $\vartheta_B$  is plotted along with the polar angle of the state  $\theta_\psi$ . For stronger noise the deviations from the adiabatic behaviour can clearly be seen above frequencies of 1/10 of the Larmor frequency of the guide field.

relative phase difference between final and initial state.

The dynamical phase difference is given by the integral over the magnetic field strength

$$\tilde{\phi}_d = i\frac{\mu}{\hbar} \int_0^T B(t) dt = i\frac{\mu}{\hbar} \int_0^T |\vec{B}_0(t) + \vec{K}(t)| dt \approx \phi_d + i\frac{\mu}{\hbar} \int_0^T \frac{\vec{B}_0(t) \cdot \vec{K}(t)}{B_0} dt, \quad (5.1.22)$$

where we have neglected contributions proportional to  $K/B_0$  and used the fact that the system is in an eigenstate of the Hamiltonian at all times, i. e.

$$\int \langle \psi(t) | \vec{\mu} \cdot \vec{B}(t) | \psi(t) \rangle dt = \mu \int B(t) \underbrace{\langle \psi(t) | \vec{\sigma} \cdot \vec{n} | \psi(t) \rangle}_1 dt.$$

From Eq. (A.4.3) the integral (5.1.22) can be calculated to find the variance of  $\tilde{\phi}_d$ ,

$$\begin{aligned} \sigma_{\phi_d}^2 &= 2P_{12}^2 \left( \frac{\mu \sin \vartheta_0}{\omega_L} \right)^2 \left[ \frac{(e^{-\Gamma_{12}T} - 1)(\Gamma_{12}^2 - \omega_r^2)}{(\Gamma_{12}^2 + \omega_r^2)^2} + \frac{\Gamma_{12}T}{\Gamma_{12}^2 + \omega_r^2} \right] \\ &\quad + 2P_3^2 \left( \frac{\mu \cos \vartheta_0}{\omega_L} \right)^2 \left[ \frac{\Gamma_3 T - 1 + e^{-\Gamma_3 T}}{\Gamma_3^2} \right], \end{aligned} \quad (5.1.23)$$

which is similar to  $\sigma_{\phi_g}^2$  with the decisive difference that it grows linearly in  $T$  for large  $T$ . In passing we note that the variance  $\sigma_\alpha^2$  of the total phase  $\alpha = \phi_d + \phi_g$  is not the sum of the variances  $\sigma_{\phi_d}^2 + \sigma_{\phi_g}^2$  since these are not independent random variables, but is given by

$$\begin{aligned} \sigma_\alpha^2 &= 2\frac{P_{12}^2}{\omega_L^2} \left( \frac{\pi \cos \vartheta_0 \sin \vartheta_0}{T} + \omega_L \sin \vartheta_0 \right)^2 \left[ \frac{(e^{-\Gamma_{12}T} - 1)(\Gamma_{12}^2 - \omega_r^2)}{(\Gamma_{12}^2 + \omega_r^2)^2} + \frac{\Gamma_{12}T}{\Gamma_{12}^2 + \omega_r^2} \right] \\ &\quad + 2\frac{P_3^2}{\omega_L^2} \left( \frac{\pi \sin^2 \vartheta_0}{T} + \omega_L \cos \vartheta_0 \right)^2 \left[ \frac{\Gamma_3 T - 1 + e^{-\Gamma_3 T}}{\Gamma_3^2} \right]. \end{aligned} \quad (5.1.24)$$

The origin of this equation is simply the calculation of the variance of the sum of the O. U. processes in Eq. (5.1.14) and (5.1.22). The sum of the coefficients of the single components from the dynamical and the geometric phase part is squared, which is different to a sum of squares as one would obtain by simply adding  $\sigma_{\phi_g}^2$  and  $\sigma_{\phi_d}^2$ .

### 5.1.4 Explanation in terms of domains of integration

The key to the understanding of the different behaviour of the dynamical and the geometric phase lies in the fact that the domains of integration are different in both cases. As for the dynamical phase it is given by the integral of the instantaneous energy  $E(t)$  over time and therefore its variance grows linear in time as well similar to the uncertainty in the position of the pollen grain in a suspension in classical Brownian motion [Bro66]. The integration domain doubles if the evolution time is doubled (Figure 5.6).

For the geometric phase the domain of integration is not time, but the path in parameter space, parametrised for example by the azimuthal angle  $\varphi \in [0, 2\pi]$ . Making the evolu-

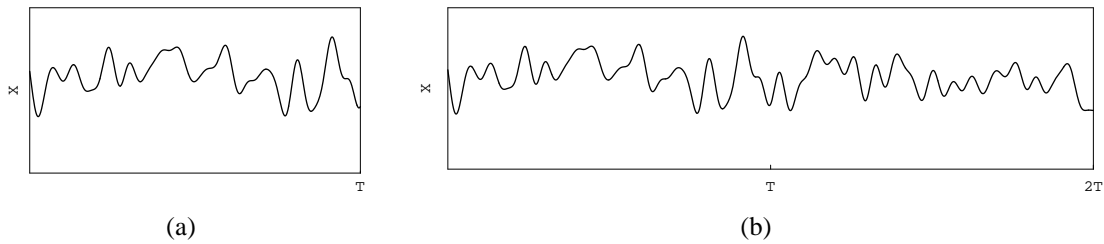


Figure 5.6: Domain of integration doubles if the evolution time is doubled for the dynamical phase. The variance  $\sigma_d^2$  grows linearly in time and is doubled as well.

tion time  $T$  for one cycle longer means that the involved frequencies relative to the angular frequency of the rotating magnetic field  $\omega_r$  are higher, but the integration domain is still  $\varphi \in [0, 2\pi]$ . The fluctuations have more time to make uncorrelated oscillations (Figure 5.7).

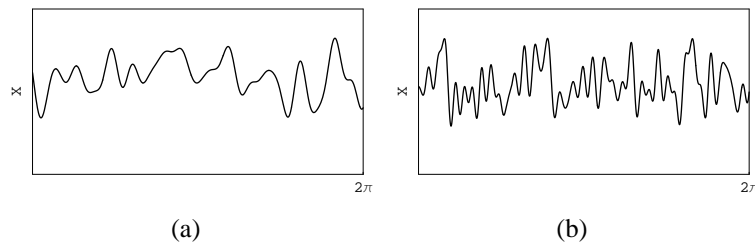


Figure 5.7: Domain of integration is the same independent of the evolution time  $T$ . Relative to the the rotation frequency  $\omega_r = 2\pi/T$  the noise frequencies are higher for larger  $T$  and the variance  $\sigma_g^2$  tends to vanish.

## 5.2 Removing the dynamical phase

To measure the geometric phase we definitely need some mechanisms to cancel dynamical phase contributions. There are a few alternatives, namely

- (i) to choose a Hamiltonian such that the dynamical phase vanishes which amounts to a parallel transport of the state vector (local compensation),
- (ii) to transport the state along a geodesic, for example by projection measurements,
- (iii) to compensate the dynamical phase afterwards by an appropriately chosen Hamiltonian (global compensation),
- (iv) to choose a system (atom) where two states have same energy and therefore same dynamical properties but different other quantum numbers [Sch06],
- (v) to use an interferometer where the evolution is such that the dynamical phase is equal in both beam paths, but the geometric phase is not,

- (vi) or to make use of a spin-echo method where the transport is executed twice but with opposite magnetic fields (or with flipped spin). Due to the opposite magnetic field the dynamical phase cancels and due to the same rotation direction the geometric phase doubles. This works only in the adiabatic case, otherwise both phase contributions vanish.

In the ideal case without fluctuations all of these methods yield the wanted results, however, if we add noise to the evolution the first three methods are not feasible since the deviations from the ideal path give rise to non-negligible dynamical phase contributions. The distorted path is not a geodesic or a parallel lift anymore, nor is the exact Hamiltonian known to compensate for it afterwards. Hence, a separation of decoherence into a geometric and a dynamic part is not possible. As for option (iv) there is no way to do this with neutrons since they only have a spin degree of freedom.

As for the interferometer option (v) the arrangement of the coils producing the magnetic field in the different paths induces a geometric phase as shown in [AKW<sup>+</sup>97]. Same noise in both coils gives rise to equal dynamical phases in both beams and the relative phase difference is then purely geometric. This issue will be addressed below in further details below (Sec.5.4.1). In the case of the spin echo the noise is also applied twice, but rather sequentially than at the same time. Choosing a specific adiabatic evolution [BDHH04] both the dynamical phase and the noise contributions from the dynamical phase are cancelled and the geometric phase remains. Clearly, one might argue that per definitionem the noise is the uncontrollable part in the course of the experiment and in order to apply the noise twice it has to be recorded and is therefore controllable in principle, a *contradictio in adiecto*. If we can record the noise we can equally well suppress it beforehand and do not have any problems in any case. However, in order to show the theoretically predicted property of vanishing variance for long exposure times to the noise we can safely neglect this objection in a proof-of-principle experiment. But we have to keep in mind that this does not resolve the problem of how to implement a unitary operation based purely on the geometric phase.

### 5.3 Spin Echo

In the adiabatic domain the dynamical phase can be removed via a spin-echo approach, namely, that the neutron is exposed to the same magnetic field twice, once in the positive eigenstate and the next time in a negative eigenstate. This can either be achieved by spin-flipping the neutron after the first magnetic field or by reversing the direction of the second magnetic field. It follows immediately that the dynamical phase cancels [BDHH04] which is the cornerstone of all our further considerations. It vanishes since it depends on the integral over the energy and this energy has opposite sign for the two magnetic fields. In contrast, the geometric phase depends only on the path and its orientation. If the path including its orientation is same in both cycles the geometric phase doubles.

For the spin echo setup we have to continue the calculations from above to include also the variance accumulated in the second round. Since just the magnetic field is flipped we can

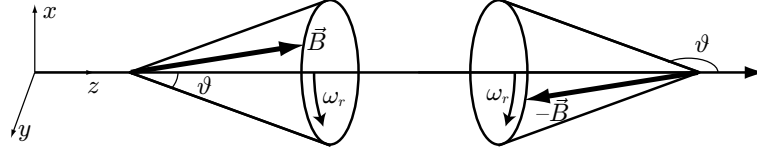


Figure 5.8: Spin-Echo Setup: The dynamical phase vanishes, since the spin is first in the positive and then in the negative eigenstate of the magnetic field Hamiltonian. Due to the equally oriented curve traced out, the geometric phase is accumulated.

already guess beforehand that the variance after the second cycle is twice the variance after the first one. But to be on the safe side, we start calculating the variance explicitly.

The magnetic field is flipped into the opposite direction now and the geometric phase for this cycle is given by

$$\phi_g^{II} = \int_T^{2T} \vec{A}^\downarrow(\vartheta') d\vec{\lambda}. \quad (5.3.1)$$

The principal direction of the magnetic field is given by  $\vartheta'_0 = \vartheta + \pi$ , i. e.  $\vec{B}$  is pointing in the opposite direction. Furthermore, the spin is now aligned anti-parallel to the magnetic field so that we need the connection  $\vec{A}^\downarrow$ . The components are given by

$$A_\vartheta^\downarrow = 0 \quad \text{and} \quad A_\phi^\downarrow(\vartheta) = -\frac{1}{2}(1 + \cos \vartheta) \quad (5.3.2)$$

For small perturbations in the magnetic field we can make a series expansion around  $\vartheta_0$ ,

$$A_\phi^\downarrow(\vartheta_0 \pm \delta\vartheta) = A_\phi^\downarrow(\vartheta_0) \pm \underbrace{\frac{\partial A_\phi^\downarrow}{\partial \vartheta} \delta\vartheta}_{\delta A_\phi^\downarrow} \Big|_{\vartheta_0} = -\frac{1}{2}((1 + \cos \vartheta_0) \mp \sin \vartheta_0 \delta\vartheta). \quad (5.3.3)$$

The  $\pm$  denotes the possibility to add the noise either in the opposite or in the same direction as in the first run. Explicitly we find for the down-spin component of the connection

$$\delta A_{\phi,\pm}^\downarrow = \pm \frac{1}{2} \sin \vartheta_0 \delta\vartheta = -\delta A_{\phi,\pm}^\uparrow. \quad (5.3.4)$$

The total geometric phase  $\tilde{\phi}_g = \tilde{\phi}_g^I + \tilde{\phi}_g^{II}$  is then

$$\begin{aligned}
 \tilde{\phi}_g &= \int_0^T [A_{\varphi,+}^\uparrow(\vartheta_0) + \delta A_{\varphi,+}^\uparrow(\vartheta_0)](\dot{\phi}_0 + \delta\dot{\phi})dt \\
 &\quad + \int_T^{2T} [A_{\varphi,\pm}^\downarrow(\vartheta'_0) + \delta A_{\varphi,\pm}^\downarrow(\vartheta'_0)](\dot{\phi}_0 + \delta\dot{\phi})dt \\
 &= \int_0^T A_{\varphi,+}^\uparrow(\vartheta_0)\dot{\phi}_0 dt + \int_0^T \delta A_{\varphi,+}^\uparrow(\vartheta_0)\dot{\phi}_0 dt + \int_0^T A_{\varphi,+}^\uparrow(\vartheta_0)\delta\dot{\phi} dt \\
 &\quad + \int_T^{2T} A_{\varphi,\pm}^\downarrow(\vartheta'_0)\dot{\phi}_0 dt + \int_T^{2T} \delta A_{\varphi,\pm}^\downarrow(\vartheta'_0)\dot{\phi}_0 dt + \int_T^{2T} A_{\varphi,\pm}^\downarrow(\vartheta'_0)\delta\dot{\phi} dt + \mathcal{O}(\delta^2).
 \end{aligned}$$

and with  $\dot{\phi}_0 = 2\pi/T$

$$\begin{aligned}
 \tilde{\phi}_g &\approx \frac{2\pi}{T} \left[ \int_0^T A_{\varphi,+}^\uparrow(\vartheta_0)dt + \int_0^T \delta A_{\varphi,+}^\uparrow(\vartheta_0)dt \right] + A_{\varphi,+}^\uparrow(\vartheta_0)(\delta\varphi(T) - \delta\varphi(0)) + \\
 &\quad + \frac{2\pi}{T} \left[ \int_T^{2T} A_{\varphi,\pm}^\downarrow(\vartheta'_0)dt + \int_T^{2T} \delta A_{\varphi,\pm}^\downarrow(\vartheta'_0)dt \right] + A_{\varphi,\pm}^\downarrow(\vartheta'_0)(\delta\varphi(2T) - \delta\varphi(T)).
 \end{aligned}$$

From the relation  $A_{\varphi,\pm}^\downarrow(\vartheta'_0) = A_{\varphi,\pm}^\uparrow(\vartheta_0)$ , since  $\vartheta' = \vartheta + \pi$ , and Eq. (5.3.4) we get

$$\begin{aligned}
 \tilde{\phi}_g &= 2\phi_g + \frac{2\pi}{T} \left[ \int_0^T \delta A_{\varphi,+}^\uparrow(\vartheta_0)dt + \int_T^{2T} \delta A_{\varphi,\pm}^\uparrow(\vartheta_0)dt \right] \\
 &\quad + \delta\varphi(T) [A_{\varphi,+}^\uparrow(\vartheta_0) - A_{\varphi,\pm}^\uparrow(\vartheta_0)] + \delta\varphi(2T) A_{\varphi,\pm}^\uparrow(\vartheta_0), \tag{5.3.5}
 \end{aligned}$$

where we have inserted the expression  $\phi_g = \frac{2\pi}{T} \int A_{\varphi,+}^\uparrow(\vartheta_0)dt$  for the unperturbed Berry's phase. We have also assumed that initially there is no noise perturbation ( $\delta\varphi(0) = 0$ ). Neglecting the terms proportional to the deviation from the final state  $\delta\varphi$  we can analyse the second term on the right hand side,

$$\begin{aligned}
 \frac{2\pi}{T} \left[ \int_0^T \delta A_{\varphi,+}^\uparrow(\vartheta_0)dt + \int_T^{2T} \delta A_{\varphi,\pm}^\uparrow(\vartheta_0)dt \right] &= \frac{2\pi}{T} \int_0^T \delta A_{\varphi,+}^\uparrow(\vartheta_0)dt \\
 &= -\frac{2\pi}{T} \int_0^T \sin \vartheta_0 \delta \vartheta dt. \tag{5.3.6}
 \end{aligned}$$

Comparing this result with Eq. (5.1.12) we find as already presumed initially that the variance of the geometric for two cycles is twice the variance after one run.

A detailed description of the ‘‘spin gymnastics’’ follows below in Section 5.5, where a possible measurement scheme is described to measure the variance of the geometric phase.

## 5.4 Possible Experimental setups

### 5.4.1 Interferometric setup

Can we use standard neutron interferometric techniques to measure the geometric phase fluctuations? Generally speaking, yes, and in contrast to the time sequential spin echo scheme it is conceptually better suited, but there are numerous technical problems. The separation of geometric and dynamical phase is rather a simple issue in an interferometer. Doing the same operation in both arms, e. g. using the same magnetic field, won't result in a shift of the interference pattern. And this works even in the case of fluctuating magnetic fields, an apparent dephasing due to an interaction with a stochastic magnetic field can be totally compensated by applying the same field with the same noise in the other path. This has been tested for slow fluctuations in [BRS03] as shown in Figure 5.3, and – from the theoretical point of view – the step towards faster fluctuations should not change the situation significantly. How can a possible evolution look like such that the dynamics are same in both paths, but with different geometry in order to obtain the same global dynamical phase but different geometric phase. For example, a rotation of the magnetic field with same strength but with opposite rotation sense yields a purely geometric phase difference between the beams. Another example is an orange-slice shaped path as depicted in Figure 5.9. Such an evolution has been implemented

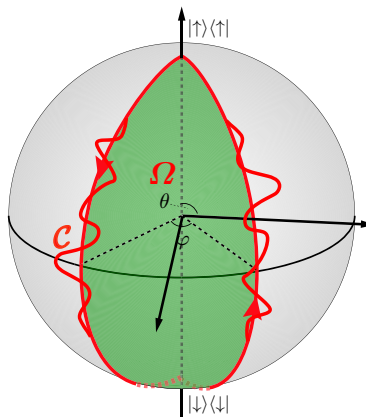


Figure 5.9: Orange-slice shaped path of the neutron spin with additive noise. The angle difference of the magnetic field in the two paths determines the opening angle of the paths from up to down spin and consequently the geometric phase.

by Allman *et al.* [AKW<sup>+</sup>97] in a neutron interferometer experiment. But in this case the magnetic field is static and the spin evolution is non-adiabatic - the neutron spin precess about the magnetic field direction. As a consequence, the formalism described above has to be altered, but this should not do any harm to the results about the robustness since the geometric picture is same. The spin traces out a path with more or less wiggles and encloses a particular surface area that is more or less smeared out.

The technical problems start, however, by trying to generate the fluctuations. These have to be faster than the transit time of neutrons through the coils producing the magnetic field.

Thermal neutrons have a typical velocity of approximately  $2000 \text{ ms}^{-1}$ . A rotation about  $2\pi$  corresponds then to about  $10^5 - 10^6 \text{ rad/s}$  for an assumed coil length of  $\approx 1 - 10 \text{ cm}$ . Such frequencies in the 10-100 kHz range are not easily achievable due to the self-inductance of the coils. An oscillating circuit has to be tuned to meet the frequency demands which restricts in turn the frequency bandwidth to a region around the resonance. Besides that, thermal radiation of a coil producing such a field will definitely lead to a loss of contrast, the produced heat disturbs heavily the visibility since the inter-atomic distances of the perfect silicon crystal change and one has to cool the coils.

If one is able to overcome these problems and one wants to implement an adiabatic evolution it is tempting to use one of the coils shown in Figure 5.10, a cylinder surrounded by helically wound wire, as used by Bitter and Dubbers [BD87]. In its moving frame of reference the neutrons feels a rotating magnetic field and the spin will follow adiabatically as long as the coil is long enough and the magnetic field is high enough. However, too long coils do not fit into the interferometer and strong magnetic fields produce lots of heat. One could also use radio-frequency spin flippers [BRS83] where the spins are flipped at resonance. The phase between the oscillations of the two spin flipping coils corresponds to the opening angle of the orange slice in Figure 5.9 resulting in a geometric phase. The problems mentioned above remain roughly the same and additionally the calculation of the behaviour of the polarisation vector when noise is added is more involved.

Common to all the different coil geometries is also that the transit time and therefore the time dependence of the geometric phase variance cannot be simply changed. Due to the Bragg condition the available range of wavelengths is rather narrow and cannot be changed easily. Unfortunately, to see the predicted behaviour depicted in Figure 5.2 the transit time should be changed. A possible workaround would be to vary the noise frequencies such that its original dependence on  $T$  is hidden in the change of the frequencies. However, this slightly misses the point of the intended experiment.

Summa summarum, the neutron interferometer does not seem the appropriate tool from the technical point of view. However, conceptually it is better suited than the concepts based on spin echo since when the coils are fed from the same source the current fluctuations will induce equal dynamical phase fluctuations in both beams. Note, that perfect control over the noise is not necessary in this case since it is automatically the same noise in both paths, if the current supply is the same. The reduction of the visibility can then only be of geometric origin and should improve with increasing evolution time, viz. longer wavelengths or higher noise frequencies.

### 5.4.2 Polarimetric setup

The difficulties with temperature and tunable evolution times leads automatically to the idea to switch over to a polarimeter setup as used for example in [HB99, WBR<sup>+</sup>00, KSH<sup>+</sup>05]. To get rid of dynamical phase contributions the idea of *neutron spin echo* [Mez72] can be adopted. Polarimetry measures - nomen est omen - the resulting polarisation of neutrons incident in a specific spin state after having carried out some evolution. In contrast to the

interferometric setup there are two coils in series such that a neutron passes through both of them. In brief, the advantages are that the heat produced by the coils does not disturb the contrast, the dimensioning is not a crucial point and there is more freedom in choosing the wavelength of the neutrons since one is not restricted to match a Bragg condition as in the interferometric case. One can use neutrons with larger wavelength, hence smaller velocity, to increase the time available for one rotation.

### Helical wounded coils

The first option are two helically twisted Helmholtz coil pairs arranged in series (Figure 5.10). Spin polarised neutrons enter the first coil and feel a rotating magnetic field due to the twist of the coils. A full  $2\pi$  rotation is executed in the first as well as in the second coil, but in the second coil the magnetic field points in the opposite direction by reversing the polarity of the coil current. As a consequence the dynamical phase vanishes and only the geometric contribution is left. The helix is additionally encircled by a coil producing a magnetic field in beam direction in order to achieve an evolution path not constrained to the equatorial plane. An advantage of this setup is that it is wavelength independent as long as the field can be made high enough to ensure adiabaticity.

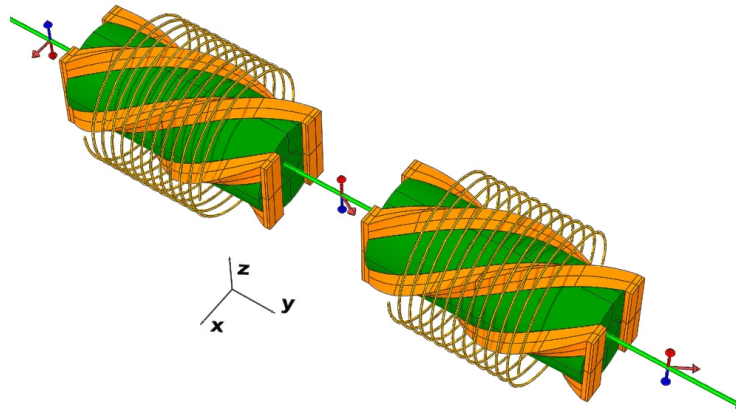


Figure 5.10: Helically twisted Helmholtz coil pairs in a spin-echo arrangement.

A few numbers will help us to estimate the results: Suppose the helix generates a field of 20 Gauss ( $\omega_L \approx 4 \times 10^5$  rad/s) in the centre along the beam axis and the unit is about 20 cm in length. Thermal neutrons will traverse this distance in 0.1 milliseconds and the angular rotation frequency is then  $\omega_r \approx 6 \times 10^4$  rad/s. Recalling Eq. (5.1.20) we find that these parameters are fine, if the noise bandwidth is made to fit in between  $\omega_r$  and  $\omega_L$ . Also, one is not restricted to thermal neutrons, one could also use slower ones and get lower rotation frequencies. That helps a lot since the self-inductance could prohibit the excitation of

high-frequency fields and when employing cold (slow) neutrons the rotation frequency  $\omega_r$  is automatically reduced.

A major problem is the needed homogeneous magnetic field field in the longitudinal as well as in the transversal direction. The geometry makes it hard to calculate the rather involved shape of the magnetic field in the interior, not to mention at the boundaries.

### Cross-coil setup

Another option is to use the type of coils described in [WB90]. Here two perpendicular coil pairs in Helmholtz-like geometry are placed around the beam. The magnetic field is also perpendicular to the forward direction of the beam and by feeding (phase-delayed) sinusoidal signals into the coils the resulting field is rotating with the frequency of the signal.

For a spin echo setup two such cross-coil devices have to be placed in sequence (Figure 5.11). The rotation frequency is adjusted such that a neutron polarised in positive  $z$ -direction, say, will be spin-flipped into a polarisation in the negative  $z$ -axis in the first coil and back to the positive  $z$ -direction in the second coil. The neutron spin will trace out an orange-slice path on the Bloch-sphere as shown in Figure 5.9. The off-axis angle towards the forward direction corresponds to the opening angle of the slice. If the axes of the cross coils are aligned with the beam the opening angle is either  $0^\circ$  or  $180^\circ$  (depending on the phase-delay between the two cross-coils) and yields a trivial geometric phase of  $0$  or  $\pi$ , which cannot be distinguished in a polarimetric measurement (c. f. Section 5.5). Only after arranging the coils inclined to each other a non-trivial geometric phase will show up.

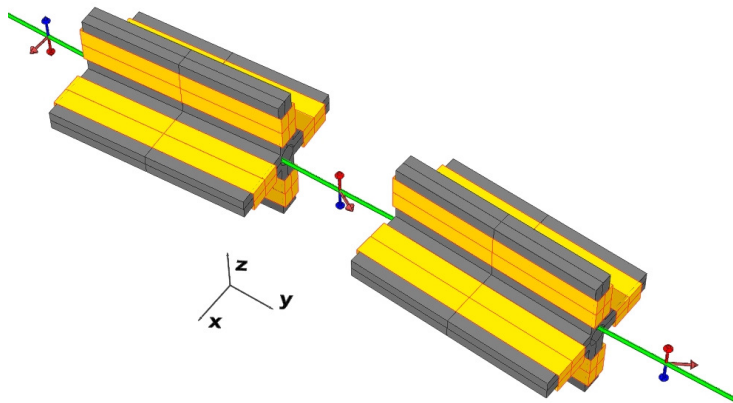


Figure 5.11: Polarimetric spin-echo setup with a coil arrangement in Helmholtz-like geometry. A sinusoidal signal fed into the perpendicular coil pair leads to a rotating magnetic field.

The problem are as above homogeneous magnetic field, boundary effects, etc. The latter might become a bigger problem since one cannot define a precise entrance time, and there-

fore not an exact initial phase. In addition, a time-of-flight measurement method has to be adopted to correlate the arrival time to the oscillating period and this setup is not that flexible in choosing a particular wavelength since the phase between these coils has to be adapted accordingly.

Finally, there is this already mentioned conceptual difficulty whether it is allowed to speak of noise even though it is artificially generated. For the moment, let us put aside this question under the working hypothesis that the artificiality of the noise does not derogate the results on the stability of the geometric phase, and move on to a similar scheme utilising stored neutrons.

### 5.4.3 Ultra cold neutrons

Although the problems in the polarimetric setup do not seem to be insuperable, instead of utilising a neutron beam there is also the possibility to use polarised ultra cold neutrons (UCNs) that can be stored in an appropriate storage vessel and then manipulated by surrounding magnetic fields. One gains flexibility in the choice of the magnetic fields, virtually any evolution can be implemented.

The storage is possible due to the very low speed of such neutrons, approximately  $< 7$  m/s corresponding to an energy of less than 250 neV. For a successful storage the wall potential (Fermi potential) has to be larger than typical kinematic energies of the neutrons. E. g., the Fermi potential of quartz is 91neV [vdGPS<sup>+</sup>99] and therefore neutrons slower than  $\approx 4.2\text{ms}^{-1}$  can be stored. Regardless of the Fermi potential the maximum time for the spin “gymnastics” is given by the lifetime of the neutrons of 886 seconds [Gro04], but for our purposes this is much larger than the typical evolution time. The neutron trap is surrounded by three pairs of coils in Helmholtz geometry. With the help of these fields the intrinsic neutron spin can be manipulated as wished and the resulting effects can be analysed by measuring the polarisation when emptying the storage vessel. The genuine Berry phase without noise fluctuations has already been measured with such a setup by Richardson *et al.* [RKGL88] at the ultra-cold neutron beam-line at the Institute Laue Langevin, Grenoble.

A typical Helmholtz-coil arrangement is shown in Figure 5.4.3. One pair of circular and two pairs of square shaped coils are used, whereas both geometries provide a fairly homogeneous field at their centre (Appendix D.1.6).

In the centre of the coil system a cylindrically shaped storage vessel made of polymer (POM) (Figure 5.13) is placed.

Incoming neutrons are polarised by virtue of totally magnetised foils (Appendix D.1.4) which are used both for preparation and later for analyzation of the polarisation. If the density of neutrons in the storage vessel is in equilibrium with the density in the neutron guide the container is closed. To produce a geometric phase  $\phi_g$  a slowly rotating magnetic field is then applied so that the spin vector of the neutrons can follow its rotation. After executing a full spin-echo cycle the final polarisation is measured with the magnetised foils in front of the detector. In the presence of adiabatic fluctuations the spin of *each* stored neutron will follow the field direction and all will end up in the same state - no dephasing has happened.

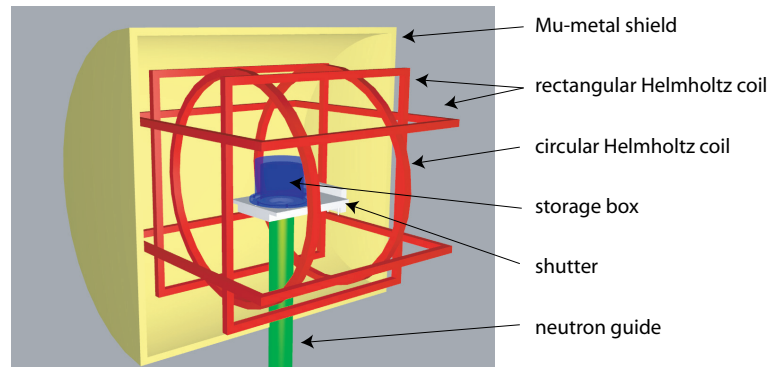


Figure 5.12: Experimental setup with one circular and two Helmholtz coil pairs perpendicular to each other surrounding the storage vessel mounted above a shutter.



Figure 5.13: Vessel made of POM coated with Fomblin.

However, for different runs of the experiment the final polarisation will be different and the average over many runs gives us information about the mean geometric phase ( $\bar{\phi}_g$ ) and its variance ( $\sigma_g^2$ ). The conclusion drawn above are valid, viz. for slow evolutions the variance  $\sigma_g^2$  tends to zero and consequently the exponential damping of the polarisation becomes negligible. In other words, the absolute error of  $\bar{\phi}_g$  in each run vanishes.

The advantages of the UCN setup are that the storage time can be chosen more or less arbitrarily as long as it is less than the neutron life-time, we do not have to rely on wavelength selection. Furthermore, arbitrary paths can be implemented due to the freedom given by the 3D-coil arrangement compared to the polarimetric or interferometric experiments where one is rather restricted in the choice of evolution paths.

Unfortunately, all that glitters is not gold. There are also severe disadvantages. For example, the magnetic field has to be highly homogeneous inside the storage box which demands for relatively large coils and small storage box. Unwanted magnetic field variations occur also due to the back and forth movements of the neutrons since the field is not 100% homogeneous inside the storage volume. From the neutron's frame of reference this amounts to time-dependent fluctuations which cannot be cancelled with the aid of a spin-echo procedure and if the magnetic field is strong the – unwanted – phase variations from these fluctuations are big . The use of weaker magnetic field might cure this defect, but, on the other hand

side, weak fields makes the experiment vulnerable to environmental non-artificial magnetic field fluctuations. These have to be shielded - for instance by means of mu-metal. Furthermore, the self-inductance of the coils prevents us to use high frequencies for the noise and the rotation sequence. A more detailed description along with an analysis of these potential pitfalls and difficulties of the UCN setup is discussed in Appendix D. It turns out that one can probably find a suitable set of parameters to get it going.

## 5.5 Spin gymnastics

In view of the potential experiment, what exactly could the spin evolution look like? In brief, the neutron spin vector points first in the positive  $z$  direction. Then, the direction of the magnetic field is changed adiabatically such that the spin vector follows its direction. After a full circle back to the initial direction the spin polarisation is again in the positive  $z$  direction, but with an additional phase factor. This phase factor comprises both dynamical and geometric contributions. The dynamical part can be cancelled by spin-echo: The field is reversed to point in the opposite direction, fast enough to induce a non-adiabatic transition. A further evolution cycle in the same direction doubles the geometric phase since the surface area enclosed by the path on the Bloch sphere doubles, whereas the dynamical part cancels, because the neutron spin is in the eigenstate with negative sign during the second cycle gathering exactly the dynamical phase with reversed sign. The final state has therefore a phase difference relative to the initial state which is purely geometric.

Where is the noise part? To test the predictions of the theory also the noise influence on the dynamical part has to vanish. If there are independent fluctuations in the first and in the second cycle the dynamical phase will cancel only in the mean, but its variance will double. However, since the quantity to be measured is in fact the variance of the total phase one can not conclude from such a measurement to the variance of the geometric phase, there are still contributions of dynamical origin. The noise must therefore be equal in both cycles which guarantees vanishing uncertainty in the dynamical phase and what is left is just contributions from the geometric phase.

### Extensive description

- (i) By use of magnetised foils a ultra cold neutron beam is prepared in the state  $|\Psi_{t_1}\rangle = |z+\rangle$ , i. e. it is polarised in the positive  $z$ -direction. The magnetic field points initially in the same direction,  $\vec{B}_{t_1} = (0, 0, B_z)^T$  (Figure 5.14). Its strength is arbitrary, but should be strong enough to prevent dephasing due to environmental influences, e. g.  $B_z \approx 1G$ .
- (ii) In the second step the magnetic field direction is suddenly switched to an axis perpendicular to the former polarisation direction (Figure 5.15). This operation has to be fast enough in order to keep the polarisation of the neutron spins,  $|\Psi_{t_1}\rangle \mapsto |\Psi_{t_2}\rangle = \frac{1}{\sqrt{2}}(|x+\rangle + |x-\rangle)$  where  $|x+\rangle$  and  $|x-\rangle$  denote the eigenstates of the field

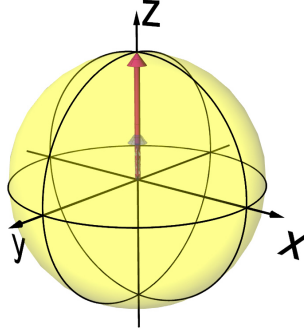


Figure 5.14: Initial spin state  $|\Psi_{t_1}\rangle = |z+\rangle$ .

$\vec{B}_{t_2} = (B_x, 0, 0^T)$ . Fast enough means that the time interval for the field flip  $\Delta t_{12}$  is shorter than the Larmor frequency of the neutron spin in the field  $\vec{B}_{t_1}$ . Quantitatively, the Larmor frequency is  $\omega_L \approx 1.8 \times 10^4$  rad/s (1 Gauss) corresponding to a frequency of  $f = \omega_L/2\pi \approx 3$  kHz and therefore  $\Delta t_{12} \approx 10^{-5}$  s. To meet these demands the rise time of the Helmholtz coils must not be neglected, but according to the test performed on a Helmholtz coil setup problems do not arise until frequencies of about 5-10 kHz (Section D.2.5).

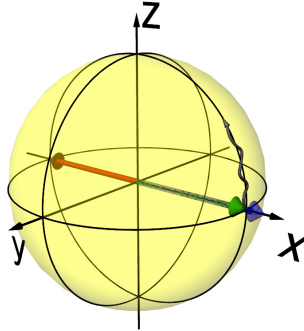


Figure 5.15: Sudden switch of the magnetic field to a direction perpendicular to the original one.

- (iii) Now comes the rotation part (Figure 5.16). The direction of the magnetic field is varied slowly (up to an angular frequency of about  $\omega_r \approx 10^3 - 10^4$  rad/s) to stay in the adiabatic domain. The state after the rotation is given by  $|\Psi_{t_2}\rangle \mapsto |\Psi_{t_3}\rangle = \frac{1}{\sqrt{2}} (|x+\rangle + e^{i2\phi} |x-\rangle)$  where  $\phi = \phi_d + \phi_g$  comprises a dynamical ( $\phi_d$ ) as well as a geometric part ( $\phi_g$ ). In the simplest case the rotation is in the  $x$ - $z$  plane with no  $y$ -component,  $\vec{B}_{t_2}(t) = (B_x \cos(\omega_r(t - t_2)), 0, B_x \sin(\omega_r(t - t_2)))^T$ . The solid angle  $\Omega$  subtended after a full cycle is then  $\Omega = 2\pi$  and consequently the geometric phase is  $\pi$ . This by itself does not cause troubles, but unfortunately both eigenstates  $|x+\rangle$  and  $|x-\rangle$  obtain the same phase with opposite sign such that the phase difference is twice the accumulated phase and having the spin-echo setup in mind, the final phase difference is given by  $\Delta = 4\phi_g$  which amounts to a trivial phase difference for  $\phi = n\pi/2$ ,  $n$

integer. Although the main focus lies on the variance, a non-trivial mean geometric phase is a more striking outcome. Adding a magnetic field pointing in the  $y$ -direction, e. g.  $\vec{B}_{t_2}(t) = (B_x \cos(\omega_r(t - t_2)), B_y, B_x \sin(\omega_r(t - t_2)))^T$ , yields  $\phi_g \neq n\pi/2$ .

During the evolution artificial fluctuations of the magnetic field both in amplitude and in direction will be added. The average power of the noise should be less than  $|B|$  and the bandwidth of the fluctuations  $\omega_n$  less than the Larmor frequency corresponding to  $|B|$  ( $\omega_n \ll \omega_L$ ). The special shape of the noise is discussed in Section 5.6.2.

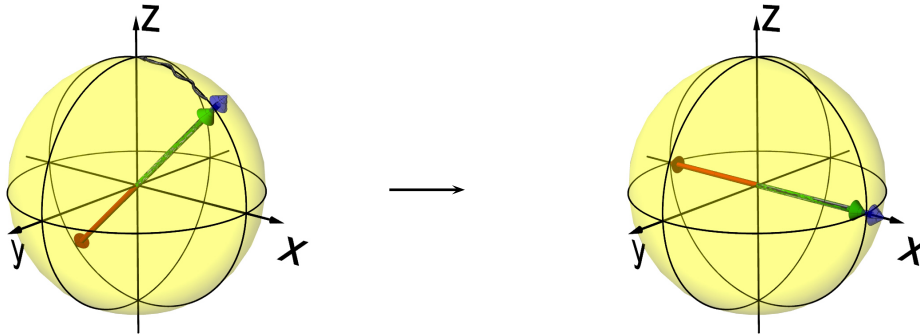


Figure 5.16: Adiabatic cyclic change of the magnetic field direction results in a relative phase difference of the constituting states  $|x+\rangle$  and  $|x-\rangle$ , respectively.

- (iv) It follows a sudden change of the magnetic field direction into its opposite  $B \mapsto -B$  (Figure 5.17). Before, maybe the amplitude of the field  $B_{t_3}$  has to be reduced in order to accomplish a sudden flip taking the finite rise time of the coils and the power supplies into account, e. g.  $B_{\Delta t_{34}} \approx 0.1 - 1\text{G} \mapsto \tilde{B}_{\Delta t_{34}} = -B_{\Delta t_{34}}$  and finally  $\vec{B}_{t_4} = (-B_r, 0, 0)^T$ . The state thereafter is  $|\Psi_{t_3}\rangle \mapsto |\Psi_{t_4}\rangle = \frac{1}{\sqrt{2}}(|x-\rangle + e^{i2\phi}|x+\rangle)$  where the basis states have changed place.

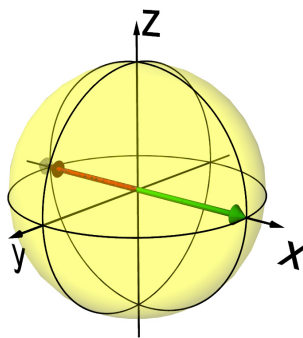


Figure 5.17: Non-adiabatic flip of the magnetic field direction.

- (v) The implementation of the spin-echo scheme necessitates a further rotation of the magnetic field in the same sense with the same rotation speed and the same fluctuations (Figure 5.18),  $\vec{B} = (-B_x \cos(\omega_r(t - t_4)), -B_y, -B_x \sin(\omega_r(t - t_4)))^T$ ,  $\omega_r = \frac{2\pi}{t_5 - t_4} = \frac{2\pi}{t_3 - t_2}$ . If these criteria can be satisfied the spin of the neutron is in the state

$|\Psi_{t_5}\rangle = \frac{1}{\sqrt{2}}(|x-\rangle + e^{i4\phi_g}|x+\rangle)$ . Note, that the phase difference is now only given by the geometric part  $\phi_g$  due to the cancellation effect. The neutron spin has spent as long in the positive eigenstate as in the negative eigenstate and since also the fluctuations have been the same there is actually no reason to expect any difference between the initial state  $|\Psi_{t_2}\rangle$  cycles and the state  $|\Psi_{t_5}\rangle$ . The phase difference is a geometric effect. But why does it not vanish?

The point is, that the geometric phase is the same for both rotations. In the present scenario the magnetic field changes in between the two rotation sequences, but neither the state is changed nor the sense of rotation. Before, we have already clarified that the energy does not play a role for the value of the geometric phase and therefore it is immaterial if the state is in the positive or negative eigenstate of the magnetic field. Consequently, the geometric phase doubles. In detail, the state after the first rotation is

$$|\Psi_{t_4}\rangle = \frac{1}{\sqrt{2}}(e^{i\phi}|x+\rangle + e^{-i\phi}|x-\rangle) \quad (5.5.1)$$

and maps to

$$|\Psi'_{t_4}\rangle = \frac{1}{\sqrt{2}}(e^{i\phi}|x-\rangle + e^{-i\phi}|x+\rangle) \quad (5.5.2)$$

after the field flip due to the swap of the basis states. After the second rotation each of the basis states accumulates a phase  $\tilde{\phi}$ ,

$$|\Psi_{t_5}\rangle = \frac{1}{\sqrt{2}}(e^{-i\tilde{\phi}}e^{i\phi}|x-\rangle + e^{i\tilde{\phi}}e^{-i\phi}|x+\rangle). \quad (5.5.3)$$

$\phi$  and  $\tilde{\phi}$  comprise a dynamical as well as a geometric part, but in contrast to  $\phi = \phi_d + \phi_g$ , there is an additional minus sign in  $\tilde{\phi} = \phi_d - \phi_g$  reflecting the constant sense of direction. Consequently,  $(\tilde{\phi} - \phi) = -2\phi_g$  and the final state is equivalent to

$$|\Psi_{t_5}\rangle = \frac{1}{\sqrt{2}}(|x-\rangle + e^{2i(\tilde{\phi}-\phi)}|x+\rangle) = \frac{1}{\sqrt{2}}(|x-\rangle + e^{4i\phi_g}|x+\rangle). \quad (5.5.4)$$

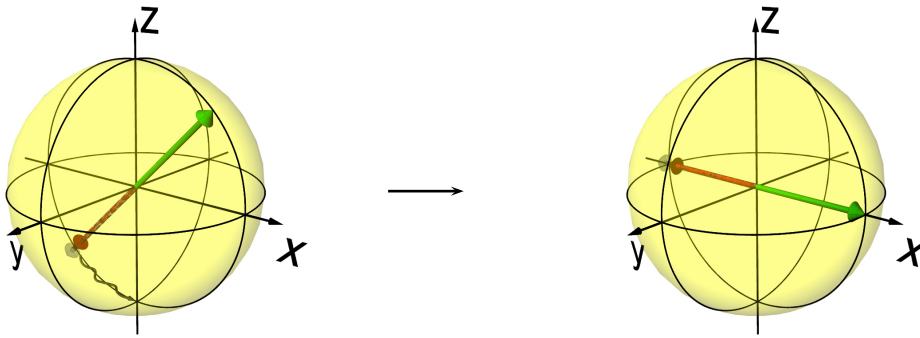


Figure 5.18: Second cycle of the spin-echo scheme where the magnetic field is reversed but not the sense of the rotation.

- (vi) Evidently the final state is different from the original one and this difference manifests itself in a different polarisation. An additional “pulse” with a small magnetic field in x-direction  $\vec{B}_{t_6} = (B_\xi, 0, 0)^T$  is applied to rotate the spin for  $\xi = 2\mu_N B_\xi t / \hbar$  about the x-axis. The meaning of this operation will be clear in a moment.  $|\Psi_{t_5}\rangle$  is transformed to the state

$$\begin{aligned} |\Psi_{t_6}\rangle &= e^{i\frac{\xi}{2}\sigma_x} |\Psi_{t_5}\rangle \\ &= \frac{1}{\sqrt{2}} (e^{i\frac{\xi}{2}} |x-\rangle + e^{-i\frac{\xi}{2}} e^{4i\phi_g} |x+\rangle) \\ &\hat{=} \frac{1}{\sqrt{2}} (|x-\rangle + e^{i(4\phi_g - \xi)} |x+\rangle). \end{aligned}$$

- (vii) Switching back to initial guide field in z-direction changes the basis of the state (Figure 5.19),

$$\begin{aligned} |\Psi_{t_6}\rangle &\mapsto |\Psi_{t_7}\rangle = \\ &= \frac{1}{2\sqrt{2}} \left( (|z+\rangle - |z-\rangle) + e^{i(4\phi_g - \xi)} (|z+\rangle + |z-\rangle) \right) \\ &= \frac{1}{2\sqrt{2}} \left( (1 + e^{i(4\phi_g - \xi)}) |z+\rangle - (1 - e^{i(4\phi_g - \xi)}) |z-\rangle \right) \\ &= \frac{1}{2\sqrt{2}} \left( e^{i(2\phi_g - \frac{\xi}{2})} \left[ (e^{-i(2\phi_g - \frac{\xi}{2})} + e^{i(2\phi_g - \frac{\xi}{2})}) |z+\rangle \right. \right. \\ &\quad \left. \left. - (e^{-i(2\phi_g - \frac{\xi}{2})} - e^{i(2\phi_g - \frac{\xi}{2})}) |z-\rangle \right] \right) \\ &\hat{=} \frac{1}{\sqrt{2}} \left( \cos(2\phi_g - \frac{\xi}{2}) |z+\rangle + i \sin(2\phi_g - \frac{\xi}{2}) |z-\rangle \right). \end{aligned}$$

It can immediately be seen that for vanishing geometric phase and vanishing  $\xi$ -pulse the original polarisation is retained. If not, the polarisation vector lies somewhere in the  $z-y$  plane depending on  $\phi_g$  and on  $\xi$ .

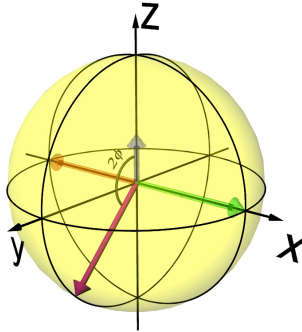


Figure 5.19: Switching the magnetic field back to the initial direction.

- (viii) In the last step the bottle is emptied and the final degree of polarisation along the z-axis

represented by the Pauli matrix  $\sigma_z$  is measured.

$$\begin{aligned} P &= \langle \Psi_{t_6} | \sigma_z | \Psi_{t_6} \rangle \\ &= \cos^2\left(\frac{\xi}{2} - 2\phi_g\right) - \sin^2\left(\frac{\xi}{2} - 2\phi_g\right) \\ &= \cos(\xi - 4\phi_g). \end{aligned}$$

Now the relevance of the extra  $\xi$  pulse becomes more obvious. To determine the value of  $\phi_g$  precisely, a sinusoidal pattern is generated by variation of  $\xi$  and compared to the case where  $\phi_g = 0$  like for interferometric measurements.

### Noise contributions

But where is the contribution of the noise in the final result? In course of the derivation of Equation (5.5.5) we have tacitly ignored the fluctuations of the magnetic field which should manifest itself in the degree of polarisation. In course of the experiment all the stored, manipulated and finally detected neutrons have had the same history when neglecting environmental influences and therefore will show the same phase  $\phi_g$ . Without artificial noise it is precisely half of the solid angle enclosed by the unperturbed path. Turning on the noise source leads to a different geometric phase  $\phi_g$  for each run of the experiment (but not for each neutron since all neutrons experience the same noise within unavoidable experimental shortcomings). Averaging over many realisations we measure a mean degree of polarisation

$$\langle P \rangle = \langle \cos(\xi - 4\phi_g) \rangle, \quad (5.5.5)$$

with a mean square deviation or variance  $\sigma_P^2 = \langle P^2 \rangle - \langle P \rangle^2$ . The variance  $\sigma_P^2$  depends on the variance of the geometric phase  $\phi_g$ . For a Gaussian distributed  $\phi_g$  with mean  $\bar{\phi}_g$  and variance  $\sigma_g^2$  we can calculate the average degree of polarisation

$$\begin{aligned} \langle P(\phi_g) \rangle &= \int P(\phi) f_{\phi_g}(\phi) d\phi \\ &= \frac{1}{\sqrt{2\pi\sigma_g^2}} \int_{-\infty}^{\infty} \cos(\xi - 4\phi) e^{-\frac{(\phi - \bar{\phi}_g)^2}{2\sigma_g^2}} d\phi \end{aligned} \quad (5.5.6)$$

with the probability density function of the geometric phase  $f_{\phi_g} = \frac{1}{\sqrt{2\pi\sigma_g^2}} e^{-(\phi - \bar{\phi}_g)/(2\sigma_g^2)}$ . Using the integral relation

$$\int_{-\infty}^{\infty} \cos(A + bx) e^{-a^2(x-x_0)^2} dx = \frac{\sqrt{\pi}}{a} \cos(A + bx_0) e^{-\frac{b^2}{4a^2}} \quad (5.5.7)$$

we obtain

$$\langle P \rangle = e^{-8\sigma_g^2} \cos(\xi - 4\bar{\phi}_g). \quad (5.5.8)$$

An exponential damping factor

$$v \equiv e^{-8\sigma_g^2}$$

due to the additional noise shows up. Intuitively one would guess that fluctuations distorting the ideal path yield vanishing mean polarisation,  $\langle P \rangle = 0$ , i. e. a total loss of contrast, provided that the fluctuations are strong enough and the neutron spends a sufficiently long time in the fluctuating magnetic field. But we have already discussed that in the case of the geometric phase, however, this is just valid with respect to the noise strength but not to the time: a slow evolution preserves the original degree of polarisation. For large variances  $\sigma_g^2$  the average degree of polarisation vanishes ( $v = 0 \rightarrow \langle P_z \rangle = 0$ ), however, for slow evolutions the variance  $\sigma_g^2$  tends to zero and consequently the exponential damping ( $v \rightarrow 1$ ) of the polarisation becomes negligible.

Thus, the variance of the geometric phase is seen as a reduction of the visibility and is recovered for longer evolution times as depicted in Figure 5.20 for several noise amplitudes. Note, that it is not possible to improve the visibility compared to its initial value. For instance, an unpolarised beam with vanishing visibility cannot be polarised just by executing some cyclic evolution, but the degree of polarisation does not change during the evolution cycle.

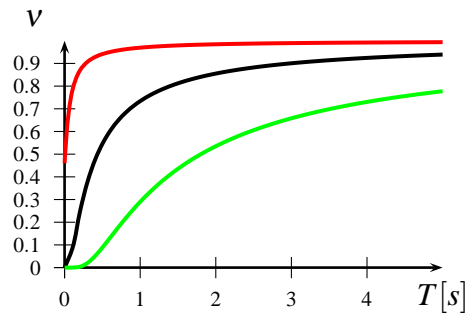


Figure 5.20: Visibility factor  $v = e^{-8\sigma_g^2}$  at  $\omega_L = 10^4$  rad/s,  $\omega_n = 50$  rad/s,  $\vartheta = \pi/2$ . The signal-to-noise ratio  $s_r = \omega_L/\sigma_3$  is set to  $2 \times 10^{1/2}$  (green),  $10^{1/2}$  (black) and  $10^1$  (red line).

### 5.5.1 Time Sequence

To gain a better understanding of the time scales for the explanation given above the currents of the different coil pairs are shown in Figure 5.21. The sinusoidal changes in the  $x$ -direction and the additional noise fluctuation in  $z$ -direction can be observed.

## 5.6 Numerical Simulations

The numerical simulation consists of two parts. On the one hand side the evolution of the spin state has to be simulated by solving the time-dependent Schrödinger equation numerically for the time-dependent Hamiltonian. On the other hand side artificial noise that alters the original Hamiltonian must be generated by a specific numerical algorithm.

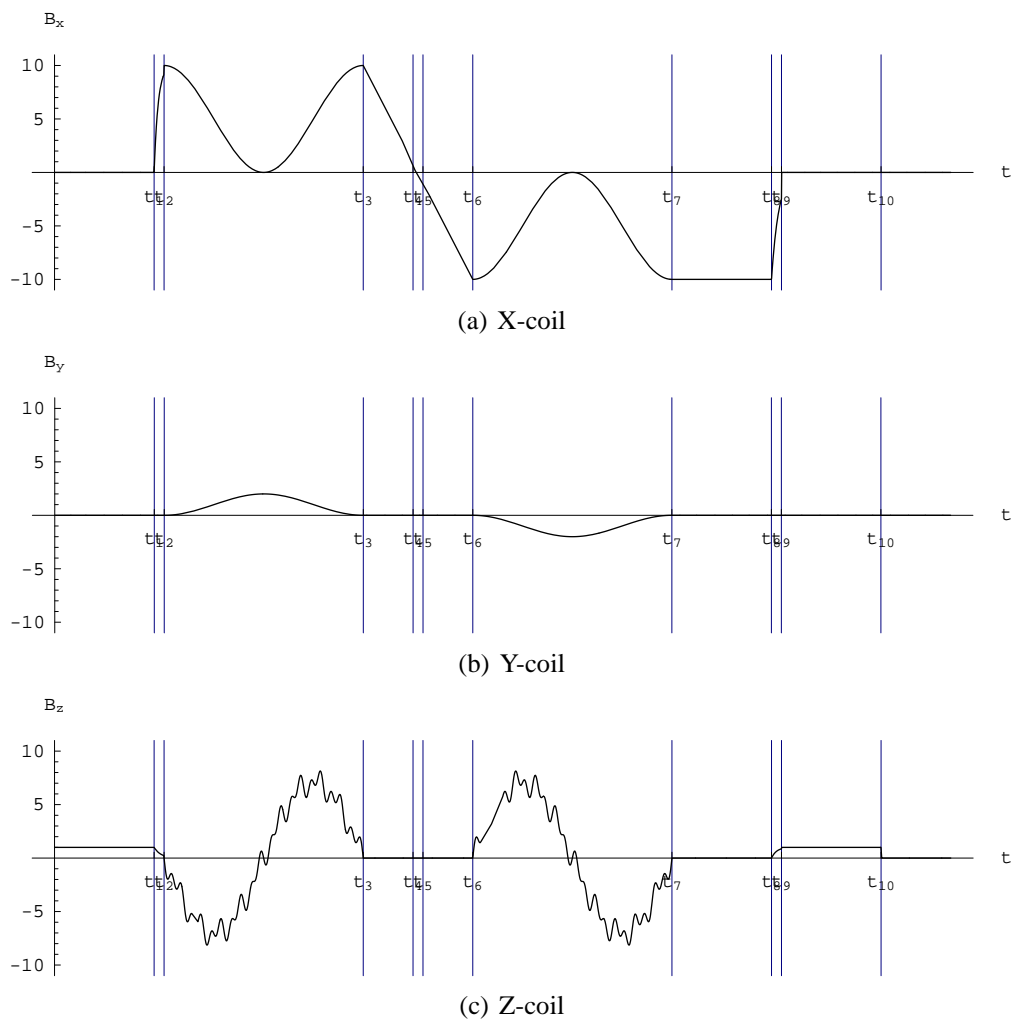


Figure 5.21: Time sequence for the different coil pairs for one experimental run.

**Why is a numerical simulation needed?** The considerations above have certain deficiencies when trying to construct an experiment. First of all, it is just a first order approximation which we expect to break down for strong noise influences (Figures 5.4 and 5.5). Furthermore, the adiabaticity condition has to be met for all participating frequencies, i.e. the bandwidth of the artificial noise contributions, the rotation frequency, and also the changes of the magnetic field as seen from the inertial frame of the neutrons due to the inhomogeneities in the storage box have to be smaller than the Larmor frequency for all times. The transition to strong noise and to non-adiabatic regions is not included in the theory and have to be tested by means of numerical simulations since the exact solution of the problem does not seem to be feasible. Of course not all effects (like all environmental influences) can be simulated, but at least the spin-trajectories of one particle subjected to a rotating noisy magnetic field can be found. Averaging over many realisations sheds light on the average geometric phase for a particular configuration and on the variance of the geometric phase as well and we can conclude on the possible parameter settings for a future “real” experiment (Appendix D).

### 5.6.1 Evolution algorithm for the spin state

Generally speaking, we would have to solve the time-dependent Schrödinger equation

$$i \frac{\partial}{\partial t} \psi(\vec{x}, t) = H \psi(\vec{x}, t), \quad (5.6.1)$$

where  $\psi(\vec{x}, t) \in \mathcal{H}_x \otimes \mathcal{H}_s$  is a tensor product state with a spatial part represented in  $\mathcal{H}_x$  and a spin angular momentum part element of  $\mathcal{H}_s$ . For the situation discussed above we can safely neglect the spatial part due to the differences in the energy scales of up to a factor  $10^{10}$  (thermal neutrons) between the Zeeman energy splitting of the spin levels (for magnetic fields in the Gauss region) and the kinetic energy of neutrons. Even for ultra-cold neutrons a factor  $10^5$  is left so that there is de facto no influence of the magnetic fields on the trajectories of the neutrons. The solution of Eq. (5.6.1) simplifies then considerably also with respect to the finite dimension of Hilbert space.  $\psi(t)$  is then a two dimensional normalised complex vector representing the spin state of the neutron.

**Implicit Crank-Nicholson scheme** The numerical solution of stochastic differential equations usually requires slightly different methods than deterministic differential equation [KP95]. Examples can be found for instance in the book by Breuer and Petruccione [BP02, p. 370] where an improved *Euler scheme* (or *Heun Method*) is used as a particular instance of a *predictor - corrector* method. However, for our purposes a standard solution method is appropriated since the fluctuations are sufficiently slow. The entire evolution is treated fully deterministic for each realisation and the stochastic nature enters when averaging over different noise realisations.

In order to approximate Schrödinger’s equation by *finite difference quotients*

(e. g. [Hea02]) a formal solution is exploited numerically,

$$\psi(t) = e^{-\frac{i}{\hbar}Ht} \psi(0). \quad (5.6.2)$$

An explicit scheme would be the approximation of the above by  $\psi(t_{n+1}) = (1 - iH\Delta t)\psi(t_n)$ , i. e. to calculate the wave function  $\psi$  at time  $t_{n+1}$  directly from the wave function  $\psi(t_n)$  one time step before. But this is unstable, meaning that the solution depends on the choice of the time increment  $\Delta t$ . A method to solve Schrödinger's equation numerically more elegant is provided by the *Crank-Nicholson scheme* which relies on the *Cayley form* of the exponential operator  $e^{-\frac{i}{\hbar}Ht}$  [GSS67]. In detail the Cayley transform  $V$  of an Hermitian operator  $A$  is defined by [AG93]

$$A = i(1 + V)(1 - V)^{-1} \quad (5.6.3)$$

where  $V$  is unitary. The latter property allows for a norm-preserving finite difference equation approximating (5.6.2). Explicitly, the exponential operator can be written as

$$e^{-iH\tau} = \frac{1 - \frac{i}{2}H\tau}{1 + \frac{i}{2}H\tau} \quad (5.6.4)$$

This approximation is accurate to second-order in time and suggests an evolution of the form

$$\left(1 + \frac{i}{2}H\Delta t\right)\psi(t_{n+1}) = \left(1 - \frac{i}{2}H\Delta t\right)\psi(t_n). \quad (5.6.5)$$

The Hamilton operator itself is evaluated at the intermediate time  $t_n + \Delta t/2$ .

The disadvantage of the Crank-Nicholson scheme is its implicit character, i. e. a linear system of equations has to be solved for each time-step. On the other hand, the advantage of this scheme is that it is unitary and stable, in other words, the norm of the wavefunction is unchanged in each time step and roundoff and discretisation errors are bounded from above.

For the Hamiltonian we insert the expression from Eq. (5.1.8), which is cyclic in the parameter  $\phi$ , the azimuthal angle of the magnetic field. According to the given angular frequency of the rotation  $\omega_r = 2\pi/T$  the state vector is iterated  $\frac{2\pi}{\omega_r\Delta t}$  times. If all the adiabatic constraints are satisfied by the specific choice of the parameters the polarisation of the final state should be equal to the polarisation of the initial state, but there is a difference of the relative phase. Before discussing the obtained results we have to discuss the modelling of the artificial noise.

## 5.6.2 Noise model

As for the numerical simulation of the noise fluctuations we resort to a Fourier series representation (Eq. A.5.1) to model the Ornstein-Uhlenbeck noise process with given power spectrum. The power spectrum is given by a Lorentzian curve with bandwidth proportional to the inverse of the relaxation time,  $\omega_n = 2\pi/\tau_n$ . The sum in Eq. (A.5.1) has to be terminated at some point where all significantly contributing frequencies are included, e. g.  $\omega_n^{max} = 7\omega_n$ .

### Division of the frequency

Still, we have to bother about the discretisation of the frequency range  $\omega \in [0, 7\omega_n]$  into small increments  $\Delta\omega$ . The frequency interval  $\Delta\omega$  in the Fourier representation of the noise process in Eq. (A.5.1),

$$X(t) = \sum_{k=1}^K [A_k \cos \omega_k t + B_k \sin \omega_k t], \quad \omega_k = k\Delta\omega, \quad (5.6.6)$$

sets a natural limit to the total time  $T$  of the process without repetitions. The lowest angular frequency  $\omega_{min} = \Delta\omega$  determines the period

$$\tilde{T} = 2\pi/\Delta\omega \quad (5.6.7)$$

of subsequent repetitions of the time series  $X(t)$ . As a consequence, the number of terms  $K = \omega_n^{max}/\Delta\omega$  has to be chosen such that  $\Delta\omega$  is small enough in order to avoid repetitions of the noise pattern during the evolution time ( $\tilde{T} > T$ ). The periodicity of the noise pattern can be seen in the correlation function  $C(t)$  (Eq. A.1.8) shown in Figure 5.22. Here, spikes appear at integer multiples of the period  $\tilde{T}$ .

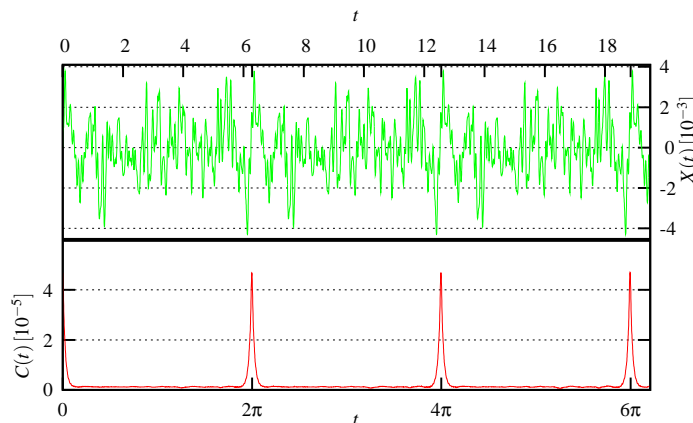


Figure 5.22: Using too low a division of the frequency range  $[0, K\Delta\omega]$  in the Fourier representation of the noise process  $X(t)$  leads to repetitions of the same process. The correlation function for a process with diffusion constant  $c = 1/7 \times 10^{-2}$ , relaxation time  $\tau_n = 2\pi/\omega_n = 14\pi \times 10^{-2}$  s,  $K = 100$  and, therefore,  $\Delta\omega = \omega_n^{max}/K = 7\omega_n/K = 1$ . The period is  $\tilde{T} = 2\pi$  and 20 realisations each for 20 seconds have been performed.

Does this have an influence on the results for the variance of the geometric phase? We test the influence with the following parameters:  $\omega_L = 10^4$  rad/s,  $T = 1$  second ( $\omega_r = 2\pi$  rad/s),  $\omega_n = 50$  rad/s,  $c = 1 \times 10^8$  rad/s ( $P = 10^3$  rad/s) and a polar angle of  $\vartheta = \pi/2$ , i. e. a rotation along the equatorial line. The time increments are  $\Delta t = 2 \times 10^{-5}$  s. The critical value for a total angular frequency range of  $7/\tau$  is at

$$K = \frac{\omega_n^{max}}{\Delta\omega} = \frac{\omega_n^{max}\tilde{T}}{2\pi} = \frac{7\omega_n}{2\pi} \approx 55.$$

Hence, we start at  $K = 10$  and watch the behaviour of the variance for increasing  $K$  by computing 100 realisations for each value. If we run the simulation with different  $K$  for the same frequency bandwidth we can see (Figure 5.23) that the variance seems to be stable after a certain frequency division higher than  $K = 55$ .

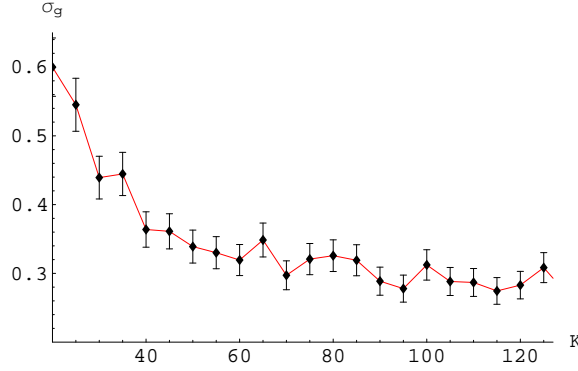


Figure 5.23: Variance for different  $K$  when constructing the stochastic process for the noise.

### Noise envelope function

Since we want the spin to end up in the same state as the initial state we have to model an adiabatic switch on and off of the noise field. If the transition to the static, non-fluctuating field is adiabatic the spin will point in the direction of the initial state at the end and only the phase carries the memory of the foregoing evolution.

We choose a smeared out rectangular envelope function for this purpose (Figure 5.24). Its mathematical form is given by

$$e(t) = \frac{1}{1 + e^{-c(t-d)}} - \frac{1}{1 + e^{-c(t-(T-d))}}, \quad (5.6.8)$$

where  $T$  is the total evolution time,  $d$  is the position where  $e(t) = 0.5$  and  $c$  is responsible for the smoothing of the edges of the function. More precisely, taking a value of  $e^{-c(t-d)}|_{t=0} \approx -10^{-4}$  as criterion that the function has approached unity reasonably well, we find

$$cd = -\ln 10^{-4} \quad \rightarrow \quad c = \frac{4 \ln 10}{d}. \quad (5.6.9)$$

The value of  $d$  depends on the Larmor frequency  $\omega_L$  of the magnetic guide field, so we set  $d = 5 \times 2\pi/\omega_L$  to guarantee adiabaticity.

### Size of time increments

Similar precautions have to be taken by choosing the size of the time increments  $\Delta t$  in the simulations. The sampling theorem tells us that for a perfect reconstruction of a continuous signal the sampling frequency has to be at least twice the bandwidth of its frequency

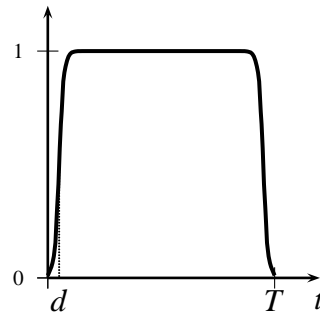


Figure 5.24: Envelope function  $e(t)$  for  $c = 90$  and  $d = 0.05$  for  $T = 1$ .

bandwidth. The other way round with a given sampling frequency the maximum frequency that can be generated without side-effects (aliasing) is half of the sampling. This critical frequency is also called *Nyquist's frequency*. In our case the highest frequency involved is the Larmor frequency determined by the magnetic guide field,  $\omega_L = 2\mu B/\hbar$  and is typically of the order  $10^{-4}$  rad/s corresponding to a frequency of  $\nu_L \approx 1.7$  kHz. The largest time increment  $\Delta t_{max}$  is determined by  $\Delta t_{max} = 1/2\nu_L \approx 3 \times 10^{-4}$  s. We choose a constant  $\Delta t$  throughout the simulations since an adaptive time increment makes sense only if the driving Hamiltonian shows changes of different time scales in different domains. Here, however,  $\omega_L$  is constant throughout the evolution.

To test the dependency on the size of the time increments we conducted the following experiments: For a given Larmor frequency  $\omega_L = 10^4$  rad/s, given noise bandwidth  $\omega_n = 100$  rad/s and power  $P_3 = \sqrt{5} \times 10^{5/2}$  rad/s we measured the variance as a function of the angular frequency  $\omega_r$  by changing time increments. From the Figures 5.25 one realises that the simulated phase and its variance do not depend significantly on the time steps chosen up to the largest time increment  $\Delta t_{max} = 3 \times 10^{-4}$  s.

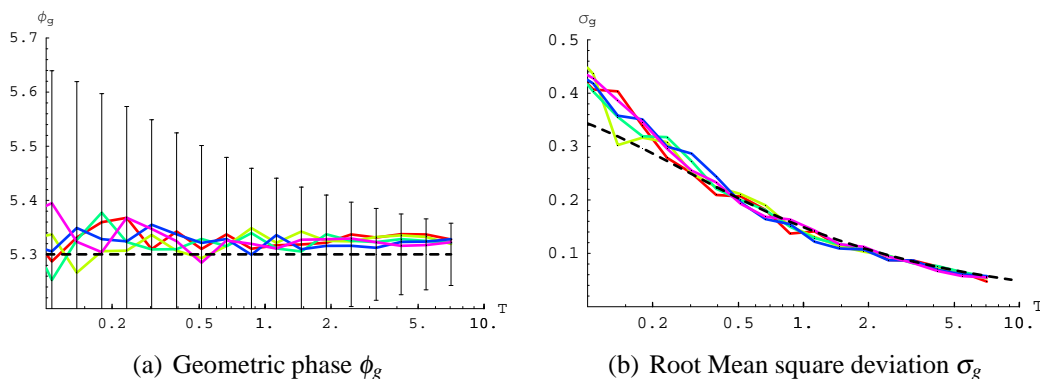


Figure 5.25: Geometric phase and its variance for different sizes of the time-increments  $\Delta t \in [2 \times 10^{-5}, 3 \times 10^{-4}]$ . The dotted line indicates the theoretical value.

### Choice of the mean geometric phase

In order to see the influences of the noise fluctuations on the variance of the geometric phase best we want to maximise  $\sigma_{\phi_g}^2$  in Equation (5.1.15) with respect to the polar angle  $\vartheta$ . We notice that the variance scales with the geometric factors  $\sin^2 \vartheta$  and  $\sin \vartheta \cos \vartheta$ , respectively. Clearly, the first term is maximal at  $\vartheta = \pi/4$ , whereas the second term is maximal at  $\vartheta = \pi/2$ . The noise fluctuations in the components in the equatorial plane have maximal effect if the magnetic field is inclined by  $45^\circ$ , and the fluctuations along the z-direction perturb the geometric phase maximal for a field circulating in the equatorial plane. The latter property becomes clear by considering the other extreme where both noise fluctuations and magnetic field are both pointing in the z-direction ( $B_0 = B_3$  and  $P = P_3$ ). Then the fluctuations change only the dynamical phase but not the path, whereas for perpendicular fluctuations the modification of the path is maximal. Without loss of generality we will consider only noise either in z-direction or along the instantaneous magnetic field direction. Although for the noise in z-direction  $\vartheta = \pi/2$  would be optimal to examine the fluctuations, the mean geometric phase is in this case just  $\pi$  and cannot be deduced from polarimetric data (Eq. 5.5.5). In conclusion, we select a polar angle close to  $\pi$ , for instance  $\vartheta = 9\pi/20$  for the following simulations.

### 5.6.3 Numerical results for different parameter settings

The main purpose of doing numerical simulations is to check the range of applicability of the expression (5.1.15) for the variance of the geometric phase. Although we can derive some rough estimations of the allowed parameter ranges, the limits of adiabaticity have to be examined more carefully via computer numerics since we do not have an analytical expression valid for all cases.

#### Fluctuating magnetic field strength

In Figure 5.26 the geometric phase and its standard deviation is depicted for weak noise in the *instantaneous* direction of the magnetic field, that is, only the strength of the magnetic field changes. In the ideal case the geometric phase must not be disturbed at all since all contributions are due to the dynamical phase since the path does not change. This simulation provides a test for the quality of the simulations, since theoretically only in the non-adiabatic region non-vanishing variance is allowed. Here,  $\omega_L = 10^4$  rad/s,  $s_r = \omega_L/P = 200$  and  $\omega_n = 100$  rad/s. Only for times smaller than the inverse noise frequency range  $2\pi/\omega_n \approx 0.06$  s we can observe deviations indicating that the noise does not have time make many uncorrelated fluctuations anymore.

#### Noise fluctuations in fixed direction

In the second scenario we choose noise added only to the z-component of the magnetic field. In contrast to the former where the noise was along the instantaneous axis and did not perturb

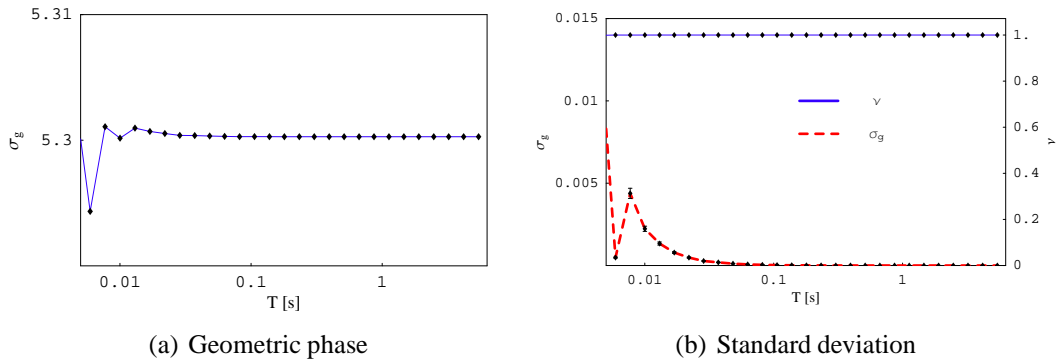


Figure 5.26: Noise along the instantaneous magnetic field direction does not disturb the geometric phase. Here the noise is two orders of magnitude smaller than the magnetic field (signal-to-noise ratio  $s_r = 200$ )

the path of the state, we expect now a deviation of the path and therefore a contribution to the standard deviation of the geometric phase due to this kind of noise.

**Varying noise strength ( $\omega_n = 50$  rad/s)** Clearly, the variance of the geometric phase depends on the amplitude of the noise fluctuations, but for long evolution time  $T$  the variance vanishes in either case. It is interesting that even for strong noise in  $z$ -direction (signal-to-noise ratio  $s_r \approx 1$ ) the variance vanishes, but the evolution time must be quite long. In Figures (5.27) the theoretical predicted standard deviation of the geometric phase along with the results from numerical simulations are shown for different amplitudes of the noise (at  $\omega_L = 10^4$  rad/s,  $\omega_n = 50$  rad/s,  $\Delta t = 10^{-4}$  s and  $\vartheta = 9\pi/20$  rad). In the right figure the exponential damping factor (visibility)  $\nu = e^{-8\sigma_g^2}$  of the polarisation (5.5.8) is shown from which we can estimate whether any difference will be noticed in a real experiment. In the last figure (c) the average geometric phase is depicted.

The theoretical predictions are different to the numerical results for fast cycles which can be explained by bearing in mind that under such circumstances the noise does not have enough time to make uncorrelated fluctuations, hence the noise process is not an O.U process anymore and the analytical expression in Eq. (5.1.15) does not have to be valid. A second property is that the numerical results are further away from the analytical curve for strong noise which is also no surprise due to the use of a first-order approximation. For weak noise and long times the computed values are in agreement with theory.

In order to get a feeling for the allowed noise strength the root-mean-square  $\sigma_g$  is plotted for increasing noise power  $P_3$  for a fixed cycle length  $T$  in Figure 5.28. According to the findings in Section 5.1.2 on the domain of validity of the adiabatic approximation, deviations from the theoretical curve start at  $s_r \approx 10$ .

**Broader noise bandwidth ( $\omega_n = 250$  rad/s)** Let us have a look at other noise frequencies. Setting the bandwidth  $\omega_n = 250$  rad/s we notice that the theoretical curve is approximately met already at a cycle time  $T \approx 0.1$  s compared to  $T \approx 0.5$  s above (c. f. Figure 5.29). The

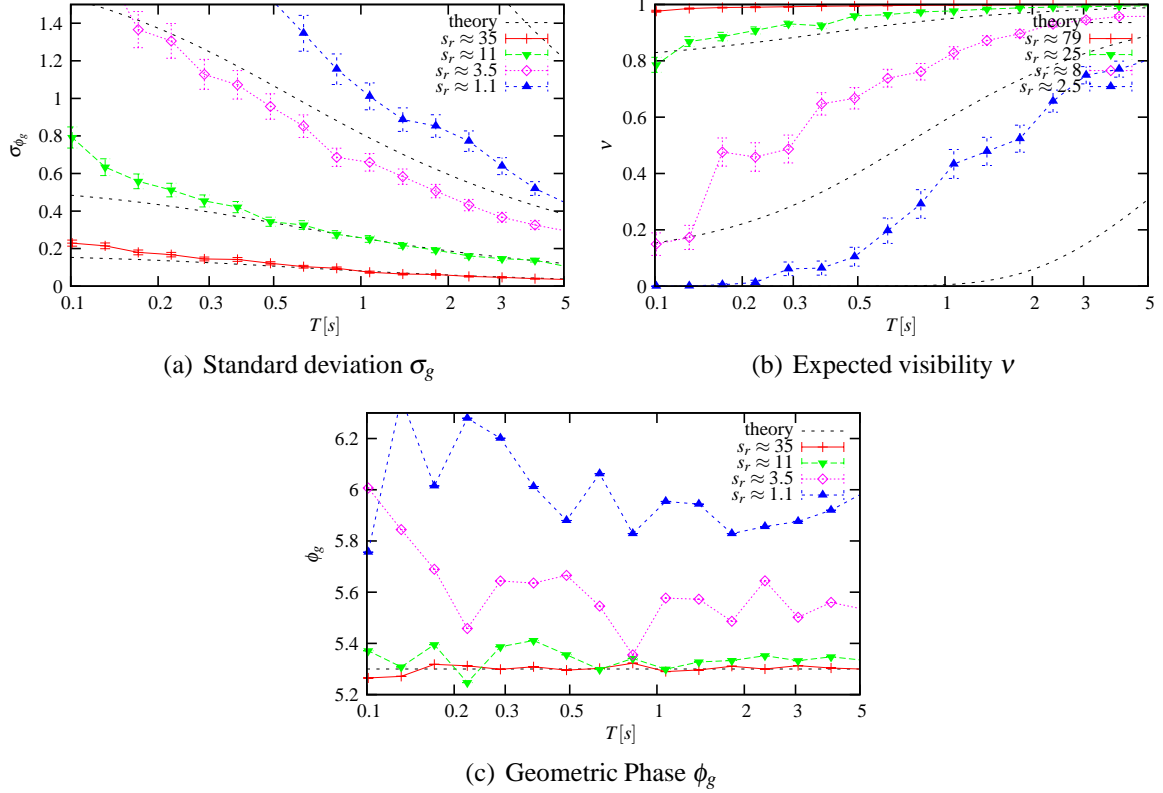


Figure 5.27: Variation of the noise amplitude  $P_3$ . The (a) standard deviation, the (b) expected visibility and (c) the mean geometric phase are shown for  $s_r = c 10^2 \approx 35$ ,  $s_r = c 10^{3/2} \approx 11$ ,  $s_r = c 10^1 \approx 3.5$  and  $s_r = c 10^{1/2} \approx 1.1$  ( $c = 1/\sqrt{8}$ ). The noise bandwidth is kept fixed at  $\omega_n = 50$  rad/s,  $\omega_L = 10^4$  rad/s and  $\vartheta_0 = 9\pi/20$ .

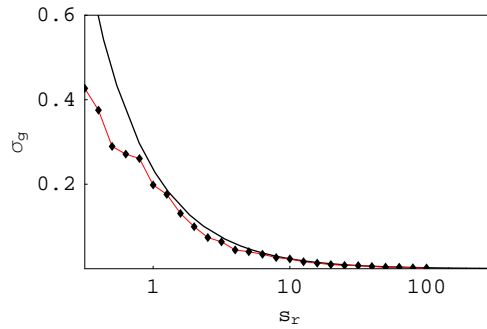


Figure 5.28: Root-mean-square of the geometric phase  $\sigma_{\phi_g}$  for varying mean noise power  $P_3$  at  $T = 1.57$  s ( $\omega_r = 4$  rad/s),  $\omega_n = 50$  rad/s. The guide-field is at  $\omega_L = 10^4$  rad/s and accordingly we notice deviations from the adiabatic approximation if  $P_3$  is about one order below  $\omega_L$  ( $s_r < 10$ ).

noise has more time to fluctuate during one cycle and the area enclosed by the path on the Bloch sphere is better approximated. The decrease of the variance compared to the former setting with  $\omega_n = 50$  rad/s is due to the weaker noise.

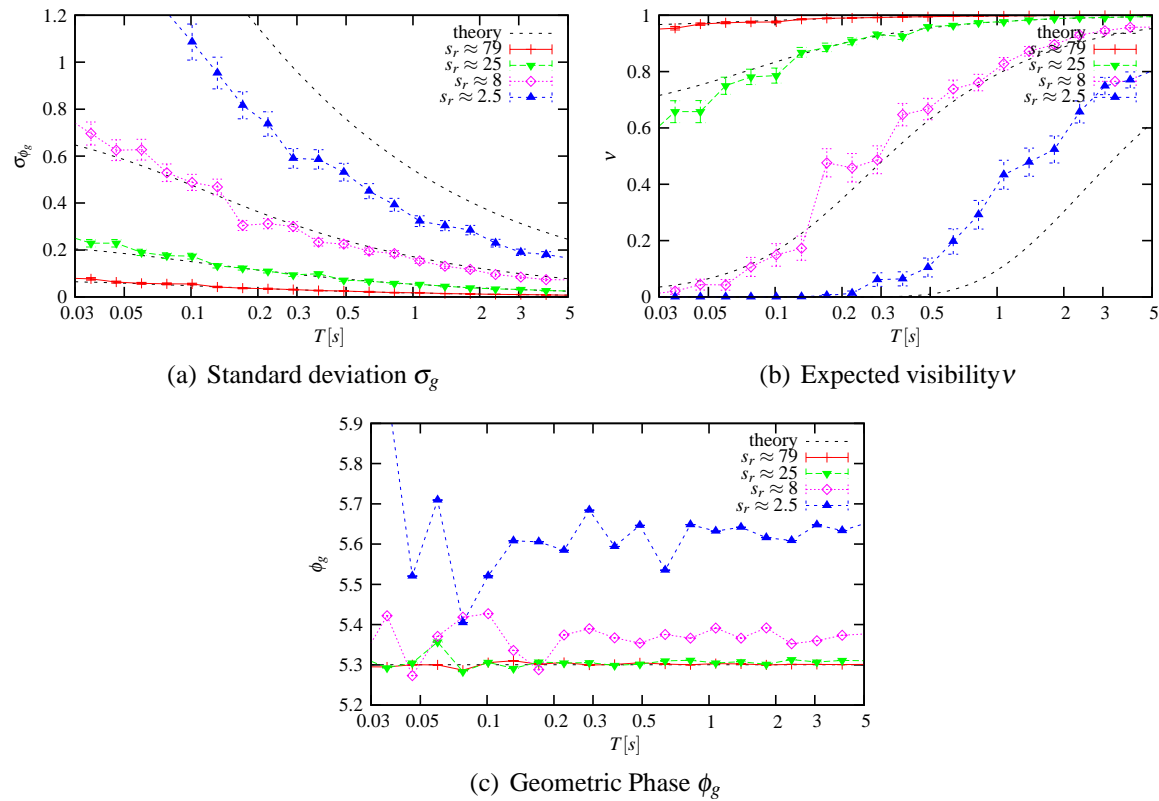


Figure 5.29: Variation of the noise amplitude  $P_3$  for a noise bandwidth  $\omega_n = 250$  rad/s. The (a) standard deviation, the (b) expected visibility and (c) the geometric phase are shown for  $s_r = c 10^2 \approx 72$ ,  $s_r = c 10^{3/2} \approx 25$ ,  $s_r = c 10^1 \approx 8$  and  $s_r = c 10^{1/2} \approx 2.5$  ( $c = 1/\sqrt{8/5}$ ).

**Even broader bandwidth ( $\omega_n = 500$  rad/s)** For  $\omega_n = 500$  rad/s we obtain similar figures (5.30). For the whole range of  $T$  the agreement with the theoretical values is very good. Looking at the visibility plot we notice, that for the setup with  $s_r = 10^{3/2}/2\sqrt{2} \approx 11$ , i. e. one order in magnitude difference between the Larmor frequency of the guide-field and the noise strength, it should be possible to observe the increase in visibility (= average degree of polarisation) also in an experiment for cycles with duration between about 0.1 - 10 seconds.

### Modification of the mean geometric phase

If one looks at the mean geometric phase in the simulations shown above, there is definitely one issue left to clarify. According to the first order deviation of De Chiara and Palma the mean geometric phase should not be affected by the noise fluctuations. However, this is valid only in the weak coupling limit for low noise amplitudes, for stronger noise one can immediately see that the mean geometric phase does not coincide with the noise-free

## 5. GEOMETRIC PHASE AND ADIABATIC FLUCTUATIONS

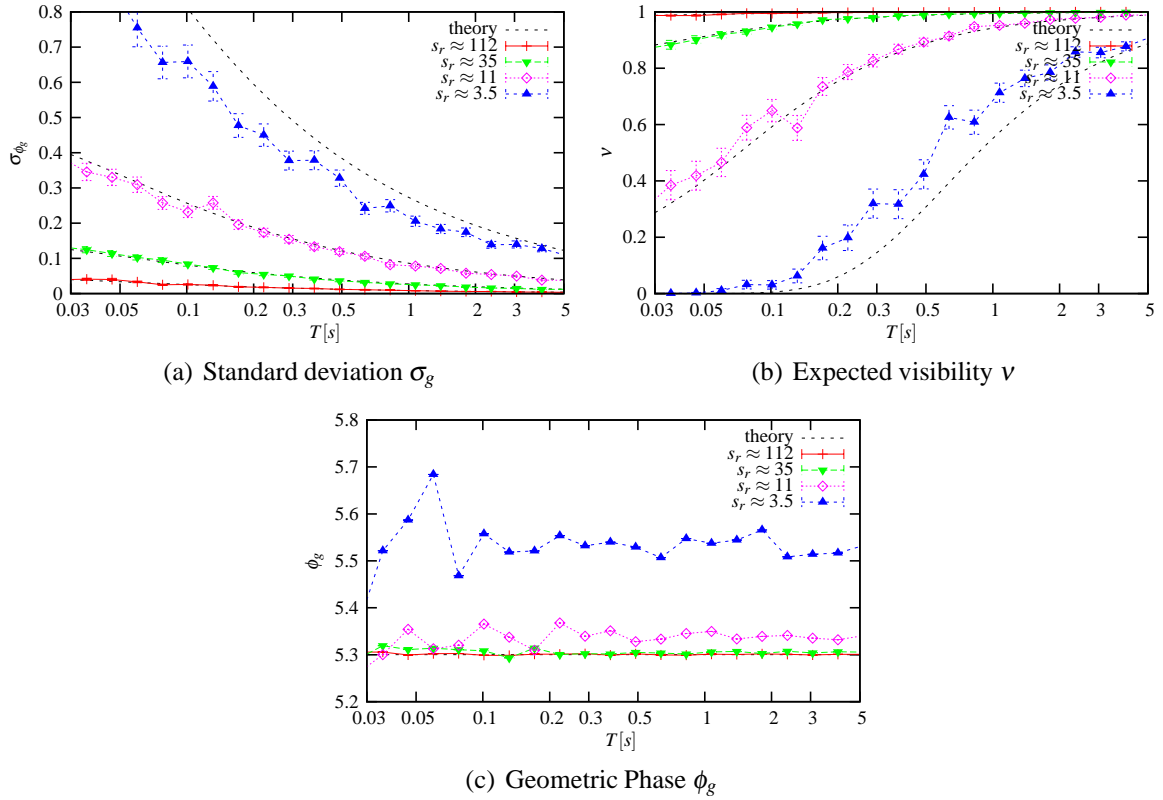


Figure 5.30: For a noise bandwidth of  $\omega_n = 500$  rad/s the noise amplitude  $P_3$  is varied. The (a) standard deviation, the (b) expected visibility and (c) the geometric phase are shown for  $s_r = c 10^{5/2} \approx 112$ ,  $s_r = c 10^2 \approx 35$ ,  $s_r = c 10^{3/2} \approx 11$  and  $s_r = c 10 \approx 3.5$  ( $c = 1/\sqrt{8}$ ).

geometric phase. In Figures 5.31 the mean geometric phase and its standard deviation are plotted for different settings of  $\vartheta \in [0, \pi]$  with large noise amplitude (signal-to-noise ratio  $s_r = 2.5$  for  $\omega_L = 10^4$  rad/s and  $P_3 = 4 \times 10^3$  rad/s). The difference between the zero-noise

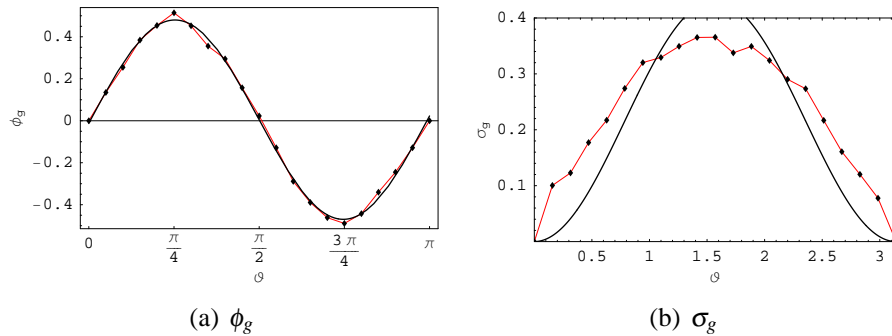


Figure 5.31: Difference between zero-noise and strong noise mean geometric phase  $\delta\phi_g$  (a) and its root-mean-square value  $\sigma_g$  (b) for strong noise for different polar angles  $\vartheta$ .

and the strong noise mean geometric phase follows evidently a sinusoidal law, a fit of the data yields  $\delta\phi_g(\vartheta) = 0.47 \sin(2\vartheta)$ .

Can this deviations be explained by geometrical considerations? Since the geometric

phase depends only on the solid angle enclosed by the path of the polarisation vector on the Bloch sphere these deviations must result from average net changes in the solid angle due to the fluctuations. The calculation of the geometric boils down to the calculation of a surface integral and we will recognise that the curvature of the surface is the reason why the average  $\phi_g$  is modified.

**Map onto a sphere** As an illustration, take for example a rectangle on a plane and modify the upper boundary by adding or subtracting rectangular areas (Figure 5.32). If the amount of added space is equal to the subtracted one, the area won't change. However, if the rectangle is mapped onto a sphere the appended and the removed areas are not of same magnitude anymore, unless the upper boundary coincides with the equator.

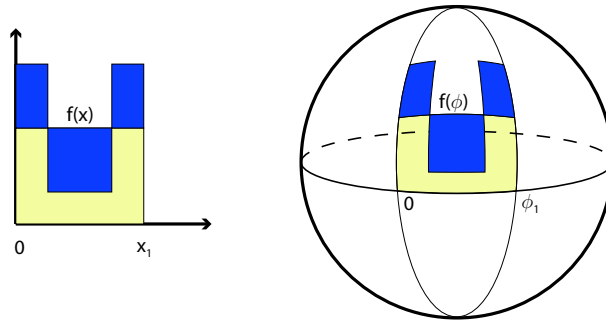


Figure 5.32: Non area-preserving map of the noise fluctuations from  $\mathbb{R}^2$  to the  $S^2$ .

The geometric phase is determined by the area enclosed by the path on the sphere along the line of latitude specified by  $\vartheta_0$ ,  $\phi_g = \pi(1 - \cos \vartheta_0)$ . Adding noise fluctuations  $\delta_z$  in the  $z$  direction modifies  $\vartheta$  to  $\vartheta_0 + \delta_\vartheta(\phi)$ , where  $\delta_\vartheta(\phi)$  depends on the instantaneous azimuthal angle  $\phi$  on the path. A calculation of the resulting geometric phase with noise  $\tilde{\phi}_g$  requires to solve the integral

$$\tilde{\phi}_g = \int_0^{2\pi} d\phi \int_0^{\vartheta(\phi)} d\vartheta \sin \vartheta. \quad (5.6.10)$$

Performing the  $\vartheta$  integration yields

$$\tilde{\phi}_g = \int_0^{2\pi} d\phi (1 - \cos \vartheta(\phi)). \quad (5.6.11)$$

For noise fluctuations in  $z$ -direction,  $\vartheta(\phi)$  describes a stochastic process which is a functional of the stochastic process  $Z_t = Z_0 + \delta_Z(t)$ , of the noise of the magnetic field in Cartesian coordinates. To solve this integral the statistical properties of  $Z_t$  have to be translated to the statical properties of the polar angle  $\vartheta(\phi)$  in spherical coordinates. This, however, is rather involved and I will stick to a simpler procedure in order to obtain at least qualitative results, whether our conjecture holds that the deviation from the noise-free geometric phase is an artifact of geometry itself.

The distribution function  $p_\vartheta(\phi)$  of  $\vartheta$  at a specific azimuthal angle  $\phi$  can already provide insight into the behaviour of the mean geometric phase. With the help of the distribution

function  $p_{\vartheta}(\phi)$  the mean value  $\overline{\vartheta}$  can be calculated. If it does not coincide with the noise-free polar angle  $\vartheta_0$  also the geometric phase as the integral over all  $\phi$  values will be shifted. It is not difficult to find the distribution function  $p_{\vartheta}$  of  $\vartheta$ .  $\vartheta$  is determined by

$$\begin{aligned} \vartheta &= \arccos \frac{Z}{B} = \arccos \frac{Z}{\sqrt{B_r^2 + Z^2}} \\ &= \begin{cases} \pi - \arccos \frac{1}{\sqrt{1+(B_r/Z)^2}} = \pi + \arctan \frac{B_r}{Z} & \text{for } Z \leq 0 \\ \arccos \frac{1}{\sqrt{1+(B_r/Z)^2}} = \arctan \frac{B_r}{Z} & \text{for } Z \geq 0 \end{cases}, \end{aligned} \quad (5.6.12)$$

where  $Z$  denotes the magnetic field component in  $z$ -direction and  $B_r = (B_x^2 + B_y^2)^{1/2}$  the magnetic field in the equatorial plane. In other words, we can write down the map  $f$  that transforms the  $Z$  component of the magnetic field to the polar angle  $\vartheta$ :

$$f: \begin{cases} Z \in (-\infty, 0) \mapsto \vartheta = \pi + \arctan \frac{B_r}{Z} \in (\pi, \pi/2) \\ Z \in (0, \infty) \mapsto \vartheta = \arctan \frac{B_r}{Z} \in (\pi/2, 0) \end{cases} \quad (5.6.13)$$

The distribution function  $p_{\vartheta}$  can be written in terms of the distribution  $p_Z$  of  $Z$  by

$$p_{\vartheta} = p_Z(f^{-1}(\vartheta)) \left| \frac{df^{-1}(\vartheta)}{d\vartheta} \right| \quad (5.6.14)$$

which follows from the substitution rule of calculus. The inverse of the map  $f$  is

$$Z = h^{-1}(\vartheta) = \frac{B_r}{\tan \vartheta} \quad (5.6.15)$$

and its derivative

$$\frac{d}{d\vartheta} h^{-1}(\vartheta) = -\frac{B_r}{\sin^2 \vartheta} \quad (5.6.16)$$

Plugging this into (5.6.14) yields

$$p_{\vartheta}(\vartheta) = \frac{B_r}{\sin^2 \vartheta} p_Z \left( \frac{B_r}{\tan \vartheta} \right). \quad (5.6.17)$$

If we assume an Ornstein-Uhlenbeck random process (Appendix A.3),  $Z$  is Gaussian distributed with mean value  $Z_0$ ,

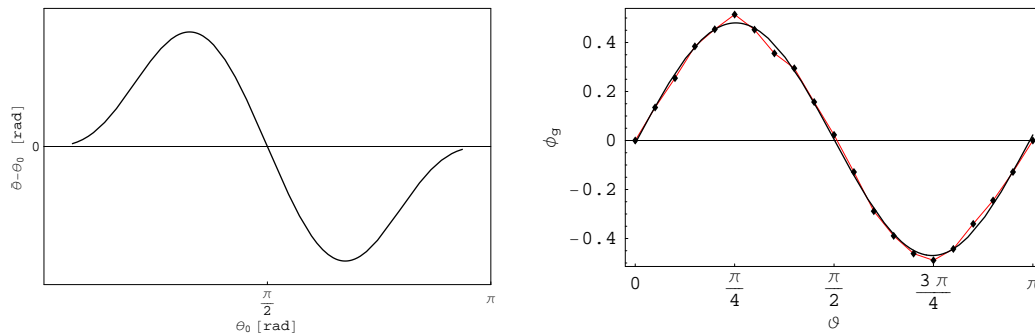
$$p_Z(z) = \frac{1}{\sqrt{2\pi\sigma^2}} e^{-\frac{(z-Z_0)^2}{2\sigma^2}}. \quad (5.6.18)$$

This leads finally to the distribution function of  $\vartheta$ :

$$p_{\vartheta}(\vartheta) = \frac{1}{\sqrt{2\pi\sigma^2}} \frac{B_r}{\sin^2 \vartheta} \exp \left[ -\frac{B_r^2 \left( \frac{1}{\tan \vartheta} - \frac{1}{\tan \vartheta_0} \right)^2}{2\sigma^2} \right]. \quad (5.6.19)$$

$p_{\vartheta}$  is not Gaussian anymore and it is therefore not surprising that the mean  $\overline{\vartheta} = \int p_{\vartheta}(t) t dt$

is not necessarily the same as the noise-less azimuthal angle  $\vartheta_0$  since the distribution is not symmetric around  $\vartheta_0$ . Only around  $\pi/2$ , an evolution along the equator, the  $(\sin\theta)^{-2}$  factor is symmetric and therefore  $\vartheta_0 = \bar{\vartheta}$ . Generally speaking, if (at least) quadratic contributions are included the mean value is shifted. In Figure 5.33(a) the difference  $\bar{\vartheta} - \vartheta_0$  is shown for different angles  $\vartheta_0$  denoting the unperturbed polar angle  $\vartheta_0 = \arctan B_0/Z_0$ . This is qualitatively in good agreement to the data from numerical simulations plotted alongside (Figure 5.33(b)). The negative offset for  $\vartheta > \pi/2$  and the positive offset for  $\vartheta < \pi/2$  corresponds to an evolution path below or above the equatorial line, respectively. For  $\vartheta_0 = \pi/2$  the fluctuations average out as predicted since the distribution is symmetric at this point. Unfortunately, there is still a mismatch to the numerical data which probably stems from the particular features of the noise process itself. Here, we have only taken the instantaneous distribution of the fluctuations into account, but not that the magnetic field is actually a random process. The correlations at different times have been totally neglected.



(a) Theory without taking the noise process properties into account. (b) Numerical simulations show about the same behaviour.

Figure 5.33: The difference  $\bar{\vartheta} - \vartheta_0$  between the mean value  $\bar{\vartheta}$  of the polar angle  $\vartheta$  and the zero noise mean  $\vartheta_0$ .

Nevertheless, this is a beautiful demonstration of the geometric nature of the geometric phase. In the previous derivation only geometry has played a role without any reference to quantum mechanical states and their phases. A future issue is to obtain a better analytical approximation to the numerical data. Also, it has to be clarified how this relates to the studies of Whitney *et al.* [WMSG05] who have calculated a non-vanishing shift of the geometric phase from fluctuating fields.

### 5.6.4 More spin flips

In the end, I want to shortly comment on the possibility to get rid of the dynamical phase if one does not know anything about the noise fluctuations. In the current scheme the dynamical phase is removed by changing the polarity of the magnetic field and apply the *same* noise twice. This is good enough for a computer simulation and for a proof-of-principle experiment, however, if one is eager to benefit from the robustness of the geometric phase in a real life experiment or even in a real life appliance the noise cannot be copied. Otherwise,

one could compensate all influences anyway without need of the geometric phase. How to solve this problem is still an open issue. Maybe a *refocusing scheme* could put things right [Ved05]: By performing not just one reversal of the magnetic field one can make many of them in the hope that the variance of the dynamical phase vanishes in the limit of many (but not infinitely many) flips. As in the spin-echo the geometric phase is not affected by reversing the magnetic field.

With the simulation program at hand this can be implemented and the results are shown in Figure 5.34. There is definitely an improvement in the standard deviation of the final phase difference, although an lower bound of the variance seems to be reached for large numbers of flips.

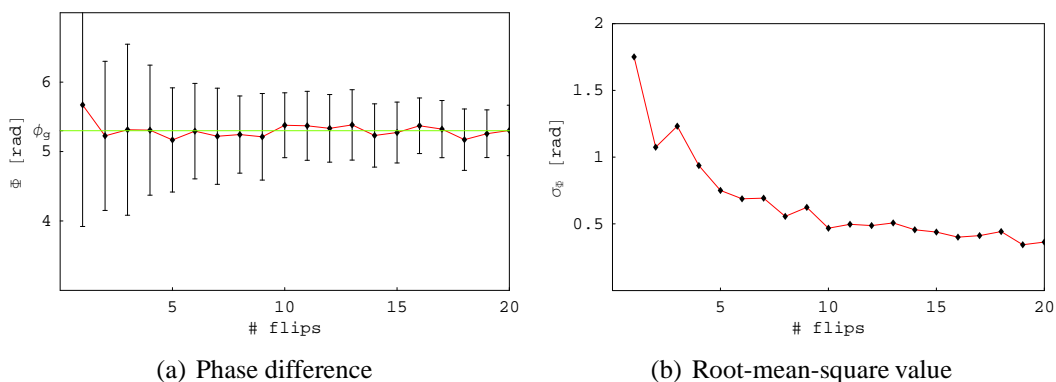


Figure 5.34: Mean and root-mean-square value of the phase difference after one rotation for an increasing number of flips of the magnetic field.

## 5.7 Conclusions

There is hope that the geometric phase is more stable than the dynamical phase, meaning that for certain perturbative influences from the environment the error (or uncertainty) in the accumulated phase is smaller in comparison. Theory indicates that this is the case for an adiabatic evolution of a neutron in a magnetic field with some not too fast perturbations such that the adiabatic approximation is still valid. However, an experiment is needed that can show the validity of this approximative result and after discussing other alternatives we ended up with a proposal of an experiment with stored ultra-cold neutrons. In order to get rid of the dynamical noise influences a spin-echo scheme can be used, with the drawback that the noisy fluctuations have to be artificially constructed. Otherwise, there is no chance to get rid of dynamical contributions. After two similar excursions of the spins there is only the geometric phase left which is spread about some mean value due to the different stochastic noise contributions in each experimental run. It is predicted that the mean value stays constant and, furthermore, that the variance tends to zero, if the evolution time is long enough.

In view of a potential experimental realisation it is not trivial to adjust the different parameters to make a verification of this feature feasible. Most problematic are the different restrictions on the involved frequency ranges in order to stay in the adiabatic domain and we have to resort to numerical simulations helping us to estimate and explore the suitable parameter range for an experiment. The theoretical predictions, i. e. the claimed stability of the geometric phase could be verified numerically for various parameter settings and it seems likely that such an experiment is possible so that the stability of the geometric phase can be tested also experimentally.

A subtle issue showing up in the simulations remains to be clarified: For stronger noise perturbations the mean geometric phase is not a constant any longer since the noise process assumed to have zero mean is mapped onto the spherical parameter space (which is equal to state space in the adiabatic case). This map from a flat to a curved manifold yields a noise process which is not centred anymore and a mean geometric phase that is not identical to the noiseless one anymore.

In the Appendix D further details on the planned setup are presented.

# Chapter 6

## Conclusions and Outlook

The geometric phase in quantum mechanics is the main issue in this thesis. In particular, three manifestations have been explored, off-diagonal geometric phases for general mixed states, a non-cyclic spatial geometric phase in a double-loop neutron interferometer experiment and a noisy geometric phase emerging from the spin evolution of a neutron. These different topics demanded for different methods. The off-diagonal mixed state geometric phase has been studied theoretically, there has been an experiment on the spatial geometric phase at the neutron reactor at the Institute Laue Langevin, Grenoble, and the connection of noise perturbations and the geometric phase has been investigated by means of numerical simulations.

As for the former, a definition of an off-diagonal geometric phase has been found which generalises the mixed state geometric phase concept of the interferometric type as well as the Uhlmann holonomies. The geometric phase, in general, gives a hint on the topological structure of the subjacent Hilbert space, but there are nodal points, i. e. points in state space where it is undefined, and nothing can be said about the underlying geometry. To have a measurable expression at hand that also works in such situations, off-diagonal extensions are needed. They share the property of reducing on the one hand side to the pure state off-diagonal geometric phase and on the other hand side including also their diagonal analogue as a special case. Furthermore, they are, as is right and proper for a geometric phase, gauge and reparametrisation invariant. In other words, they are a property only of paths of mixed states, while dynamical quantities like energy and time are immaterial. Clearly, one can also find physical examples where such phases come in useful. Two coupled Mach-Zehnder-interferometers with an entangled photon pair as input state can be used to measure the interferometric off-diagonal geometric phase for mixed states.

Next, it has been substantiated that a geometric phase can be ascribed to the paths of neutrons through an interferometer. A previous experiment demonstrated the cyclic case, but there was harsh criticism denying the correct measurement of a geometric phase. With the present experiment it has become clear that the measured shift in the interference fringes can be ascribed to a geometric phase of the non-cyclic case. First, the paths in state space, that is, on the Bloch-sphere, have been devised and the enclosed solid angle proportional to

---

the geometric phase has been calculated. Secondly, one can easily calculate the expected phase shift in a neutron interferometer without falling back onto any kind of geometric argument by merely superposing all the possible beam paths. It turns out that these descriptions are equivalent resulting in the same phase shift whenever one imposes a parallel transport condition on the transport of the neutron state, i. e. for vanishing dynamical phase. Finally, these prediction have been verified experimentally using neutrons travelling through a double-loop perfect-crystal interferometer. The results are coherent with theory to a high degree. Qualitatively, the data plots show the same behaviour as expected, for example, that the sign of the enclosed surface area matters, which depends on the orientation of the surrounding path. Or, if the endpoint of the evolution is opposite to the starting point on the Bloch-sphere one cannot ascribe a certain path since there are infinitely many alternatives to connect these points via a geodesic. This manifests itself in vanishing interference contrast and therefore undefined phase. However, quantitatively, one must admit that there are discrepancies between theory and experiment. The intrinsically different contrasts of the interferometer loops and differently sized phase shifting slabs give rise to additional phase contributions. These systematic effects have been explored in order to quantify the deviations from theory. Altogether, the results substantiate the geometric nature of the measured phase shift.

In the third part, the canonical example of Berry's phase (adiabatic geometric phase), namely a spin-1/2 particle subjected to an adiabatically varying magnetic fields is reviewed for stochastically fluctuating magnetic fields. Recently, it has been shown theoretically [CP03] that the geometric phase stays robust for long evolution times in a classically fluctuating magnetic field, the spread in the measured phase is then only caused by dynamical contributions. The basic idea was to verify this behaviour also experimentally and neutrons seemed to be particularly suited. We have discussed that a neutron interferometry experiment is conceptually best suited, but unfortunately there are sound counter-arguments, like the difficulties in implementing appropriate magnetic fields in an interferometer by coils which produce heat that destroys the contrast. Or, the frequency range for the noise is band-limited by the inductance of the coils and high-frequencies needed for rather fast thermal neutrons are not implementable. The final idea is to use polarised ultra-cold neutrons that can be stored in a box due to their low kinetic energy and by wrapping Helmholtz coils around, their spin can be manipulated. Numerical studies have been made in order to find suitable parameters for the guide-field strength, the evolution speed, the noise strength and the noise bandwidth that can be used to demonstrate the stability of the geometric phase experimentally. These simulations are crucial for spotting the demarcation line to non-adiabatic behaviour. This, in turn, is important since the parameters have to be chosen quite close to the non-adiabaticity regime in order to be able to observe measurable modification of the geometric phase variance also in an experiment. It turns out that there is a set of parameters suited for an experiment. Furthermore, it turns out that the first order approximation of the theory may not be sufficient. At least for stronger noise contributions, an unpredicted deviation of the mean geometric phase is visible as well. This can nicely be visualised again by

means of the spherical shape of state space. A noise process although having zero mean that is mapped onto a sphere yields a shift in the mean geometric phase.

At the end, a detailed description of the ultra-cold neutron experiment is presented in the Appendix D along with some difficulties one has to face when building a real-life experiment. For example, inhomogeneities and external fluctuations of the magnetic field cannot be neglected. To have negligible external influences a strong guide field is needed, but this in turn gives larger phase differences among the different trapped neutrons with different paths in the slightly inhomogeneous magnetic field. The plan is to overcome this and suchlike problems and measure the stability of the geometric phase at soonest. The first experiments are scheduled for the end of the year 2006 and will hopefully be along the lines of the theoretical and numerical predictions.



# Appendix A

## About Noise

Stochastic processes appear at every turn, financial markets, the spreading of diseases, the travelling of dollar banknotes [BHG06], etc. are nowadays modelled using random processes or *noise processes*. Such descriptions go back to the well known example of the *Brownian motion* of a grain particle suspended in fluid [Bro66]. Since we touch here this huge field only peripherally I will just give a short sketch of the basic principles without raising the claim of mathematical rigour. The latter can be found for example in [Öks03, Bil95]. A collection of seminal papers of stochastic processes relevant in physics can be found in [Wax54]. In the following short introduction we will adopt the presentation in [Réf04].

### A.1 Definition of a stochastic process

The notion of a stochastic process is based on *random variables* which are variables that are determined by a random experiment. A simultaneous measurement of, say, the temperature with different apparati does not yield one precise value, but a distribution of values used to determine the average value that we accept then as the current temperature. This distribution makes up a random variable. A (temporal) sequence of random variables constitutes a stochastic process, i. e. if one thermometer is called many times in succession the sequence of values is a single *realisation* of a random process. Taking the whole ensemble of thermometers at each time step we can determine the instantaneous distribution of values and characterise the stochastic process itself, instead of merely one realisation or *trajectory*.

More abstractly, a random variable  $X$  is a map from some abstract sample space  $\Omega$  into the real numbers,  $X : \Omega \mapsto \mathbb{R}$ . For the sake of simplicity, let us stick to a discrete valued example like throwing a die. The sample space is given by the six faces of the die,  $\Omega = \{\cdot, \cdot\cdot, \cdot\cdot\cdot, \cdot\cdot\cdot\cdot, \cdot\cdot\cdot\cdot\cdot, \cdot\cdot\cdot\cdot\cdot\cdot\}$ . When performing an experiment, i. e. throwing the die we assume that one face shows up. The result of an experiment is called an *event*  $\lambda \in \Omega$ . Apparently the simplest example of a random variable is to count the number of dots,  $X_{\cdot}^d = 1, X_{\cdot\cdot}^d = 2, \dots$ . Another example is the random variable  $X_{odd}^p = 0, X_{even}^p = 1$  if just the parity is of interest for the experimenter.

Each time the die is thrown we get a realisation of  $X$  denoted by  $x = X(\lambda)$  with  $x \in$

$\{1, 2, 3, 4, 5, 6\}$  for the first example and  $x \in \{0, 1\}$  for the second. So for each throw (each measurement) we get the outcome  $x_i$ , i. e. the random variable  $X$  takes on the value  $x_i$ .

Now, to each event  $\lambda_i$  out of the sample space  $\Omega$  we can assign a probability  $p_i = P(\lambda_i)$  that  $\lambda_i$  is realised in the experiment. It is not difficult to guess that for the die example  $p_i = 1/6$ , if the die is sufficiently “healthy”. In the second example the sample space  $\Omega$  is partitioned into the subsets  $\{\bullet, \bullet, \bullet, \bullet, \bullet, \bullet\}$  and  $\{\bullet, \bullet, \bullet, \bullet, \bullet, \bullet\}$ . The probability for an event belonging to one of these subsets is  $p_i = 1/2$ .

A stochastic process is then a family of random variables  $X_\lambda(t)$  where  $t$  usually denotes the time parameter. The dependence on  $t$  reflects the possible changes of the stochastic properties of  $X_\lambda(t)$  in time. In a formal definition a stochastic process is defined as a map

$$X : \Omega \times \mathbb{R} \mapsto \mathbb{R}.$$

$X_\lambda(t)$  associates with each  $t \in \mathbb{R}$  and  $\lambda \in \Omega$  a real number  $x_t = X_\lambda(t)$ , one can think of it as a function in two variables: Given  $t$ , the possible values of  $X_\lambda(t)$  are called *states* of the process at  $t$ . Keeping all the events  $\lambda = \lambda'$  fixed and varying  $t$ ,  $X_{\lambda'}(t)$  is a deterministic function, so  $t \mapsto X_{\lambda'}(t)$ , is called a *realisation* or *trajectory* or *sample path* of the stochastic process. In other words, we look at one possible process by choosing a particular outcome of the experiment at each time as depicted in Figure A.1. The *mean* of a random variable

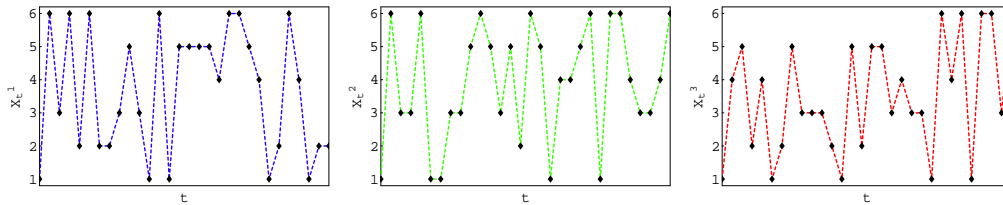


Figure A.1: Three different realisations of the random process “Throwing a die”

$X_\lambda(t_1)$  is denoted by

$$\mu_X(t) \equiv \langle X_\lambda(t) \rangle = \sum x_i p_i(t) \quad \text{or} \quad \mu_X(t) \equiv \int x f_X(x, t) dx, \quad (\text{A.1.1})$$

where  $f_X(x, t)$  is the probability distribution of  $X_\lambda(t)$  and  $x_i$  are the possible outcomes, if  $X_\lambda(t)$  is a discrete map as in the dice example. For continuous random variables  $X_\lambda(t)$  the sum is converted into an integral over all possible values of  $x$ . Similarly, other moments are defined ( $\langle X_\lambda^r \rangle \equiv \sum x_i^r p_i$ ), especially the second moment is needed to define the variance

$$\sigma_X^2(t) \equiv \langle (X_\lambda(t) - \mu_X(t))^2 \rangle = \int (x(t) - \mu_X(t))^2 f_X(x, t) dx. \quad (\text{A.1.2})$$

Examining two random variable  $X$  and  $Y$  correlations between them can be grasped by

calculating the *covariance* function

$$G_{XY}(t_1, t_2) \equiv \langle (X_\lambda(t_1) - \mu_X(t_1))(Y_\lambda(t_2) - \mu_Y(t_2)) \rangle = \langle X_\lambda(t_1)Y_\lambda(t_2) \rangle + \mu_X(t_1)\mu_Y(t_2). \quad (\text{A.1.3})$$

It is common to use the *correlation coefficient*  $\rho_{XY}(t_1, t_2) = G_{XY}(t_1, t_2)/\sigma_X(t_1)\sigma_Y(t_2)$  taking values between  $-1$  and  $+1$ . It is equal to  $1$  if two random variables are perfectly correlated and  $0$  if they are independent. For a stochastic process the correlation function between the noise process at different times  $t_1$  and  $t_2$  is of particular importance. Qualitatively, it tells us something about the memory loss, since if the random variables  $X_\lambda(t_1)$  and  $X_\lambda(t_2)$  are correlated after a finite time  $\Delta t = t_2 - t_1 \neq 0$ , it means that the process at  $t_2$  knows something about its past at time  $t_1$ . If there is no correlation what has happened in the past is immaterial for the present status. The vanishing of correlations determines a specific time scale, the *relaxation time*.

A process is called *stationary*, if the mean  $\mu_X(t)$  is independent of  $t$  and if the covariance function depends only on the time difference  $\Delta t$ . For such a process the covariance simplifies to

$$G_{XX}(t_1, t_2) = G_{XX}(\Delta t) = \langle X_\lambda(0)X_\lambda(\Delta t) \rangle + \mu_X^2. \quad (\text{A.1.4})$$

For a stochastic process  $X_\lambda(t)$  we can define also the time average for fixed  $X_\lambda$ ,

$$\overline{X_\lambda(t)} = \lim_{\substack{T_1 \rightarrow -\infty \\ T_2 \rightarrow \infty}} \left[ \frac{1}{T_2 - T_1} \int_{T_1}^{T_2} X_\lambda(t) dt \right], \quad (\text{A.1.5})$$

where the limits are taken to ensure that the time average does not depend on the integration limits. Similarly, the (*auto*)*correlation function* is defined by the time average

$$C_X(\Delta t) \equiv \overline{X_\lambda(t)X_\lambda(t + \Delta t)} = \lim_{\substack{T_1 \rightarrow -\infty \\ T_2 \rightarrow \infty}} \left[ \frac{1}{T_2 - T_1} \int_{T_1}^{T_2} X_\lambda(t)X_\lambda(t + \Delta t) dt \right], \quad (\text{A.1.6})$$

If  $C_X(\Delta t)$  does not depend on  $\lambda$  it is called *ergodic*, the time averaging removes the dependence on  $\lambda$ , i. e. on the particular trajectory over which the time average is taken. For a stationary and ergodic process the time average is equal to the average at fixed time  $t$  (ensemble average),  $C_X(\Delta t) = G_{XX}(\Delta t)\langle X_\lambda(t)X_\lambda(t + \Delta t) \rangle$ , a property widely used in statistical physics [Réf04].

As for the discussion about coherence in Section 4.8.1 note, that the correlation functions used there are analogous to the definition of  $G_{XX}$  in Eq. (A.1.3). In classical optics the electrical field of light  $E_\lambda(\vec{r}, t)$  is considered as a (complex) random variable. The covariance function

$$G(\vec{r}_1, t_1; \vec{r}_2, t_2) = \langle E_\lambda^*(\vec{r}_1, t_1)E_\lambda(\vec{r}_2, t_2) \rangle - \langle E_\lambda^*(\vec{r}_1, t_1) \rangle \langle E_\lambda(\vec{r}_2, t_2) \rangle$$

is used to define the coherence properties of the beam. The same formalism can be adopted to neutron optics [RWK<sup>+</sup>96, RW00].

The importance of the autocorrelation function is based on the *Wiener-Khinchine* theorem

that relates it to the *power spectral density* function via a Fourier transform,

$$S_X(\nu) = \int_{-\infty}^{\infty} C_X(\tau) e^{-i2\pi\nu\tau} d\tau \quad (\text{A.1.7})$$

for a stationary stochastic process  $X_\lambda(t)$ . Vice versa, the autocorrelation function  $C_X(t)$  can be found via the inverse Fourier transformation ,

$$C_X(t) = \int_{-\infty}^{\infty} S_X(\nu) e^{i2\pi\nu t} d\nu. \quad (\text{A.1.8})$$

The instantaneous power of the fluctuations is defined by the

$$P_X^2(t) = \langle X_\lambda(t) X_\lambda(t) \rangle$$

which is in the stationary case independent of time  $t$  and thus equal to the *mean power*  $P_X^2$ . It can be associated to the covariance  $G_{XX}(t) = \langle X_\lambda(0) X_\lambda(t) \rangle$  by

$$P_X^2 = G_{XX}(0). \quad (\text{A.1.9})$$

From the Wiener-Khinchine theorem the mean power can be expressed in terms of the power spectral density

$$P_X^2 = \int_{-\infty}^{\infty} S_X(\nu) d\nu, \quad (\text{A.1.10})$$

in other words,  $S_X(\nu)$  gives the portion of the mean power in the frequency range  $[\nu, \nu + d\nu]$ .

**White noise** Take a *Gaussian white noise process* as an example: This process comprises all possible frequencies (and is therefore strictly speaking just a theoretical construct that cannot be realised in reality) with a uniform power distribution over all frequencies. It is defined to have zero mean,  $\mu^{WN}(t) = 0$ , at all times  $t$  and  $X_\lambda(t)$  is Gaussian distributed. Its correlation function is proportional to the delta function,  $C_X^{WN}(\tau) \propto P_X^2 \delta(\tau)$ . It follows that its power spectral density is constant,  $S_X(\nu) = P_X^2$  according to (A.1.7).

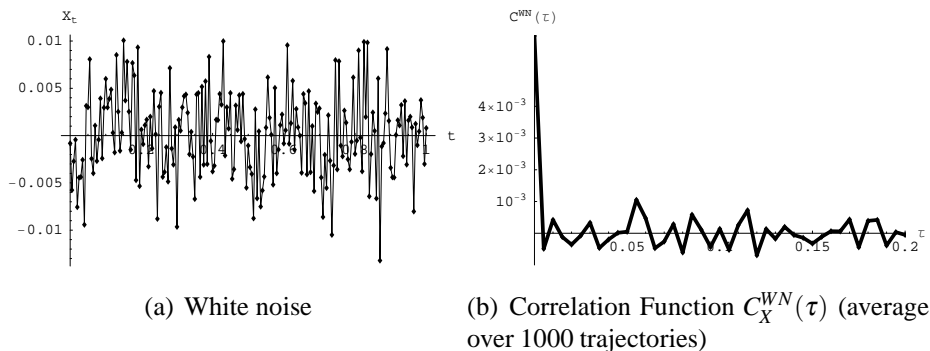


Figure A.2: White noise process

The white noise process is a typical instance of a *Markovian process* which is basically

a process with no memory. The value at time  $t$  depends only on the value at time  $t - \Delta t$  ( $\Delta t \dots$  time increment) but not on the total history. The correlation function in Figure A.2(b) shows the  $\delta$ -peak at zero time difference.

## A.2 Langevin equation

In physics differential equations are essential to describe the dynamical behaviour of a system. The most prominent example is the equation of motion that determines the acceleration  $\vec{a} = \dot{\vec{v}}$  of a particle of mass  $m$ ,  $m\dot{\vec{v}} = -b\vec{v} + \vec{\eta}(t)$ , where  $\vec{\eta}(t)$  describes the a conservative force acting on the particle and  $b$  the *viscous* force proportional to the velocity  $\vec{v}$ .

Consider now a particle surrounded by many other particles that are much smaller. Due to the collision with these smaller particles the big particle experiences a series of stochastic changes of its velocity. This has been examined already by the botanist Brown [Bro66] and is nowadays known as *Brownian motion*. He looked at grain pollens under the microscope and found them moving around without apparent cause. To account for this in a mathematical formula the stochastic changes of the velocity can be subsumed in the force vector  $\vec{\eta}$  which comprises a deterministic term  $\vec{\eta}_{det}$  and the stochastic fluctuations  $\vec{\eta}_{stoch}$ . We end up with the *Langevin* equation,

$$m \frac{d\vec{v}}{dt} = -b\vec{v} + \vec{\eta}_{stoch}(t) \quad (\text{A.2.1})$$

by assuming vanishing deterministic forces (e. g. gravitation).

Such examinations may not sound that spectacular and one is urged to say: “But it was clear beforehand that the grain pollen will be kicked and therefore it will move around.” But atomic theory was not well established until the end of the nineteenth century, it was not clear at all that there exists an atom per se without being only a convenient picture in mind. “Haben’s eins gesehen?” (“Have you seen one?”) is the striking quote attributed to Ernst Mach in discussions on the existence of atoms. It was none less than Albert Einstein who established with his theory on diffusion the atomistic view [Ein05].

Another form of writing down the *Langevin* equation is [Gil95]

$$X(t + dt) = X(t) + A(X(t), t)dt + D^{1/2}(X(t), t)N(0, 1)(dt)^{1/2}, \quad (\text{A.2.2})$$

where the velocity  $\vec{v}$  and the viscosity  $b$  have been replaced by a general random variable  $X(t)$  and the *drift function*  $A(X(t), t)$ , respectively. The stochastic driving force  $\eta(t)$  is split into the *diffusion function*  $D^{1/2}(X(t), t) > 0$  and the reduced Gaussian random variable  $N(0, 1)$  with zero mean and unit variance. The occurrence of the strange looking square root of the differential  $dt$  can be justified if we have a look at the mean square displacement of a Brownian particle. If we take  $X(t)$  as the vertical displacement of a particle suspended in a fluid its mean value will be zero,  $\langle X(t) \rangle = 0$  neglecting the influence of gravity. Furthermore, the observable mean square displacement is proportional to the time [Ein05, Per98],  $\langle X^2(t) \rangle = a^2 t$  and the root mean square deviation is therefore proportional to the square root of the time  $t$ ,  $\Delta X(t) = \sqrt{\langle X^2(t) \rangle} = a\sqrt{t}$ .

### A.3 Ornstein-Uhlenbeck process

We consider as one of the simplest stochastic processes the Ornstein-Uhlenbeck (O. U.) process which describe the velocity of a particle in Brownian motion [UO30] and can also be used to model Johnson (thermal) noise in electrical circuits [Gil00]. In contrast to the white noise process it does not have a flat, but a Lorentzian power spectrum and is therefore called *coloured noise* in general, or *Brown noise* in particular.

Setting  $A(X, t) = -\frac{1}{\tau_n}X$  and  $D(X, t) = c$  with the *relaxation time*  $\tau_n$  and the *diffusion constant*  $c$  in the Langevin equation (A.2.2) defines the Ornstein-Uhlenbeck process.

$$X(t + dt) = X(t) - \frac{1}{\tau_n}X(t)dt + c^{1/2}N(0, 1)(dt)^{1/2}, \quad (\text{A.3.1})$$

From Eq. (A.2.1) we easily see that the O. U. process is a *Markov process* since the knowledge of  $X(t)$  is sufficient to calculate its value  $X(t + dt)$  at an infinitesimal time  $dt$  later. It is also a Gaussian process (all  $X(t)$  are Gaussian random variables) with mean  $\langle X(t) \rangle = x_0 e^{-(t-t_0)/\tau_n}$  for the initial condition  $\langle X(t) \rangle = x_0$ . The variance at time  $t$  can be calculated to

$$\sigma_X^2(t) = \langle X^2(t) \rangle - \langle X(t) \rangle^2 = \frac{c\tau_n}{2}(1 - e^{-2(t-t_0)/\tau_n}) \quad (\text{A.3.2})$$

and its covariance

$$G_{XX}(t_1, t_2) = \langle X(t_1)X(t_2) \rangle = \frac{c\tau_n}{2}e^{-(t_2-t_1)/\tau_n} \left(1 - e^{-2(t_1-t_0)/\tau_n}\right) \quad (t_0 \leq t_1 \leq t_2) \quad (\text{A.3.3})$$

since  $\mu_X = 0$ . The characteristics of the process are subsumed in the random variable

$$X(t) = N(x_0 e^{-(t-t_0)/\tau_n}, \frac{c\tau_n}{2}(1 - e^{-2(t-t_0)/\tau_n})) \quad (\text{A.3.4})$$

and in the limit  $t_0 \rightarrow -\infty$ ,

$$X(t) = N(0, \frac{c\tau_n}{2}). \quad (\text{A.3.5})$$

The nomenclature for  $\tau_n$  as the *relaxation time* is now justified since it characterises the time scale over which the mean and variance of  $X(t)$  relax to their asymptotic values 0 and  $c\tau_n/2$ , respectively. In its relaxed form the O.U. process is also stationary, the probability density function of  $X(t)$  does not change anymore in time. For the relaxed form the correlation function is given by

$$C_{OU}(t') = \frac{c\tau_n}{2}e^{-t'/\tau_n}. \quad (\text{A.3.6})$$

This implies (Eq. A.1.7) that the noise has a Lorentzian power spectrum

$$S(\omega) = \frac{1}{2\pi} \int_{-\infty}^{\infty} C(t')e^{-i\omega t'} dt' = \frac{2c\tau_n^2}{1 + (\tau_n\omega)^2}. \quad (\text{A.3.7})$$

The integral over all frequencies  $\nu = \omega/(2\pi)$ ,  $\int d\nu S(\nu) = \frac{1}{2\pi} \int d\omega S(\omega)$  gives the mean

power

$$P_{OU}^2 = c\tau_n/2.$$

The bandwidth  $\omega_n$  of the power spectrum is given by  $\omega_n = 2\pi/\tau_n$ .

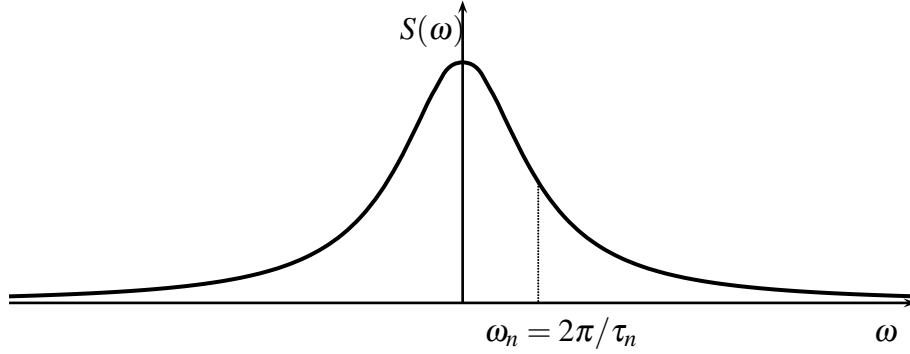


Figure A.3: Lorentzian shape of the spectral distribution  $S(\omega)$  of the O.U.-process

## A.4 Integral of an O.U. process

Since Brownian motion describes the velocity of a particle in a suspension the integral of this process results in the particle position and is therefore not unattractive to calculate. Indeed, one can also find for the position analytic expressions for its mean and variance. The mean value of the random variable

$$Y(t) = Y(0) + \int_{t_0}^t X(t') dt' \quad (\text{A.4.1})$$

is given by

$$\mu_Y = \langle Y(t) \rangle = 0 \quad (\text{A.4.2})$$

since  $\langle Y(t) \rangle = Y(0) + \langle \int_{t_0}^t X(t') dt' \rangle = Y(0) + \int_{t_0}^t \langle X(t') \rangle dt' = Y(0) = 0$  when exchanging the time and the ensemble average (*Fubini's theorem*), assuming that the initial position  $Y(0)$  is zero and taking the relaxed form of  $X(t)$  ( $t_0 \rightarrow -\infty$ ). Its variance is given by [Doo42]

$$\sigma_Y^2(t) = c\tau_n^3 \left[ e^{-\frac{t}{\tau_n}} - 1 + \frac{t}{\tau_n} \right],$$

or

$$\sigma_Y^2(t) = 2\tau_n^2 P_{OU}^2 \left[ e^{-\frac{t}{\tau_n}} - 1 + \frac{t}{\tau_n} \right] \quad (\text{A.4.3})$$

in terms of the mean power  $P_{OU}^2 = c\tau_n/2$ .

It is instructive to explicitly derive the formula for the variance  $\sigma_Y^2(t)$  in Equation A.4.3. Inserting (A.4.1) into  $\sigma_Y^2(t) = \langle Y^2(t) \rangle$  and using (A.3.3) in its relaxed form ( $G_{XX}(t_1, t_2) =$

$\frac{c\tau_n}{2}e^{-(t_2-t_1)/\tau_n}$  it follows that

$$\begin{aligned}\langle Y^2(t) \rangle &= \int_0^T \int_0^T \langle X(t')X(t'') \rangle dt' dt'' \\ &= \frac{c\tau_n}{2} \int_0^T \int_0^T e^{-|t''-t'|/\tau_n} dt' dt''.\end{aligned}\quad (\text{A.4.4})$$

This can be simplified to

$$\begin{aligned}\langle Y^2(t) \rangle &= 2\frac{c\tau_n}{2} \int_0^T \left( \int_0^{t''} e^{-(t'-t'')/\tau_n} dt' \right) dt'' \\ &= c\tau_n \int_0^T e^{t''/\tau_n} \int_0^{t''} e^{-t'/\tau_n} dt' dt'' \\ &= c\tau_n^3 \left( e^{T/\tau_n} - 1 + \frac{T}{\tau_n} \right)\end{aligned}\quad (\text{A.4.5})$$

as in Eq. (A.4.3).

In Section 5.1.1 a slightly modified form has to be calculated, namely the integral of an O. U. process  $X(t)$  times a cosine,  $\int_0^T \cos \omega t X(t)$ . Similarly to the above the integral

$$2 \left( \frac{c\tau_n}{2} \right)^2 \int_0^T \cos \omega t'' e^{t''/\tau_n} \int_0^{t''} \cos \omega t' e^{-t'/\tau_n} dt' dt''$$

which is already a more tedious task. At the final time  $T = 2\pi/\omega$  a simple form can be obtained,

$$\sigma_{Yc}^2 = 2P_X^2 \tau_n^2 \left( \frac{e^{-T/\tau_n} - 1}{((1/\tau_n)^2 + \omega^2)^2} + \frac{T/\tau_n}{(1/\tau_n)^2 + \omega^2} \right).\quad (\text{A.4.6})$$

Similarly, for  $\int_0^T \sin \omega t X(t)$  the variance can be calculated to

$$\sigma_{Ys}^2 = 2P_X^2 \tau_n^2 \left( \frac{\omega^2 (e^{-T/\tau_n} - 1)}{((1/\tau_n)^2 + \omega^2)^2} + \frac{T/\tau_n}{(1/\tau_n)^2 + \omega^2} \right).\quad (\text{A.4.7})$$

## A.5 Generation of an O. U.-process by its spectral representation

An approximation to the O. U.-process is obtained by decomposing it into a Fourier sum of trigonometric functions with random amplitudes and/or phases [Ric44a, Ric44b],

$$X(t) = \sum_{k=1}^K [A_k \cos \omega_k t + B_k \sin \omega_k t].\quad (\text{A.5.1})$$

The coefficients are independent zero-mean random variables which are taken to be Gaussian and their variances are determined by the spectral density function of the process,

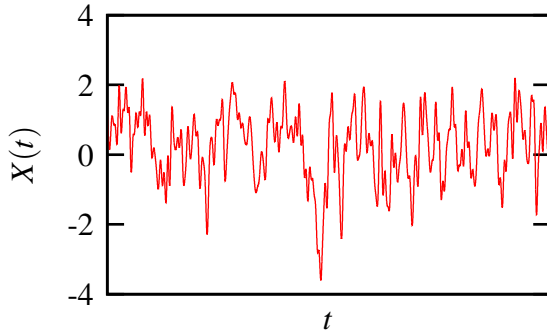
$$\sigma_{A_k}^2 = \sigma_{B_k}^2 = S(f_k)\Delta f, \quad (\text{A.5.2})$$

with the relations  $f_k = \omega_k/(2\pi)$  and  $f_k = k\Delta f$ . The spectral representation of the noise process in Eq. (A.5.1) can be used for different kind of noise characterised by their spectral density. Thus, the O. U. process is obtained by choosing  $S(f_k)$  according to Equation (A.3.7). The properties of the random variables  $A_k$  and  $B_k$  determine these characteristics and in the limit of  $K$  tending to infinity the approximation to the desired noise process is exact.

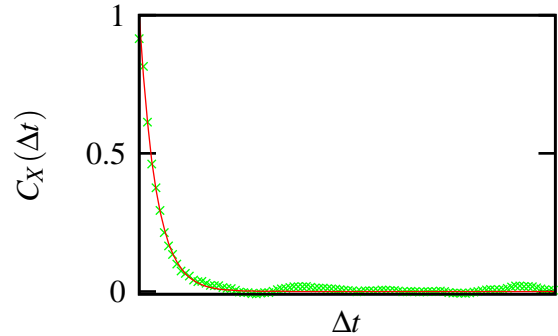
An alternative representation makes use of random phases  $\phi_n$  uniformly distributed in the interval  $[0, 2\pi]$ ,

$$X(t) = \sum_{k=1}^K C_k \cos(\omega_k t - \phi_k) \quad (\text{A.5.3})$$

with fixed amplitude  $C_k = \sqrt{S(\omega_k)\Delta\omega/\pi}$  (or  $C_k = \sqrt{2S(f_k)\Delta f}$ ). This is the form we have used for the numerical simulations since it is “cheaper” in the way that just one uniform distributed random variable has to be generated instead of two normal distributed ones. Sample trajectory of an O. U. process generated in such a way are shown in Figure A.4(a). The correlation function shows the exponential characteristics  $C_X(\Delta t) = P_{OU}^2 e^{-\Delta t/\tau_n}$  of the memory of the process (Figure A.4(b)).



(a) Sample trajectory.



(b) Correlation function averaged over 100 trajectories.

Figure A.4: Sample Ornstein-Uhlenbeck process with parameters  $c = 2$ ,  $\tau_n = 1$  and therefore  $P_{OU}^2 = 1/2$ . The red solid line shows the fitted correlation function  $C_X(\Delta t)$  with the fit parameters  $c_f = 2.02 \pm 0.006$  and  $\tau_f = 0.98 \pm 0.003$  in accordance to the input parameters values.

## A.6 Example: Current noise in an electric circuits

A resistance at nonzero temperature in an electric circuit produces current noise (*Johnson noise*) that can be described by an O. U. process [Gil00]. For example, in an electric circuit

comprising a resistance  $R$  and self-inductance  $L$  – for example, a Helmholtz coil arrangement as described in Appendix D – one can estimate the Lorentzian shaped power spectrum at a temperature  $T$ . The equation describing this circuit is

$$\frac{dI_J(t)}{dt} = -\frac{I_J(t)}{L/R} + \frac{1}{L}V_J(t), \quad (\text{A.6.1})$$

where  $I_J(t)$  is the fluctuating electrical current and the randomly fluctuating voltage  $V_J(t)$ . The connection to the O. U. process is established by  $\tau_n = L/R$  and  $V_J(t) = Lc^{1/2}\Gamma(t)$ , where  $\Gamma(t)$  denotes Gaussian white noise with zero mean and  $1/dt$  variance<sup>1</sup>. Furthermore, it can be shown [Gil00] that

$$c = \frac{2k_B T R}{L^2}$$

with the Boltzmann constant  $k_B = 1.3806 \times 10^{-23} \text{ J/K}$ . The frequency spectrum has a bandwidth of  $\Gamma = 1/\tau_n = R/L$  and the mean square current is  $\langle I_J^2 \rangle = c\tau_n/2 = k_B T/L$ . At room temperature and for  $L = 10^{-5}$ , the value found for the Helmholtz coils used for the UCN storage experiment below (Appendix D) a mean noise current of 20 nA is found.

---

<sup>1</sup>To see the equivalence with Eq. (A.2.2) write  $dI_J(t) = I_J(t+dt) - I_J(t)$  and use  $\alpha + \beta N(m, \sigma^2) = N(\alpha + \beta m, \beta^2 \sigma^2)$  for the normal random variable  $N(m, \sigma^2)$  with mean  $m$  and variance  $\sigma^2$ .

# Appendix B

## Calculation of a geodesic on a sphere

For the following derivation of a geodesic we refer to Ref. [Nak03] or any other book on (differential) geometry will probably do as well. The metric on the  $S^2$  embedded in  $\mathbb{R}^3$  is induced by the Riemann metric defined on  $\mathbb{R}^3$  given by [Nak03, p. 245]

$$g_p = g_{\mu\nu}(p)dx^\mu \otimes dx^\nu, \quad (\text{B.1})$$

where in our Euclidean geometry  $g_{\mu\nu} = \delta_{\mu\nu}$  and  $\mu, \nu = 1, 2, 3$ , i. e.

$$g_p = dx^1 \otimes dx^1 + dx^2 \otimes dx^2 + dx^3 \otimes dx^3. \quad (\text{B.2})$$

Using the transformation property of the dual basis  $dx^\mu = \frac{\partial x^\mu}{\partial y^\nu} dy^\nu$  we can write

$$\begin{aligned} g_p &= dx^\mu \otimes dx^\mu \\ &= \frac{\partial x^\mu}{\partial y^\sigma} dy^\sigma \otimes \frac{\partial x^\mu}{\partial y^\rho} dy^\rho \end{aligned} \quad (\text{B.3})$$

$$= \frac{\partial x^\mu}{\partial y^\sigma} \frac{\partial x^\mu}{\partial y^\rho} dy^\sigma \otimes dy^\rho \quad (\text{B.4})$$

In general [Nak03, p. 246] let  $M$  be an  $m$ -dimensional sub-manifold of an  $n$ -dimensional Riemannian manifold  $N$  with the metric  $g_N$ . If  $f : M \mapsto N$  is the embedding which induces the sub-manifold structure of  $M$ , the pullback map  $f^*$  induces the natural metric  $g_M = f^* g_N$  on  $M$ . The components of  $g_M$  are given by

$$g_{M\mu\nu}(x) = g_{N\alpha\beta}(f(x)) \frac{\partial f^\alpha}{\partial x^\mu} \frac{\partial f^\beta}{\partial x^\nu} \quad (\text{B.5})$$

where  $f^\alpha$  denote the coordinates  $f(x)$ .

In particular the metric of the unit sphere embedded in  $\mathbb{R}^3$  is provided by the coordinate transformation  $f$  from  $(\theta, \phi)$ , the polar coordinates of  $S^2$  to the coordinates  $(x, y, z)$  in Euclidean space. It is defined by

$$f : (\theta, \phi) \mapsto (\sin \theta \cos \phi, \sin \theta \sin \phi, \cos \theta), \quad (\text{B.6})$$

from which we obtain the induced metric

$$g_{\mu\nu} dx^\mu \otimes dx^\nu = \delta_{\alpha\beta} \frac{\partial f^\alpha}{\partial x^\mu} \frac{\partial f^\beta}{\partial x^\nu} dx^\mu \otimes dx^\nu = \frac{\partial f^\alpha}{\partial x^\mu} \frac{\partial f^\alpha}{\partial x^\nu} dx^\mu \otimes dx^\nu.$$

Evaluating  $\frac{\partial f^\alpha}{\partial x^\mu} \frac{\partial f^\alpha}{\partial x^\nu}$  to

$$\frac{\partial f^\alpha}{\partial x^1} \frac{\partial f^\alpha}{\partial x^1} = \frac{\partial f^\alpha}{\partial \theta} \frac{\partial f^\alpha}{\partial \theta} = \cos^2 \phi \cos^2 \theta + \sin^2 \phi \cos^2 \theta + \sin^2 \theta = 1, \quad (\text{B.7})$$

$$\frac{\partial f^\alpha}{\partial x^2} \frac{\partial f^\alpha}{\partial x^2} = \frac{\partial f^\alpha}{\partial \phi} \frac{\partial f^\alpha}{\partial \phi} = \sin^2 \phi \sin^2 \theta + \cos^2 \phi \sin^2 \theta = \sin^2 \theta, \quad (\text{B.8})$$

$$\frac{\partial f^\alpha}{\partial x^1} \frac{\partial f^\alpha}{\partial x^2} = \frac{\partial f^\alpha}{\partial \theta} \frac{\partial f^\alpha}{\partial \phi} = 0, \quad (\text{B.9})$$

$$\frac{\partial f^\alpha}{\partial x^2} \frac{\partial f^\alpha}{\partial x^1} = \frac{\partial f^\alpha}{\partial \phi} \frac{\partial f^\alpha}{\partial \theta} = 0, \quad (\text{B.10})$$

$$(\text{B.11})$$

finally yields

$$g_{S^2 ij} dx^i \otimes dx^j = d\theta \otimes d\theta + \sin^2 \theta d\phi \otimes d\phi. \quad (\text{B.12})$$

Now we want to derive the geodesic connecting two points  $q = (\theta_0, \phi_0) \in S^2$  and  $p = (\theta_1, \phi_1) \in S^2$ . The geodesic is per definition the straightest possible curve between these two points which can be derived by minimising the length  $I(\mathcal{C})$  along a curve  $\mathcal{C} : s \mapsto \vec{x}(s)$  on the sphere,

$$I(\mathcal{C}) = \int_{\mathcal{C}} ds = \int_{\mathcal{C}} \sqrt{ds^2} = \int_{\mathcal{C}} \sqrt{g_{ij} dx^i \otimes dx^j} = \int_{\mathcal{C}} \sqrt{g_{ij} \frac{dx^i}{ds} \frac{dx^j}{ds}} ds \quad (\text{B.13})$$

parametrised by the distance  $s$ . The minimisation of  $I(\mathcal{C})$  leads to the Euler-Lagrange equation

$$\frac{d}{ds} \left( \frac{\partial L}{\partial x'^i} \right) - \frac{\partial L}{\partial x^i} = 0 \quad (\text{B.14})$$

with  $x' = dx/ds$  and  $L = \sqrt{g_{ij} dx^i dx^j}$ . Note that  $L \equiv 1$  from  $\int_{\mathcal{C}} ds = \int_{\mathcal{C}} L ds$  and therefore  $dL/ds = 0$  along the curve. In order to circumvent difficulties arising from the square root solving Eq. (B.14) can be shown to be equivalent to solving the Euler-Lagrange equations for the function  $F = L^2/2 = g_{ij} x'^i x'^j$ .

Doing so we obtain

$$\frac{d}{ds} (g_{kj} x'^j) - \frac{1}{2} \frac{\partial g_{ij}}{\partial x^k} x'^i x'^j \quad (\text{B.15})$$

$$= \frac{\partial g_{kj}}{\partial x^i} x'^j x'^i + g_{kj} \frac{d^2 x^j}{ds^2} - \frac{1}{2} \frac{\partial g_{ij}}{\partial x^k} x'^i x'^j \quad (\text{B.16})$$

$$= g_{kj} \frac{d^2 x^j}{ds^2} + \frac{1}{2} \left( \frac{\partial g_{kj}}{\partial x^i} + \frac{\partial g_{ki}}{\partial x^j} - \frac{\partial g_{ji}}{\partial x^k} \right) \frac{dx^j}{ds} \frac{dx^i}{ds} = 0 \quad (\text{B.17})$$

Multiplying the last line by  $g^{lk}$  we obtain the geodesic equation

$$\frac{d^2 x^k}{ds^2} + \Gamma_{ij}^k \frac{dx^i}{ds} \frac{dx^j}{ds} = 0 \quad (\text{B.18})$$

by use of the *Christoffel symbols*

$$\Gamma_{ji}^l \equiv \frac{1}{2} g^{lk} \left( \frac{\partial g_{kj}}{\partial x^i} + \frac{\partial g_{ki}}{\partial x^j} - \frac{\partial g_{ij}}{\partial x^k} \right).$$

In our particular example  $F = \frac{1}{2} \theta'^2 + \sin^2 \theta \phi'^2$  and the Euler-Lagrange equations are

$$\frac{d^2 \theta}{ds^2} - \sin \theta \cos \theta \left( \frac{d\phi}{ds} \right)^2 = 0 \quad (\text{B.19})$$

$$\frac{d^2 \phi}{ds^2} + 2 \cot \theta \frac{d\phi}{ds} \frac{d\theta}{ds} = 0. \quad (\text{B.20})$$

which define the Christoffel symbols  $\Gamma_{\phi\phi}^\theta = -\sin \theta \cos \theta$  and  $\Gamma_{\theta\theta}^\phi = \Gamma_{\theta\phi}^\phi = \cot \theta$ . To finally obtain the geodesic curve  $C_g : s \mapsto (\theta(\phi), \phi)$  we insert

$$\frac{d\theta}{ds} = \frac{d\theta}{d\phi} \frac{d\phi}{ds}, \quad \frac{d^2 \theta}{ds^2} = \frac{d^2 \theta}{d\phi^2} \left( \frac{d\phi}{ds} \right)^2 + \frac{d\theta}{d\phi} \frac{d^2 \phi}{ds^2}$$

into the first equation of (B.19) and get

$$\frac{d^2 \theta}{d\phi^2} \left( \frac{d\phi}{ds} \right)^2 + \frac{d\theta}{d\phi} \frac{d^2 \phi}{ds^2} - \sin \theta \cos \theta \left( \frac{d\phi}{ds} \right)^2 = 0. \quad (\text{B.21})$$

Plugging the second equation of (B.19) into Eq. (B.21) results in

$$\frac{d^2 \theta}{d\phi^2} - 2 \cot \theta \left( \frac{d\theta}{d\phi} \right)^2 - \sin \theta \cos \theta = 0. \quad (\text{B.22})$$

Defining a function  $f(\theta) \equiv \cot \theta$  by explicit calculations one finds that

$$\frac{d^2 f}{d\phi^2} + f = 0 \quad (\text{B.23})$$

is sufficient for Equation B.22 to hold. The general solution is  $f(\theta) = \cot \theta = A \cos \phi + B \sin \phi$  or

$$A \sin \theta \cos \phi + B \sin \theta \sin \phi - \cos \theta = 0, \quad (\text{B.24})$$

the equation of a great circle which lies in a plane whose normal vector is  $(A, B, -1)$ .  $A$  and  $B$  have to be determined by the initial conditions.  $\theta(\phi)$  is therefore

$$\theta(\phi) = \arctan \left[ (A \cos \phi + B \sin \phi)^{-1} \right]. \quad (\text{B.25})$$

# Appendix C

## Adiabatic Theorem

The adiabatic theorem says that if the system is initially in an eigenstate of a time-dependent Hamiltonian it will stay in an eigenstate at each instant of time under the condition that the Hamilton operator is changing slowly enough. Can we also quantify this condition? Following Messiah [Mes62] let us assume a system initially in the state  $|\psi(0)\rangle$  which is also an eigenstate of the Hamiltonian,  $|\psi(0)\rangle = |n_0\rangle$  with  $H(t)|n_t\rangle = E_n(t)|n_t\rangle$ . For all  $t = 0$  we therefore have a complete set of basis states  $|n_t\rangle$  belonging to the respective energy eigenvalues  $E_n(t)$ , which are taken to be non-degenerate. We also assume that the Hilbert space spanned by the basis vectors is compact, hence, the number of basis states is finite. The time evolution is given by the Schrödinger equation

$$H(t)|\psi(t)\rangle = i\hbar \frac{\partial}{\partial t} |\psi(t)\rangle.$$

At any time the state  $|\psi(t)\rangle$  can be written as a superposition of the  $|n_t\rangle$ ,

$$|\psi(t)\rangle = \sum_n c_n(t) e^{-\frac{i}{\hbar} \int_0^t E_n(t') dt'} |n_t\rangle \quad (\text{C.1})$$

by absorbing the time dependency into the coefficients  $c_n(t) \in \mathbb{C}$ . Inserting (C.1) into the Schrödinger equation we obtain

$$\begin{aligned} \sum_n c_n(t) H(t) e^{-\frac{i}{\hbar} \int_0^t E_n(t') dt'} |n_t\rangle &= i\hbar \sum_m [\dot{c}_m(t) e^{-\frac{i}{\hbar} \int_0^t E_m(t') dt'} |m_t\rangle \\ &\quad + c_m(t) \left(-\frac{i}{\hbar}\right) E_m(t) |m_t\rangle + c_m(t) e^{-\frac{i}{\hbar} \int_0^t E_m(t') dt'} |\dot{m}_t\rangle]. \end{aligned}$$

Multiplying this equation from the right with the instantaneous eigenvector  $\langle l_t |$  we obtain

$$\begin{aligned} e^{-\frac{i}{\hbar} \int_0^t E_l(t') dt'} c_l(t) E_l(t) \\ = i\hbar \dot{c}_l(t) e^{-\frac{i}{\hbar} \int_0^t E_l(t') dt'} + c_l(t) E_l(t) e^{-\frac{i}{\hbar} \int_0^t E_l(t') dt'} + i\hbar \sum_m c_m(t) e^{-i \int_0^t E_m(t') dt'} \langle l_t | \dot{m}_t \rangle \end{aligned}$$

from which

$$\dot{c}_l(t) = - \sum_m c_m(t) e^{-i \int_0^t [E_m(t') - E_n(t')] dt'} \langle l_t | \dot{m}_t \rangle \quad (\text{C.2})$$

follows. We have assumed that  $H(t)$  is Hermitian so that its eigenvectors are orthogonal ( $\langle m_t | n_t \rangle = \delta_{mn}$ ).

The expression  $\langle l_t | \dot{m}_t \rangle$  can be found from the time derivative of the eigenvector equation,

$$\begin{aligned} \frac{d}{dt} \cdot \left| \begin{array}{l} H(t) |m_t\rangle = E_m(t) |m_t\rangle \\ \dot{H}(t) |m_t\rangle + H(t) |\dot{m}_t\rangle = \dot{E}_m(t) |m_t\rangle + E_m(t) |\dot{m}_t\rangle, \quad l \neq m \\ \langle l_t | \dot{H} |m_t\rangle + E_l(t) \langle l_t | \dot{m}_t\rangle = E_m(t) \langle l_t | \dot{m}_t\rangle \end{array} \right. \\ \langle l_t | \dot{m}_t \rangle = \frac{\langle l_t | \dot{H} |m_t\rangle}{E_m(t) - E_l(t)}. \end{aligned} \quad (\text{C.3})$$

Inserting Eq. (C.3) into (C.2) we finally obtain

$$\dot{c}_l(t) = - \langle l_t | \dot{l}_t \rangle + \sum_m c_m(t) e^{-i \int_0^t [E_m(t') - E_n(t')] dt'} \frac{\langle l_t | \dot{H} |m_t\rangle}{E_m(t) - E_l(t)}. \quad (\text{C.4})$$

The state will remain in an eigenstate of the instantaneous Hamiltonian if the eigenstates do not mix, i. e. if the matrix element

$$\left| \frac{\langle l_t | \dot{H} |m_t\rangle}{E_m(t) - E_l(t)} \right| \ll 1. \quad (\text{C.5})$$

The rate of change of the Hamiltonian must be smaller than the energy splitting in order to stay in the adiabatic region. In terms of a spin-1/2 particle subjected to a magnetic field the Larmor frequency  $\omega_L$  corresponding to the Zeeman energy level splitting  $E_\uparrow - E_\downarrow$  must be smaller than the rotation frequency of the magnetic field. Numerically, it is shown in Section 5.1.2 that they should differ by approximately one order of magnitude.

# Appendix D

## Stability of the geometric phase - UCN measurement in details

A possible test of the robustness of the geometric phase under the influence of classical fluctuations can be designed using ultra cold neutrons. In brief, polarised UCNs have to be stored in the storage volume for a certain time interval and appropriate magnetic fields are applied to manipulate their spin degree of freedom. After the controlled spin evolution the resulting polarisation is measured by both counting neutrons with spin up and neutrons with spin down and the ratio of the count rates provides the polarisation. The apparatus is constructed in such a way that both the preparation and the analyzation is accomplished by use of a totally magnetised foil which transmits neutrons with parallel spin polarisation and reflects anti-parallel polarised ones. To get this going a switch has to be attached to the neutron guide. The complete setup is shown in Figure D.

In detail, the measurement scheme is as follows:

- (i) First the shutter is open and the switch directs neutrons from the source to the storage volume.
- (ii) The magnetised foil blocks neutrons with spin aligned anti-parallel to the applied guide field surrounding the neutron guide between the polarisation foil and the storage box.
- (iii) The hereby polarised neutrons go straight into the storage volume and if density equilibrium is established the shutter of the box is closed. The RF spin flipper is not operating.
- (iv) The evolution cycle is started as described in Section 5.5. Meanwhile the switch is toggled to prevent “fresh” neutrons entering the apparatus and to connect the storage vessel to the detector.
- (v) After finishing the spin gymnastics the shutter is opened, but here we have to pay attention that all neutrons lingering in the area between the switch and the shutter have already hit the detector.

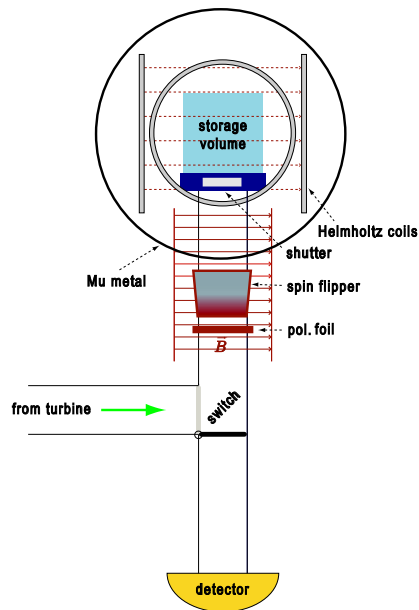


Figure D.1: Complete setup for the UCN measurement of Berry’s phase stability. Neutrons coming from the turbine are directed into a storage volume enclosed by Helmholtz coils and released after some spin evolution in order to hit the detector.

- (vi) Before arriving at the detector all neutrons have to surmount the magnetised foil once again with the effect that in the first place only neutrons with spin pointing again in the initial direction can pass.
- (vii) To measure also neutrons with opposite spin the resonance spin flipper attached to the apparatus is switched on after a specific time delay so that only neutrons with opposite spin can pass through the magnetised foils.
- (viii) After the detection the shutter is opened, the switch is toggled again, and the next run can be started.

## D.1 Description of the components

The basic apparatus consists of the neutron guide, a shutter, a beam switch, a polarisation foil, a storage vessel attached directly to the (second) shutter all surrounded by three pairs of mutually orthogonal Helmholtz coils. The latter parts (storage vessel, shutter and coils) have to be placed inside a magnetically shielding chamber, for example a mu-metal box.

### D.1.1 Neutron guides

We do not make any special demands on the neutron guides, except that in the region between the polarisation foil and the storage bottle non-magnetic material should be used in order to

preserve the spin polarisation. PVC tubes coated with a thin copper layer in the interior will be used.

### D.1.2 Shutter

There are no particular requirements neither on the switch nor on the first shutter redirecting neutrons either from the source to the storage bottle or from the bottle to the detector.

As for the second shutter it is of highest priority to avoid any kind of magnetic stray fields either by using magnetic materials or electro-mechanical mechanisms. Tests have shown that already a few millimetre thick aluminium plate reduces the higher frequencies of the magnetic field considerably. Thus, it is unfortunately not enough to build a shutter using only non-magnetic metal like aluminium, but the shutter must be made of insulating material as well to prevent spurious absorption effects due to induced eddy currents. At present the plans are to build a shutter made of some kind of polymer (POM - Polyoxymethylen) which is rigid enough to sustain mechanical stress (Figure D.3).

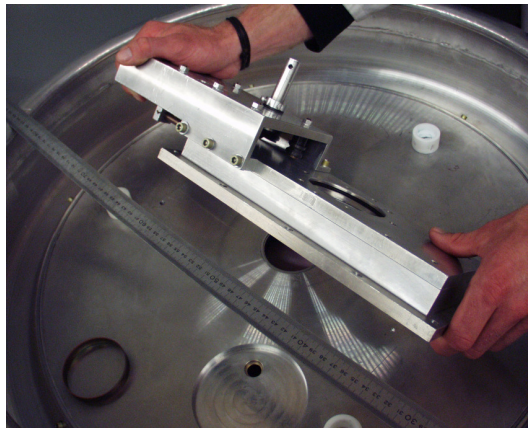


Figure D.2: Picture of a non-magnetic shutter that cannot be used to seal the storage vessel since for fluctuating magnetic fields eddy currents shield and distort them. The fingers belong to Dr. Plonka.

### D.1.3 Switch

The switch is nothing special, just a piece of neutron guide that can be toggled between two possible positions to redirect the beam.

### D.1.4 Polarisation foil

The UCNs are to be prepared in a spin-polarised state by transmission through a totally magnetised foil. As already pointed out by Bloch [Blo36] the index of refraction of the magnetised foil is different for different spin polarisations due to the interaction between the magnetic field  $\vec{B}$  and the neutron magnetic moment  $\vec{\mu}$ . The optical potential (4.1.15) is

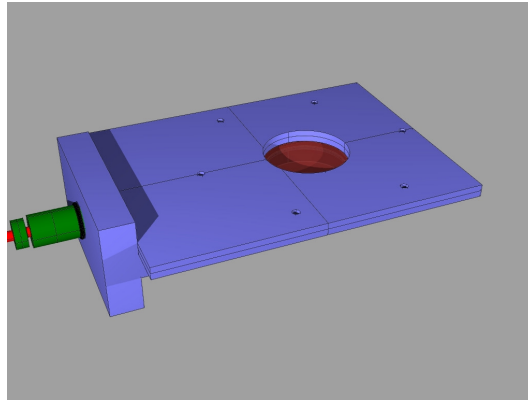


Figure D.3: A new shutter has to be design that lacks metallic materials as far as possible in order to avoid stray magnetic fields.

modified by a magnetic term  $-\vec{\mu} \cdot \vec{B}$  and therefore neutrons are either reflected or transmitted for large enough  $B$ . With this method a degree of polarisation close to 100% can be achieved.

### D.1.5 Storage volume

In the centre of the coil system a cylindrically shaped storage vessel out of the polymer POM (Figure D.4) is placed. Its inner surface is coated with Fomblin oil [MAB<sup>+</sup>89] which totally reflects UCNs of energies below its Fermi potential (106.5 neV corresponding to a maximum velocity of  $4.55 \text{ ms}^{-1}$  and loss probability  $2 - 3 \times 10^{-5}$ /bounce at  $20^\circ \text{ C}$ ). Furthermore, by using this non conductive material the problem of induced eddy currents can be tackled. The effective storage volume is 100 mm in height and 120 mm in diameter corresponding to  $\approx 1.1$  litre. The wall thickness is 15 mm.

The storage volume must be sufficiently small to fit into the homogeneous region of the magnetic field (c. f. Section D.2.1). Compared to the bottle used in the EDM experiment [BDG<sup>+</sup>06] our volume is rather small. They reported a UCN count rate of 15.000 counts per charge for storage volume of 21 litres. By comparison we can expect maximally around 700 counts per charge which may not be ideal.

### D.1.6 Helmholtz coils

Finally, the Helmholtz coils constitute the central part of the apparatus. Three perpendicular pairs of coils in Helmholtz geometry (c. f. for instance in [Gre98]) are placed such that the storage vessel sits in their centre. In order to achieve a maximally homogeneous field, the distance between the coils has to be equal to the radius for circular coils. For square shaped coils the ratio of the distance of the coils to their side length has been determined numerically to  $r_H \approx 1.84$ . In order to achieve a magnetic field as homogeneous as possible two square shaped coils are combined with an innermost circular coil. In Figure D.1.6 this construction is shown. The dimensions have to be chosen in such a way that the coils fit inside the Mu-metal shielding which is 950 mm in diameter and at the same time maximise



Figure D.4: Vessel made of POM coated with Fomblin.

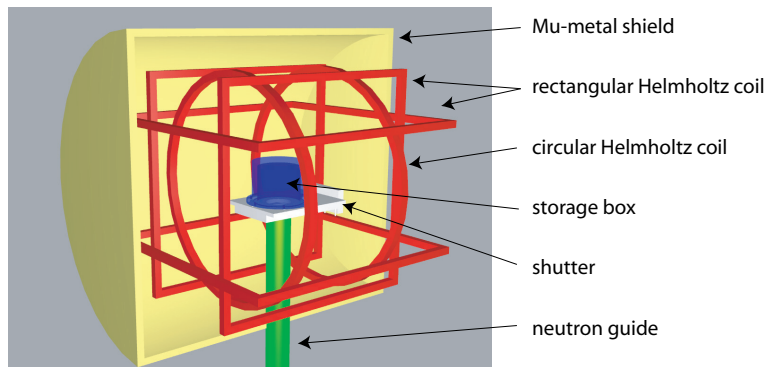


Figure D.5: Apparatus with two square shaped and a circular Helmholtz coil pairs surrounding the storage vessel mounted above a shutter.

the homogeneous region in the centre. The material used for the coil frame is aluminium. To reduce eddy currents each coil frame has a insulating insert and the joints between the coil frames are also insulated.

### Circular coil

The outer diameter of the circular coil is 634 mm corresponding to a standard 28'' bicycle rim (Mavic A119). The cross section of the wire duct is about  $8 \text{ mm} \times 20 \text{ mm} \approx 160 \text{ mm}^2$  (Figure D.6). Wire of 0.9 mm in diameter is used for  $N = 100$  windings.

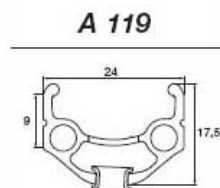


Figure D.6: Profile of the Mavic A119 rim.

### Square shape

The (outer) side lengths for the rectangular coils are 660 mm and 620 mm. In the setup depicted in Figure D.1.6 the innermost and the middle coil is perpendicular to the axis of the cylindrical storage vessel. The third (largest) coil is parallel to the axis of the cylindrical storage box. The material of the coil frame is aluminium. One has to cut the profiles to avoid the formation of eddy-currents that could disturb the measurements. The cross section of the wire duct is  $20 \times 20 \text{ mm}^2$  (Figure D.7) and as in for the circular coils 100 windings of wire 0.9 mm in diameter are attached.

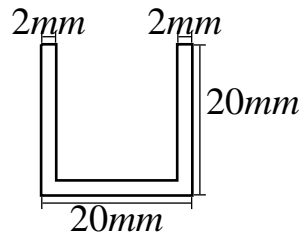


Figure D.7: Coil cross section and dimensions of the wire duct.

**Heat issues** For the following calculations we are always using an average diameter (or side lengths for the square shaped coils) since the changes in the different layers of the coils are negligible compared to the dimension of the coil. For the circular coil we need  $2\pi r \times N = 198 \text{ m}$  meters wire ( $r = 315 \text{ mm}$ ,  $N = 100$ ). For a rectangular coil we need  $4a \times N$  meters wire, for the largest coil  $\approx 260 \text{ m}$  ( $a = 650 \text{ mm}$ ,  $N = 100$ ) and for the intermediate coil  $\approx 244 \text{ m}$  ( $a = 610 \text{ mm}$ ). For a resistance of  $\approx 27.9 \Omega/\text{km}$  we can calculate the power consumption according to  $P = I^2 R$ . For a coil current of 2 A it is about 50 W, so altogether  $\approx 150 \text{ W}$  (Figure D.8). This could be a problem if the whole setup is placed inside a vacuum chamber as originally planned, but otherwise this should be fine. Also, for an intended magnetic field of one Gauss we just need circa 0.35 A (Figure D.9) resulting in pretty low power of  $< 5 \text{ W}$  which is definitely acceptable.

**Field homogeneity** Even more interesting is a discussion about the achievable field in the centre of the coil arrangement along with the theoretical homogeneity of the field. In Figure D.9 the calculated magnetic fields in the centre of the different Helmholtz coils is shown. To avoid excessive numerical integrations the particular geometry of the wire duct has been neglected, that is, a single infinitesimally (and nonphysically) thin wire models the square shaped actual current distribution. We will see later that the deviations from the real setup is negligible (Figure D.13). Calculations of the magnetic field of a Helmholtz coils 315 mm in radius show that about 100 windings will be enough to produce a magnetic field of  $\approx 5 \text{ Gauss}$  at a current of 2 A. With 100 windings around the inner coil radius a current of  $\approx 0.35 \text{ A}$

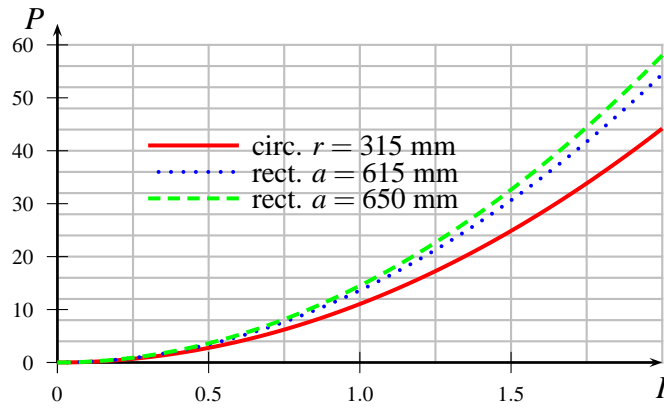


Figure D.8: Power consumption of a Helmholtz coil pair with 100 windings and a 0.9 mm wire diameter.

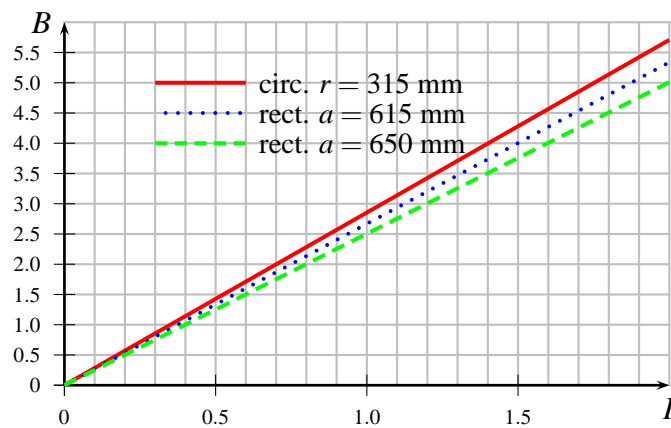


Figure D.9: Magnetic Field at the centre of a square Helmholtz coil with 100 windings.

## D. DETAILS OF UCN MEASUREMENT

yields approximately a magnetic field of 1 Gauss in the centre of the coil arrangement. The current values for one Gauss for the other coils can be found in Table D.1. In Figure D.11 a

coil	current [A]
circ. (315 mm)	0.35
rect. (610 mm)	0.38
rect. (650 mm)	0.40

Table D.1: Currents of the Helmholtz coils to generate 1 G at the centre.

cut in the  $x$ - $z$ -plane (Figure D.10) shows the  $z$ -component of the field for the different coils. The box in the middle indicates the storage volume of 120 mm in length and 100 mm in height. The contour lines indicate deviations of 0.1 % of the magnetic field at the coil centre, thus, the field seems to be fairly homogeneous – at least theoretically. In Figure D.12 the

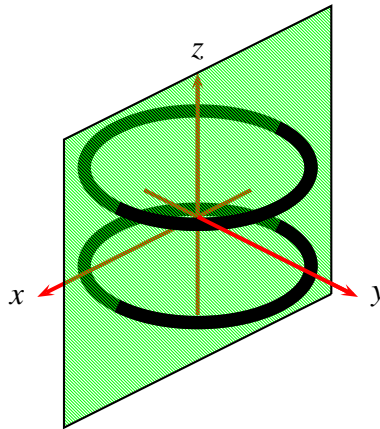
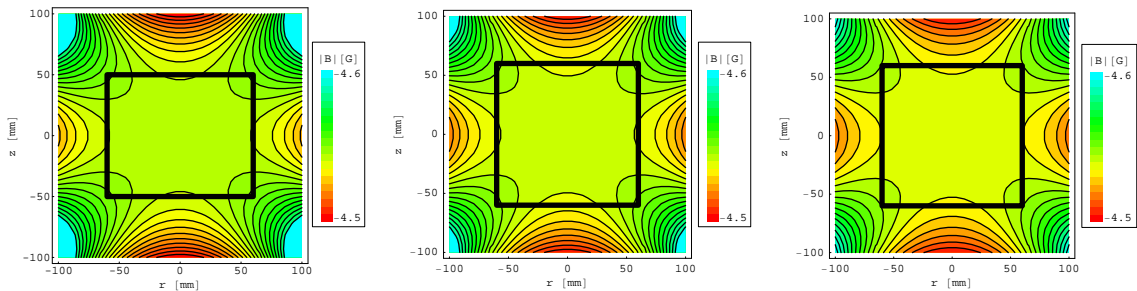


Figure D.10: Choice of coordinates for a Helmholtz coil pair.



(a) Circular coil ( $r=315$  mm)    (b) Rectangular coil ( $a=610$  mm)    (c) Rectangular coil ( $a=650$  mm)

Figure D.11: Cut in the  $x$ - $z$ -plane. The contours indicate a magnetic field deviation of 0.1 % of the magnetic field at the centre of the Helmholtz coil pairs.

storage cylinder (red) is shown along with the contours indicating 0.1% deviation of the  $z$ -component of the magnetic field at the centre of the setup. The yellow surface indicates the

field of the generated by the circular Helmholtz coil pair ( $r=315$  mm) and the green surface the  $\pm 0.1\%$  contour of the the smaller square Helmholtz coil pair having a side length of 610 mm. If one can build perfectly aligned coils the field should be fairly homogeneous around the centre. For a discussion whether the degree of homogeneity is sufficient for our purposes the reader is referred to Section D.2.1.

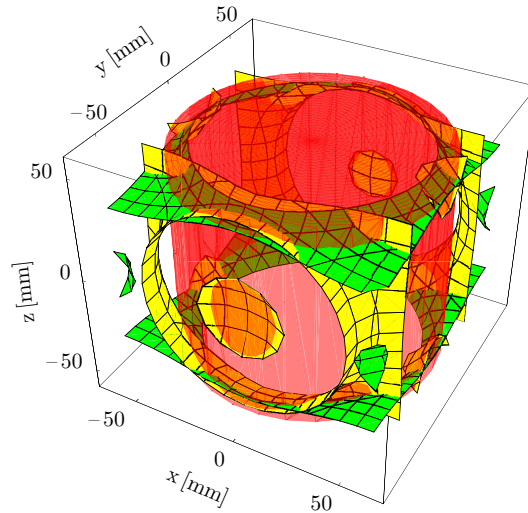


Figure D.12: Deviations from the maximal magnetic field at the centre of a circular Helmholtz coil with radius 315 mm and a square shaped Helmholtz coil ( $a=610$  mm). Inside the storage vessel (red) the field is homogeneous up to deviations smaller than 0.2%. The green surfaces denote the  $\pm 0.1\%$  contour of the rectangular and the yellow surface the field of the circular coil.

What we did not clarify yet is the error we introduce by neglecting the finite dimensions of the wire duct. The deviation from a more realistic calculation is shown in Figure D.13. The plot is for a coil with 315 mm radius and the wire duct is assumed to have a cross section of  $16 \times 18$  mm comprising 100 windings at a current of 2 A. The relative deviations are of order  $10^{-4}$ , one order of magnitude less than the inhomogeneities in the magnetic field, and can therefore be safely neglected.

### D.1.7 Mu-metal shielding chamber

Additional to the inhomogeneities in the magnetic fields, any influences of environmental fields will result in unwanted depolarisation effects as well. To minimise these disturbing effects the whole setup is to be placed in a magnetically shielding chamber. A cylindrical box made of Mu-metal, a soft magnetic alloy, 950 mm in diameter will be utilised to provide sufficient shielding - c. f. Section D.2.2.

### D.1.8 Detector

A standard detector will do.

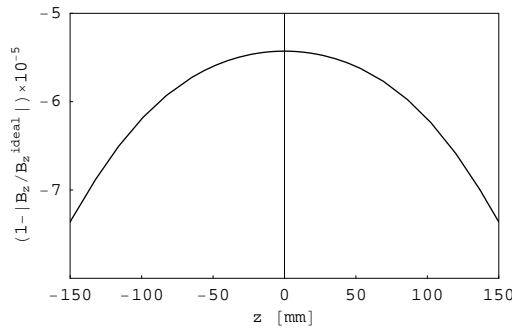


Figure D.13: Deviation induced by approximating the geometry of the wire by an infinitesimally thin one. The absolute ratio of the real magnetic field (with finitely thick wire duct) over the ideal B-field (with an infinitesimally thin wire) is plotted ( $1 - |B_z^{real} / B_z^{ideal}|$ )

### D.1.9 Control units

For the control of the experiment one controllable power supply is needed for each of the coils. The expected frequencies involved are up to 1-5 kHz resulting in a required rise time of the electrical circuits in the 10 kHz region. The signal of the noise fluctuations is modelled on a personal computer in order to easily simulate different types of noise. The standard audio output of the PC will be sufficient as the noise frequencies used will be small enough and therefore not distorted by the low sampling rate of such a device. The noise signal superposed with the unperturbed coil currents is then fed into the amplifier.

Furthermore, a static power supply for the guide field is needed and another one for the polarisation foil, if one does not use a permanent magnet and attach a resonant spin flipper to flip the spin instead of the analyzation direction. In this case a high-frequency amplifier and signal generator is needed.

## D.2 Unavoidable influences

What we have neglected so far are unavoidable decoherence effects by stray magnetic fields, inhomogeneities, improper reconstruction of the noise, non-zero switching times of the magnetic fields, a.s.o. These effects will modify the polarisation regardless of whether there is a rotation or not. The final answer, whether these problems can be overcome have to be answered by experiments, however, theoretical estimates will provide first insights.

### D.2.1 Inhomogeneities of the magnetic field of the coils

One of the main problems is as already indicated the inhomogeneous magnetic field. Let us assume that the magnitude of the field is about 1 Gauss which corresponds to a Larmor frequency  $\omega_L$  of about  $2 \times 10^4$  rad/s, and therefore an additional phase  $\omega_L t$ . This means that the spin of a neutron spending one second in this field rotates  $\omega_L / 2\pi \approx 3000$  times.

To measure the geometric phase the averaged phase of the ensemble of stored neutrons is observable. By allowing for inhomogeneities of the field in the storage volume of 0.1 % we induce fluctuations of the phase of individual neutrons, say, of the same order of magnitude. But this is already a phase difference larger than  $2\pi$  and the phase difference we wanted to measure will be totally smeared out. Note, that this is the noise that we cannot circumvent. This is not the noise we intend to apply at will but an intrinsic source of error. A more optimistic way of thinking is to assume that the majority of neutrons will stay in a more homogeneous region at the centre than in the regions of inhomogeneity near to the surface of the vessel.

### Induced frequency of inhomogeneities

What about the frequency of this kind of noise as seen from the neutron's frame of reference. The mean free path length is  $\Lambda = 4 * Volume / Surface \approx 80 \text{ mm}$  [MAB<sup>+</sup>89], so that we expect approx.  $4.55 \text{ ms}^{-1} / \Lambda * s \approx 56$  bounces per second. This means that for one second storage in the bottle the neutron will traverse the storage volume about 50 times and therefore the frequency of this noise is of the order of 50 Hz, in the same frequency domain as the artificial noise, but much weaker. The adiabaticity condition is still fulfilled.

### Flight of a neutron through the vessel

The deviation in the accumulated dynamical phase is the integral over the magnetic potential experienced during this flight. I have tried to estimate the variance to be expected if a neutron travels through inhomogeneous magnetic fields. A simple model is to simulate not a cylinder, but a cuboid shaped neutron storage container and implement periodic boundary conditions,  $B(x_i + L) = B(x_i)$  for the function  $B(x)$  describing the magnetic field at the point  $x$ .  $L$  is the side length of the cuboid. For the simulation we choose  $L = 50 \text{ mm}$  corresponding roughly to the size of the projected vessel. The magnetic field shall be  $\approx 1$  Gauss in the middle of the coil. The magnetic field along possible neutron trajectories is show in Figures D.14, on the left for neutrons having only velocity components in the  $x - y$  plane and on the right for an additional  $z$ -component, where the calculated magnetic field distribution as shown in Figures D.11 has been used.

The integration along a path  $C$ ,  $\int_C B(x) d\vec{s}$  yields the total magnetic field the neutron has experienced and therefore the total phase shift is  $\omega_L t = \hbar^{-1} \int_C \mu B(x) d\vec{s} = \hbar^{-1} \int \mu B(x(t)) |ds/dt| dt$ . We assume now a slightly collimated beam, i. e.  $v_x > v_y, v_z$  and generate trajectories with random velocity components, for example uniform distributed random variables taken out of the interval

$$v_x \in [0, 1], \quad v_y \in [0, 0.2], \quad v_z \in [0, 0.2].$$

The velocity is afterwards normalised to the typical velocity of 4.4 m/s. From the ensemble of generated stochastic trajectories the mean and the variance can be calculated.

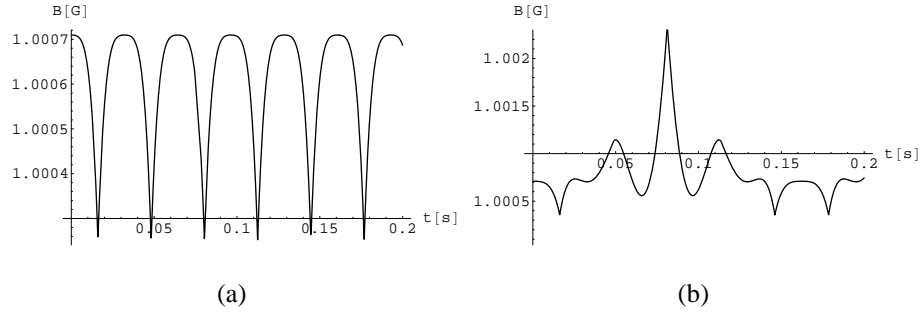


Figure D.14: Magnetic field along neutron trajectory (a) restricted to the  $x - y$  plane ( $\vec{v} = (3.1, 3.1, 0)^T$ ) and with a small velocity component in the  $z$ -direction ( $\vec{v} = (3.08, 3.08, 0.6)^T$ ). The modulus of the velocity  $|\vec{v}| = 4.4$  m/s.

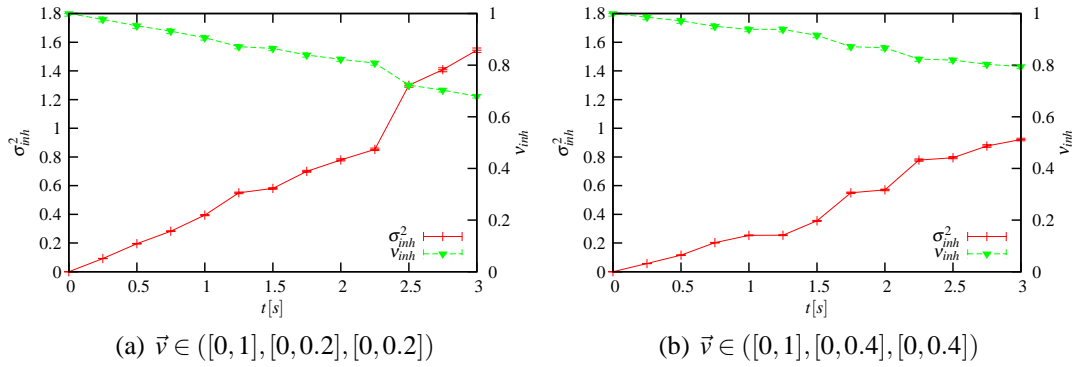


Figure D.15: Variance  $\sigma_{inh}^2$  of the accumulated phase of neutrons (solid line) propagating through the storage vessel with inhomogeneous magnetic field distribution. 2000 realisations have been computed for a mean field of 1 Gauss. On the right axis the visibility reduction  $V_{inh} = e^{-\sigma_{inh}^2/4}$  is plotted (dotted line).

What is the influence on the visibility of such fluctuations. An additional random phase shift has to be added to the average polarisation (c. f. Eq. 5.5.8) to obtain

$$\langle P \rangle = e^{-8\sigma_g^2} \cos(\xi - 4\bar{\phi}_g + \phi_{inh}). \quad (\text{D.2.1})$$

We assume for convenience that  $\phi_{inh}$  is Gaussian distributed with zero mean and variance  $\sigma_{inh}^2$ . The latter can be read off from Figures D.15. Accordingly, we find the second average according to Eq. (5.5.7)

$$\langle\langle P \rangle\rangle = e^{-8\sigma_g^2} \cos(\xi - 4\bar{\phi}_g) e^{-\frac{\sigma_{inh}^2}{4}} \quad (\text{D.2.2})$$

and notice, that the influence is much weaker due to the factor  $1/4$ . Maybe this can save the experiment. However, it depends on the time spent in the box and may cause additional complications for longer cycle times. In the experiment one has to pay attention to this additional time-dependent contribution since it antagonises the expected increase of the visibility.

## D.2.2 Fluctuating stray magnetic fields

One might argue that the effect of spurious inhomogeneities can be diminished by using weaker magnetic fields. However, another problem in connection with magnetic fields are stray fields of the environment which are disturbing the measurements more seriously the weaker the magnetic guide field is. In the section above we have reasoned that the magnetic field has to be fairly homogeneous up to Milligauss deviations. But can we provide a shielding that guarantees that there are not even larger unwanted influences from other sources?

In passing we note also that there is a subtle difference between the inhomogeneities of the artificial magnetic field and the magnetic fluctuations of the environment in that the former affect individual neutrons depending on their path through the box. In contrast the external fluctuations act on the ensemble of stored neutrons as a whole. It is an interesting question whether this makes a difference in the decoherence behaviour.

### Magnetic Shielding

In order to maintain the homogeneous magnetic field the magnetic shielding should be large enough to keep the influences from the exterior as low as possible, i. e. in our case at least less than 0.1% of the coil fields which corresponds to less than 0.1 Milligauss. Mu-metal<sup>1</sup> shielding should be sufficient to fulfil these requirements. Mu-metal is a nickel-iron alloy with high magnetic permeability,  $\mu_r = \mu/\mu_0 \approx 10^5$  relative to the vacuum permeability  $\mu_0$ . To calculate the effect of an external field inside a shielding we use the equations

$$S_A \approx \frac{(1 + 4N^{ell} S_T)}{1 + \frac{1}{2} \frac{D}{L}} \quad \text{and} \quad (\text{D.2.3})$$

$$S_T = \frac{\mu_r d}{D} \quad (\text{D.2.4})$$

for the axial and the transverse shielding factor  $S = B_e/B_i$  [PKS00] of a cylindrically shaped magnetic shield.  $B_e$  and  $B_i$  denote the external and the resultant internal magnetic field,  $d$  the wall thickness,  $D$  the diameter and  $L$  the axial length of the shielding cylinder.  $N^{ell}$  is the demagnetising factor of an equivalent ellipsoid [Os45].

The expected fluctuations in the magnetic field are about  $\pm 0.5 \text{ Gauss}$  as was measured in the course of examining the properties of a Helmholtz coil. Hopefully these are less in the vicinity of the PF2, the ultra-cold-neutrons beam line at the ILL in Grenoble, France, since for a 1 mm thick Mu-metal sheet the transverse attenuation factor is  $S_T = 125$  ( $\mu_r = 10^5$ ,  $D = 800$  mm) and the axial attenuation factor is  $S_A$  approximately same since the length-to-diameter-ratio  $L/D$  is close to 1 in our case [PKS00]. The external fluctuations are therefore damped to  $\approx 0.005G$  for a closed cylinder. Simulations show that a cylinder without the base caps has an attenuation factor of about  $S_T = 10$ . To see if this is sufficient for our purposes we have to measure the magnetic field fluctuations at the UCN beam-line itself.

---

<sup>1</sup>see e. g. <http://en.wikipedia.org/wiki/Mu-metal>

### D.2.3 Vessel too small

Besides reducing the flux, hence increasing the measurement time, the small size of the storage volume influences also the loss-rate and in turn again the count rate. The loss rate  $\alpha$  can be estimated [MAB<sup>+</sup>89] from the UCN reflection-loss probability of  $r = 2 - 3 \times 10^{-5}$ /bounce at the Fomblin surface (Section D.1.5), the mean free path length  $\lambda \approx 80$  mm (Section D.2.1), the neutron's velocity ( $v \approx 4.5 \text{ms}^{-1}$ ) and the storage time  $s < 10$  seconds,

$$\alpha \approx rvs/\lambda \approx 1 \times 10^{-3}, \quad (\text{D.2.5})$$

which is rather small for the short storage times assessed for the experiment. The major obstacle, however, remains probably the size itself in that the number of particles in each run is rather low.

### D.2.4 Insufficient rise & fall time of the electrical components

The typical rise and fall time of the amplifiers to be used in this experiment<sup>2</sup> is about  $20 - 30 \mu\text{s}$  (10% - 90%) equivalent to  $\approx 30 - 50$  kHz. Non-adiabatic switching has to be considerably faster than the maximal frequency present, which is the Larmor frequency  $\omega_L$  of about 3 kHz for 1 Gauss. If stronger magnetic fields are used there is also the possibility to reduce the magnetic field in strength just before the sudden change to guarantee a non-adiabatic transition. Moreover, the timing of the signal sequence in Section 5.5.1 has to be precise enough to assure no unpredictable phase accumulations, if the evolution is slightly longer or shorter from one run to another. The argument is the same as before, the Larmor frequency is the benchmark and the precision has to be on a time scale much lower than  $2\pi/\omega_L \approx 0.3$  ms.

### D.2.5 Inductance of Helmholtz coil could spoil high frequency noise

Another problem might be that the coils act as a low-pass filter for the noise current due to their inductance  $L$ . To estimate the influence from this source an already existing Helmholtz coil pair similar to the projected coils (530 mm inner and 567 mm outer diameter, 100 windings, wire 1 mm in diameter) has been tested. The cross section of the wire duct is  $17 \times 12 \text{mm}^2$  and its specific electrical resistance is  $7.9 \Omega$ .

From the equation

$$U(t) = U_0 e^{-tR/L} \quad (\text{D.2.6})$$

the inductance  $L$  can be derived by applying for example a periodic rectangular pulse and read off the exponential term at the falling edge (c. f. Figure D.16).

The fit yields the exponential function  $f(t) = -3.5 + 6.5 e^{-2.6 \times 10^5 t}$ . Inserting the resistivity  $R = 7.9 \Omega$  along with the damping coefficient  $-2.6 \times 10^5$  into Eq. (D.2.6) we get for

---

<sup>2</sup>KEPCO BOP 20-5M - <http://www.kepco.com/bopdyn.htm>

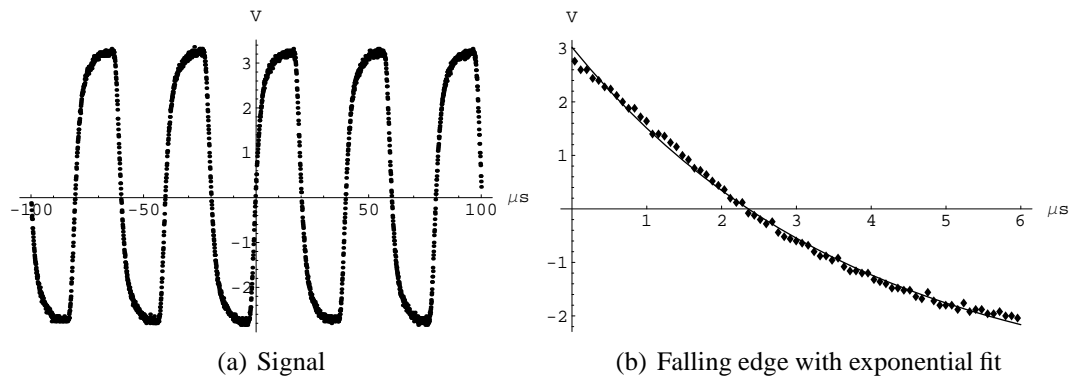


Figure D.16: A periodic rectangular signal is fed into the coils. The non-vanishing inductance of the coil distorts the shape of the rectangle.

the inductance  $L \approx 3 \times 10^{-5} H$ . From the complex resistivity

$$|Z| = |R + i\omega L| = \sqrt{R^2 + (\omega L)^2}$$

(neglecting the capacity of the circuit) we find that at frequencies where  $\omega L \approx 1$  the resistivity due to the self-inductance becomes non-negligible, i. e. for  $\omega \approx 3.3 \times 10^4$  rad/s or  $\nu = \omega/2\pi \approx 5$  kHz.

The maximal frequency we can apply is therefore about 5 kHz. As for the noise this is not alarming, we just want to use up to 1 kHz. However, the non-adiabatic reversal of the magnetic field is more critical. The problems can be circumvented by ramping down the magnetic guide field before flipping.

### D.3 How to measure?

In the measurement scheme unavoidable decoherence processes have to be taken into account. Therefore, we have to quantify the dephasing both due to the field inhomogeneities (Section D.2.1) and due to the external fluctuations (Section D.2.2). The sinusoidal oscillations of the average polarisation  $\langle P \rangle$  (Eq. 5.5.5) as a function of the additional phase  $\xi$  reveal the influence of these factors. A more dispersed polarisation manifests itself in a lower contrast.

- (i) First of all, stored neutrons are merely exposed to a static magnetic guide field. The polarisation changes sinusoidally as a function of storage time  $T$  and linearly with the strength of the magnetic field  $B$ . Both inhomogeneous field distribution and external fluctuations derogate the visibility for increasing  $T$ , but increasing  $B$  affects the visibility only via the inhomogeneous field distribution.

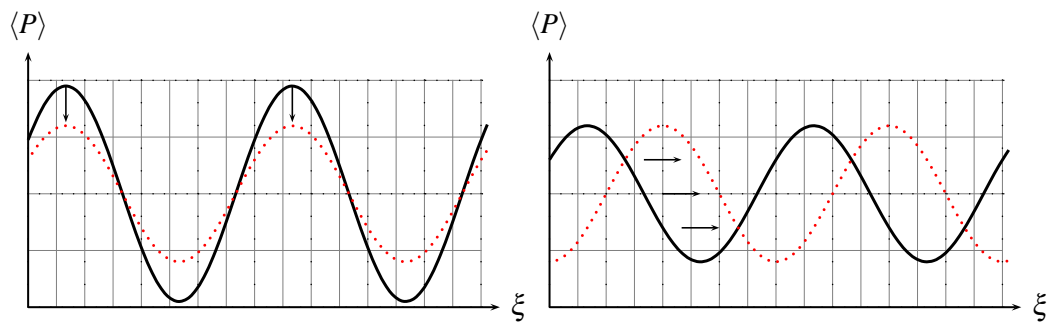
How can we separate the inhomogeneity influence from the external fluctuation influence?

- (ii) For constant  $T$  the field strength  $B$  can be varied. The amount of dephasing due to inhomogeneities depends linearly on  $B$ , so for  $B = 0$  there should be no dephasing

under ideal circumstances. However, the external fluctuations are present nevertheless, hence the limit of the contrast values  $B \rightarrow 0$  provides evidence of this kind of dephasing mechanism.

To find the effective unavoidable decoherence contribution to the contrast reduction the spin-echo scheme has to be implemented.

- (iii) Reversing the polarisation of the magnetic field strength exactly at half storage time ( $T/2$ ) the dynamical phase is cancelled (spin-echo). For a static magnetic field there should be no phase shift in the interference pattern, but only a reduction of contrast. The hereby found contrast value is the maximal contrast attainable (Figure D.17(a))



(a) The contrast (signal-to-noise ratio) is reduced by unavoidable noise fields and non-uniformity of the magnetic field.

(b) The oscillations are shifted as a function of the geometric phase.

Figure D.17: Average degree of polarisation.

By virtue of these preliminary measurements one must strive to find a compromise between a strong magnetic guide field to mask the external fluctuations and a weak field to avoid decoherence due to the non-uniform magnetic field. This is the main aim of the preliminary measurements scheduled in autumn 2006 at the ILL. If we succeed to spot a suitable set of parameters, the changeover to a rotating magnetic field can be attempted.

- (iv) The magnetic field is now rotated according to the time sequence described in Section 5.5, but still without artificial noise. By adjusting the off-axis angle  $\theta$  with the coil pair surrounding the  $y$ -axis the opening angle of the cone traced out by the magnetic field vector and consequently the expected geometric phase is set. The interference pattern is shifted, but the contrast stays constant (Figure D.17(b)).
- (v) Finally, artificial noise is added to test the predictions of theory [CP03] and numerical simulations (Section 5.6).

# Appendix E

## Notation

$m_n$  neutron mass ( $1.67492716(13) \times 10^{-27} \text{kg}$ )

$\mu_n$  neutron magnetic moment ( $-9.6623 \times 10^{-27} \text{JT}^{-1}$ )

$\sigma_x, \sigma_y, \sigma_z$  Pauli matrices

$\Phi$  total phase  $\Phi \equiv \arg\langle \psi_f | \psi_i \rangle$

$\phi_g, \gamma$  pure state geometric phase

$\phi_d$  pure state dynamical phase

$\tilde{\phi}$  noisy phase

$\gamma_{ij} \dots$  off-diagonal geometric phase

$\phi_\rho$  mixed state geometric phase

$\gamma_{\rho_i \rho_j} \dots$  off-diagonal mixed state geometric phase

$v$  visibility, contrast

$\eta$  usually used for the phaseshift responsible for interference fringes

$n$  refraction index ( $n = n' + in''$ )

$\lambda$  wavelength

$\vec{k}$  wavevector with magnitude  $k = |\vec{k}| = 2\pi/\lambda$

$X_i$  total phaseshift in the  $i$ -th beam in the second interferometer loop

$\tilde{X}_i$  spatial displacement,  $\tilde{X}_i = X_i/\bar{k}$

$\bar{k}$  mean momentum

$\chi_i^0$  phaseshift at parallel position ( $45^\circ$ )

## E. NOTATION

---

- $\chi_i$  phaseshift due to rotation ( $\chi_i = X_i - \chi_i^0$ )
- $\Delta\chi$  relative phase shift  $\Delta\chi = \chi_2 - \chi_1$
- $\Delta_n^c$  coherence length in direction  $n$
- $d$  thickness of phaseshifter
- $d_{eff}$  effective thickness
- $d_\lambda$   $\lambda$ -thickness
- $b_c$  coherent scattering length
- $N_{al}$  particle density (of aluminium)
- $\mathcal{H}$  complex Hilbert space
- $\mathcal{P}$  projective Hilbert space (Ray space)
- $\mathcal{N}$  set of nonzero vectors in Hilbert space  $\mathcal{H}$
- $\mathcal{N}_0$  set of unit vector in  $\mathcal{N}$  ( $\mathcal{N}_0 \subset \mathcal{N} \subset \mathcal{H}$ )
- $P_\psi$  ray space representative of  $|\psi\rangle \in \mathcal{H}$ , projection operator
- $\mathcal{H}_S$  system Hilbert space
- $\mathcal{H}_A$  ancilla (environmental) Hilbert space
- $\mathcal{H}_E$  extended Hilbert space ( $\mathcal{H}_E = \mathcal{H}_S \otimes \mathcal{H}_A$ )
- $\mathcal{O}(\mathcal{H})$  operator algebra of Hilbert space  $\mathcal{H}$
- $N$  dimension of Hilbert space,  $\dim \mathcal{H} = N$
- $\mathcal{C}$  curve in Hilbert space
- $\mathcal{C}_0$  curve of unit vectors in Hilbert space
- $\tilde{\mathcal{C}}$  curve in projective Hilbert space
- $\hat{\mathcal{C}}$  curve in extended Hilbert space
- $c$  parallel lifted curve
- $\mathcal{G}$  geodesic path in Hilbert space
- $U(K)$  unitary group of dimension  $K$
- $\text{Tr}_A$  partial trace over the environment

- 
- $T$  total evolution time
- $\omega_L$  angular Larmor frequency
- $\omega_r$  angular frequency of the magnetic field rotation
- $\omega_n$  angular frequency bandwidth of noise
- $\Gamma_j$  frequency bandwidth of noise (in direction  $j$ ) ( $\omega_n = 2\pi\Gamma$ )
- $\mu_X$  mean of the random variable  $X$
- $\sigma_X^2$  variance of the random variable  $X$
- $\langle Y \rangle$  ensemble average of the random variable  $Y$
- $\bar{Y}$  time average of  $Y$
- $G_{YZ}$  covariance of the random variables  $Y$  and  $Z$
- $C_X(t)$  autocorrelation function of the stochastic process  $X$
- $S_X(\nu)$  power spectral density of the stochastic process  $X$  ( $\nu \dots$  frequency)
- $P_X^2$  mean power of the stochastic process  $X$
- $s_r$  signal-to-noise ratio  $\omega_L/P_X$

# Bibliography

- [AA87] Y. Aharonov and J. S. Anandan, *Phase change during a cyclic quantum evolution*, Phys. Rev. Lett **58** (1987), 1593–96.
- [AB59] Y. Aharonov and D. Bohm, *Significance of electromagnetic potentials in quantum theory*, Phys. Rev. **115** (1959), 485–91.
- [AG93] N. I. Akhiezer and I. M. Glazman, *Theory of linear operators in hilbert space*, vol. II, Dover Publications, Inc., New York, 1993.
- [AKW<sup>+</sup>97] B. E. Allman, H. Kaiser, S. A. Werner, A. G. Wagh, V. C. Rakhecha, and J. Summhammer, *Observation of geometric and dynamical phases by neutron interferometry*, Phys. Rev. A **56** (1997), 4420–4439.
- [Ana92] J. Anandan, *The geometric phase*, Nature **360** (1992), 307–13.
- [ASP<sup>+</sup>01] J. S. Anandan, E. Sjöqvist, A. H. Pati, A. Ekert, M. Ericsson, D. K. L. Oi, and V. Vedral, *Reply to "singularities of the mixed states phase"*, e-print: quant-ph/0109139, 2001.
- [Bar64] V. Bargmann, *Note on Wigner's theorem on symmetry operations*, J. Math. Phys. **5** (1964), 862.
- [BD87] T. Bitter and D. Dubbers, *Manifestation of Berry's topological phase in neutron spin rotation*, Phys. Rev. Lett. **59** (1987), 251–254.
- [BDG<sup>+</sup>06] C. A. Baker, D. D. Doyle, P. Geltenbort, K. Green, M. G. D. van der Grinten, P. G. Harris, P. Iaydijiev, S. N. Ivanov, D. J. R. May, J. M. Pendlebury, J. D. Richardson, D. Shiers, and K. F. Smith, *An improved experimental limit on the electric dipole moment of the neutron*, eprint: hep-ex/0602020, 2006.
- [BDHH04] R. Bertlmann, K. Durstberger, Y. Hasegawa, and B. Hiesmayr, *Berry phase in entangled system: A proposed experiment with single neutrons*, Phys. Rev. A **69** (2004), 032112.
- [Bel64] J. S. Bell, *On the Einstein-Podolsky-Rosen paradox*, Physics **1** (1964), 195–200.

## BIBLIOGRAPHY

---

- [Ber84] M. V. Berry, *Quantal phase factors accompanying adiabatic changes*, Proc. Roy. Soc. Lond. A **392** (1984), 45–57.
- [Ber87] ———, *Interpreting the anholonomy of coiled light*, Nature **326** (1987), 277–278.
- [Ber96] R. A. Bertlmann, *Anomalies in quantum field theory*, Int. Series of Monographs on Physics, vol. 91, Oxford University Press, New York, 1996.
- [Bha91] R. Bhandari, *Evolution of light beams in polarization and direction*, Physica B **175** (1991), 111–122.
- [Bha97] ———, *Polarization of light and topological phases*, Phys. Rep. **281** (1997), 1–64.
- [Bha99] ———, *Comment on "Neutron interferometric observation of noncyclic phase"*, Phys. Rev. Lett. **83** (1999), 2089.
- [Bha02] ———, *Singularities of the mixed state phase*, Phys. Rev. Lett. **89** (2002), 268901.
- [BHG06] C. Brockmann, L. Hufnagel, and T. Geisel, *The scaling laws of human travel*, Nature **439** (2006), 462–465.
- [Bil95] P. Billingsley, *Probability and measure*, 3rd ed., Wiley-Interscience, New York, 1995.
- [Blo36] F. Bloch, *On the magnetic scattering of neutrons*, Phys. Rev. **50** (1936), 259.
- [BP02] H.-P. Breuer and F. Petruccione, *The theory of open quantum systems*, Oxford University Press, 2002.
- [Bro66] R. Brown, *A brief account of microscopical observations on the particles contained in the pollen of plants*, The miscellaneous works of Robert Brown (J. J. Bennet, ed.), vol. Vol I., R. Hardwicke, London, 1866.
- [BRS83] G. Badurek, H. Rauch, and J. Summhammer, *Time-dependent superposition of spinors*, Phys. Rev. Lett. **51** (1983), 1015–1018.
- [BRS03] M. Baron, H. Rauch, and M. Suda, *First attempt of neutron quantum state reconstruction*, J. Opt. B **5** (2003), 8241–8244.
- [BT57] R. H. Brown and R. Q. Twiss, *Interferometry of the intensity fluctuations in light. I. Basic theory.*, Proc. Roy. Soc. Lond. A **242** (1957), 300–324.
- [BT58] ———, *Interferometry of the intensity fluctuations in light. II. An experimental test of the theory for partially coherent light*, Proc. Roy. Soc. Lond. A **243** (1958), 291–319.

## BIBLIOGRAPHY

---

- [BT03] A. Blais and A.-M. S. Tremblay, *Effect of noise on geometric logic gates for quantum computation*, Phys. Rev. A **67** (2003), 012308.
- [Bur69] D. Bures, *An extension of Kakutani's theorem on infinite product measures to the tensor product of semifinite  $w^*$ -algebras*, Trans. Am. Math. Soc. **135** (1969), 199–212.
- [CBDMDB77] Y. Choquet-Bruhat, C. DeWitt-Morette, and M. Dillard-Bleick, *Analysis, manifolds and physics*, vol. I, Elsevier, Netherlands, 1977.
- [CEM<sup>+</sup>04] S. Chaturvedi, E. Ercolessi, G. Marmo, G. Morandi, N. Mukunda, and R. Simon, *Geometric phase for mixed states: a differential geometric approach*, Eur. Phys. J. C **35** (2004), 413–423.
- [CFGSV03] A. Carollo, I. Fuentes-Guridi, M. F. Santos, and V. Vedral, *Geometric phase in open systems*, Phys. Rev. A **90** (2003), 160402.
- [CFGSV04] A. Carollo, I. Fuentes-Guridi, M. F. Santos, and V. Vedral, *Spin-1/2 geometric phase driven by decohering quantum fields*, Phys. Rev. Lett. **92** (2004), 020402.
- [CKW<sup>+</sup>91] R. Clothier, H. Kaiser, S. A. Werner, H. Rauch, and H. Wölwitsch, *Neutron phase echo*, Phys. Rev. A **44** (1991), 5357–5368.
- [COW75] R. Colella, A. W. Overhauser, and S. A. Werner, *Observation of gravitationally induced quantum interference*, Phys. Rev. Lett. **34** (1975), 1472–1474.
- [CP03] G. D. Chiara and G. Palma, *Berry phase for a spin-1/2 particle in a classical fluctuating field*, Phys. Rev. Lett. **91** (2003), 090404.
- [DCZ01] L.-M. Duan, J. I. Cirac, and P. Zoller, *Geometric manipulation of trapped ions for quantum computation*, Science **292** (2001), 1695–1697.
- [dFdTPN03] J. P. de Faria, A. de Toledo Piza, and M. Nemes, *Phases of quantum states in completely positive non-unitary evolution*, Europhys. Lett. **62** (2003), 782–788.
- [Doo42] J. L. Doob, *The Brownian movement and stochastic equations*, Ann. Math. **43** (1942), 319–337, Also published in [Wax54].
- [DZS<sup>+</sup>03] J. Du, P. Zou, M. Shi, L. C. Kwek, J.-W. Pan, C. H. Oh, A. Ekert, D. K. L. Oi, and M. Ericsson, *Observation of geometric phases for mixed states using NMR interferometry*, Phys. Rev. Lett. **91** (2003), 100403.
- [EAB<sup>+</sup>05] M. Ericsson, D. Achilles, J. Barreira, D. Branning, N. Peters, and P. Kwiat, *Measurement of geometric phase for mixed states using single photon interferometry*, Phys. Rev. Lett. **94** (2005), 050401.

- [Eco88] U. Eco, *Il pendolo di Foucault*, Gruppo Editoriale Fabbri, 1988.
- [EEH<sup>+</sup>00] A. Ekert, M. Ericsson, P. Hayden, H. Inamori, J. A. Jones, D. K. L. Oi, and V. Vedral, *Geometric quantum computation*, *J. Mod. Opt.* **47** (2000), 2501–2513.
- [Ein05] A. Einstein, *On the motion of small particles suspended in a stationary liquid according to the molecular kinetic theory of heat*, *Ann. Phys. Leipzig* **17** (1905), 549–60.
- [EPR35] A. Einstein, B. Podolsky, and N. Rosen, *Can quantum-mechanical description of physical reality be considered complete?*, *Phys. Rev.* **47** (1935), 777–80.
- [EPS<sup>+</sup>03] M. Ericsson, A. K. Pati, E. Sjöqvist, J. Brännlund, and D. K. L. Oi, *Mixed state geometric phases, entangled systems, and local unitary transformations*, *Phys. Rev. Lett.* **91** (2003), 090405.
- [ESB<sup>+</sup>03] M. Ericsson, E. Sjöqvist, J. Brännlund, D. K. L. Oi, and A. Pati, *Generalization of the geometric phase to completely positive maps*, *Phys. Rev. A* **67** (2003), 020101.
- [FFP<sup>+</sup>00] G. Falci, R. Fazio, G. M. Palma, J. Siewert, and V. Vedral, *Detection of geometric phases in superconducting nanocircuits*, *Nature* **407** (2000), 335–358.
- [FHLR05a] S. Filipp, Y. Hasegawa, R. Loidl, and H. Rauch, *Noncyclic geometric phase due to spatial evolution in a neutron interferometer*, *Phys. Rev. A* **72** (2005), 021602, eprint: quant-ph/0412038.
- [FHLR05b] ———, *Spatial non-cyclic geometric phase in neutron interferometry*, *NIST J. Res.* **110** (2005), 251–257.
- [Fra89] J. D. Franson, *Bell inequality for position and time*, *Phys. Rev. Lett* **62** (1989), 2205–08.
- [FS03a] S. Filipp and E. Sjöqvist, *Off-diagonal generalization of the mixed-state geometric phase*, *Phys. Rev. A* **68** (2003), 042112.
- [FS03b] ———, *Off-diagonal geometric phase for mixed states*, *Phys. Rev. Lett.* **90** (2003), 050403.
- [FS04a] S. Filipp and K. Svozil, *Generalizing Tsirelson’s bound on Bell-inequalities using a min-max principle*, *Phys. Rev. Lett.* **93** (2004), 130407.
- [FS04b] ———, *Testing the bounds on quantum probabilities*, *Phys. Rev. A* **69** (2004), 032101.

## BIBLIOGRAPHY

---

- [FS05] S. Filipp and E. Sjöqvist, *Off-diagonal quantum holonomy along density operators*, Phys. Lett. A **342** (2005), 205–212.
- [FVH57] R. P. Feynman, F. L. Vernon, and R. W. Hellwarth, *Geometrical representation of the Schrödinger equation for solving maser problems*, J. Appl. Phys. **29** (1957), 49–52.
- [Gab56] D. Gabor, *Theory of electron interference experiments*, Rev. Mod. Phys. **28** (1956), 260–276.
- [GF89] D. Gamliel and J. Freed, *Berry’s geometrical phases in ESR in the presence of stochastic process*, Phys. Rev. A **39** (1989), 3238–3255.
- [Gil95] D. Gillespie, *The mathematics of Brownian motion and Johnson noise*, Am. J. Phys. **64** (1995), 225–240.
- [Gil00] D. Gillespie, *A mathematical comparison of simple models of Johnson noise and shot noise*, J. Phys. Cond. Mat. **12** (2000), 4195–4205.
- [GK06] A. Ghosh and A. Kumar, *Experimental measurement of mixed state geometric phase by quantum interferometry using NMR*, Phys. Lett. A **349** (2006), 27–36.
- [Gla63] R. J. Glauber, *The quantum theory of optical coherence*, Phys. Rev. **130** (1963), 2529–2539.
- [GLN05] A. Gilchrist, N. Langford, and M. Nielsen, *Distance measures to compare real and ideal quantum processes*, Phys. Rev. A **71** (2005), 062310.
- [Gre98] W. Greiner, *Classical electrodynamics*, Springer Verlag, Berlin Heidelberg, 1998.
- [Gro04] S. E. P. D. Group), *Review of particle physics*, Phys. Lett. B **592** (2004), 1–5, <http://pdg.lbl.gov>.
- [GS22] W. Gerlach and O. Stern, *Der experimentelle Nachweis der Richtungsquantelung im Magnetfeld*, Z. Phys. **9** (1922), 349–355.
- [GSS67] A. Goldberg, H. M. Schey, and J. L. Schwartz, *Computer-generated motion pictures of one-dimensional quantum-mechanical transmission and reflection phenomena*, Am. J. Phys. **35** (1967), 177–186.
- [GW88] J. C. Garrison and E. M. Wright, *Complex geometrical phases for dissipative systems*, Phys. Lett. A **128** (1988), 177–181.
- [Haa96] R. Haag, *Local quantum physics: Fields, particles, algebras*, 2<sup>nd</sup> ed., Springer, Berlin Heidelberg, 1996.

- [Hal87] F. D. M. Haldane, *Comment on "Observation of Berry's topological phase by use of an optical fibre"*, Phys. Rev. Lett. **59** (1987), 1788.
- [HB99] Y. Hasegawa and G. Badurek, *Noncommuting spinor rotation due to balanced geometrical and dynamical phases*, Phys. Rev. A **59** (1999), 4614–4622.
- [HBG<sup>+</sup>99] P. Harris, C. Baker, K. Green, P. Iaydjiev, S. Ivanov, D. May, J. Pendlebury, D. Shiers, K. Smith, M. van der Grinten, and P. Geltenbort, *New experimental limit on the electric dipole moment of the neutron*, Phys. Rev. Lett. **82** (1999), 904–907.
- [Hea02] M. T. Heath, *Scientific computing - an introductory survey*, 2nd ed., McGraw-Hill, 2002.
- [HLB<sup>+</sup>01] Y. Hasegawa, R. Loidl, M. Baron, G. Badurek, and H. Rauch, *Off-diagonal geometric phase in a neutron interferometer experiment*, Phys. Rev. Lett. **87** (2001), 070401.
- [HLB<sup>+</sup>02] Y. Hasegawa, R. Loidl, G. Badurek, M. Baron, N. Manini, F. Pistolesi, and H. Rauch, *Observation of off-diagonal geometric phases in polarized-neutron-interferometer experiments*, Phys. Rev. A **65** (2002), 052111.
- [HLB<sup>+</sup>03] Y. Hasegawa, R. Loidl, G. Badurek, M. Baron, and H. Rauch, *Violation of a Bell-like inequality in single-neutron interferometry*, Nature **425** (2003), 45–48.
- [HS00] B. Hessmo and E. Sjöqvist, *Quantal phase for nonmaximally entangled photons*, Phys. Rev. A **62** (2000), 062301.
- [HSKH<sup>+</sup>05] H. Häffner, F. Schmidt-Kaler, W. Hänsel, C. Roos, T. Körber, M. Chwalla, M. Riebe, J. Benhelm, U. Rapol, C. Becher, and R. Blatt, *Robust entanglement*, Appl. Phys. B **81** (2005), 151–153.
- [Hüb93] M. Hübner, *Holonomy on Lie groups and energy uncertainty*, Phys. Lett. A **179** (1993), 221–225.
- [HZR96] Y. Hasegawa, M. Zawisky, and H. Rauch, *Geometric phase in coupled neutron interference loops*, Phys. Rev. A **53** (1996), 2486–92.
- [IOS<sup>+</sup>06] M. Iannuzzi, A. Orecchini, F. Sacchetti, P. Facchi, and S. Pascazio, *Direct experimental evidence of free-fermion antibunching*, Phys. Rev. Lett. **96** (2006), 080402.
- [Joz94] R. Jozsa, *Fidelity for mixed quantum states*, J. Mod. Opt **41** (1994), 2315–2323.

## BIBLIOGRAPHY

---

- [JVEC00] J. A. Jones, V. Vedral, A. Ekert, and G. Castagnoli, *Geometric quantum computation using NMR*, *Nature* **403** (200), 869–71.
- [KCS04] I. Kamleitner, J. D. Cresser, and B. C. Sanders, *Geometric phase for an adiabatically evolving open quantum system*, *Phys. Rev. A* **70** (2004), 044103.
- [KDM77] H. Kimble, M. Dagenais, and L. Mandel, *Photon antibunching in resonance fluorescence*, *Phys. Rev. Lett.* **39** (1977), 691–695.
- [KP95] P. E. Kloeden and E. Platen, *Numerical solution of stochastic differential equations*, Springer, 1995.
- [Kra83] K. Kraus, *States, effects and operations*, Lecture Notes in Physics, vol. 190, Springer Verlag, Berlin, 1983.
- [KRH02] H. Kiesel, A. Renz, and F. Hasselbach, *Observation of Hanbury Brown-Twiss anticorrelations for free electrons*, *Nature* **418** (2002), 392–394.
- [KSH<sup>+</sup>05] J. Klepp, S. Sponar, Y. Hasegawa, E. Jericha, and G. Badurek, *Noncyclic Pancharatnam phase for mixed state  $SU(2)$  evolution in neutron polarimetry*, *Phys. Lett. A* **342** (2005), 48–52.
- [KWW<sup>+</sup>99] P. G. Kwiat, E. Waks, A. G. White, I. Appelbaum, and P. H. Eberhard, *Ultrabright source of polarization-entangled photons*, *Phys. Rev. A* **60** (1999), R773.
- [Leo94] W. Leo, *Techniques for nuclear and particle physics experiments. A how-to approach.*, ch. Statistics and the Treatment of Experimental Data, Springer, Berlin, 1994.
- [MAB<sup>+</sup>89] W. Mampe, P. Ageron, C. Bates, J. M. Pendlebury, and A. Steyerl, *Neutron lifetime measured with stored ultracold neutrons*, *Phys. Rev. Lett.* **63** (1989), 593.
- [MACS01] N. Mukunda, Arvind, S. Chaturvedi, and R. Simon, *Bargmann invariants and off-diagonal geometric phases for multi-level quantum systems: A unitary group approach*, *Phys. Rev. A* **65** (2001), 012102.
- [May03] S. Mayer, *Experimente zur phasenstabilität eines neutroneninterferometers*, Master's thesis, Atominstitut der Österr. Universitäten, 2003.
- [Mes62] A. Messiah, *Quantum mechanics*, vol. 2, North-Holland, Amsterdam, 1962.
- [Mez72] F. Mezei, *Neutron spin echo: A new concept in polarized thermal neutron techniques*, *Z. Phys.* **255** (1972), 146–160.

- [MP00] N. Manini and F. Pistolesi, *Off-diagonal geometric phases*, Phys. Rev. Lett. **85** (2000), 3067–71.
- [MS93] N. Mukunda and R. Simon, *Quantum kinematic approach to the geometric phase*, Ann. Phys. **228** (1993), 205.
- [Nak03] M. Nakahara, *Geometry, topology and physics*, Institute of Physics Publishing, London, 2003.
- [NC00] M. A. Nielsen and I. L. Chuang, *Quantum computation and quantum information*, Cambridge University Press, Cambridge, U. K., 2000.
- [NSM02] A. Nazir, T. P. Spiller, and W. J. Munro, *Decoherence of geometric phase gates*, Phys. Rev. A **65** (2002), 042303.
- [Öks03] B. Öksendal, *Stochastic differential equations*, Springer-Verlag, 2003.
- [Osb45] J. A. Osborn, *Demagnetizing factors of the general ellipsoid*, Phys. Rev. **67** (1945), 351–357.
- [Pan56] S. Pancharatnam, *Generalized theory of interference and its applications*, Proc. Ind. Acad. Sci. **A44** (1956), 247–62.
- [Per98] I. Percival, *Quantum state diffusion*, Cambridge, 1998.
- [Pet87] D. Petrascheck, *Coherence lengths and neutron optics*, Phys. Rev. B **35** (1987), 6549–6553.
- [PHS<sup>+</sup>04] J. M. Pendlebury, W. Heil, Y. Sobolev, P. G. Harris, J. D. Richardson, R. J. Baskin, D. D. Doyle, P. Geltenbort, K. Green, M. G. D. van der Grinten, P. S. Iaydjiev, S. N. Ivanov, D. J. R. May, and K. F. Smith, *Geometric-phase-induced false electric dipole moment signals for particles in traps*, Phys. Rev. A **70** (2004), 032102.
- [PKS00] E. Paperno, H. Koide, and I. Sasada, *A new estimation of the axial shielding factors for multishell cylindrical shields*, J. Appl. Phys. **87** (2000), 5959–5961.
- [Pre98] J. Preskill, *Lecture notes for physics 229: Quantum information and computation*, 1998.
- [Pur56] E. M. Purcell, *The question of correlation between photons in coherent light rays*, Nature **178** (1956), 1449–1950.
- [Rau04] H. Rauch, *Interferometrie mit Neutronen*, Physik Journal **3** (2004), 39–45.
- [Réf04] P. Réfrégier, *Noise theory and application to physics*, Springer, 2004.

## BIBLIOGRAPHY

---

- [Ric44a] S. O. Rice, *Mathematical analysis of random noise*, Bell System Technical Journal **23** (1944), 282–332, Also published in [Wax54].
- [Ric44b] ———, *Mathematical analysis of random noise*, Bell System Technical Journal **24** (1944), 46–156, Also published in [Wax54].
- [RKGL88] D. Richardson, A. Kilvington, K. Green, and S. Lamoreaux, *Demonstration of Berry’s phase using stored ultracold neutrons*, Phys. Rev. Lett. **61** (1988), 2030–2033.
- [RLBL02] H. Rauch, H. Lemmel, M. Baron, and R. Loidl, *Measurement of a confinement induced neutron phase*, Nature **417** (2002), 630–632.
- [Ros84] J. Ross, *The rotation of the polarization in low birefringence monomode optical fibres due to geometric effects*, Opt. Quantum Electron. **16** (1984), 445.
- [RP76a] H. Rauch and D. Petrascheck, *Grundlagen für ein Laue-Neutroneninterferometer - teil 1*, 1976.
- [RP76b] ———, *Grundlagen für ein Laue-Neutroneninterferometer - teil 2*, 1976.
- [RS80] M. Reed and B. Simon, *Methods of modern mathematical physics*, vol. I. Functional Analysis, Academic Press, 1980.
- [RS84] H. Rauch and J. Summhammer, *Static versus time-dependent absorption in neutron interferometry*, Phys. Lett. **104** (1984), 44–46.
- [RTB74] H. Rauch, W. Treimer, and U. Bonse, *Test of a single crystal neutron interferometer*, Phys. Lett. **47** (1974), 369–371.
- [RW00] H. Rauch and S. A. Werner, *Neutron interferometry: Lessons in experimental quantum mechanics*, Clarendon Press, Oxford, 2000.
- [RWK<sup>+</sup>96] H. Rauch, H. Wölwitsch, H. Kaiser, R. Clothier, and S. A. Werner, *Measurement and characterization of the three-dimensional coherence function in neutron interferometry*, Phys. Rev. A **53** (1996), 902–908.
- [RZB<sup>+</sup>75] H. Rauch, A. Zeilinger, G. Badurek, A. Wilfing, W. Bauspiess, and U. Bonse, *Verification of coherent spinor rotation of fermions*, Phys. Lett. **54** (1975), 425–427.
- [SB88] J. Samuel and R. Bhandari, *General setting for Berry’s phase*, Phys. Rev. Lett. **60** (1988), 2339–42.
- [SBRK82] J. Summhammer, G. Badurek, H. Rauch, and U. Kischko, *Explicit experimental verification of quantum spin-state superposition*, Phys. Lett. A **90** (1982), 110–112.

- [Sch35] E. Schrödinger, *Discussion of probability relations between separated systems*, Proc. Camb. Phil. Soc. **31** (1935), 555–563.
- [Sch36] ———, *Discussion of probability relations between separated systems*, Proc. Camb. Phil. Soc. **32** (1936), 446–451.
- [Sch06] J. Schmiedmayer, private communication, 2006.
- [Sea89] V. F. Sears, *Neutron optics*, Oxford University Press, 1989.
- [SF03] E. Sjöqvist and S. Filipp, *Off-diagonal mixed state phases in unitary evolution*, Foundations of probability and physics - 2 (Växjö) (A. Khrennikov, ed.), Math. Modelling in Physics, Engineering and Cognitive Sciences, Växjö Univ. Press, 2003.
- [Sim83] B. Simon, *Holonomy, the quantum adiabatic theorem, and Berry's phase*, Phys. Rev. Lett. **51** (1983), 2167–2170.
- [Sjö01] E. Sjöqvist, *Quantal phase in split-beam interferometry*, Phys. Rev. A **63** (2001), 035602.
- [Sjö02] ———, *Pancharatnam revisited*, Quantum Theory: Reconsideration of Foundations (A. Khrennikov, ed.), Math. Modelling in Physics, Engineering and Cognitive Sciences, Växjö University Press, 2002, p. 343.
- [SL06] M. S. Sarandy and D. A. Lidar, *Abelian and non-Abelian geometric phases in adiabatic open quantum systems*, Phys. Rev. A **73** (2006), 062101.
- [SPE<sup>+</sup>00] E. Sjöqvist, A. K. Pati, A. Ekert, J. S. Anandan, M. Ericsson, D. K. L. Oi, and V. Vedral, *Geometric phases for mixed states in interferometry*, Phys. Rev. Lett. **85** (2000), 2845–49.
- [STB<sup>+</sup>03] K. Singh, D. M. Tong, K. Basu, J. L. Chen, and J. F. Du, *Geometric phases for nondegenerate and degenerate mixed states*, Phys. Rev. A **67** (2003), 032106.
- [TC86] A. Tomita and R. Chiao, *Observation of Berry's topological phase by use of an optical fiber*, Phys. Rev. Lett. **57** (1986), 937–940.
- [TS03] J. Tidström and E. Sjöqvist, *Uhlmann's geometric phase in presence of isotropic decoherence*, Phys. Rev. A **67** (2003), 032110.
- [TSF<sup>+</sup>05] D. M. Tong, E. Sjöqvist, S. Filipp, L. C. Kwek, and C. H. Oh, *Kinematic approach to off-diagonal geometric phases of nondegenerate and degenerate mixed states*, Phys. Rev. A **71** (2005), 032106.

- [TSKO04] D. M. Tong, E. Sjöqvist, L. C. Kwek, and C. H. Oh, *Kinematic approach to the mixed state geometric phase in nonunitary evolution*, Phys. Rev. Lett. **93** (2004), 080405.
- [Uhl76] A. Uhlmann, *The 'transition probability' in the state space of a  $*$ -algebra*, Rep. Math. Phys. **9** (1976), 273.
- [Uhl86] ———, *Parallel transport and "quantum holonomy" along density operators*, Rep. Math. Phys. **24** (1986), 229–40.
- [Uhl91a] ———, *A gauge field governing parallel transport along mixed states*, Lett. Math. Phys. **21** (1991), 229–36.
- [Uhl91b] ———, *Symmetry in physics v, (algebraic systems, their representations, realizations, and physical applications)*, ch. Algebra and Geometry in the Theory of Mixed States, pp. 565–583, Plenum Press, New York, 1991.
- [Uhl93] ———, *Symmetry in science vi, (from the rotation group to quantum algebras)*, ch. Parallel lifts and holonomy along density operators: Computable examples using  $O(3)$ -orbits, pp. 741–748, Plenum Press, New York, 1993.
- [Uhl95] ———, *Geometric phases and related structures*, Rep. Math. Phys. **36** (1995), 461–81.
- [UJA<sup>+</sup>04] R. Ursin, T. Jennewein, M. Aspelmeyer, R. Kaltenbaek, M. Lindenthal, P. Walther, and A. Zeilinger, *Quantum teleportation across the Danube*, Nature **430** (2004), 849.
- [UO30] G. Uhlenbeck and L. Ornstein, *On the theory of Brownian motion*, Phys. Rev. **36** (1930), 823–841.
- [vdGPS<sup>+</sup>99] M. G. D. van der Grinten, J. M. Pendlebury, D. Shiers, C. A. Baker, K. Green, P. Harris, P. S. Iaydijiev, S. N. Ivanov, and P. Geltenbort, *Characterization and development of diamond-like carbon coatings for storing ultracold neutrons*, Nucl. Instr. Meth. A **423** (1999), 421–427.
- [Ved05] V. Vedral, private communication, 2005.
- [Wag99] A. G. Wagh, *Comment on "Geometric phase in coupled neutron interference loops"*, Phys. Rev. A **59** (1999), 1715–16.
- [Wax54] N. Wax (ed.), *Selected papers on noise and stochastic processes*, Dover Publications, New York, 1954.
- [WB90] H. Weinfurter and G. Badurek, *Measurement of Berry's phase for noncyclic evolution*, Phys. Rev. Lett. **64** (1990), 1318–1321.

## BIBLIOGRAPHY

---

- [WBR<sup>+</sup>00] A. Wagh, G. Badurek, V. Rakhecha, R. Buchelt, and A. Schricker, *Neutron polarimetric separation of geometric and dynamical phases*, Phys. Lett. A **268** (2000), 209–216.
- [Wei] E. Weisstein, *Harmonic addition theorem*, Mathworld - A Wolfram Web Resouce, <http://mathworld.wolfram.com/HarmonicAdditionTheorem.html>.
- [WMSG05] R. S. Whitney, Y. Makhlin, A. Shnirman, and Y. Gefen, *Geometric nature of the environment-induced Berry phase and geometric dephasing*, Phys. Rev. Lett. **94** (2005), 070407.
- [WRFI98] A. G. Wagh, V. C. Rakhecha, P. Fischer, and A. Ioffe, *Neutron interferometric observation of noncyclic phase*, Phys. Rev. Lett. **81** (1998), 1992–95.
- [WRS<sup>+</sup>97] A. Wagh, V. Rakhecha, J. Summhammer, G. Badurek, H. Weinfurter, B. Allman, H. Kaiser, K. Hamacher, D. Jacobson, and S. Werner, *Experimental separation of geometric and dynamical phases using neutron interferometry*, Phys. Rev. Lett. **78** (1997), 755–759.
- [WZ84] F. Wilczek and A. Zee, *Appearance of gauge structure in simple dynamical systems*, Phys. Rev. Lett. **52** (1984), 2111–2114.
- [ZBLR02] M. Zawisky, M. Baron, R. Loidl, and H. Rauch, *Testing the world’s largest monolithic perfect crystal neutron interferometer*, Nucl. Instr. Meth. A **481** (2002), 406.
- [ZR99] P. Zanardi and M. Rasetti, *Holonomic quantum computation*, Phys. Lett. A **294** (1999), 94–99.
- [ZZ05] S.-L. Zhu and P. Zanardi, *Geometric quantum gates robust against stochastic control errors*, Phys. Rev. A **72** (2005), 020301.

# Curriculum Vitae

## Personal details

---

Name: Stefan Filipp  
Address: Herzgasse 14/5, 1100 Wien, Austria  
Nationality: Austria  
Email: sfilipp@ati.ac.at  
Place/Date of birth: Mistelbach, 16/11/1977  
Military Service: Dec. 1996 - July 1997 in Mistelbach

## Education and University Studies

---

1988 - 1996 Gymnasium Laa/Thaya, Austria  
June 1996 Matura with distinction.  
1997 - 2003 Physics studies at the Vienna University of Technology  
March 2003 Master's Degree (Dipl.-Ing.) in Technical Physics, Vienna University of Technology, Austria  
Thesis: "Bounds on Quantum Probabilities"  
(Supervisor: Dr. Karl Svozil)  
Jan. - July 2002 Physics studies at the Uppsala University, Sweden  
July 2002 Master's Degree (MSc.) in Physics, Uppsala University, Sweden  
Thesis: "Off-diagonal geometric phases for mixed states"  
(Supervisor: Dr. Erik Sjöqvist)  
2003-2006 PhD-Studies at the Atominstitut der Österr. Universitäten, Austria

## Academic Positions

---

Oct. 2001 - Jan. 2002, Teaching assistant at the Institute of Theoretical Physics,  
Oct. 2002 - Jan. 2003 Vienna University of Technology  
2004 - 2006 Doctorand at the Institut Laue - Langevin, Grenoble, France  
since May 2003 Research assistant at the Atominstitut der Österr. Universitäten

## Publications (refereed)

---

1. Non-cyclic geometric phase due to spatial evolution in a neutron interferometric Setup. **S. Filipp**, *Y. Hasegawa, R. Loidl and H. Rauch*. Phys. Rev. A **72**, 021602(R) (2005).
2. Off-diagonal quantum holonomy along density operators. **S. Filipp** and *E. Sjöqvist*. Phys. Lett. A **342**, 205 (2005).
3. Spatial non-cyclic geometric phase in neutron interferometry. **S. Filipp**, *Y. Hasegawa, R. Loidl and H. Rauch*. NIST Journal of Research **110**, 251 (2005).
4. Kinematic approach to off-diagonal geometric phases of nondegenerate and degenerate mixed states. *D.M. Tong, E. Sjöqvist, S. Filipp, L.C. Kwek and C.H. Oh*. Phys. Rev. A **71**, 032106 (2005).
5. Generalizing Tsirelson's bound on Bell inequalities using a min-max principle. **S. Filipp** and *K. Svozil*. Phys. Rev. Lett. **93**, 130407 (2004).
6. Testing the bounds on quantum probabilities. **S. Filipp** and *K. Svozil*. Phys. Rev. A **69**, 032101 (2004).
7. Off-diagonal generalization of the mixed state geometric phase. **S. Filipp** and *E. Sjöqvist*. Phys. Rev. A **68**, 042112 (2003).
8. Off-diagonal geometric phase for mixed states. **S. Filipp** and *E. Sjöqvist*. Phys. Rev. Lett. **90**, 050403 (2003).

## Publications (Proceedings)

---

1. Tracing the Bounds on Bell-Inequalities. **S. Filipp** and *K. Svozil*. AIP Conference Proceedings **750**. Foundations of Probability and Physics - 3, ed. by A. Khrennikov (American Institute of Physics, Melville, NY, 2005).
2. Off-diagonal mixed state phases in unitary evolution. *E. Sjöqvist and S. Filipp*. Foundations of probability and physics - 2, ed. A. Khrennikov; series "Math. Modelling in Physics, Engineering and Cognitive Sciences", Växjö Univ. Press (2003).
3. Boole-Bell-Type Inequalities in Mathematica. **S. Filipp** and *K. Svozil*. Proceedings of the 5<sup>th</sup> International Mathematica Symposium. Challenging the Boundaries of Symbolic Computation. ed. P. Mitic, P. Ramsden and J. Carne. Imperial College Press (2003).